DESIGN DEFINITION OF A MECHANICAL CAPACITOR

(NASA-CR-152613) DESIGN DEFINITION OF A MECHANICAL CAPACITOR Final Report, Jun. 1976 - Apr. 1977 (RCA Advanced Technology Labs.) 292 p HC A13/MF A01 CSCL 10B

N77-33603

G3/44 Unclas 49972

T. D. Michaelis, E. W. Schlieben, R. D. Scott

Advanced Technology Laboratories
Government Systems Division
RCA
Camden, New Jersey

May 1977

Final Report for Period June 1976-April 1977

Prepared for

GODDARD SPACE FLIGHT CENTER
Greenbelt, MD., 20771

1. Report No.	2. Government Accession No.	3. Recipient's Catalog No.

4. Title and Subtitle	5. Report Date
Design Definition of a Mechanical Capacitor	May 1977
	6. Performing Organization Code ---

7. Author(s)	8. Performing Organization Report No.
T. Michaelis, E. Schlieben, R. Scott	

9. Performing Organization Name and Address	10. Work Unit No.
RCA, Advanced Technology Laboratories Government Systems Division Camden, New Jersey 08102	--- 11. Contract or Grant No. NAS5-23650
12. Sponsoring Agency Name and Address National Aeronautics and Space Administration Goddard Space Flight Center, Greenbelt, MD 20771	13. Type of Report and Period Covered Final Report for Period June 1976 - April 1977 14. Sponsoring Agency Code ---

15. Supplementary Notes

16. Abstract

A design study and analyses of a 10 kW-hr, 15 kW Mechanical Capacitor (Energy Storage Wheel) System has been concluded. It has been determined that magnetically supported wheels constructed of advanced composites have the potential for high energy density (50 W-hr/lb) and high power density. Two structural concepts are analyzed that yield the highest energy density of any structural design yet reported. Particular attention has been paid to the problem of 'friction' caused by magnetic and I^2R losses in the suspension and motor-generator subsystems and low design friction levels have been achieved. The potentially long shelf life of this system, and the absence of wearing parts, can provide superior performance over conventional flywheels supported with mechanical bearings.

The costs and economies of energy storage wheels have been reviewed briefly. Vehicle applications appear to be feasible.

(Cont'd)

17. Key Words (Selected by Author(s))		18. Distribution Statement
Mechanical Capacitor Flywheels Energy wheels Composites Magnetic bearings	Advanced composite application	

19. Security Classif. (of this report)	20. Security Classif. (of this page)	21. No. of Pages	22. Price*
Unclassified	Unclassified	266	

* For sale by the National Technical Information Service, Springfield, Virginia 22151.

16. Abstract (Cont'd)

Finally, the engineering problems (or assumed problems) that require solution are summarized.

It is concluded that magnetically supported energy storage wheels are technically feasible and can be economic for certain applications. Further development is warranted in the light of the growing need for efficient energy storage devices acting as energy buffers between time varying prime power sources and loads.

PREFACE

Mechanical Capacitor is the short descriptor for a special form of electro-mechanical energy storage system comprising a magnetically supported energy wheel (flywheel) coupled to the electrical supply and the load by a motor-generator and a power conditioning subsystem.

This report contains the results and details of a design study and analyses, performed by RCA for the NASA-Goddard Space Flight Center, of a Mechanical Capacitor System satisfying a set of performance requirements. The objectives of the study were:

Major Objective:

Define a long-life, efficient, energy-storage system for public utility peaking power generation at terminal locations.

Secondary Objective:

Exploit evolving technologies from space programs.

And the scope of work was:

Scope of Program - First Phase

-Design definition and analysis of a complete energy storage system meeting the Statement of Work requirements, including a system of maximum efficiency and minimum cost.

-Study and select other system applications with attractive cost-benefits.

The study is significant because it addresses questions relating to the performance of a complete energy-storage system rather than the wheel element alone. The operational domain of energy wheels is thus more clearly defined.

Also, the study includes an analytical treatment of a magnetically supported rotating wheel as a gyroscopic mass requiring control in six degrees. The analysis can be extended to other systems and is a contribution to the art of magnetic bearing design.

CONCLUSIONS

Magnetically supported energy storage wheels of the type studied may approach an energy density of 110 to 128 W-hr/kg, depending on performance requirements. (Advanced battery systems may approach the same energy density.)

For the point design contained in this report, energy storage density is strongly influenced by power density requirements. A maximum power density of 100 to 200 W/lb or 220 to 440 W/kg is realizable at an energy density of approximately 66 W-hr/kg. (Advanced batteries have comparable power density goals.)

Higher power density is attainable (110 to 120 W-hr/kg) if the metal elements on the wheel can serve also as structure. However, energy density is reduced as the weight of metal on the rim is increased. (Fortunately, the wheel configurations analyzed meet the power density needs for many applications.)

Energy-wheel losses can be made diminishingly low (0.16% for a 24-hr powered cycle and 0.04% for 24 hr when coasting) but power conditioning losses are critically dependent on:

- Power level
- Nature and quality of electrical supply and electrical load, etc.

The system throughput efficiency can vary over wide limits.

For maximum system efficiency, both load and supply should be dc to reduce energy power-conversion losses. Storage system costs are sensitive to physical scale, production rate, and electrical performance requirements. System costs can vary greatly (from $1.75/W-hr to $0.28/W-hr for the systems studied).

With sufficient production, the energy wheel may be competitive with advanced batteries and internal-combustion engine power trains in small cars and other vehicles.

Other applications may be economically feasible, depending on the cost-benefits assigned to the energy-wheel attributes of environmental immunity, minimum safety hazard, absence of noise, and expected minimal maintenance and repair.

RECOMMENDATIONS

The problems cited in Section VI are, for the most part, best approached through experiments. However, because of the dynamic environment that gives rise to a number of problems, the experimental solutions must be sought, using test apparatus that resembles the energy-wheel configuration. The question is: how far short of a full system can the test apparatus be and still yield meaningful design data relating to the problems?

Accordingly, it is thought that a test apparatus that permits the initial preliminary determination of:

- Material rheological performance,
- Combined structural and magnetic stresses,
- Suspension-system idling losses,
- Motor-generator output and losses,
- Wheel dilation,
- Growth (or no growth) in wheel unbalance,

without introducing a full servo suspension system, is a relatively low-risk approach. Accordingly, it is recommended that a scale model of the Mechanical Capacitor be built incorporating the wheel inner rim (complete with the suspension electromagnets), rim electromagnet keepers, and motor-generator stator and rotor. The rim would be directly driven with an external brushless dc motor and the fixed and moving parts of the system radially constrained to avoid the use of a magnetic suspension servo system.

LIST OF ABBREVIATIONS AND SYMBOLS

Symbol	Description	Units
A	rotor transverse inertia	meter-kilogram-second ^{2}
a	permanent magnet spring constant	newton meter/radian
B	magnetic induction	gauss
b	Routhe coefficient	$10^3 \tau_2$
c	Routhe Coefficient	$1/\omega_n^2$
d	Routhe coefficient	10^{-6}x2a/Aω_n^2
E	energy	joules
EM	electromagnet	
F	force	newton
f	frequency	Hz
G_7	transfer function	-----
g	acceleration of gravity	9.804 meters/second
H	momentum	kilogram-meter-second
H_g	gap flux density	kilogauss
J	moment of inertia	-----
k_1	servo gain	-----
K_m	vertical spring constant	newton/meter
K'_m	vertical spring constant per unit of circumference	newton/meter^2
m	meter	
m	rotor mass	90.7 N second^2/m
N	newton	
PM	permanent magnet	
s	Laplace transform complex frequency	-----

LIST OF ABBREVIATIONS AND SYMBOLS (Continued)

Symbol	Description	Units
R	bearing radius	meter
r	radius	meter
T	torque	newton-meter
t	thickness	cm
TC	time constant	-----
V	lineal velocity	meter/second
VZP	virtual zero power	-----
W	weight	kilogram
y	lateral displacement	meter
z	vertical displacement	meter
δ	damping factor	-----
α	cone angle	25 degrees
γ	fiber density	kilogram/meter^3
θ	tilt angular displacement	radian
ρ	resistivity	ohm cm
σ_{max}	maximum fiber stress	kilogram/meter^2
τ_1	lead time constant	second
τ_2	lag time constant	second
ω	rotational velocity	radians/second
ϕ	tilt angular displacement	radian
χ	lateral displacement	meter
ω_n	rotor nutational frequency	radian/second
ω_o	earth's rate	7.27×10^{-5} radians/second

TABLE OF CONTENTS

TABLE OF CONTENTS (Continued)

LIST OF ILLUSTRATIONS

LIST OF TABLES

Section I

INTRODUCTION

Section I

INTRODUCTION

There is growing interest in the use of energy wheels (flywheels) as storage devices. This interest stems from the expectation that light, high-strength fibers can be used in specially designed wheels to store more energy per pound than flywheels made of high-strength steels or other stores, such as batteries. It is possible that lightweight mechanical energy stores may show significant cost savings because of the reduced weight of materials used, long life, and the economic advantage of weight savings in systems to which they may be applied.

NASA and RCA have addressed these possibilities in earlier studies and experimental programs. Their conclusions appear in technical notes and papers (see References 1 to 3). In summary, magnetically supported, thin-rim, circumferentially wound energy wheels are conceived to be the most efficient type of rotating mechanical device for energy storage.

However, this conclusion has been obtained mainly from the examination and analyses of the rotating element only and does not include the total system performance of the energy store.

The study reported here was established by NASA to examine the magnetic-energy wheel concept in more detail and determine the technical and economic feasibility of one system for a selected use.

The system studied comprises a magnetically supported wheel for energy storage, integral with a motor-generator (m-g) for electrical-mechanical and mechanical-electrical energy conversion, and a separate subsystem to process the electrical power from the supply to the energy wheel and from the energy wheel to the load.

This introduction comprises a statement of the performance requirements for the system specified by NASA, the study logic, and a description of the point design developed during the study.

A. SYSTEM PERFORMANCE REQUIREMENTS

The statement of work for this study has been reduced for reference purposes and is summarized in Figures 1-1 and Table 1-1.

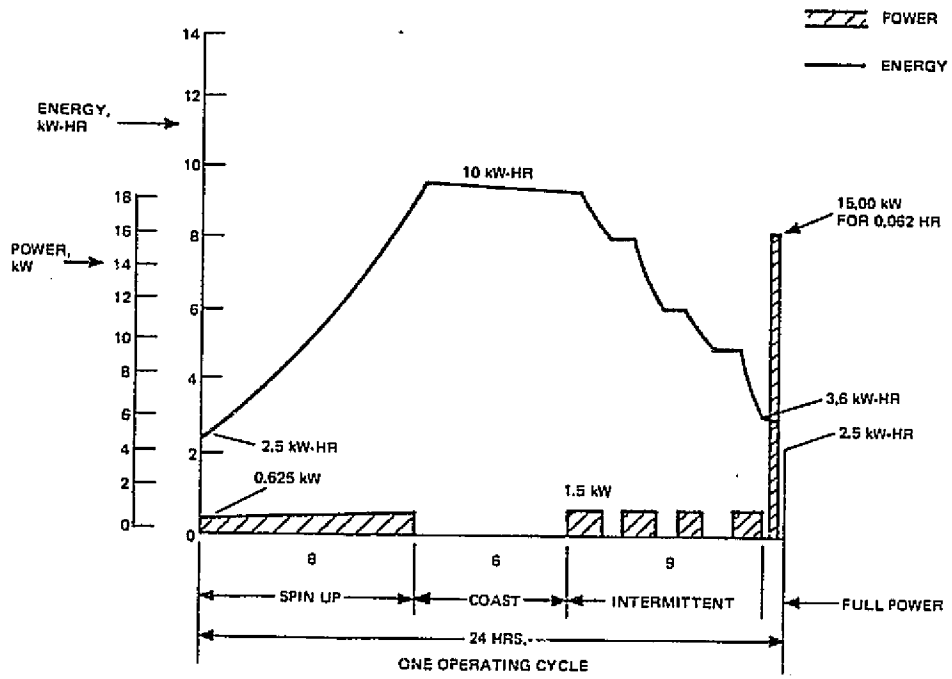

Figure 1-1. Mechanical Capacitor power and energy profiles; 24-hour cycle.

As shown in Figure 1-1 the system operates on a 24-hour cycle. Maximum storage is 10 kW-hr, and the maximum electrical load is 15 kW. The wheel speed varies from full to 50% of full speed (75% depth of discharge). The charge period is 8 hours, at constant wheel acceleration. The coast period is 6 hours and intermittent loads are supplied with up to 10% maximum power during the next 9 hours. The wheel speed is reduced to 60% of full speed. In the last hour, full power is taken from the wheel until the wheel speed is reduced to 50% of full speed.

The energy-power profile is not based on energy use data for a particular application, but it is a reasonable one for system analysis. The effects of major changes in the requirements are brought out in several succeeding sections of the report. Some of the general requirements are:

- Mean time to failure $\geq$50,000 hrs.
- No overspeed possibility
- Safe coast down with loss of line power
- Self contained, only 110/220 V, 3ϕ, 60 Hz in and out
- 15 kW to maximum load - 1/2 to maximum speed
- 25% over speed in qualification test with no permanent deflection
- $\leqslant$50% over-speed in qualification test with no burst

TABLE 1-1. MECHANICAL CAPACITOR DESIGN REQUIREMENTS

Subsystem	Design for following:	System Design Goals
Supply → Power Conditioner	110/220 v, 60 Hz 3 ϕ line power in load power out.	Maximize: — Energy density — Power density — Energy thruput efficiency (>60%)
Wheel	- 1.25 max speed (without deformations) - 1.50 max speed (without burst) - natural frequencies outside speed range - Balance dynamically to 300 μin. - Balance statically to 0.03 ft. lb. with axis vert.	
Motor/Generator	- <80 W internal loss during spin up - <45 W -motor loss during steady state - <75 W-generator losses - <50 W-commutation rectification loss - charging <50 W loss discharging 15 kW to load - 300% overload - 1 s	
Magnetic Suspension (Bearing)	- Support 2 x wheel weight - Handle worst-case seismic loading and earth rate with 50% margin of safety - Radial stiffness-1600 lb/in. - Radial damping - 60% of min. value. - Stable during speed changes and expansion	
Support	- Natural frequencies outside of suspension - Smooth Base	

The design requirements are listed in Table 1-1. Additional requirements were added during the study and are set forth in the appropriate sections.

B. DESIGN LOGIC

The 'bottom line' in this study is maximum energy storage capacity per dollar of system cost, and as a function of storage time. These objectives lead to several design guidelines:

- Stress low-cost designs
- Stress low "friction" suspension and motor-generator designs.

Low friction is required if mechanical capacitors are to compete with long-shelf life batteries and other energy stores.

Further, the complexity of an energy wheel system gives rise to a number of other guidelines. The system is located at the end of a utility distribution grid; it interfaces with the utility system and the load(s) (see Figures 1-2 and 1-3). Hence, if many storage systems are used, the dynamic performance of all three systems must be evaluated for interactive effects. However, as discussed in Appendix B, a simplifying assumption has been made that there is no interaction.

In the energy wheel system, the major design features derive primarily from the system performance requirements (the independent variables shown in Figure 1-4). But each subsystem also is sensitive to the other subsystem design parameter values, to varying degrees, as shown by the width of the arrows.

Design logic requires that all the subsystems be modeled to include the values of the independent variables for all the interactive subsystems except the one being designed, and include also the design variables for the subsystem in question. Further, cost, dynamic, and weight models can be developed. A full systems model would include the parameters shown in Figure 1-4, plus others-- perhaps more than 200.

The brevity of this study does not permit this treatment. Instead, some modeling of subsystems has been completed and tradeoffs among subsystems arrived at by relying on experience, on some sensitivity analyses, and by testing for upper and lower design bounds. Therefore, the resulting point design is an optimal design but not totally optimum.

C. POINT DESIGN

The principal features of this point design are shown in sketch SK2294234 (Sheets 1 and 2 of which appear at the end of this report). Some discussion of these features appear, starting on page 1-11.

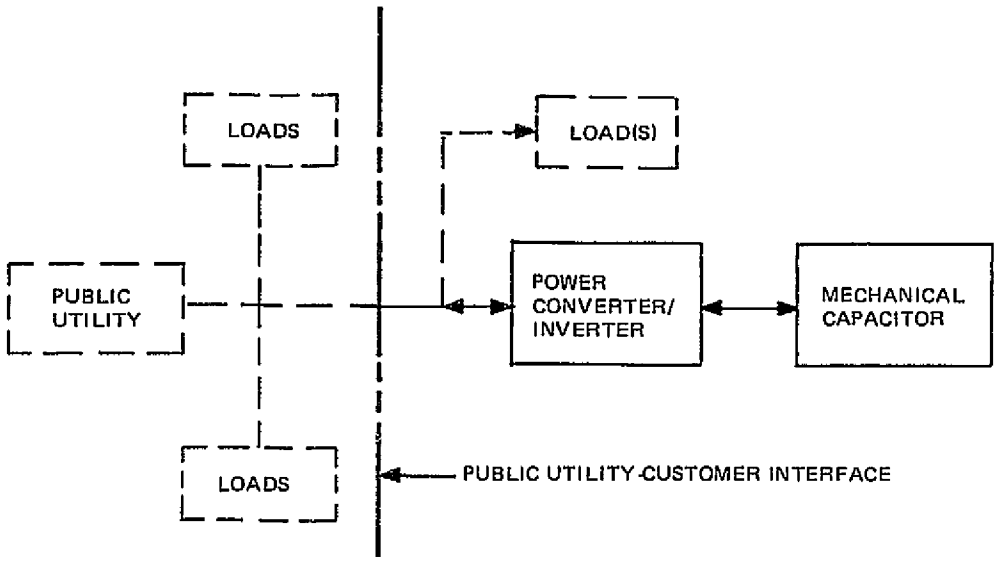

Figure 1-2. Mechanical capacitor connections.

Three wheel configurations A, B and C and two motor generator configurations were proposed originally. These appear in Figures 1-5, 1-6, and 1-7, showing wheel system cross sections. All these configurations comprise a composite rim (or rims), magnetic suspension of the wheel, and motor-generator elements to accelerate and decelerate the wheel (add or subtract energy).

The wheel is a gyroscopic body rotating close to but not in physical contact with the supports. The function of the magnetic bearings is to maintain the space gap between the wheel and the supports in the presence of gravity and disturbing forces.

As the wheel spins up to high speed, it can expand 1% or more on the diameter. Therefore provision was made for an axial adjustment of the support surfaces to maintain the space gap for proper operation of the electromagnetic bearings. However, this approach was abandoned during the study in favor of the use of a very stiff inner rim so that expansion is limited to a small increase in gap growth. Further, the angled bearing support was chosen to further minimize gap increase due to wheel growth. Configurations B and C were eliminated; configuration B for the reason stated last and configuration C because it was determined at the outset that the physical strength properties of the rim of the wheel must be significantly derated to allow for stress concentrations due to centrifugal forces imposed by the metal elements. The principal values and materials chosen for the point design energy wheel are shown in sketches SK-2294234 and in Table 1-2.

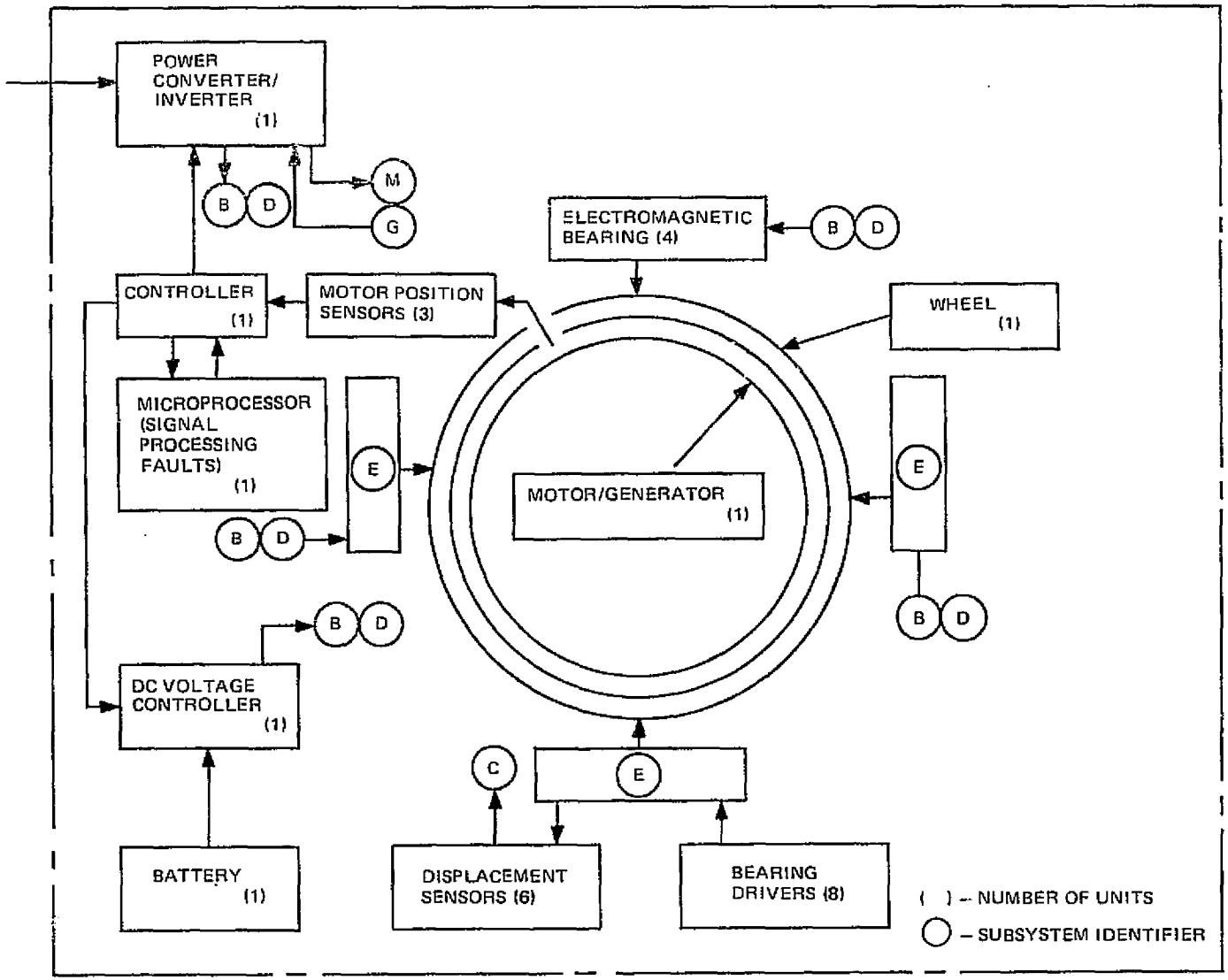

Figure 1-3. Major components of Mechanical Capacitor.

E. Schlieben

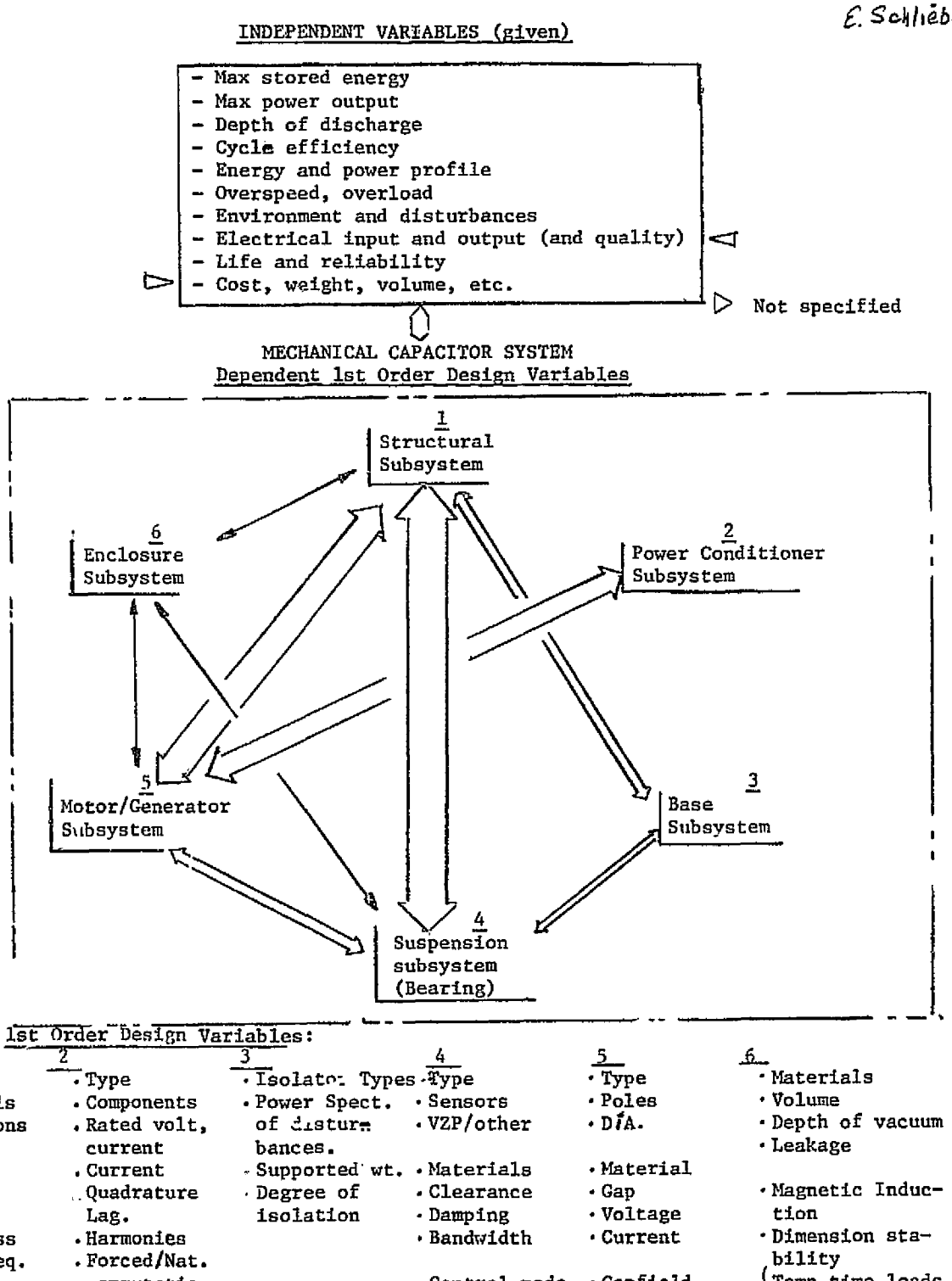

Figure 1-4. Independent variables, dependent variables, and interactive relationships of Mechanical Capacitor

Mechanical Capacitor Concept

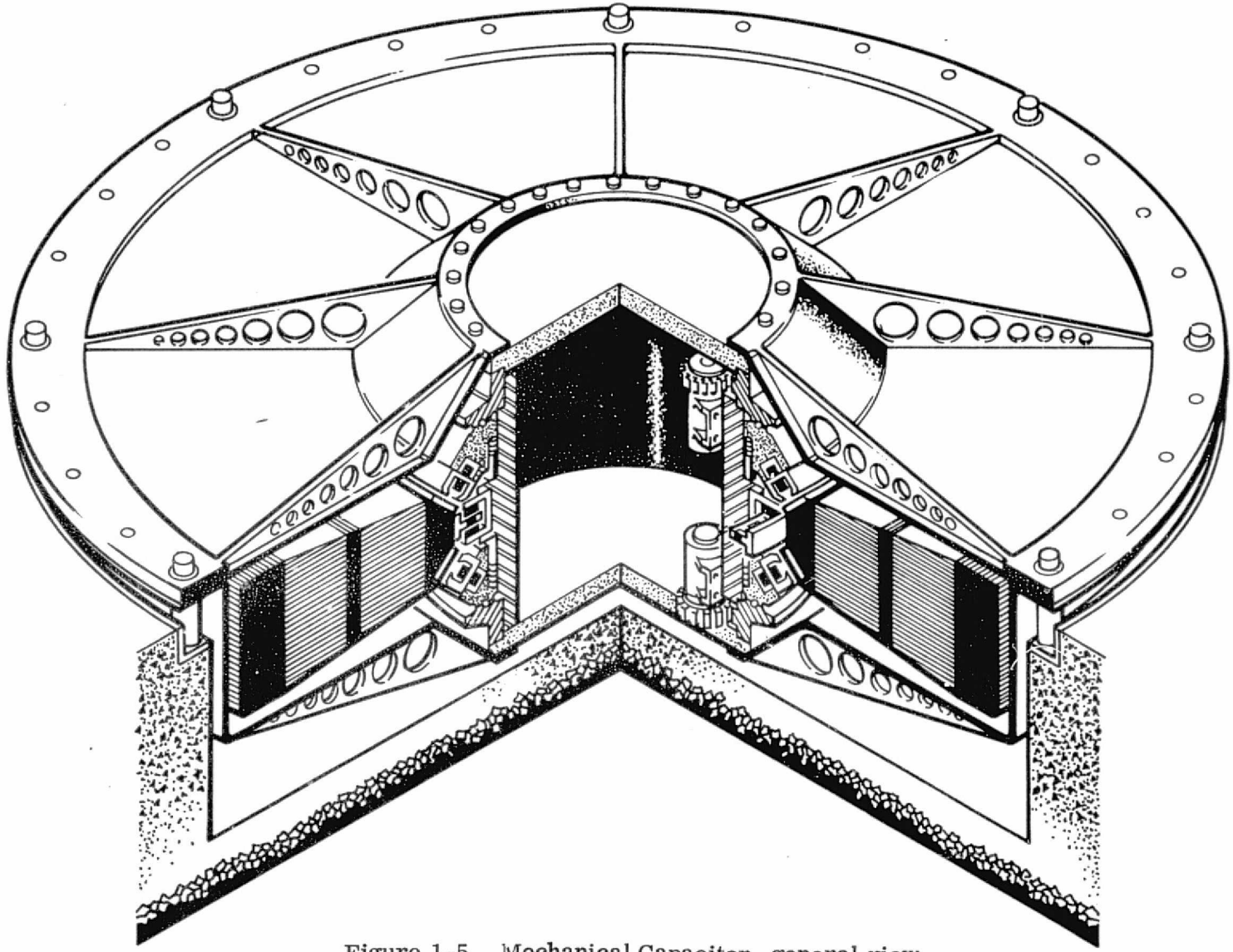

Figure 1-5. Mechanical Capacitor, general view.

Review of Proposal Concept

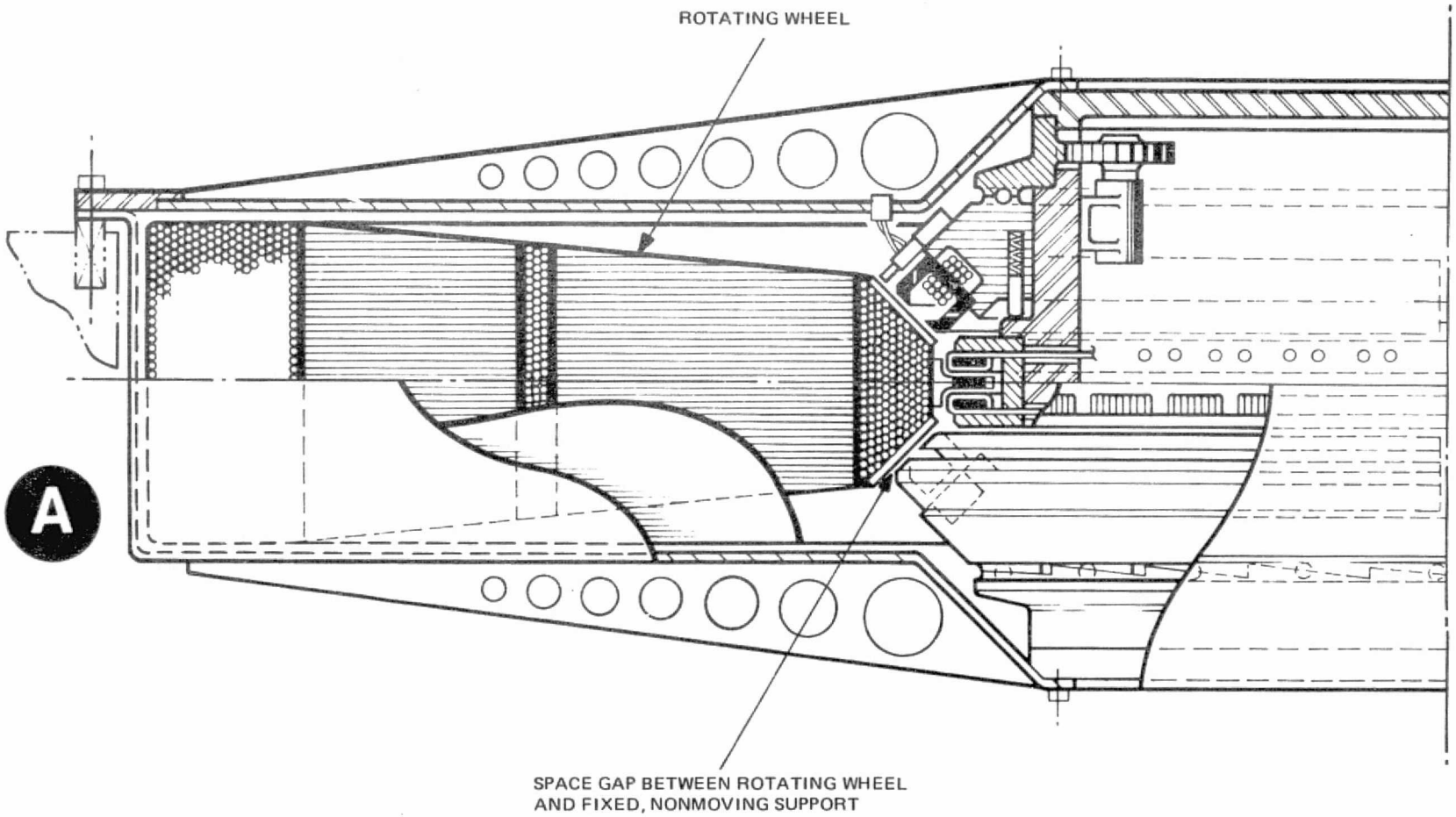

Figure 1-6. Mechanical Capacitor, concept A cross section.

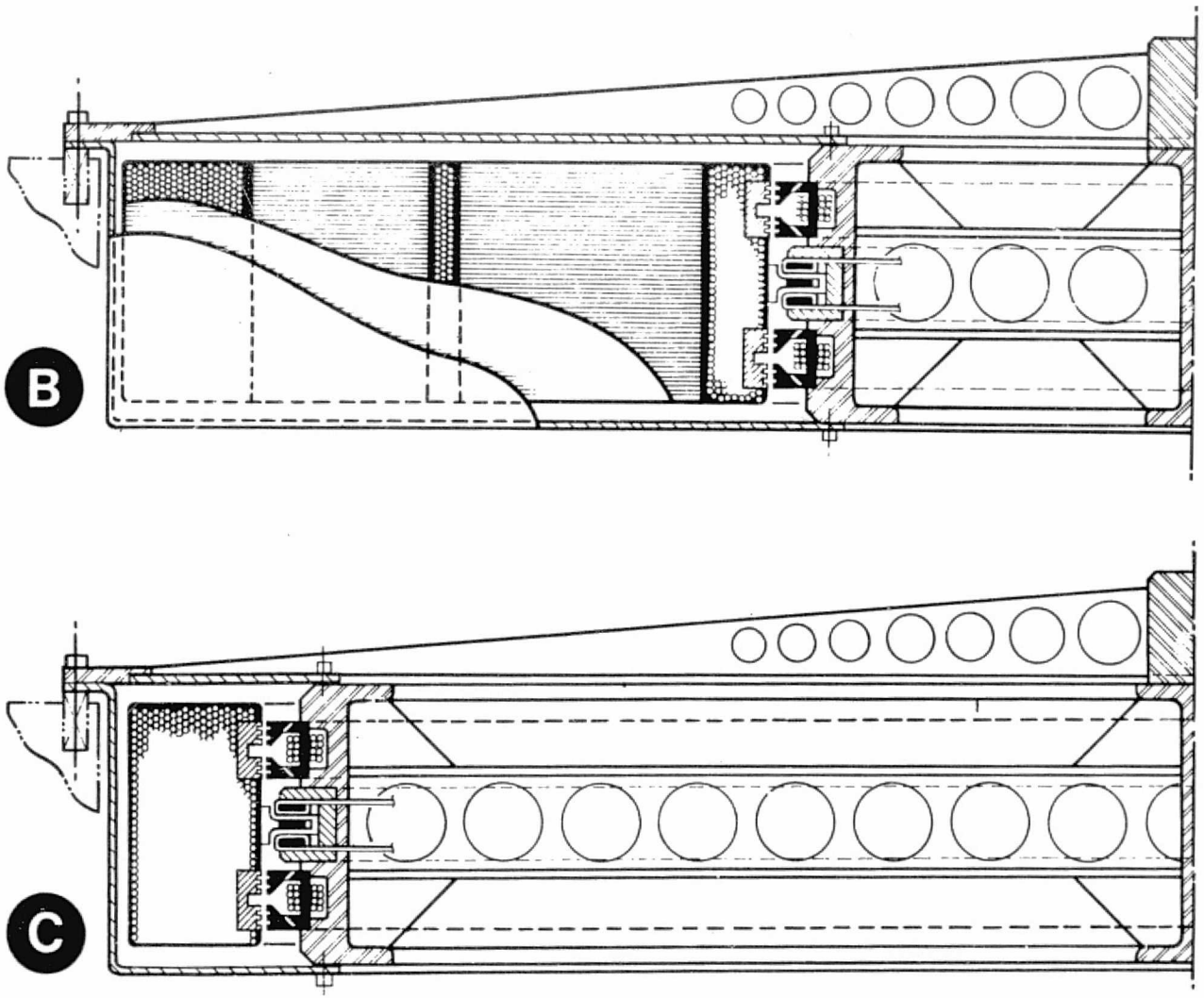

Figure 1-7. Mechanical Capacitor, concept B and C cross sections.

TABLE 1-2. MECHANICAL CAPACITOR POINT DESIGN FEATURES

Wheel OD ID	4 Ft. 2 Ft.
Max. Normal Speed	17,000 rpm
50% Normal Speed	8,500 rpm
Rim Material	Kevlar 49 and resin matrix
Rim Fiber Content	79%
Inner Rim Material	Graphite GY-70 and resin matrix
Fiber Content	60%
Soft Magnetic Material	Carbonyl Iron or a glassy metal (Metglas)
Perm. Magnetic Material	$SmCo_5$
Attractive Suspension	VZP (virtual Zero Power)
Nominal Gap Clearance	0.030 In.
Maximum Excursion	±0.020 In.

Although configuration A was the only one selected for more design analysis, a number of subsystem options were analyzed. First, two wheel structures were designed and analyzed:

1. A prestressed solid multiring wheel, which will be referred to as the NASA configuration.

2. A multiring wheel with light weight fillers between the rings, which will be referred to as the RCA configuration (this is a proprietary configuration).

1. Motors

Four motor-generator configurations and four variants were examined instead of the two proposed configurations (a homopolar and a dc torquer). The basic configurations are shown in Figure 1-8. The upper sketches are cross sections of the inner rim of the energy wheel. The lower sketches are views looking radially from the wheel axis of rotation. Two motor-generator configurations have fixed fields, and the others variable fields. In the first two, the generator voltage varies 2:1 with wheel speed. In the others, the field can be varied to maintain constant output voltage. A trade must be made, taking into account the effect on the power conditioner subsystem design, motor-generator losses, wheel dynamic stability, weight, and cost. The Inland Motors Division of the Kollmorgan Corporation consulted with RCA and examined its motor analyses and selection. Configuration 2A-1 was considered as the optimum selection. A qualitative

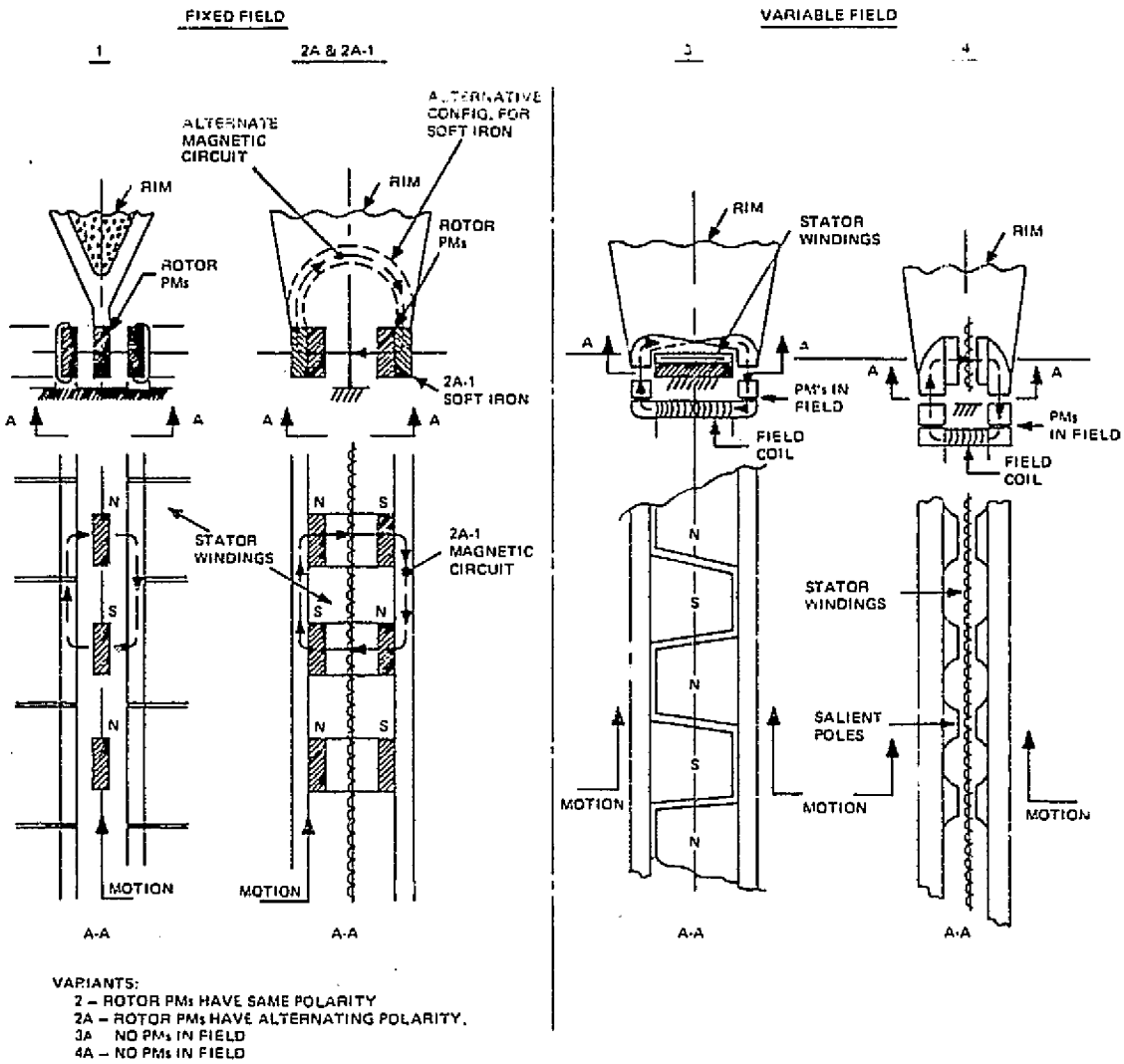

Figure 1-8. Mechanical Capacitor m-g configurations.

rating appears in Table 1-3. This is a 3-phase, Delta connected motor-generator operating at a high commutation rate with a permanent magnet field structure carried on the wheel and the ironless armature supported by the fixed structure. Details of the motor-generator analyses appear in Appendix C.

2. Structure

The two structures considered for the wheel, the NASA and the RCA configurations, were stress-analyzed using the structures model shown in Appendix A. The objective was to determine an optimum design (maximum energy density) through a choice of material and dimensions that exploits the high intrinsic energy composites in such a way that the radial and tangential stresses in the wheel are everywhere close to the allowable stresses.

A number of design parameters are involved in each tested design. Some boundary conditions were: the choice of two structural fibers, one rim id-od ratio, one wheel id-od ratio, and a pancake configuration.

Two idealized configurations, of the many analyzed, are shown in Figures 1-9 and 1-10 and the point designs are shown in sketch 2294234.

The NASA configuration comprises prestressed circumferentially wound rims with no fillers. The RCA configuration comprises separate rims with honeycomb fillers. The honeycomb does not contact the rim directly but is bedded in an elastomer as shown in the detail in Figure 1-11. The function of the elastomer is to accommodate changes in the radial direction dimension between rims as the wheel speed changes.

A number of configurations were analyzed, some of which are listed in Table 1-4.

The analysis indicates that the NASA and RCA configurations theoretically are superior in energy density capacity to all known energy wheel configurations. The detailed structural analysis appears in Appendix A.

3. Suspension

The electromagnets, comprising part of the magnetic suspension subsystems, are shown in sketch SK-2294234. These are biased electromagnets with integral permanent magnets that provide a 'bias' field across the gaps that can be modulated by coil currents. Coil currents variation with the electromagnet force is fairly linear. The suspension has the following features or capabilities:

- Support twice the rotor weight
- Conical bearing

TABLE 1-3. M-G CONFIGURATIONS (COMPARISON)

	1	2A-1	3	4
Rotor Weight	Lowest 1	2-3	3	4
Air Gap, in. (Complete Circuit)	Smallest 1 0.12	1 0.14 (min.)	2 0.234	3 0.314
Flux Density (For some length mags. or equiv. electromags)	Highest 1	2	4	3
I^2R Losses	Lowest 1 Armature Coils-Long End Turns	2	3 (I^2R for field is added)	4 Armature Coils - Long End Turns (I^2R for field is added)
Magnetic Losses		Lowest		
-Running	3	1	2	2
-Coasting	3	1	2	2
Crosstalk (Between M/G and Bearing				
-Powered	Yes (axial)	No	Yes (Radial)	Yes (Radial)
-Coasting	Yes (axial)	No	Yes	Yes
Mfg. Cost		Lowest		
	2	1	4	3

Notes:

Wheel growth with m-g dia. of 22 in.
$E = 70 \times 10^6$ lbs/in^2
Maximum Strain = 0.017 in. on radius.

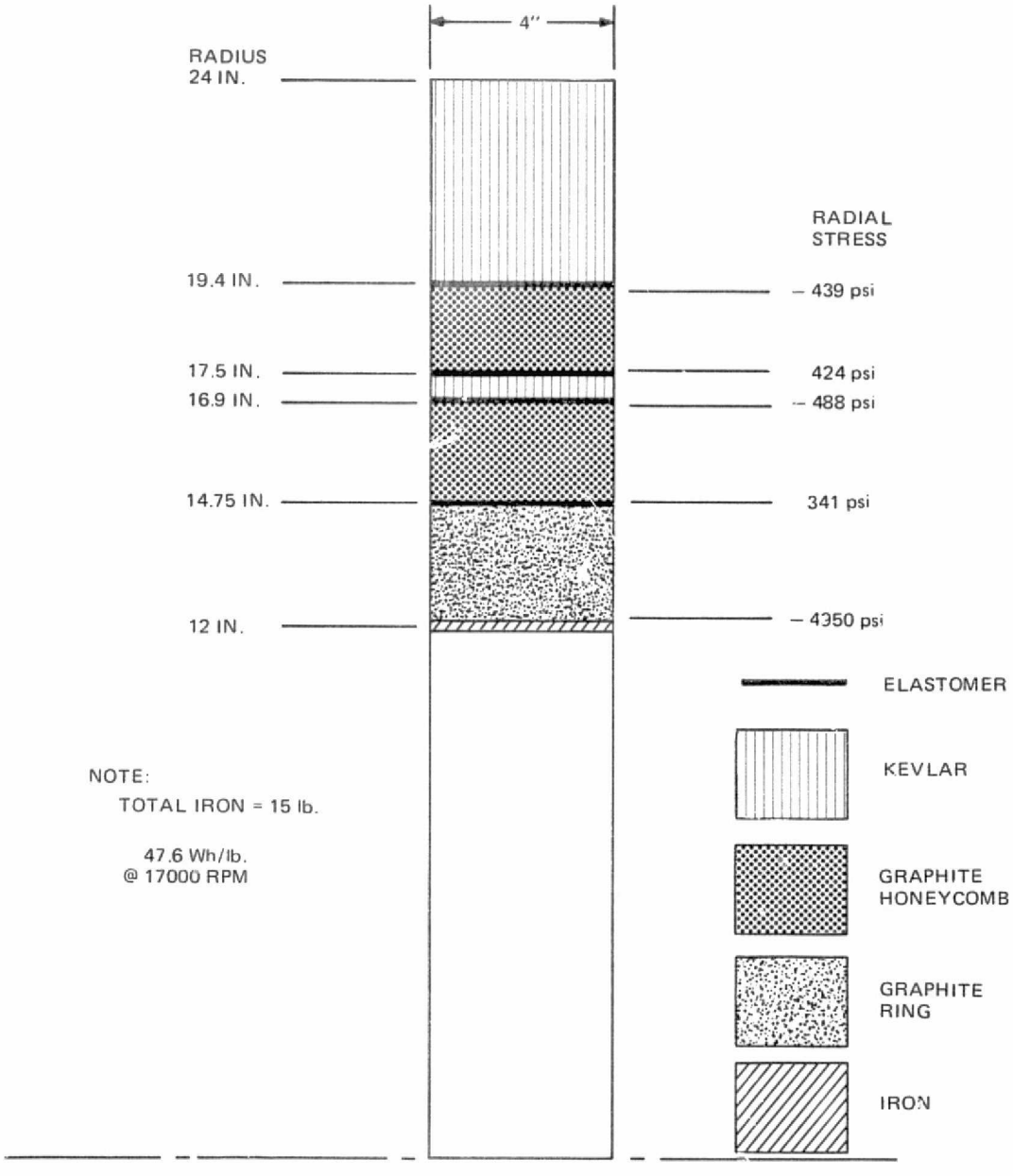

Figure 1-9. RCA graphite, graphite-honeycomb, Kevlar energy-wheel configuration.

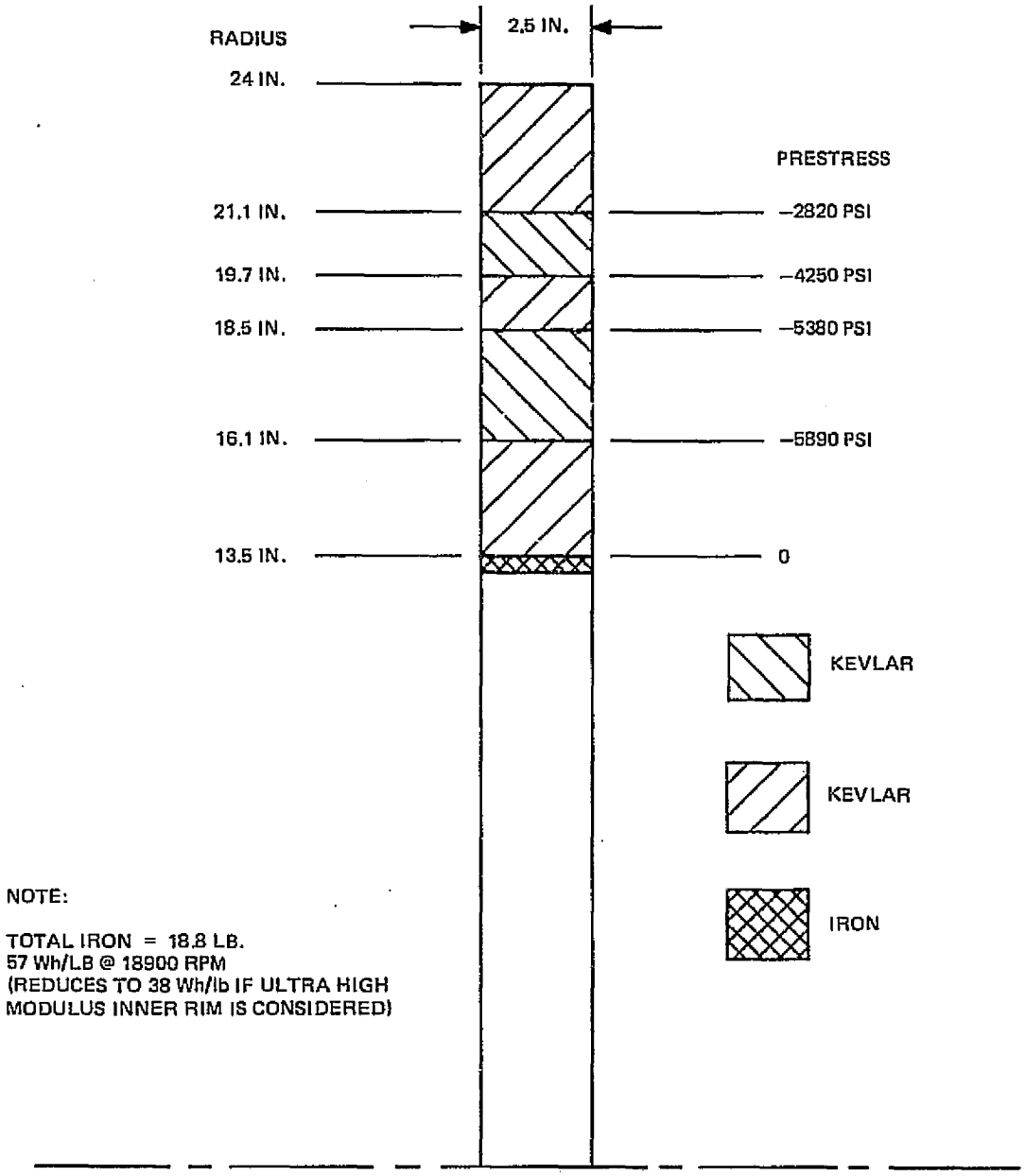

Figure 1-10. NASA all-Kevlar energy-wheel configuration.

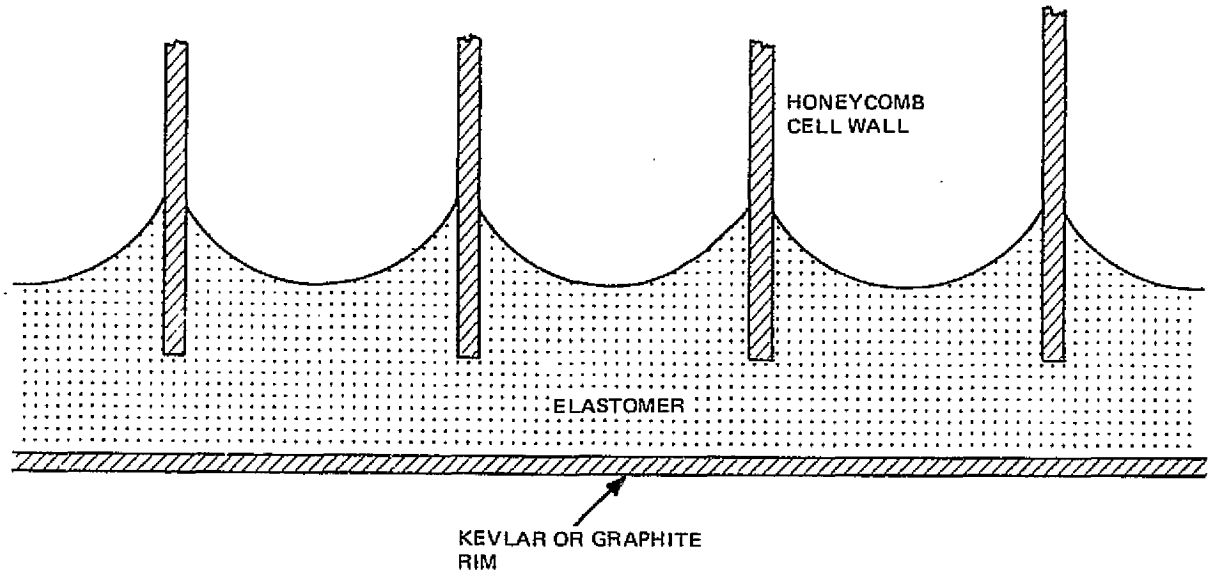

Figure 1-11. RCA honeycomb-elastomer rim configuration.

- All-active axes
- Biased magnetic field
- Symmetrical surface sensing

The block diagram of the system is shown in Figure 1-12. Five degrees of freedom of the wheel are controlled by the system and the sixth by the m-g. Six displacement sensors (five and one redundant) are needed to determine all motions. The sensors measure displacements (gaps) normal to the bearing surface. The design axial and radial loop parameters are shown in Table 1-5. The system is stable for the rigid wheel. An elastic model of the wheel is needed to determine if stability can be obtained for this case. The suspension system analysis appears in Appendix B.

4. Power Conditioning Subsystem

The subsystem requirements were refined during the study to include the following assumptions and statements:

- Supply and load 3 ϕ, 110/220 V
- Supply has infinite tolerance for converter reactive volt-ampere demand and converter-injected harmonics

TABLE 1-4. WHEEL STRESS ANALYSIS RESULTS

Iron Wt. (lb.)	Wheel Wt. (lb.)	ID (in.)	Thickness (in.)	Radial Growth (in.)	Construction	RPM
15.2	500	12	10	0.008	I-G-R-H-R-K-R-H-R-K	11,000
15.2	200	12	4	0.019	I-G-R-H-R-K-R-H-R-K	17,000
16.0	263	13.4	4	0.040	I-G-K (prestress)	15,280
18.8	175	13.5	2.5	0.017	I-K (prestress)	18,900
9.2	526	12.1	3.6	0.035 (Est)	I-G-K (prestress)	14,000
22	167	12.1	2.5	0.017	I-K (prestress)	19,600
15	370	12	4/8.5	0.01	I-G-H-K-H-K	12,000
15	209	12	4.1	0.02	I-G-H-K-H-K	17,000
30	308	12	5.5	0.02	I-G-H-K-H-K	14,300
15.2	208	12	4	0.022	I-G-R-H-K-R-H-K	17,000
22.5	330	12	5.7	0.021	I-G-R-H-K-R-H-K	13,800
45	227	12	4	0.12	I-K-R-H-K	17,000
0	203	12.5	4.3	0.02	I-G-R-H-K-R-H-K	17,000
20	270	12.5	5.1	0.031	I-G-R-H-K-R-H-K	15,000
39.9	362	12.5	6.5	0.037	I-G-R-H-K-R-H-K	13,300
0	199	11.5	4.2	0.018	I-G-R-H-K-R-H-K	17,000
20	250	11.5	4.5	0.02	I-G-R-H-K-R-H-K	16,000
40	320	11.5	5.5	0.02	I-G-R-H-K-R-H-K	14,500
0	197	13.5	4.1	0.025	I-G-R-H-K-R-H-K	17,000
39.6	400	13.5	7	0.023	I-G-R-H-K-R-H-K	12,900

Notes:
I: Iron
G: Graphite
R Elastomer
H: Honeycomb
K: Kevlar

All wheels: 48 in. OD
Energy store: 10 kWh

Working Stress:
Kevlar 49 = 225 ksi
Honeycomb = 500 psi
Graphite = 120 ksi

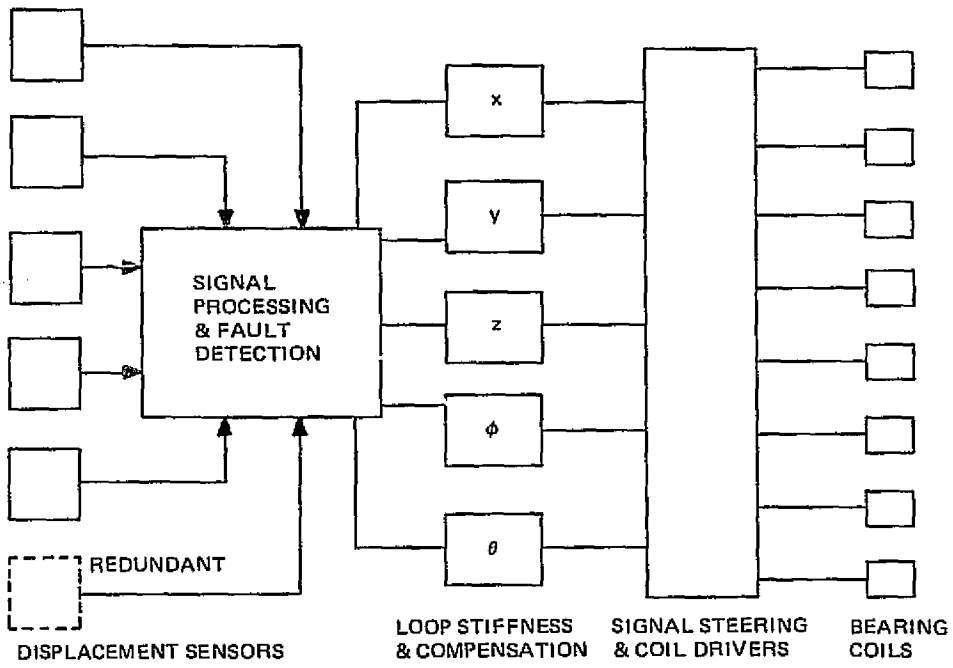

Figure 1-12. Suspension system block diagram.

TABLE 1-5. AXIAL AND RADIAL LOOP PARAMETERS

Parameter	Axial	Radial
Gain	96.3 dB	78.9 dB
Crossover Frequency	500 rad/s.	168 rad/s.
Phase Margin	54°	55°
P.M. Bearing Spring Constant	-59,500 lb/in.	$-\frac{59,500}{2}\sin^2\alpha$ lb/in.
Motor Fld. Spring Constant	0	$-\frac{59,500}{4}\sin^2\alpha$ lb/in.
Axial Defl. for Twice Weight	11.8 mil-in.	—
Total Spring Constant	+59,500 lb/in.	+7970 lb/in.
δ		0.6

Note:
$\alpha = 25°$

- Parallel tie-line operation
- Motor harmonic impedance high
- No filtering between converter and m-g.

Motor configuration 2A-1 (Figure 1-12) was used for the analysis.

The Westinghouse R&D Center Systems Analysis Group consulted on the subsystem design and cost estimate. The elemental schematic of the system is shown in Figures 1-13, 1-14, and 1-15.

The high frequencies involved and the high-efficiency requirement leads to a double-conversion transistor voltage and current fed scheme as shown in Figure 1-13 with switch details shown in Figures 1-14 and 1-15. The cost of this system in the 1980-1985 time frame is very high and becomes a principal consideration in the application of energy wheels. A detailed discussion leading to choice of power converter subsystem appears in Appendix D.

5. Vacuum Housing, Base, and Isolation

These topics have been treated lightly because they are low-risk items with little impact on systems optimization and costs.

The vacuum housing shown in sketch SK-2294234 is overdesigned for a vacuum pressure of 10^{-5} torr. The housing and support structure is made of fiber glass mat (to eliminate magnetic losses due to stray fields from the suspension and m-g systems) and sheathed on the outside with butyl rubber to provide a low-leak barrier. The housing has no openings, hence a small vacuum pump operating intermittently can provide the vacuum pressure.

The housing is supported by shock mounts to provide isolation from seismic and local noise (traffic, etc.). Low-frequency earthquake shock waves can be handled by the magnetic suspension. One alternative view is that the housing can be bolted solidly to the base structure because normal seismic noise is likely to have a small effect on suspension power expenditure. Some supporting information is contained in Appendix E.

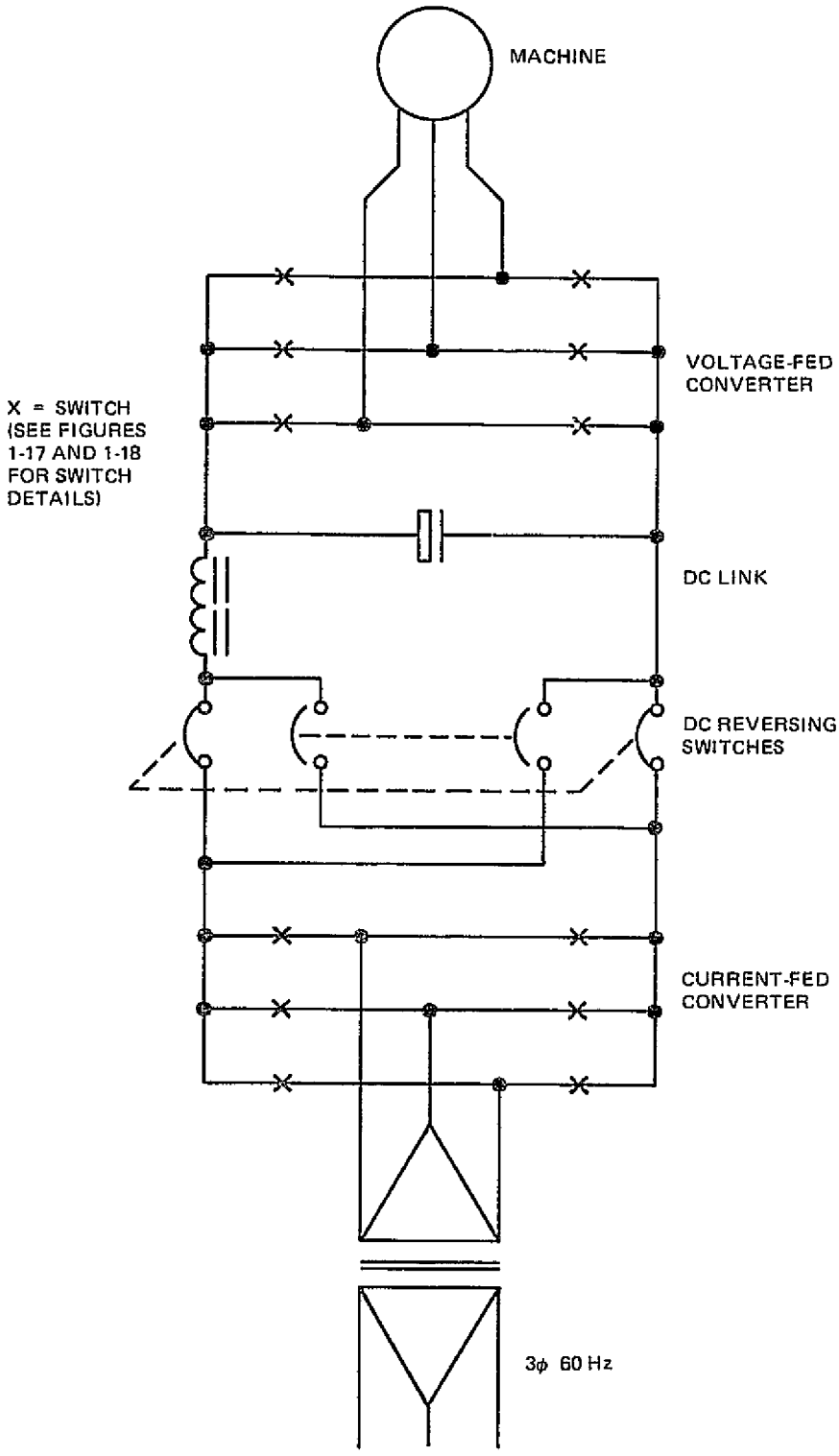

Figure 1-13. Elemental schematic diagram of complete double conversion system.

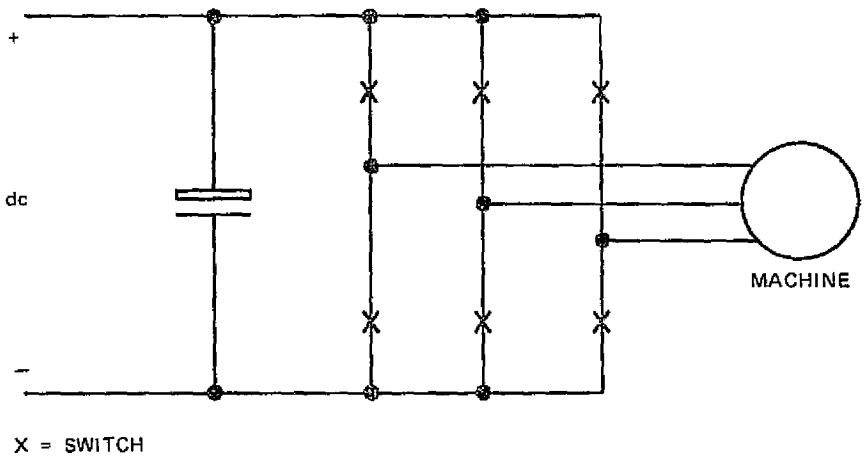

a. Elemental schematic diagram of voltage-fed converter.

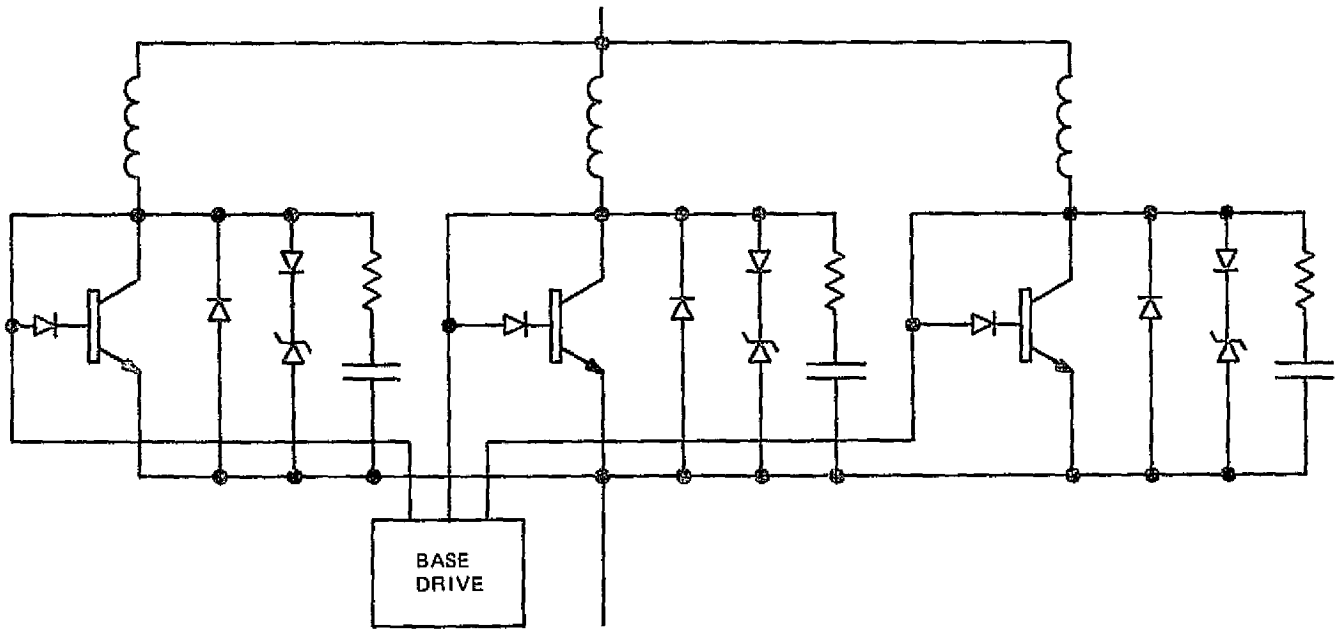

b. Switch details.

Figure 1-14. Voltage-fed converter schematic diagrams.

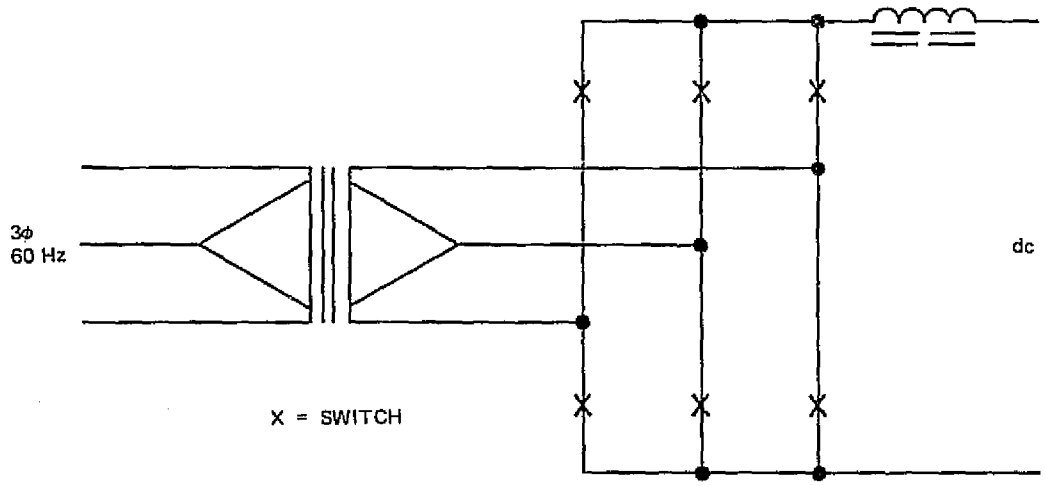

a. Elemental schematic diagram of current-fed converter.

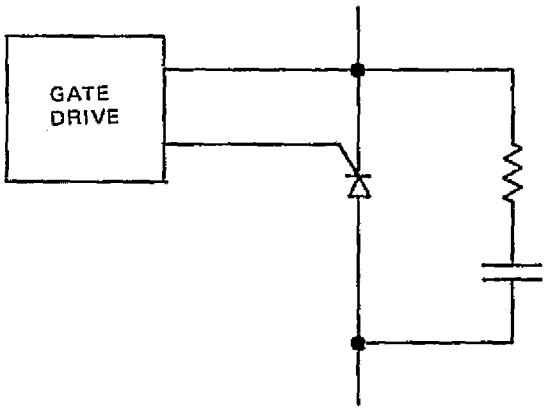

b. Switch details.

Figure 1-15. Current-fed converter schematic diagrams.

Section II

LOSSES AND SYSTEM EFFICIENCY

Section II

LOSSES AND SYSTEM EFFICIENCY

Energy losses are encountered in the suspension and motor-generator (m-g) subsystems. The determinants of losses are shown in Table 2-1, and the localized hardware-based sources of losses in Table 2-2.

When the wheel is in neutral equilibrium, the Virtual Zero Power (VZP) suspension system does not require electrical power if the magnetic bearings have symmetry. The magnetic field in the gaps does not vary as the wheel rotates; hence, the metal in the electromagnet circuits will not be exposed to time-varying coercive fields. However, Group I causes in Table 2-1 will in fact result in dB/dt variations and hence eddy-current and hysteresis losses. Group II imposed inertial forces require that the suspension system expend power also in countering these mechanical noises. Group III are first-order determinants of losses, controllable through fundamental design decisions. And Group IV determinants are, in the main, independent variables that tend to determine the absolute value of the losses.

Accurate determination of losses is rendered difficult because of the complex nature of the operating environment. For example, the magnetic induction in the rim metal is modulated in a complex manner. All suspension system magnetic changes occur mainly in the first B-H quadrant at high frequencies. The hysteresis and eddy-current losses are determined by:

- The effective permeability
- Power spectrum of frequencies contained in the variations in magnetic induction
- Range of variation in the magnetic induction about the normal bias values
- Magnitude and distribution of instantaneous flux density across the thickness of the laminations
- Magnetic property changes due to physical stresses in the rim metal
- Other causes.

Input values for the determinants marked with asterisks in Table 2-1 are not obtainable during the design phase for the computation of losses. Conservative assumptions can be made, based on manufacturer's measured bulk properties, manufacturing experience, etc., and losses computed from these assumptions. This procedure has the merit of permitting estimates to be made, but will not lead to an accurate determination of absolute losses a priori.

TABLE 2-1. MECHANICAL CAPACITOR; DETERMINANTS OF SYSTEM LOSSES

	First Order	Second Order
Group I - Physical Causes		
*Wheel Dimensional Variations		X
*Wheel Unbalance		X
*Electromagnet Assembly Magnetic Variations	X	
*Magnet Variations	X	
*Soft Iron Variations	X	
*Sensor Noise		X
Group II - Inertial Sources		
Earth Rotation		X
*Seismic Noise		X
*Motor-Gen. - Suspension System Cross Talk Forces		X
*Local Noise		X
Group III - Miscellaneous		
Basic Choice of M-G and PCU Configurations	X	
Stray & Residual	X	
Group IV - Performance Related		
Speed	X	
M-G Diameter	X	
Suspension (Bearing) Diameter	X	
Wheel Weight	X	
System Operating Cycle (Energy and Power Profiles)	X	

In addition to the losses enumerated, stray fields from the magnetic suspension system and motor-generator can interact with the vacuum housing and supports if these are made of ferrous metals, aluminum, etc.

Following are estimates based on the foregoing loss sources.

TABLE 2-2. MECHANICAL CAPACITOR; POWER LOSS SOURCES

1. Suspension Subsystem
   a. Electromagnets
      I^2R
      Eddy Current
      Hysteresis
   b. Keepers and Other Metals
      Eddy Current
      Hysteresis
   c. Electrical & Electric Circuits and Components
      I^2R
   d. Quiescent Power
      I^2R

2. M-G
   a. Rotor Magnets & Circuit Elements
      Hysterisis
      Eddy Current
   b. Stator
      I^2R
      Hysterisis
      Eddy Current

3. Harnesses
   I^2R

4. Power Conditioner Unit
   I^2R and Magnetic Losses

A. SUSPENSION SUBSYSTEM LOSSES

1. Dimensional Variations Effects

The effect of wheel dimension variations is to cause variations in the gap field. The slope of the gap field flux, from the test electromagnet data in Table B-1, Appendix B is $\frac{4.20 - 1.95}{0.04} \cong 5.6$ kilograms/in. If wheel out of round and out of flat is ±0.002 in., the B variation is 5400 x 0.002 = ±10.8 at a once around frequency.

2. Effect of Unbalance

If the maximum unbalance is 0.0003 in. (from the SOW) the B field variation is: 5400 x .003 = ±16.2 gauss.

The effect of these small variations in the gap field should be negligible, compared to other losses determined in the following pages.

3. Electromagnet Variations

These include magnet variations and soft iron variations. Variations in the magnetic properties of the electromagnets (EMs), magnetic, and soft iron circuit elements can cause dB/dt changes under steady-state operation. With high quality materials, the variation in the biased gap field may be held to ±5%. The nature of the variations seen by the rim soft magnetic material, however, is not known a priori. If a sinusoidal variation is assumed with a wavelength of 4.3 x the keeper width, or approximately 5.6 in., the field will vary with a frequency as follows:

wheel frequency x keeper diameter x π /2.6

for wheel frequency of 17,000 rpm and keeper diameter of 26 in. approximately,

$$f = \frac{17000}{60} \times \frac{26\pi}{5.6} \cong 4.1 \text{ kHz}$$

The metal on the wheel (the moving portion of the electromagnet circuit) sees an external dc field due to the biased EMs and an ac field due to the variations mentioned. The hysteresis loop that results appears like Figure 2-1. The loop is in the first quadrant of the B-H characteristic curve.

The true dynamic environment is considerably more complex because the assumed sinusoidal ac circuit field component is, in fact, made of many frequencies and strengths and can result in many interior hysteresis loops as shown in Figure 2-2(d) (first quadrant), taken from Reference 4.

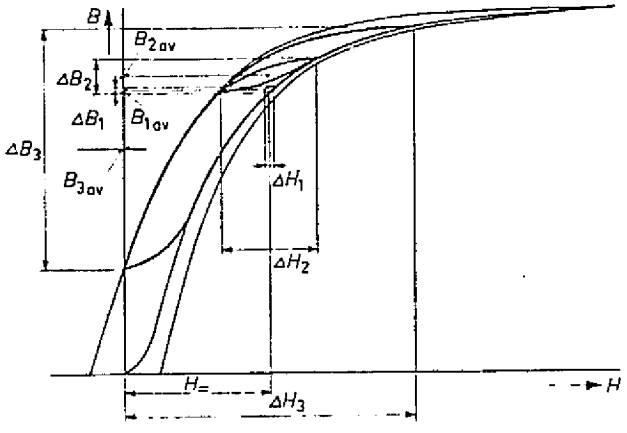

(a)

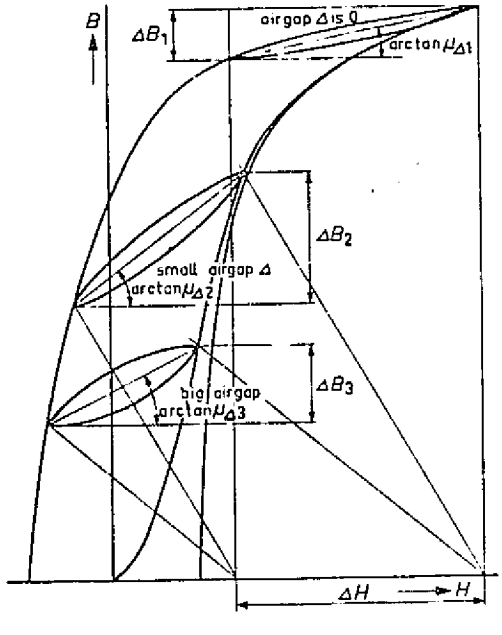

(b)

Figure 2-1. Influence of superimposed alternating field strength on value of mean induction.

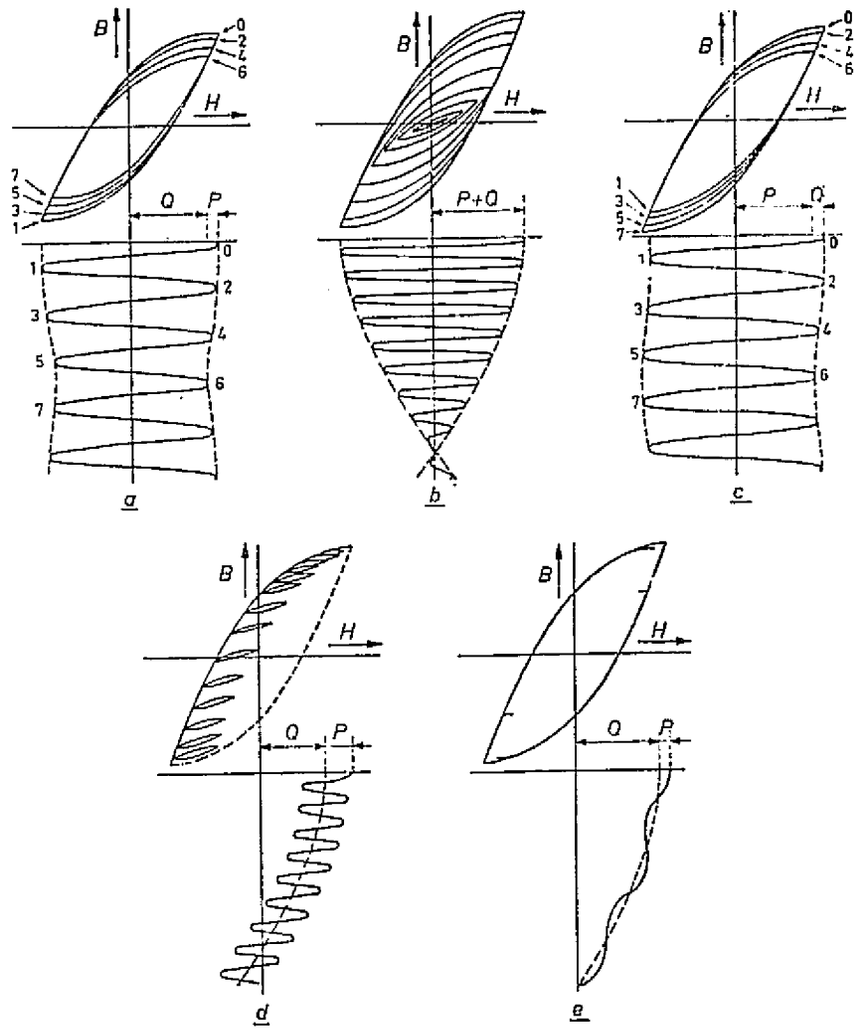

Figure 2-2. Examples of hysteresis loops with the field strength of two components of different frequency and different amplitudes.

It is assumed the small interior loop is 5% of the complete loop, also that the keeper is made of laminated Metglas 2605 whose bulk loss characteristics are shown in Table 2-3. The loss in the suspension keeper is then:

$$\text{Loss (Watts)} = \frac{W}{2.2} \left(\frac{B_1}{B_0}\right)^{1.6} \left(\frac{f_1}{f_0}\right)^{1.4} \frac{t_1/p_1}{t_2/p_2} \times 0.1$$

The keeper weight is $0.290 \times 1.32 \times 26\pi \times 2 \times 0.20 = 12.5$ lbs. The lamination thickness is 0.002 in.

$$\text{Loss (W)} = \frac{12.5}{2.2} \left(\frac{250^*}{1000}\right)^{1.6} \left(\frac{4.1}{1.0}\right)^{1.4} \times 1 \times 0.1$$

$$= 0.44 \text{ watt.}$$

The loss in the soft iron EM cores will be much less due to the low duty factor and the lower frequencies of induction due to coil current modulation.

The above loss dominates all magnetic losses from causes in Paragraphs A.1 through A.3 in the no load wheel condition. The uncertainty in the estimate must be emphasized.

4. Other Effects

The suspension servo loop must deal with earth rotation, seismic noise, sensor noise, and unbalance motor forces. However, the last named loss determinant does not apply to m-g configuration 2A-1, which does not produce cross-talk forces affecting the suspension system.

The effects of the remaining loss determinants are small. The first is determinable; the others could be specified for the design and evaluated in a simulation of the suspension system to determine power requirements. However, this analysis is beyond the scope of the study.

For preliminary design, it is assumed that in steady-state operation, a 5% gap field modulation at a once-around rate is required to counter the inertial forces and sensor noise. The loss calculated, as before, is then approximately 0.44 watt. The electromagnetic power losses must also be accounted for.

*5% modulation.

TABLE 2-3. SOFT MAGNETIC METALS FOR ENERGY WHEEL BEARINGS

Material (2 Mils Thick)	Watts/KG Hysteresis and Eddy Current Loss at Frequency and Induction Noted		
	60 Hz 13,000 Gauss	10^3 Hz 1000 Gauss	10^4 Hz 1000 Gauss
50% Silicon Iron	1.5	0.26	7.0
50% Nickel Iron	0.77	0.22	5.5
2605 Metglas*	0.53	0.10	2.9

*The resistivity is 125 μohm cm.

In general, at the higher frequencies, METGLAS 2605 losses vary from those shown as:

$$\left(\frac{B_1}{B_0}\right)^{1.6} \cdot \left(\frac{f_1}{f_0}\right)^{1.4} \cdot \left(\frac{t_1/\rho_0}{t_0/\rho_0}\right)$$

where B is the magnetic induction, f is the frequency, and t and ρ the thickness and resistivity, respectively.

The EM assemblies have 473 turns of No. 26 AWG copper wire. The length of the coils is 477 x 19/12 x 32 = 24168 ft; for No. 26, R = 41.6 ohms/1000 ft.

$$R_{total} = 41.6 \times 24.2 = 1006 \text{ ohms}$$

Assume 5% of full current or 0.15 ampere:

$$\text{Average } I^2R = (0.15 \times 0.707)^2 \times 1006 = 11.31 \text{ watts.}$$

Hence, in the idling condition, the wheel suspension system loss is: 0.88 + 11.31 = 12.2 watts.

5. Motor-Generator Losses

The motor-generator is a 3-phase, delta-connected, electronically commutated configuration with an ironless armature. In the coast phase, the motor-generator losses should be approximately zero, because the fixed field (which is part of the wheel) is not acting on any fixed-stator soft magnetic material.

There is a question, however, of possible eddy-current losses in the armature windings. These losses are ignored in conventional motor design, but ought to be considered in an energy wheel system sensitive to 'friction' while in the coast condition. An upper bound estimate of losses made in Technical Note 2-1 'Upper Bound Eddy Current Losses'* is 74 watts. A reasonable assumption is 10% of this value or 7.4 watts, approximately.

The remaining motor-generator losses have been determined in Appendix C. A summary appears in Table 2-4.

These losses are based on a 28-pole, 11,000-rpm motor-generator. The design wheel speed was later changed to 17,000 rpm and the number of motor-generator poles reduced proportionately to maintain commutation switching speeds. Accordingly, eddy-current and hysteresis losses will remain, to a first approximation, the same as do the armature and field currents. However, the number of field coils is reduced. Therefore, the I^2R losses are reduced by the pole ratio or 18/28. Table 2-5 lists the revised losses. The armature eddy-current loss is accounted for also.

6. Power Conditioning Losses

Efficiency calculations for both variable-voltage and constant-voltage motor-generators are displayed in Figures 2-3 and 2-4. It can be seen that efficiencies hold up quite well down to a 40 to 50% load, but fall off quite rapidly below that level.

This behavior can be explained quite simply. There are, in essence, three categories of loss in power conversion equipment, as follows:

(1) I^2R Loss - A loss component proportional to the square of the rms current in transformer and reactor windings, in busses and connections, and to an approximation, in a portion of the conducting drop of semiconductor devices.

(2) A loss component directly proportional to current, mainly in the switching losses of semiconductor devices and losses due to voltage transient protection therefor. These losses are also, in general, a function of voltage level and switching rate (operating frequency). Also, a portion of semiconductor conducting loss is, to an approximation, directly proportional to current level.

(3) "Constant losses", mainly from two factors - the excitation losses of magnetic components (transformers and reactors) and the losses of R-C "snubbers" used to control dV/dt and transient voltage phenomena as applied to semiconductor devices. These latter are also, in general, dependent on voltage level and switching rate.

*Found at the end of this Section.

TABLE 2-4. MOTOR GENERATOR LOSSES (WATTS) (11,000 RPM RATED SPEED, 28 POLES)

	Charge From 50% to 100% rated speed in 8 hours	Coast Zero Input & Output Power for 6 hours	Low Power Intermittent Op. at 10% rated power to 60% Rated Speed in 9 hrs.	High Power 15 kW (rated power) During last hour down to 50% Speed
2. M/G 1				
- Stator				
I^2R	0.15	-	.30 - .83	77.8 - 120.80
Eddy Current	12.5 - 33.0	33.0	33.0 - 16.20	16.20 - 12.55
Hysterisis				
- Rotor				
EddyCurrent				
Hysterisis				
Total Losses:	12.7 - 33.2	33.0	33.3 - 17.0	94.0 - 133.4
2. M/G 2A-2				
- Stator				
I^2R	.25	—	.5 - 1.4	135.2 - 194.7
Eddy Current	—	—	—	—
Hysterisis				
- Rotor				
Eddy Current	—	—	—	—
Hysterisis				
Total Losses:	0.3	—	0.5 - 1.4	135.2 - 194.7
2. M/G 3				
- Stator				
I^2R	0.5	—	2.1	233.8
Eddy Current	—	—	—	—
Hysterisis				
- Rotor				
Eddy Current	12.3 - 22.9	22.9	22.9 - 6.2	6.2 - 12.30
Hysterisis			200.0 - 64.3	64.3 - 200
Total Losses:	12.8 - 23.4	22.9	225.0 - 72.6	304.3 - 446.1
2. M/G 4				
- Stator				
I^2R	1.0	—	4.4	451.0
Eddy Current	—	—	—	—
Hysterisis				
- Rotor				
Eddy Current	12.3 - 22.9	22.9	22.9 - 6.2	6.2 - 12.30
Hysterisis			200 - 64.3	64.3 - 200.0
Total Losses:	13.3 - 23.9	22.9	227.3 - 74.9	521.2 - 663.3

Note: Eddy current armature wire losses not included.

TABLE 2-5. MOTOR-GENERATOR LOSSES (WATTS)
(17,000 RPM RATED SPEED, 18 POLES)

	Charge From 50% to 100% rated speed in 8 hours	Coast Zero Input & Output Power for 6 hours	Low Power Intermittent Op. at 10% rated power to 60% Rated Speed in 9 hours	High Power 15 kW (rated power) During last hour down to 50% Speed
2. M/G 1				
- Stator				
I^2R	0.10		0.19 - 0.53	50 - 77.7
Eddy Current	12.5 - 33.0	33.0	33 - 16.2	16.2 - 12.5
Hysteresis				
- Rotor				
Eddy Current				
Hysteresis				
Total Losses:	12.6 - 33.1	33.0	33.2 - 16.7	66.2 - 90.2
2. M/G 2A-1				
- Stator				
I^2R	0.16		0.32 - .90	86.9 - 125.2
Eddy Current				
Hysteresis				
Eddy Current (Armature)	3.8 - 7.5	7.5	7.5 - 4.5	4.5 - 3.8
Total Losses	4.0 - 7.7	7.5	7.8 - 5.4	91.4 - 129.10
2. M/G 3				
- Stator				
I^2R	0.32		1.35	150.3
Eddy Current				
Hysteresis				
Rotor				
Eddy Current				
Hysteresis	12.3 - 22.9	22.9	22.9 - 6.2	6.2 - 12.3
- Field Coil			200.0 - 64.3	64.3 - 200.0
Total Losses	12.6 - 23.2	22.9	223.3 - 71.9	220.8 - 362.6
2. M/G 4				
- Stator				
I^2R	0.67		2.8	289.9
Eddy Current				
Hysteresis				
- Rotor				
Eddy Current				
Hysteresis	12.3 - 22.9	22.9	22.9 - 6.2	6.2 - 12.30
- Field Coil			200 - 64.3	64.3 - 200.0
Total Losses:	13.0 - 23.6	22.9	225.7 - 73.3	350.4 - 302.2

*This armature eddy current loss estimate is included only in the motor generator finally chosen (2A-1).

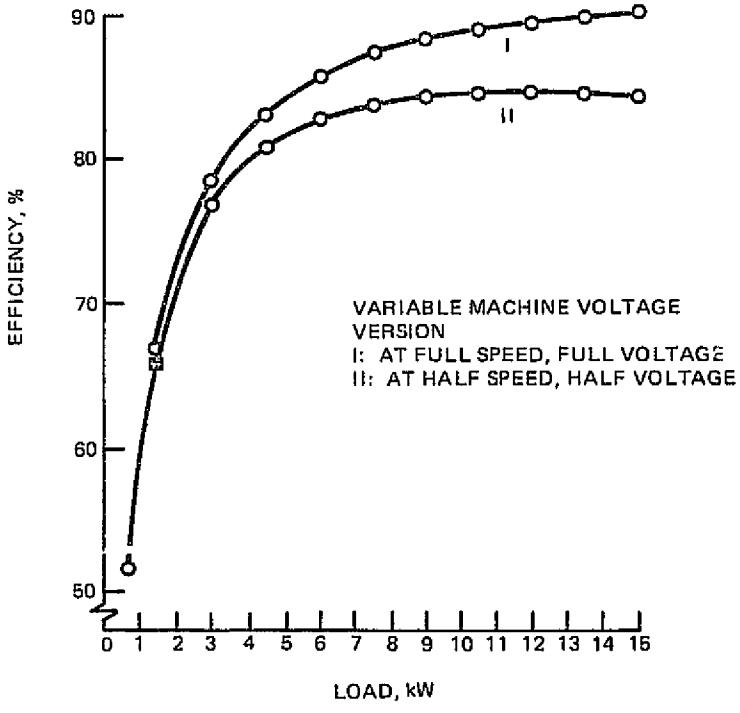

Figure 2-3. Efficiency vs. loading for power conversion equipment - Flywheel Energy Storage application, variable voltage.

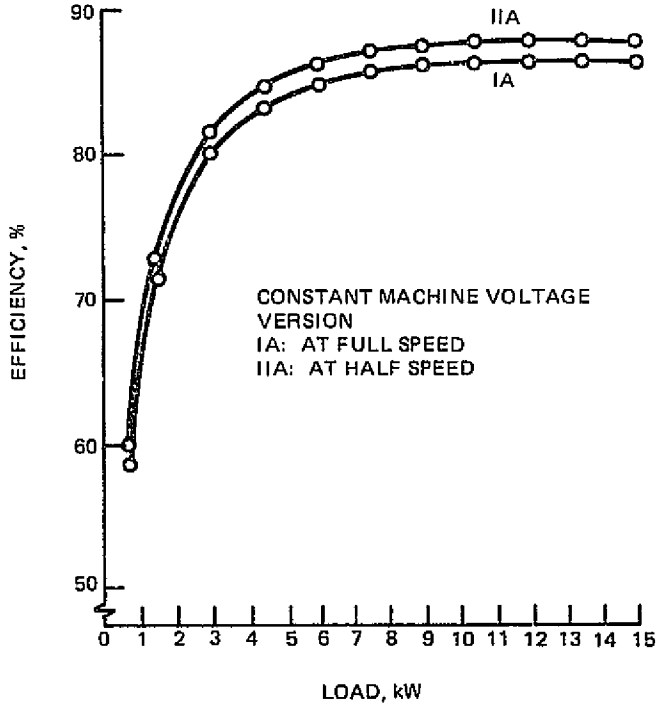

Figure 2-4. Efficiency vs. loading for power conversion equipment - Flywheel Energy Storage application, constant voltage.

The "constant" loss contributions are, obviously, responsible for the drastic reductions in efficiency at light loads. Since there is very little that can be done to reduce these losses in equipment designed for a given power level, there is little prospect of improving the light-load efficiency to any significant degree.

Observing the curves for a variable voltage (fixed field) machine, the reduction in I^2R and I-proportional losses at full voltage, full speed (and hence half current) more than offsets the increases in voltage-dependent, switching-rate-dependent losses that occur as compared to the half voltage, half speed, and full rated current condition. Comparing to the curves for a constant voltage (controlled field) machine, the increase in frequency-dependent losses there causes a reduction in efficiency as machine speed increases, the current being essentially constant at any given load level.

The efficiencies for a constant-voltage machine lie between those for variable voltage operation - while not so good as for the high voltage (curve I) condition, they are better than is obtained at low voltage (curve II).

The curves indicate that good efficiency over a very wide load range could be obtained by using two converters, one rated at about 75% and the other at about 25% of system requirements, and operating with an appropriate strategy. This approach is, in general, going to add considerably to the cost of the equipment; however, energy costs may be high enough to justify its adoption.

Of the system components, the major loss contributors are the input transformer, which is also responsible for much of the "constant" loss contribution, and the high-frequency self-commutated (transistorized) machine converter. While the biggest single factor in that element's losses is transistor conduction loss, transistor switching loss, transient overvoltage protection loss, and dV/dt control loss combined make up an equally important contribution. The 60-Hz converter and dc reactor losses are, by comparison, relatively minor contributors.

Some improvements in efficiency could be made, then, by reducing the frequency of the machine's generated voltages and/or improved switching transistor characteristics (in all respects - saturation voltage, rise and fall times, and switching voltage capabilities). However, the input transformer contributes 1/3 to 1/2 of all loss, and thus dramatic improvements in efficiency are unlikely unless a transformerless scheme is adopted. The hazards of such an approach make it seem unlikely that it would be acceptable.

Some key electrical design parameters of the conversion equipment are as follows:

- Machine Frequency - 1283 to 2567 Hz
- Machine Voltage (Variable) - 131 to 263 V rms (line-to-line)

- Machine Voltage (Fixed) - 131 V rms (line-to-line)
- DC Link Voltage (Variable) - 170 to 340 V
- DC Voltage (Fixed) - 170 V
- Average dc Link Current (Variable) - 52 to 104 A
- Average dc Link Current (Fixed)- 104 A
- Transistor Peak Current Assuming 0.75 pF Machine Loading On Converter - 145 A Max.
- Transistor Conduction Angle - 138.6 Degrees
- Transistor Switching Current, Peak - 96 A Max.
- Diode Conduction Angle - 41.4 Degrees
- Transistor Average Current - 40.4 A Max.
- Diode Average Current - 5.8 A Max.
- DC Link Capacitor (Variable Voltage Version) - 6000 μF
- DC Link Capacitor (Fixed Voltage Version) - 33,000 μF
- DC Link Reactor (Variable Voltage Version) - 2.28 mH @ 104 A to 39 mH @ 6 A
- DC Link Reactor (Fixed Voltage Version) - 0.4 mH @ 104 A to 3.6 mH @ 12 A (Swinging chokes are necessary)
- Transistor and Diode Voltage Ratings:

  Variable Voltage Version - 600 V

  Fixed Voltage Version - 400 V
- 60-Hz Converter Line Voltage:

  Variable Voltage Version - 344 V

  Fixed Voltage Version - 175 V
- Thyristor Average Current - 35 A Max.
- Thyristor Peak Current - 105 A Max.
- Thyristor Conduction Angle - 120 Degrees
- Thyristor Voltage Ratings:

  Variable Voltage Version - 1200 V

  Fixed Voltage Version - 800 V
- Input Transformer kVA Ratings (nearest standard)

  Variable Voltage Version - 50 kVA

  Fixed Voltage Version - 25 kVA

7. System Efficiency

System efficiency is defined for a 24-hour cycle. The ratio of energy extracted to that supplied, for the 24-hour cycle, should be greater than 60%. The primary losses in the energy wheel system are caused by the magnetic suspension, the motor generator, and the power converter.

Table 2-6 contains a summary of the losses for motor-generator 2A-1 and the suspension. These values are used in this determination of system efficiency.

TABLE 2-6. POWER LOSS SUMMARY; M-G 2A-1 AND SUSPENSION

	Charge From 50% to 100% rated Speed in 8 hours	Coast Zero Input & Output Power for 6 hours	Low Power Intermittent Op. at 10% rated power to 60% Rated Speed in 9 hours	High Power 15 kW (rated) power) During last hour down to 50% Speed
1. Suspension				
- Electromagnets				
I^2R	11.31	11.31	11.31	11.31
Eddy Current	—	—	—	—
Hysterisis				
- Keepers				
Eddy Current / Hysterisis	0.44 - 0.88	0.88	0.88 - 0.54	0.54 - 0.44
- Sensor & Electronics	6.0	6.0	6.0	6.0
Subtotal	18.0	18.0	18.0	18.0
2. M/G				
- Stator				
I^2R	0.16	—	0.32 - 0.90	86.9 - 125.2
Eddy Current (Armature)	3.8 - 7.5	7.5	7.5 - 4.5	4.5 - 3.8
Hysterisis	—	—	—	—
- Rotor				
Eddy Current / Hysterisis	—	—	—	—
Subtotal	4.0 - 7.7	7.5	7.5 - 5.4	9[illegible] - 129.10
Total	22.0 - 25.7	25.5	25.5 - 23.4	109.4 - 147.1

a. Spin-Up - 8 Hours

The average power is approximately $\frac{0.625 + 1.25}{2}$ or 0.9375 kW

Average power loss is approximately (4.0 + [0.70 x 3.7]) + 18 = 24.6 W

Power converter efficiency ≅ 55%

Input energy = $\frac{(937.5 + 24.6)}{0.55}$ x8 = 14.08 W-hr

Efficiency = 1 - $\frac{14.008 - 7.5}{14.008}$ = 0.54 or 54%

This is clearly unacceptable. The low efficiency of the power converter at low loads is the cause. The alternative is to charge the wheel at full load.

Average loss = (91.4 + [0.7 x 37.6]) + 18 = 136 W

Power Converter efficiency ≅ 0.90

Power to wheel = 15 + 0.136 = 15.136 kW

Charge time = $\frac{7.5}{15.136}$ ≅ 0.50 hr

Utility power input = $\frac{15.136}{0.90}$ = 16.817 kW

Utility energy input = 8.4087 kW-hrs

Efficiency = 1 - $\frac{8.409 - 7.500}{8.40}$ = 0.89 or 89%.

Clearly this method of charging is preferred.

b. Remaining Phases

The remaining phases are treated in like manner. The results are shown in Table 2-7.

From Table 2-7 and this spin up analysis, the combined losses are 3.218 kW-hr. per 24 hr cycle. The system round trip efficiency is

$$1 - \frac{3.218}{8.408} = 0.62 \text{ or } 62\%.$$

It is important to note that the low efficiency is due almost entirely to the power converter. The wheel round trip efficiency alone is approximately 97%.

TABLE 2-7. OPERATIONAL PHASE EFFICIENCY

	Coast	Intermittent Load	Full Load
Actual time (hr)	8	2.50	0.066
Losses - In. wheel (kW-hr)	0.153	0.050	0.009
Wheel Energy (kW-hr)			
Start of period	10.000	9.847	3.600
End of period	9.847	3.600	2.500
Loss-Power Conversion (kW-hr)			
(70% Efficiency)		1.987	
(90% Efficiency)			0.11
Efficiency	98.47%	68.20%	89.10%

C. TECHNICAL NOTE 2-1.

Upper Bound Edge Current Losses

Upper Bound Eddy Current Losses

Introduction:

Eddy current losses in the motor windings may be appreciable due to the relatively high surface speed of this design.

Therefore, a study was made to calculate upper bounds for this loss and to see how it varies parametrically.

These upper bounds result in large power dissipation even when small diameter wires are paralleled to produce the required current carrying cross sectional area.

A more rigorous analysis based on a three dimensional field approach utilizing Maxwell's equations is needed as well as test data.

The motor windings experience flux reversals as the rotor pulses move past them. Each conductor in the coil experiences a flux gradient across its cross-section, causing eddy currents.

Two cases have been studied; the field changes step wise and ramp wise.

In Fig. 1, the magnetic field moves from left to right across the conductor of length 1 with side dimensions of x_1. A square cross sectional wire was chosen for convenience in analysis. The induced voltage between the ends of the shaded portion of the wire is

$$e = Bl\nu \qquad (1)$$

This portion of the wire has a resistance

$$R_1 = \frac{\rho \ell}{x_1 x} \tag{2}$$

The remaining portion of the wire has a resistance

$$R_2 = \frac{\rho \ell}{x_1 (x_1 - x)} \tag{3}$$

$$R_1 + R_2 = \frac{\rho \ell}{x (x_1 - x)} \tag{4}$$

From the equivalent circuit of Fig. 1, the power is

$$P = \frac{\mathcal{E}^2}{R} = \frac{B^2 \ell^2 v^2 x (x_1 - x)}{\rho \ell} \tag{5}$$

The resistance approaches zero as $x \to 0$ and $x \to x_1$.

Utilizing Eq. (5) and the relation

$$x = vt \qquad x = 0, t = 0 \tag{6}$$

$$P = \frac{B^2 \ell}{\rho} v^3 (x_1 - vt) t \tag{7}$$

Eq. (7) can be integrated to find the energy dissipation for a complete unidirectional traversal.

$$E = \int_0^{t_1} P\,dt = \frac{B^2 \ell n^3}{\rho}\left[x_1 \int_0^{\frac{x_1}{n}} t_c\,it - n\int_0^{\frac{x_1}{n}} t^2\,dt\right] \qquad (8)$$

$$E = \frac{B^2 \ell n x_1^3}{6\rho} \qquad \text{watt-sec. per conductor} \qquad (9)$$

For a given current carrying capacity the motor winding will have a cross-sectional area, A.

$$\text{then} \qquad A = N x_1^2 \qquad (10)$$

where N is the number of parallel conductors. Substituting into Eq. (9) from Table 1 (MKS units)

$$E = \frac{B^2 \ell n A^{3/2}}{6\rho N^{3/2}} \qquad \text{watt-sec per conductor} \qquad (11)$$

$$E = \frac{B^2 \ell n A^{3/2}}{6\rho \sqrt{N}} \qquad \text{watt-sec for N parallel conductors}$$

E = .3082 watt sec. ONE #10 wire (12)

E = .01517 watt-sec. 413 #36 WIRES

The energy per event given by Eqs. (12) and (13) must be converted to an average power.

E = energy per event

4 = events per coil per pole

(each coil has 2 sides; each pole, 2 edges)

P = 18 poles per resolution

S = 283.3 revolutions per sec.

n = 54 coils

Then $P_{Av} = 2E_o PS n$ (14)

Pav_1 = 339,600 watts 1 - #10 wire

Pav_2 = 16,711 watts 413 - #36 wires

These eddy current losses are excessive and, therefore, another more realistic upper bound model must be constructed. The obvious change is to introduce a more realistic spatial flux function; i.e., replace the step with a ramp.

Fig. 2 shows the geometry for a ramp function. It is assumed that the gradient is small enough that the end effects (conductor just leaving or entering the field) can be neglected. A gradient is developed as shown in Fig. 2. The dc component of the field, common to all elements of the conductor, can be neglected.

All elemental conductors are assumed terminated in a perfect conductor at each end. Therefore, a terminal voltage, E, will exist due to all the elemental conductors.

The induced voltage in an element at x is: (see Table 1 for symbols)

$$e = Blv \qquad (1)$$

$$B = \frac{B_m (x_1 - x)}{x_f} \qquad 0 \le x \le x_1 \qquad (15)$$

then

$$R = \frac{\rho \ell}{x_1 \, \ell_y} \tag{16}$$

and

$$di = \frac{\mathcal{E}-E}{R} = \frac{\frac{B_m (x_1 - x)}{x_f} \ell v - E}{\frac{\rho \ell}{x_1 \, \ell_y}} \tag{17}$$

The total current must be zero:

$$I = \int_0^{x_1} di = 0 \tag{18}$$

From Eq. 17 and 18 ;

$$E = \frac{B_m \ell v \, x_1}{2 x_f} \tag{19}$$

The voltage across each elemental conductor is (substituting from Eq. 19 and 17)

$$(\mathcal{E} - E) = \frac{B_m}{x_f}(x_1 - x)\ell v - \frac{B_m \ell v x_1}{2 x_f} \tag{20}$$

$$(\mathcal{E} - E) = \frac{B_m \ell v}{x_f}\left(\frac{x_1}{2} - x\right) \tag{21}$$

The power dissipated in each element is

$$dP = \frac{(\mathcal{E}-E)^2}{\frac{\rho \ell}{x_1 \, \ell_y}} \tag{22}$$

$$dP = \frac{B_m^2 \ell^2 v^2 x_1}{x_f^2 \rho \ell}\left(\frac{x_1^2}{4} - x_1 x + x^2\right) dx \tag{23}$$

Integrating from $x = 0$ to $x_1 = x_1$

$$P = \frac{B_m^2 \ell v^2 x_1^4}{12 x_c^2 \rho} \quad \text{watts per conductor} \tag{24}$$

For a given total conductor cross sectional area, A,

$$A = N x_1^2 \tag{25}$$

Substituting from Eq.(25)into Eq. (24)

$$P = \frac{B_m^2 \ell v^2 A^2}{12 x_c^2 \rho N^2} \quad \text{watts per conductor} \tag{26}$$

For N parallel conductors,

$$P = \frac{B_m^2 \ell v^2 A^2}{12 x_c^2 \rho N} \quad \text{watts for } N \text{ parallel conductors} \tag{27}$$

Eq. (27) gives the eddy current power where the gradient is:

$$\frac{B_m}{x_c} \quad \frac{\text{tesla}}{\text{meter}}$$

Substituting values from Table 1 into Eq. (27) for 413 parallel #36 copper wires;

$$P = 2.639 \text{ watts} \tag{28}$$

This is the power dissipated while one side of the coil is traversing the field gradient.

As before, four of these events will occur per pole-coil combination. However, each event has a duty cycle of $\frac{x_c}{2\pi r}$

where r is the motor radius.

Therefore, the total average power is:

$$P_{av} = P \times 4 \times 18 \times 54 \times \frac{6.0127}{2\pi (0.217914)} \qquad (29)$$

[where $P = 2.639$ from Eq. (28)]

$$P_{av} = 74.22 \text{ watts}$$

The average power varies inversely with the gradient distance since, although χ_f^2 appears in the denominator of Eq. (27), the power is dissipated for a longer time (Eq. 29).

The eddy current power loss (74.22 watt) is excessive even though a rather gradual gradient (0.5 inch) was used in the calculation. Actual eddy current losses will be less for several reasons:

1. Increased resistance due to finite end resistance.
2. Increased resistance due to non-uniform current distribution.
3. Increased impedance due to inductive effects.

The upper bound losses are excessive such that a more rigorous analysis based on Maxwell's field equations is warranted.

Table 1

Motor Parameters for Eddy Current Loss Calculations

Symbol	Description	Units	Value
B	Flux density	Tesla	0.45
l	Conductor length in field	Meter	.0254
	Rotor speed	RPM	17,000
r_o	Rotor RADIUS	METER	0.2794
v	Rotor lineal speed	Meter/sec.	497.4
A	Cross sect. area #10 wire	Meter^2	5.261×10^{-5}
ρ	Resistivity, copper	Ohm-meter	1.67×10^{-8}
N	No. of equivalent parallel #36 wires	—	413
K_f	"Fringing distance" ZERO TO FULL FIELD	Meter	.0127

FIG 1

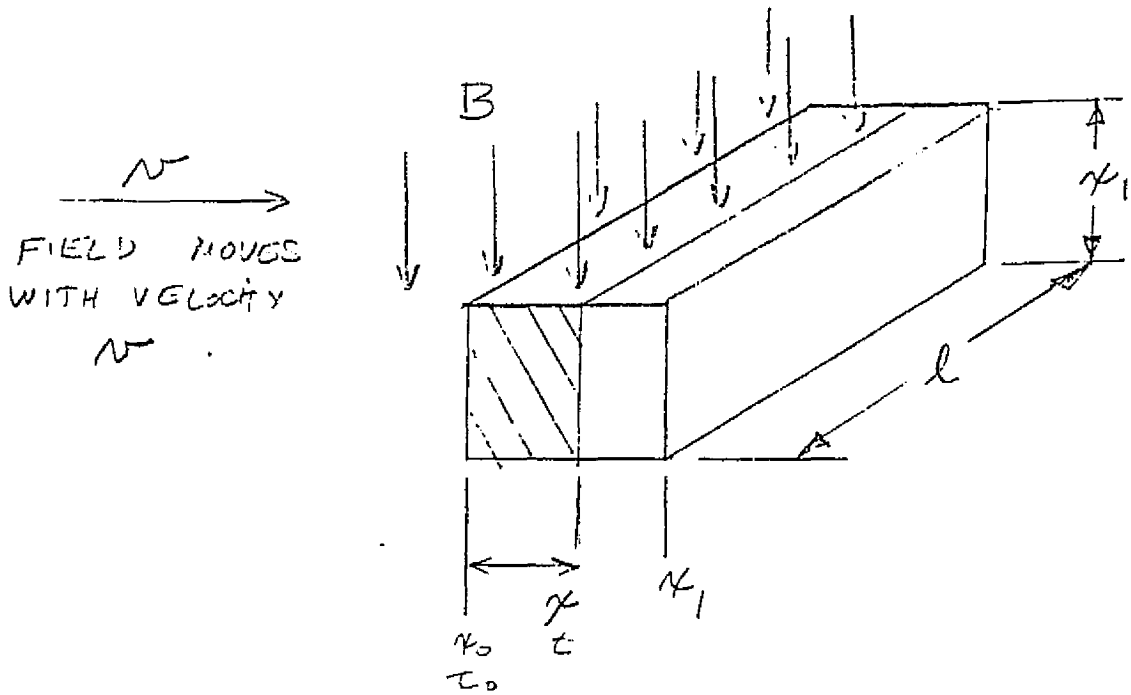

EQUIVALENT CIRCUIT

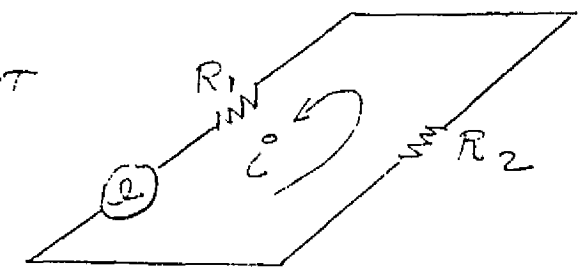

$R = R_1 + R_2$

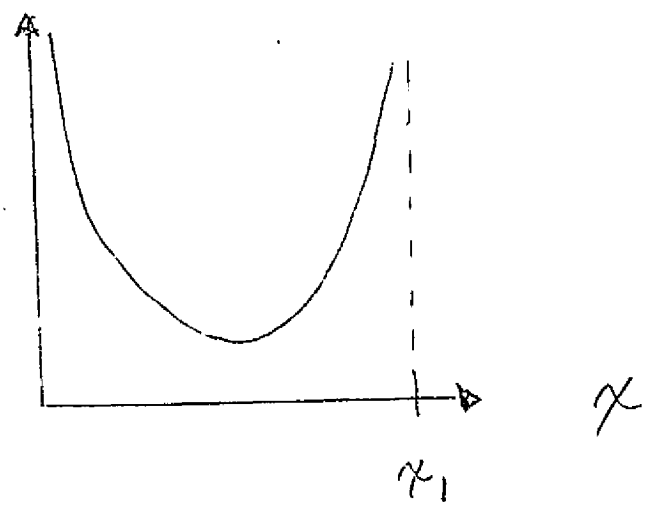

FIG 2

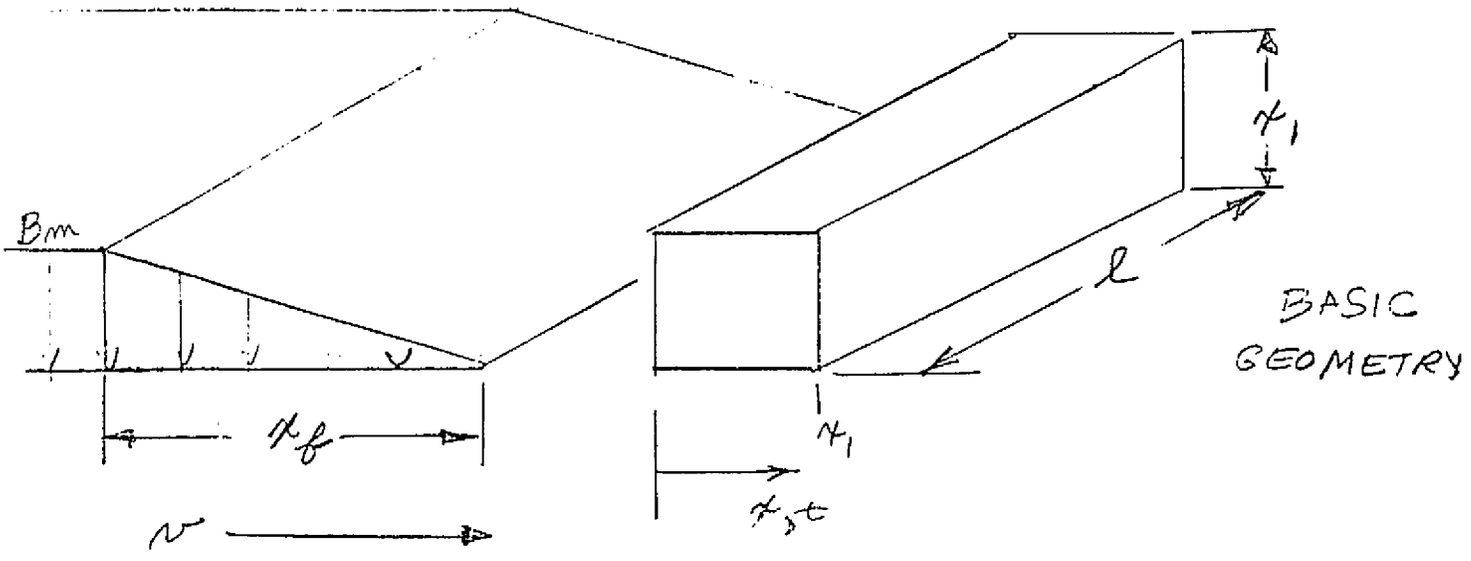

BASIC GEOMETRY

l ; INDUCED EDDY CURRENT VOLTAGE WHEN CONDUCTOR IS IN FRINGING AREA

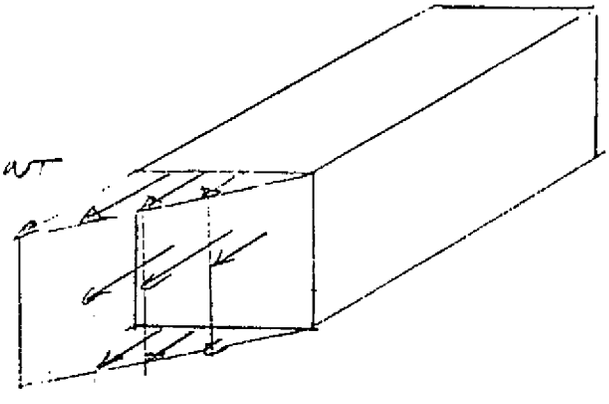

EQUIVALENT CIRCUIT

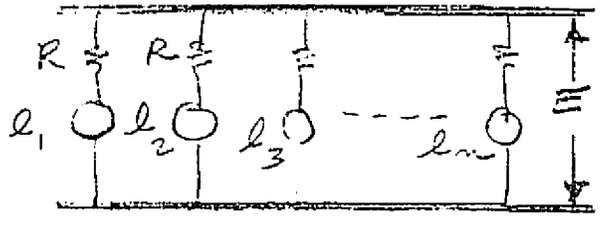

Section III

ENERGY STORAGE WHEELS AND COMPETITIVE STORES

Section III

ENERGY STORAGE WHEELS AND COMPETITIVE STORES

A. ENERGY WHEELS

Secondary energy storage is required in virtually all power systems because the energy supply and demand are rarely matched in time and power. The secondary store may be thought of as a buffer store. Figure 3-1 illustrates the use of an energy-wheel system for acceptance of energy from time varying prime energy sources and delivery to assumed loads.

The energy store requirements are established by system characteristics, including the energy to be stored, the rates at which (power) energy is to be stored or extracted, and the forms of the energy supplied to and delivered by the store. Energy wheels are one of an array of means for energy storage. Table 3-1 lists others. Of these, only batteries are used extensively as stores. Super-conducting magnets, hydraulic pumped storage, compressed gas storage, and fuel cells are under study for electrical utilities for power peaking. The choice in a particular power system depends on selection criteria that may differ between systems. Two excellent studies (References 5 and 6) report on the competitive aspects of some of these stores. In this study, the emphasis is placed on energy wheel systems design and cost optimization. The competitive position of wheel energy stores is treated in a peripheral fashion. However, it may be instructive to note the "domain" of the object of this study relative to other primary and secondary stores. In Figure 3-2, taken from Reference 7, the capability of advanced energy wheels has been inserted. It appears that the energy wheel is operationally competitive, particularly for high power density applications. The 'best' energy wheels, made of light, strong materials (such as the so-called engineering fibers like graphite, fiberglass, and the aramids) are potentially capable of storing more energy per pound than wheels made of traditional materials. In Table 3-2, a comparison is made of two wheels, identical except for the density of the materials. If the maximum allowable strength is the same for both, the lighter wheel is capable of storing more energy per unit mass by a factor equal to the mass ratio $m/\frac{m}{n}$ or n.

For materials with anisotropic physical strength properties, the comparison with isotropic structural materials is more difficult to draw, but in the main, it has been shown that the relationship still holds.

RCA
Government and
Commercial Systems

Energy Wheel Store

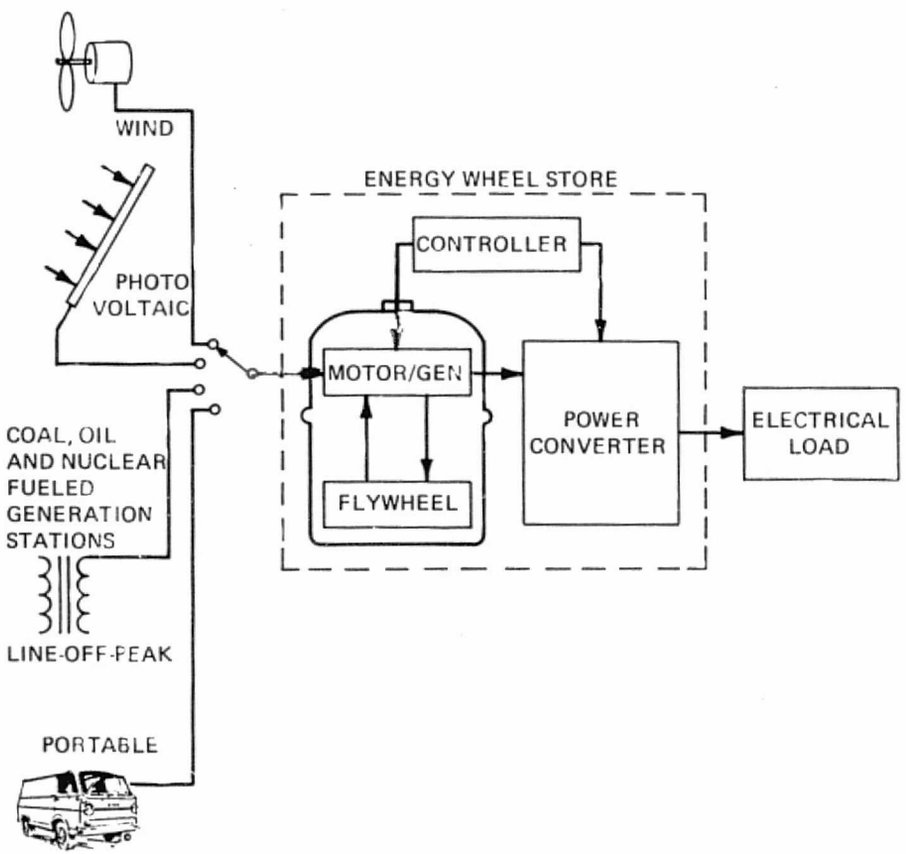

CIVIL
HOME
25–75 KW HR.
HOSPITAL
1500–3000 KW HR.
INDUSTRIAL PARK
1000–3000 KW HR.
SHOPPING MALL
3000–8000 KW HR.
GENERATION STATIONS
100 MW HR.
COMPUTER CENTERS

MILITARY
TACTICAL – PORTABLE
25–100 KW HR.
UNDERSEA TOOL AND LIGHTS
10–50 KW HR.
AIRCRAFT
1–5 KW HR.

SPACE
0.5–1.0 KW HR.

VEHICULAR
COMPACT CAR (100 MI)
30 KW HR.
INDUSTRIAL HANDLING
10 KW HR.
BUSES, VANS, ETC.
50–100 KW HR.

Figure 3-1. Energy wheel store.

TABLE 3-1. FORMS OF SECONDARY ENERGY STORAGE

	Available Energy	
	Btu/lb Material	Btu/ft^3 Material
Thermal Energy		
Heat of Fusion Only		
Lithium Hydride (1256°F)	1,250	63,900
Lithium Fluoride (1558°F)	450	73,000
Lithium Hydroxide (884°F)	378	33,700
Heat of Vaporization Only		
Steam Accumulator (3000 psia at 695°F)	1,115	67,500
Sensible Heat Only (2420-620°F)		
Boron	996	206,800
Lithium (liquid)	991	28,750
Magnesium Oxide	539	120,300
Silicon Carbide	524	105,000
Silicon Dioxide	511	74,000
Sensible Heat and Change of State		
Lithium Hydride (1300-800°F)	2,061	105,300
Lithium Fluoride (1900-800°F)	1,056	171,000
Lithium Hydroxide (1600-800°F)	1,057	94,100
Eutectic, 4/1 LiOH/LiF (1600-800°F)	1,033	98,250
Electrical Energy		
Batteries (for 15 h discharge)		
Lead-acid	46.4	6,960
Cadmium-Nickel	46.4	6,960
Silver-Cadmium	110	16,500
Silver-Zinc	110	16,500
Tape-Fed Battery	683	51,200[a]
Inductance		
Superconducting Solenoid[b]	419	1,636
Mechanical Energy[c]		
Compressed Solid (steel)	0.06	29
Compressed Liquid[d] (ether at 29,400 psia)	0.39	117
Compressed Gas[d] (air at 6,000 psia)	28.94	3,200
Flywheel	204.78	17,690

[a]Assumed storage density: 75 lb/ft^3

[b]125,000 gauss coil storing 1.08×10^{12} joules at 1.3×10^5 A/cm^2, volume of core included.

[c]Metal stressed at 100,000 psi in tension or 50,000 psi in shear.

[d]Includes weight of container.

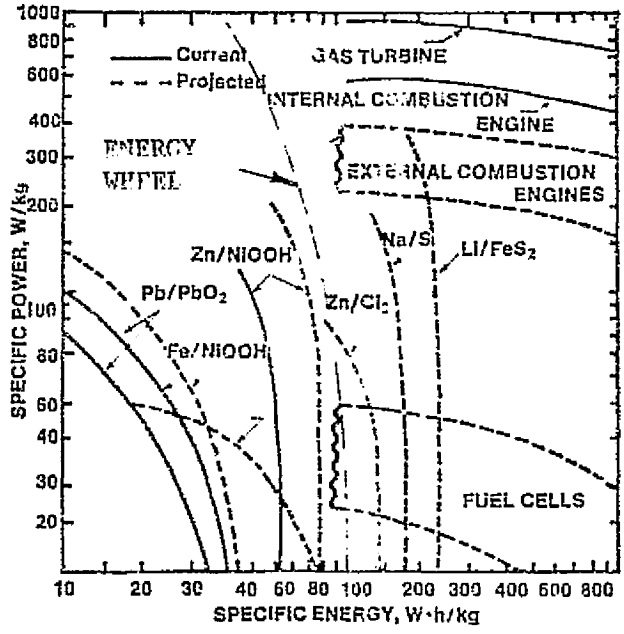

Fig. 3-2. Energy and power capabilities of various devices.

TABLE 3-2. COMPARISON OF TWO DIMENSIONALLY IDENTICAL WHEELS WITH DIFFERENT MATERIALS WITH THE SAME TENSILE WORKING STRESS

	Heavy Material	Light Material
Mass, m	m	$\frac{m}{n}$
Inertia, j	mk^2	$\frac{mk^2}{n}$
Speed, ω	ω	$\sqrt{n}\,\omega$
Stress, f_t	$cmk^2\omega^2$	$cmk^2\omega^2$ (by definition)
Momentum, $j\omega$	$mk^2\omega$	$\frac{mk^2}{n}\,\partial\sqrt{n}\omega$ or $\frac{mk^2\omega}{\sqrt{n}}$
Momentum/Mass	$k^2\omega$	$k^2\omega\sqrt{n}$
Energy, $1/2\, j\omega^2$	$1/2\, mk^2\omega^2$	$1/2\,\frac{mk^2}{n}\, n\omega^2$ or $1/2mk^2\omega^2$
Energy/Mass	$1/2k^2\omega^2$	$1/2nk^2\omega^2$

1. Geometric and Material Tradeoffs for Rim

It is necessary to consider the relationships among geometry, material, and speed that maximize the storage energy for a given system weight. The energy storage in a rotating body per unit weight can be expressed as:

$$E_W = K_W \left(\frac{\sigma_{max}}{\gamma} \right), \text{ (in.)} \tag{3-1}$$

and energy per unit volume as

$$E_V = K_V \left(\frac{\sigma_{max}}{\gamma} \right), \text{ (lb/in.}^2\text{)} \tag{3-2}$$

where

σ_{max} = working tensile strength, lb/in.^{2}

γ = weight density, lb/in.^{3}

K_W, K_V = dimensionless geometric factors

The factor (σ_{max}/γ) is also referred to as the specific strength of the material. (To obtain Wh/lb and Wh/in.^{3}, multiply Eqns. 3-1 and 3-2 by 3.14×10^{-5} Wh/in.-lb.)

Within the framework of Eqns. 3-1 and 3-2, the comparison of energy wheels is simplified by considering a materials factor and a shape factor, each of which can be discussed separately. For preliminary matters, this approach is very useful, but certain aspects of detail design blur the distinction somewhat, as will be shown later.

Historically, a handful of basic shapes practical for flywheel use have emerged. Figure 3-3 (from Reference 8) displays the character of K_W versus K_V for some of these practical shapes. At first glance, it would seem that the isotropic disc is the obvious choice over a filament wound shape, but the available material properties tell a different story. Table 3-3 gives representative values for a number of substances. Of the isotropic family, the solid, high-strength steel disc has the advantage, considering volume as well as weight. Of the filament, or laminated family, the Kevlar composite has the clear advantage for both cost and volume tradeoff.

If one compares energy storage for a high-strength steel wheel with that for the Kevlar wheel (at approximately 50% of the shape factor), it is discovered that, pound for pound, the Kevlar wheel will outperform the steel wheel by a factor of

TABLE 3-3. ENERGY WHEEL MATERIALS

Material	Density (ρ) (lb/in.^{3})	Poisson's Ratio (ν)	Ultimate Tensile (F_{tu}) ksi	Yield Tensile (F_{ty}) ksi	Working Stress (σ) ksi	Specific Strength σ/ρ ($x;10^6$)	Material Cost ($/lb)	Normalized Cost ($/lb)
1SN1-400 (Maraging Steel)	0.289	0.26	409	400	260	0.900	2.25	5.30
1SN1-300 (Maraging Steel)	0.289	0.30	307	300	200	0.062	2.25	6.89
4340 Steel	0.288	0.32	260	217	130	0.459	0.60	2.78
1040 Steel	0.288	0.30	87	58	36	0.127	0.30	5.00
1020 Steel	0.283	0.30	68	43	25	0.088	0.30	7.23
Cast Iron	0.280	0.30	55	37	20	0.071	0.30	8.94
2021-T81 (Aluminum)	0.103	0.33	62	52	26	0.252	0.53	4.45
2024-T851 (Aluminum)	0.100	0.33	66	58	35	0.350	0.50	3.03
6A1-4V (Titanium)	0.160	0.32	150	140	82	0.512	4.00	16.55
E-Glass	0.075	0.29	200	-	67	0.890	0.42	1.00
S-Glass	0.072	0.29	260	-	87	1.210	0.75	1.31
KEVLAR 49(1)	0.050	0.30	350	-	225	4.500	3.00(2)	1.42
Sitka Spruce	0.015		19	-	10	0.67	0.20	0.63
Graphite Fiber(1)	0.061			-	120	1.97	15.00	16.10
Graphite Whisker(3)	0.060		1500	-	1080	18.00	200.00	23.50
Boron Filament/ Aluminum	0.096			-	254	2.61	200.00	162.00
Music Wire	0.283		600		431	1.52		

(1) in epoxy composite (60% fiber by volume)
(2) projected - 1975-77
(3) in epoxy composite (70% fiber by volume)

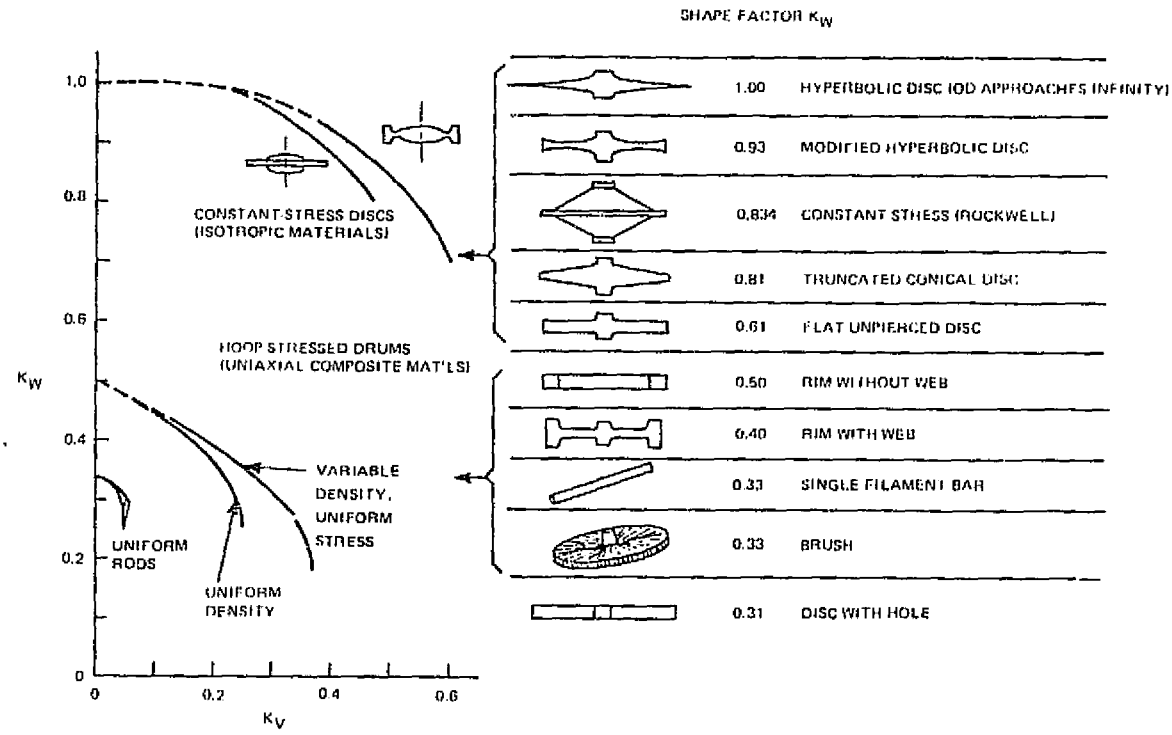

Figure 3-3. Relationship of weight efficiency factor, K_W, and volumetric efficiency factor, K_V, for high performance flywheel designs.

about 2:1. Volumetrically, of course, it is the steel wheel that has approximately a 2:1 advantage. On a materials cost basis, the Kevlar wheel will be less expensive in dollars per unit energy stored.

Table 3-3 (from Reference 8) shows a few projected values of energy density for certain storage configurations assumed to be stressed in their optimum configuration.

Of course, the preceding discussion only establishes a trend, based on inherent material and shape factors. Nothing has been said about manufacturing considerations, geometric compromises, system weight, safety, life cycle costs, and the like. Each of these additional factors tends to change the relative merit of a candidate system; trade-offs have been continually made during the design process.

Inherent in the definition of both shape and material factors is the assumption of theoretical uniformity. If the shape is manufactured with errors, or if the material properties vary, then the energy storage capacity will also change. It comes as no surprise that the performance of the wheel usually suffers, whatever the variation.

For utility system use, where life cycle cost is the overriding consideration, the specific energy on a weight basis is the controlling factor, rather than volumetric

efficiency. As the weight increases, the cost of material rises for the rim. At the same time, the size of the suspension increases as well as the energy to run the servos. All of this adds to system losses and, hence, life-cycle cost. The effect is so critical that the commonly accepted outlook for energy wheels for utility use is pessimistic. However, as in all matters, new developments can bring about a re-examination of the competitive position of this type of store.

2. Magnetically Supported Energy Wheel

If, as shown, the thin-rim, circumferentially wound wheel is the best form of store, practical considerations must be taken into account in the design of this type.

If a shaft is used, the spokes, web or other means to support the thin rim can only add weight, stress concentrations, and other effects that reduce the energy density.

If the rim is magnetically supported, the support can be at the rim, but design problems still remain. However, the use of magnetic bearings does appear to lead to the most efficient configuration for maximum energy density.

Nevertheless, it is not the object here to make final judgments. It is generally agreed that both types may find increasing use.

B. COMPETITIVE STORES

A detailed comparison with competitive stores has not been made for the application being considered because it is not feasible to do so in the limited time available.

Reference 5 contains a table on page 1-19 (Table 3-4) listing comparative data for nine stores sized for peak power application in electric utility systems. The findings of that study are that battery systems are the choice for the period 1985-2000.

However, all energy stores are uneconomical if used on the customers premises to satisfy the energy and power profile of this study. The total energy throughput per 24 hours is 5.19 kW-hr approximately. If it is assumed that the cost of off-peak charging electricity is $0.02 per kWh vs $0.05 per kW-hr for normal demand, the electricity cost saved for 24 hours is $0.03 x 5.19, or $0.154. Assuming a 21-year life for the energy store, the cost of electricity is $1180, which must be compared to the "cradle to grave" costs of the energy store.

TABLE 3-4. EXPECTED TECHNICAL AND COST CHARACTERISTICS OF SELECTED ENERGY STORAGE SYSTEMS

Characteristics	Near Term					Intermediate Term			Long Term
	Hydro Pumped Storage	Compressed Air	Thermal		Lead Acid Batteries	Advanced Batteries	Flywheel	Hydrogen Storage	Superconducting Magnetic
			Steam	Oil					
Commercial Availability	Present	Present	Before 1985	Before 1985	Before 1985	1985-2000	1985-2000	1985-2000	Post 2000
Economic Plant Size (MWh or MW)	200-2000 MW	200-2000 MW	50-200 MW	50-200 MW	20-50 MWh	20-50 MWh	10-50 MWh	20-50 MW	Greater than 10,000 MWh
Power Related Costs (a) ($/kWh)	90-160	100-210	150-250	150-250	70-80	60-70	65-75	500-860	50-60
Storage Related Costs (a) ($/kWh)	2-12	4-30	30-70	10-15	65-110	20-60	100-300	6-15	30-140(c)
Expected Life (Years)	50	20-25	25-30	25-30	5-10	10-20	20-25	10-25	20-30
Efficiency (d) (%)	70-75	(e)	65-75	65-75	60-75	70-80	70-85	40-50	70-85
Construction Lead Time (Years)	8-12	3-12	5-12(f)	5-12(f)	2-3	2-3	2-3	2-3	8-12

(a) Constant 1975 dollars; does not include cost of money during construction.
(b) Could be considerably higher.
(c) These numbers are very preliminary.
(d) Electric energy out to electric energy in, in percent.
(e) Heat rate of 4200-5500 Btu/kWh and compressed air pumping requirements from 0.58 to 0.80 kWh (out).
(f) Long lead time includes construction of main power plant.

Caveat - Data applies only to designs as considered in the study.

Section IV

COSTS

Section IV

COSTS

The objective of the study is to determine the lowest cost Mechanical Capacitor system that meets the performance requirements.

The cost of an energy system is the sum of the costs of the subsystems and the integration and test costs. Some of the costs are independent of scale, but sensor system costs (sensors, signal processing, etc.) and some other costs are not. Table 4-1 is an initial estimate of the effects of scale on component costs. All costs are subject also to the experience curve of production.

The baseline production for cost estimates was assumed to be 1,000 systems per year.

Costs were determined in two ways: bottom up and top down. The bottom up estimates are based on costs estimated by RCA, and by suppliers, for the year 1985, and takes into account the suppliers estimates of their 'learning experience' and projected markets for their products. The year 1985 is the estimated date for the first use of an operational Mechanical Capacitor. All dollars are on a 1977 base. The costs of materials are listed in Table 4-2 for 1977 and 1985. Using these costs, and motor-generator and PCU estimates from Inland Motors and Westinghouse Electric, the system costs are shown in Table 4-3.

The costs for the system, under the assumption of limited production (1000 per year or 83 per month approximately) is high. These costs do not include authorization of R&D, tooling, and other costs, taken into account in the top down estimate.

The top down estimates were generated through the use of PRICE - a cost modeling technique described in the Technical Note in Appendix H.

The comparable center cost (the estimated range is ±6% of center costs) for the Mechanical Capacitor system, drawn on the same basis as the bottom up estimate, is $22,134 (compared to the bottom up estimate of $18,950). The total cost, including authorization of development, production engineering, tooling, and test equipment is $30,217.

The total cost for 10,000 per year is $16,098 per system, which shows clearly the effect of the learning experience.

TABLE 4-1. COSTS VS. SCALE (PEAK ENERGY AND PEAK POWER)

	Material	Fabrication
Wheel	Kw_m X Pe	Kw_f X $(Pe)^{0.9}$
Suspension		
Electrical (power)	$Ksep_m$ X Pe	$Ksep_f$ X $(Pe)^{0.9}$
Electronics (info)	$Ksel_m$ X 1	$Ksel_f$ X 1
M/G	Kg_m X Pp	Kg_f X $(Pp)^{0.9}$
PCU	$Kpcu_m$ X Pp	$Kpcu_f$ X Pp
Vacuum Housing	Kv_m X Pe	Kv_f X $(Pe)^{0.9}$
Base	Kb_m X Pe	Kb_f X $(Pe)^{0.9}$
Vacuum Pump	Kup_m X Pe	----
Power Controls	Kc_m X $(Pe)^{0.9}$	Kc_f X $(Pe)^{0.9}$

K = Production cost of point design

Pe = Peak Energy ratio

Pp = Peak Power ratio

A PRICE computer printout for one subsystem and for the complete system are shown as Figure 4-1.

It can be seen from Table 4-3 that in the case of the system studied, the power conditioning costs dominate systems costs. The high speed of the motor-generator and the requirement that the system accept and deliver 3-phase electrical power, determines the PCU configuration and hence the costs.

TABLE 4-2. SOME PROJECTED COSTS OF PURCHASED MATERIALS

	1977	1985	Source
Kevlar 49	$8.5/lb	$4.5/lb*	DuPont
Honeycomb (Aircraft grade)	6.8/lb	6.8/lb	Hexcel
Graphite Fiber	35/lb	7.5/lb	Celanese
Resin	1/lb	1/lb	RCA
Elastomer	1.4/lb	1.4/lb	RCA
Electromagnet Cores	2/lb	2/lb	RCA
Samarium Cobalt Permanent Magnets	30/lb	30/lb	Strnat/Univ. of Dayton
Wire No. 26	31/1000 ft.	31/1000 ft.	Adelphi
Wire No. 16	96/1000 ft.	96/1000 ft.	Adelphi
Eddy Current Sensors	435/unit	200-350/ unit	Kaman
Drivers & Electronics	482/2 sets of servos	482/2 sets of servos	RCA (IR&D Project estimate)
Dynel (Engr. Plastic)	1.40/lb	1.40/lb	RCA
Fiberglas Mat and Polyester Resin.	0.50/lb	0.50/lb	RCA
Low Carbon Steel	0.20/lb	0.20/lb	Materials Selector
Vacuum Pump	$415/unit	$243/unit	Sergeant Welch

*Based on presently forecasted markets

TABLE 4-3. SYSTEM COST FOR 1,000 PER YEAR PRODUCTION

	Wt., lbs.	$ Mat.	$ Fab.	$ Assem.	$ Test
Rim					
Resin	39	39			
Graphite	12	434			
Kevlar	121	544			
Honeycomb	4	27	200		
Elastomer	1	2			
PMs	9	258			
Keepers (Soft Iron)	14	28			
	200	1332			
Suspension					
EMs	59	118	124		
PMs	3	75			
Sensors	6	1650	623		
Electronics	---	241			
(purchased)	68	2084			
Motor-Generator (purchased)	17	942 (less PMs)		1 man week @ $15./hr. $600.00	1/2 man week @ $15./hr. $300.00
Harness					
Wire, etc.	10	100	100		
Vacuum Housing					
Enclosure	200	100	200		
Pump (purchased)	20	243	---		
Base	100	100	200		
Housing	100	100	200		
PCU	20	11400			
	735	16401	1647	600	300

Costs = $18,950
Cost/wt - hr = $1.90

SUSPENSION SYSTEM, SERVO LOOPS

INPUT DATA

QTY	32000.	PROTOS	96.0	WT	2.230	VOL	0.007	MODE	1.
QTYSYS	32.	INTEGE	0.500	INTEGS	0.700	AMULTE	100.00%	AMULTM	100.00%

MECH/STRUCT

WS	2.130	MCPLXS	4.800	PRODS	0.000	NEWST	1.000	DESRPS	0.000

ELECTRONICS

USEVOL	0.498	MCPLXE	6.700	PRODE	0.000	NEWEL	1.000	DESRPE	0.000
PWR	1.000	CMPNTS	15.	CMPID	0.000	PWRFAC	0.000	CMPEFF	0.000

ENGINEERING

ENMTHS	6.0	ENM.HP	24.0	ENMTHT	48.0	ECMPLX	1.600	PRNF	0.000

PRODUCTION

PRMTHS	54.0	PRMTHF	70.0	LCURVE	0.850	ECNE	0.000	ECNS	0.000

GLOBAL

YEAR	1978.	ESC	0.00%	PROJCT	1.000	DATA	1.000	TLGTST	1.000
PLATFM	1.800	SYSTEM	1.000	PPROJ	1.000	PDATA	1.000	PTLGTS	1.00

PROGRAM COST	DEVELOPMENT	PRODUCTION	TOTAL COST
ENGINEERING			
DRAFTING	13.	0.	14.
DESIGN	53.	1.	54.
SYSTEMS	11.	0.	11.
PROJ MGMT	23.	85.	108.
DATA	6.	4.	11.
SUBTOTAL (ENG)	106.	90.	197.
MANUFACTURING			
PRODUCTION	0.	1122.	1122.
PROTOTYPE	76.	0.	76.
TOOL-TEST EQ	9.	737.	746.
SUBTOTAL (MFG)	85.	1859.	1944.
TOTAL COST	192.	1949.	2141.

VOL	0.007	AVCOST	0.04	TOTAL AV PROD COST		0.06	LCURVE	0.850	
WT	2.230	ECNE	0.082	ECNS	0.024	DESRPE	0.000	DESRPS	0.000

MECH/STRUCT

WS	2.130	WSCF	317.910	MECID	0.000	PRODS	2.921	MCPLXS	4.800

ELECTRONICS

WE	0.100	WECF	30.000	CMPID	0.000	PRODE	3.888	MCPLXE	6.700
PWR	1.000	CMPNTS	15.			PWRFAC	0.767	CMPEFF	19.238

SCHEDULES

ENMTHS	6.000	ENMTHP	24.000	ENMTHT	48.000	ECMPLX	1.600	PRNF	0.152
PRMTHS	54.000	PRMTHF	70.000	AVER. PROD RATE PER MONTH					2000.000

COST RANGES	DEVELOPMENT	PRODUCTION	TOTAL COST
FROM	170.	1628.	1798.
CENTER	192.	1949.	2141.
TO	231.	2613.	2844.

Figure 4-1. PRICE Computer Printout
(Sheet 1 of 2)

TOTAL COST, LESS INTEGRATION COST

PROGRAM COST	DEVELOPMENT	PRODUCTION	TOTAL COST
ENGINEERING			
DRAFTING	649.	3.	652.
DESIGN	2787.	7.	2794.
SYSTEMS	969.	0.	969.
PROJ MGMT	1297.	339.	1636.
DATA	549.	17.	566.
SUBTOTAL (ENG)	6251.	365.	6617.
MANUFACTURING			
PRODUCTION	0.	6267.	6267.
PROTOTYPE	956.	0.	956.
TOOL-TEST EQ	72.	1145.	1218.
PURCH ITEMS	68.	13570.	13638.
SUBTOTAL (MFG)	1097.	20982.	22079.
TOTAL COST	7348.	21348.	28696.

COST RANGES	DEVELOPMENT	PRODUCTION	TOTAL COST
FROM	6501.	20015.	26517.
CENTER	7348.	21348.	28696.
TO	8721.	23837.	32558.

TOTAL COST, WITH INTEGRATION COST

PROGRAM COST	DEVELOPMENT	PRODUCTION	TOTAL COST
ENGINEERING			
DRAFTING	680.	5.	685.
DESIGN	2930.	14.	2944.
SYSTEMS	1009.	0.	1009.
PROJ MGMT	1345.	390.	1736.
DATA	567.	19.	586.
SUBTOTAL (ENG)	6531.	429.	6960.
MANUFACTURING			
PRODUCTION	0.	7370.	7370.
PROTOTYPE	976.	0.	976.
TOOL-TEST EQ	78.	1194.	1272.
PURCH ITEMS	68.	13570.	13638.
SUBTOTAL (MFG)	1122.	22134.	23257.
TOTAL COST	7654.	22563.	30217.

COST RANGES	DEVELOPMENT	PRODUCTION	TOTAL COST
FROM	6772.	21018.	27790.
CENTER	7654.	22563.	30217.
TO	9080.	25400.	34480.

FUNCTION:

Figure 4-1. PRICE Computer Printout
(Sheet 2 of 2)

Section V

APPLICATIONS

Section V

APPLICATIONS

A. GENERAL

Although the application originally chosen falls short of a good 'fit' for energy wheels, there are others that will meet the requirements. Some effort was undertaken in the last month of the study to determine more attractive applications. This is a report of the findings.

The attractive features of magnetically supported energy wheels are:

Capability for high power density

Immunity to environment (wheel operates in closed vacuum system)

High system energy density

Absence of noise and effluents

Long life

Potential for low maintenance

Table 5-1 lists some possible applications and a feature check indicating wheel characteristics of value. It is seen that moving base applications capitalize on the energy wheel's strong points. The 'Economic' column indicates, without analytical verification, whether the application is believed to be an economic one. However, one application has been examined in more depth — the small energy-wheel electric car whose requirements are listed in the last line of Table 5-2. This application has energy and power requirements close to the point design of the study. Further, the power conditioning requirements are less restrictive.

It is assumed that the charger is not part of the vehicle, and that the energy wheel generator delivers power to a dc load (motors at the wheels).

The energy-wheel electric car competes with the battery-electric car, which it resembles in all respects except for the type of energy store.

If automobile industry production is postulated at, say, 1,000,000 small cars per year, the cost of the energy wheel system is as shown in Table 5-3 for production costs of 1,000 and 1,000,000 per year. In arriving at these costs, the weight of the off-wheel

TABLE 5-1. MECHANICAL CAPACITOR APPLICATIONS

	Economic		Application	Lt. Wt.	Environ. Immunity	No Noise, Effluent, Hazards	Long Life	Min. Maint.	High Power Density
	Y	N							
Fixed base									
		X	• Emergency Power Supply (P.S.) Supermarkets, Hospitals, etc.	-	-	-	-	-	-
		X	• Load Peaking for utilities	-	-	-	X	X	-
	X		• Mine equipment	-	X	X	X	X	X
	X		• Remote unattended windmills, solar thermal	-	X	-	X	X	X
	X		• Military remote Base Secondary P.S.	X	X	X	X	X	X
Moving base			Spacecraft						
	X		• Energy storage	X	X	X	X	X	X
	X		• Laser power	X	X	X	X	X	X
			Aircraft						
	X		• Landing gear	X	X	X	X	X	X
	X		• Laser Power	X	X	X	-	X	X
	X		• Emergency power	X	X	X	-	X	X/-
	X		• RPV prime power	X	X	X	-	X	X
			Land						
			• Materials handling						
		X	industrial	-	-	X	X	X	X
	X		military	X	X	X	X	X	X
	X		• Car, truck, bus, etc.	X	X	X	X	X	X
	X		• Subways	X	X	X	X	X	X
		?	• Trailered P.S.	X	X	X	X	X	X
	X		• Light army tank	X	X	X	X	X	X
		?	• Transportable Welders (peak power)	X	X	X	X	X	X
	X		• Earth movers	X	X	X	X	X	X
	X		• Draglines	-	X	X	X	X	X
			Sea						
	X		• Undersea vehicles	X	X	X	X	X	X
	X		• Power packs	X	X	X	X	X	X
	X		• Buoys (solar elec.)	-	X	X	X	X	X
	X		• Catapults	-	-	-	-	X	X
	X		• Lasers	X	X	X	X	-	X
		?	• Ferry boat	-	-	-	X	X	X
		?	• Harbor craft	-	-	-	X	X	X
		?	• Merchant ship Emergency power	-	-	-	X	X	X

TABLE 5-2. ENERGY STORAGE SYSTEM REQUIREMENTS

	Source/Load	Power, kw		Cycle Min./Hrs.	Life, Years	Energy Storage kW-Hrs.
		Max.	Avg.			
Residential	3ϕ, 110/220V to 1ϕ, 110/220V	15	0.31	-/24	6	7.5
Fork Lift	3ϕ, 110/220V to dc	10 to 20	2.8	-/3	20	7.5
Laser Pump	dc to dc	4,000 to 10,000		1/-	?	80
UPS	3ϕ, 110/200V to 3ϕ, 110/220V	1-7	?	*	20-40	small to 3.5
Small Car	3ϕ, 110/220V** to dc	21.4	3.5	-/24	21	16.2

*Time for charged condition is variable. Discharge time can vary from 10 seconds to 1/2 hr. typically.

**Power supply converter is not part of car.

subsystems has been reduced in recognition of the fact that this is a vehicle application. In arriving at the costs for 1,000,000 a year production rates, the procedure contained in References 9 and 10 has been used. An experience curve slope of 90% has been assumed (somewhat more conservative than the 85% slope assumed in the PRICE analysis).

B. COMPARISON OF SMALL CAR COSTS OF OWNERSHIP

The required performance for an electric car has been taken from Reference 7. Table 5-4 has been taken from the reference and the axle power requirements used. Acceleration has been set at 0 to 50 km/hr in 9 seconds rather than 10. Table 5-4 also lists candidate batteries for electric cars and the authors projected performance estimates. These data are for information only.

From Reference 11, the proposed battery goals for electric vehicles are as shown in Table 5-5. The comparable values for the Mechanical Capacitor have been added.

The estimated future costs of advanced batteries are listed also from Reference 5 for information.

TABLE 5-3. MECHANICAL CAPACITOR, SMALL CAR APPLICATION (1000 kg)

(System Cost for 1,000 & 1,000,000/yr. Production*)

	Wt., lbs.	$ Mat.	$ Fab.	$ Assem.	$ Test
Rim					
Resin	83	83			
Graphite	27	946			
Kevlar	259	1161			
Honeycomb	9	59	430		
Elastomer	4	6			
PMs	18	555			
Keeper	30	60			
	430	2870			
Suspension					
EMs	127	254	254		
PMs	5	150	10		
Sensors		1650			
Electronics	10	241	623		
M/G	37	2025			
Harness					
Wire, etc.	10	100	100		
	189	4420			
Vacuum Housing					
Enclosure	70	70	140		
Pump	5	50			
Mechanical Supports and Suspension	60	60	180		
	135	180			
PCU	20	1875			
Subtotals	774	9345	1737	600	300

1 man week @ $15./Hr. - $600.00

1/2 man week @ $15./Hr. - $300.00

For 1000 per year production
$\sum$ costs = $12,756.

Learning factor for 1,000,000 Production = 0.345, so system average cost = $4600
90% Learning Curve

*Not including wheel drive motor/generators.

TABLE 5-4. POWER AND BATTERY REQUIREMENTS FOR ELECTRIC VEHICLE

energy and power requirements
for urban electric vehicles

energy consumption*	
At Axle	0.10 to 0.12 kW-h/T-km
From Battery	0.14 to 0.17 kW-h/T-km
From Plug	0.18 to 0.23 kW-h/T-km
peak power required (0 to 50 km/h, ≤ 10s)	
At Axle	18 to 20 kW/T (Test wt)
From Battery	25 kW/T (Test wt)

average power required	at axle	from battery
urban driving (avg. 32 km/h)	3 to 3.5 kW/T	4 to 5 kW/T
50 km/h cruise	3 to 3.5 kW/T	4 to 5 kW/T

* These energy consumption figures correspond to urban driving profiles, such as the Federal Register driving profile, and represent an average speed of about 32 km/h.

specific energy and specific power
requirements for electric vehicle batteries
under urban driving conditions

battery weight, percent of vehicle test weight	specific energy W-h/kg (for 80 km range)	average specific power W/kg	peak specific power W/kg
20	55-68	20-25	125
25	44-54	16-20	100
30	37-45	13-17	85

candidate batteries for electric vehicle propulsion

			status			projection			
system	cell voltage	theor. W-h/kg	W-h/kg[a]	W/kg[b]	cycle[c] life	W-h/kg[a]	W/kg[b]	cycle[c] life	year[d]
$Pb/H_2SO_4/PbO_2$	2.1	175	20-40	50-100	300+	40-50	150-250	500+	1977
Zn/KOH/NiOOH	1.7	326	50-65	100-200	100+	70-90	200-300	500+	1978
Fe/KOH/NiOOH	1.4	267	30-45	50-100	500+	45-50	100-200	1000+	1979
Fe/KOH/Air	1.2	720	90	30	200	120	50	300	1978
$Zn/ZnCl_2/Cl_2$	2.1	825	65	60	<100	110	100	500	1979
$Na/Na_2O \cdot X\ Al_2O_3/S$	2.1	760	80	150	1000+*	170-190	150-200	1000+	1985
Li/LiCl-KCl/FeS	2.3	1300	155	50	1000+*	200-220	150-200	1000+	1985

a. Specific energy at 10 W/kg
b. Peak specific power or maximum recommended specific power.
c. Cycle life for deep discharge (>60%).
d. Estimated date for initial availability at projected performance.
* These cycle lives are representative values for laboratory cells and have not necessarily been demonstrated with lightweight cells.

TABLE 5-5. PROPOSED GOALS FOR ELECTRIC VEHICLE

Cell Performance	Battery Storage		Mechanical-Electrical Energy Storage
	Mark I	Eventual	Mark I
Cycle Life	200-400	700-1000	>> 100,000
Specific Energy, W-hr/kg	110	160	110
Specific Power, W/kg	110 (75)*	200	200**
Discharge Period, hr	4	4	As short as 1/2
Charge Period, hr	8	8	As short as 1/2
Cell Cost			
Cost for Initial Order, $/kW-hr	2000	-	≅ 900 (1000 units)
Projected Cost, at a Production Rate of 2000 MW-hr/yr, $/kW-hr	-	35-40	≅ 280
Storage-Road Efficiency		63%	85%
Schedule			
Order	10/77		?
Begin Tests	6/78		?
Install	9/78		?
Test Prototype	-	1/81	?

*For batteries rather than cells
**Design variable

For the energy-wheel electric car, the energy-wheel requirements are as follows:

- Assume wheel-to-road efficiency = 0.85 (0.95 x 0.95 x 0.95) (Gen.) (Chopper) (Motor)
- Assume 80% wheel discharge
- Energy required for 100 km = 11 kW-hr
- Energy stored = 11/(0.85 x 0.80) = 16.18 kW-hr

- Power at road - 21.4 kW
- Power generated in wheel = 21.4/0.85 = 25.15 kW

C. COSTS FOR BATTERY ELECTRIC CAR

Assume: Battery system weighs 1.1 x battery weight

Battery energy density - 34.1 W-hr/lb

System energy density - 34.1/1.1 = 31 W-hr/lb

Conversion efficiency (one way) = 0.70 x 0.95 x 0.95

= 0.63

Battery cost is - $40/kW hr - lower limit (Refer Table 5-6)

$75/kW/hr - upper limit (From R&D sources)

Cost of converter - $75/kW

Depth of discharge - 80%

Maintenance - 4%/yr of first cost

Battery life - 3 years

Battery salvage value - 5%

Fixed portion of system - salvage value = 50%

Electricity cost - $0.06/kW-hr

10% cost of money (11% avg. for 3 or 4 years on straight line amortization)

4 yr financing of non-battery portion of system

Cost of drive motor - $1200

Cost of System for 21 yrs:

Total Cost = First cost + interest on non-battery portion for 4 yrs. + interest on battery portion for seven 3-yr. periods + six sets of batteries + electricity costs - salvage value of seven sets of batteries and fixed portion of system

= $27026 for $40/kW-hr batteries

= $33611 for $75/kW-hr batteries

TABLE 5-6. RESULTS OF REVIEW OF MANUFACTURER ESTIMATES OF SELECTED BATTERIES

Type	Operating Temperatures (°C)	Suggested[1] Approximate Module Cost ($/kWh)
Lead-Acid	20 - 50	35[2]-65
Sodium-Sulfur	300 - 350	15-25
Lithium-Metal Sulfide	400 - 450	30-35
Sodium-Chloride	180 - 210	15-25
Zinc-Chlorine	0 - 80	12-30
Redox	20 - 50	30-35[3]

Notes:

1. Further studies are required before the differences in the advanced systems can be used to distinguish between them. Assumes success in R&D for advanced batteries.
2. Lower value estimate for an advanced battery module.
3. These estimates may be low and include a portion of power related costs. Highly suspect.

D. COSTS FOR ENERGY-WHEEL ELECTRIC CAR

Assume: Energy wheel system = 1.8 x wheel weight

Wheel energy density = 50 W-hr/lb

System energy density = 50/1.8 = 27.8 W-hr/lb

Conversion efficiency = 0.95 x 0.95 x 0.95

(wheel to road) = 85%

System cost = $4600/16.18 = $284/kW-hr

System life = 21 yrs.

20% salvage at end of life

Maintenance = 1%/yr of first cost

System cost = First cost + interest for 4 yrs + maintenance for 21 yrs + electricity - salvage

= $16,308

E. COSTS FOR INTERNAL COMBUSTION ENGINE (ICE) CAR - 21 YRS.

Assume: Car cost = $4500

Propulsion system - 4500/3 = $1500

Life = 7 yrs.

No salvage value

Maintenance = 10%/yr of initial cost

Finance period - 4 yrs

Fuel economy - 30 mpg, daily mileage - 100 km
- 61 mi

System cost = first cost + interest for 4 yrs + maintenance + fuel

Cost at $0.60/gal gas = $17,991

at $1.00/gal gas = $24,225

at 1.40/gal gas = $30,458

The summary of costs are shown in Table 5-7.

TABLE 5-7. COST SUMMARY

a. GM Car (1000 kg)

Trip distance	100 km
Energy/trip	11 kW-hr
Maximum power	21.4 kW
Acceleration	0 to 50 km/hr in 9 sec.

b. Life Costs for GM Car Propulsion System

(21 yr. term)

Ice	Batteries	Mechanical Capacitor
$17,991 ($0.60/g fuel)	$27,026 ($40/kw-hr)	$16,308
$24,225 ($1.00/g fuel)	$33,611 ($75/kw-hr)	
$30,458 ($1.40/g fuel)		

Section VI

PROBLEMS

Section VI

PROBLEMS

The preliminary design and analysis of the Mechanical Capacitor requires a number of assumptions, which should be replaced by firm engineering data before an operating prototype is attempted. There are a number of subsidiary problems that require solution by modeling, testing, or literature search. Following is a short review of the more important problem areas:

A. RHEOLOGICAL BEHAVIOR OF COMPOSITES

The long time behavior of Kevlar, graphite fiber and epoxy or elastomer composites is not understood. The energy wheel will be under cycling, ever-present stresses throughout its life. If it is balanced at the outset, the high self-imposed loads from the metal elements on the rim and from the fibers and resin matrix, can result in plastic flow of the matrix around the fibers, relaxation of the fibers, and metal embedment in the composite.

The effects may be of little consequence, but if deformations are significant and/or not uniform, wheel unbalance can increase with time, requiring constant monitoring and rebalancing.

B. MAGNETIC-STRESS INTERACTIONS

It is known that soft magnetic metals and hard magnetic metals exhibit changes in magnetic properties when stressed. The metal elements on the wheel can be stressed in shear, compression, and tension. Their behavior must be known to determine if the stresses impair their magnetic performance.

C. AGING

The long term effects on all the wheel materials must be assessed to determine, for example, whether the polymer structure of the Kevlar fibers and the matrix resin will remain stable over 20 years, or whether the magnets will develop microcracks that propagate with cycling stress, and destroy them or impair their strength.

D. MAGNET QUALITY

Rare earth magnets are subject to manufacturing anomolies, including micro-cracks, non-uniform magnetic structure, variation in magnetic strength, and varying stability with time. The effect of manufacturing variations must be related to their long-term performance in the energy wheel.

E. POWER LOSSES

Reliable estimates of power losses are not feasible without operational experience with a large enough sample of energy wheels - in the manner of motor-generator experience. The need for data is particularly important in coasting operations after the wheel is 'charged'. Losses will determine the shelf life of the wheel. The competitive position of energy wheels vis-a-vis batteries requires that shelf-life performance data be available.

Therefore all loss producing elements of the system must be evaluated by carefully designed tests and measurements.

Some power losses can be calculated or estimated fairly closely. For others, upper bounds can be calculated that show negligible loss. One loss source that has turned out to be elusive is eddy current loss in the motor windings due to time-changing, transverse-flux gradients. A simplistic upper bound calculation showed these losses to be excessive. A literature search uncovered a paper (Reference 12) that treats this general problem for sinusoidally time varying flux and recommends twisted ribbon conductors to minimize the loss.

Differences in geometry and flux-time variation (it is not sinusoidal for the motor windings) preclude direct application of the referenced article to the problem at hand.

Analytically, the pr m is to solve Maxwell's equations (with a valid assumption of zero displacement current) for the given geometry and magnetic field time variation for various conductor arrangements, including standard copper wire, twisted ribbons, and litz wire.

Practically, tests should be conducted utilizing these sample configurations with a realistic, time-varying field. Loss measurement poses problems since the eddy currents are local short circuits.

Voltage or temperature measurements can be used to arrive at the needed data. Obviously, the measurement experiments must be carefully planned to insure valid results.

F. FAIL SAFE OPERATION

The mechanical capacitor can be designed to rely completely on magnetic suspension through the use of redundant critical components and systems. Some of these are the sensors, electronic elements, and controllers. Thus, if the power supply fails, the wheel can power itself down to a stop without a catastrophic failure due to mechanical grounding of the bearing surfaces. This problem has not been addressed in the study but requires a solution.

Also, in the event the wheel should fail structurally, the vacuum housing, or the enclosure in which the wheel is housed must be capable of containing the debris leaving the wheel at projectile speeds.

G. DYNAMIC PERFORMANCE

The wheel structure is an elastic body exhibiting a number of mode shapes and frequencies when externally excited by vibratory forces. The dynamic performance of the wheel, which is a flexible gyroscopic body, must be examined for the effect of its elastic behaviour on the stability and power consumption of the magnetic suspension system. General methematical models of the elastic wheel subsystem and the suspension subsystem can be developed and programmed for use in the computer simulation of a complete system.

H. POWER CONVERSION

The high costs and low efficiency at partial power, of the power-conversion system chosen for the mechanical capacitor seriously affects overall system performance, and has a first-order effect on cost. The problem is of such import in this system (and in other energy storage systems) that it warrants an independent program of research and development directed at the development of solid-state switches with higher speed and power handling capabilities and lower costs.

I. FABRICATION

The wheel configurations analyzed in this study pose fabrication problems. Composite material density and uniformity must be of a high order to attain the dynamic balance required. Tight dimensional tolerances must be satisfied. And, in the prestressed wheel, ways must be found to achieve the initial stresses specified by the design. Finally, the cost of fabrication of these sophisticated structures must be reduced through innovations in tooling and fixturing.

REFFRENCES

Reference	Title
1.	Kirk, James A., Studer, Philip A., and Evans, Harold E. "Mechanical Capacitor," Goddard Space Flight Center, National Aeronautics and Space Administration, NASA, TND-8185, March 1976.
2.	Schlieben, E.W., "Systems Aspects of Energy Wheels," Proceedings of the 1975 Flywheel Technology Symposium, Lawrence Hall of Science, Berkeley, CA, ERDA 76-85, Nov. 10-12, 1975.
3.	Schlieben, E. W., "System Aspects of Magnetically Suspended Energy Wheels," Second International Workshop on Rare Earth-Cobalt Permanent Magnets and Their Applications, University of Dayton.
4.	Olson, E., "Approach Magnetism - A Study in Quantities," New York Springer Verlag, 1966.
5.	"An Assessment of Energy Systems Suitable for use by Public Utilities," Final Report EPRI, EM-264, Project 225, ERDA E(11-1)-2501 in three volumes, prepared by Public Service Electric and Gas Co., Newark, NJ. for EPRI and ERDA, July 1976.
6.	"Economic and Technical Feasibility Study for Energy Storage Flywheels," SO 75-SA-0166, by Rockwell International for ERDA, December 1975.
7.	Cairns, Dr. Elton J. and McBreen, Dr. James, "Batteries Power Urban Autos," Industrial Research, June 1975.
8.	Fulman, R. L., "Energy Storage by Flywheels," Record of the Tenth Inter-society Energy Conversion Conference, University of Delaware, Newark, Delaware, August 18-22, 1975.
9.	Asher, Harold, "Cost-Quantity Relationships in the Airframe Industry," R-291, US Air Force Project Rand, July 1, 1956.
10.	Grant, Eugene L. and Ireson, W. Grant, "Principles of Engineering Economy," The Ronald Press Co., NY.
11.	First Annual ERDA Battery Contractors Coordination Meeting, Collection of Vugraphs from Invited Guests, Germantown, MD. January 25-28, 1977.
12.	Stoll, R.L. and Hindmarsh, R., "Turbogenerator Stator Windings Using Composite Subconductors," Proc. IEE, V123 No. 11, Nov. 1976, p. 1217.

APPENDIXES

Appendix A

WHEEL STRUCTURE

Appendix A

WHEEL STRUCTURE

A. WHEEL STRESS AND DYNAMICS

Two considerations limit the range of choice of rim proportions: stress concentrations, and natural rim vibrational modes and frequencies. For every rim configuration consisting of the Kevlar composite ring plus accompanying magnetic structure, there exists a radial and tangential stress distribution in the fiber composite that is unique to that configuration. The bond strength of the epoxy matrix generally limits the radial stresses to 3000 to 5000 psi, and the tensile strength (fatigue limit) of the Kevlar limits the peak tangential stress to about 225,000 psi. The greater the ratio of peak to minimum stresses across the rim, the less effective the design, because the lower stressed fibers are carrying less than their share of the energy. The ideal rim contains the least amount of magnetic material possible, and is uniformly stressed.

The vibrational frequencies of the rim must lie outside the range of operating rotational frequencies in order to avoid resonance and attendant power losses. The modes that tend to lie in this range are the bending modes. Generally, the method of raising the modal frequencies is to provide a stiff beam cross section for the rim, and minimize the loading imposed by high density (deadweight) elements. The two structural concepts analyzed drive the design in this direction.

B. SYSTEM DYNAMICS

The dynamic behavior of the total rim plus suspension system can be investigated by analytic simulation, but must be left as a future investigation due to its extensive scope. The rim behaves as a gyroscope, acted upon by forces supplied by the magnetic bearing elements. In addition, the motor-generator may apply moments to the rim. Of interest is the behavior and stability of the rim under normal steady-state operation with small perturbations from the suspension; under transient conditions due to spin-up and spin-down; under shock and vibration input via the foundation; and under the effects of nominal unbalance and geometric imperfections in both the rim and supports. This requires considerable computer investment.

Two types of wheel structure have been analyzed with the same analytical procedure. The Technical Note in Appendix G prepared by Dr. James A. Kirk, a consultant to RCA, contains the rationale and analytical mode for the NASA (prestressed

ring) configuration. The RCA configuration avoids the need for prestressed rings and the possible difficulty in fabricating a wheel of that configuration. But the RCA configuration also is an unproved design. In the RCA configuration,* two or more rings are separated by a lightweight filler with adequate strength in the radial direction to withstand self loading and the loads imposed by differential expansion of the joined rims. In the following discussion, both configurations are examined and compared.

C. RIM DESIGN

Choosing a configuration for an energy wheel and its subsystems—the suspension system and the drive system—involves a number of design compromises. The energy wheel rim is a multifunctional device in a technical sense. The rim is not only a structural element for storing kinetic energy, but it is part of the magnetic bearing system and the motor-generator system. It is axiomatic in engineering that a multifunctional device is usually not as efficient and cost effective as a group of separate devices, each optimized for its own function. Provision for magnetic suspension and drive degrades the energy-density efficiency of the rim. The design objective is to minimize the effect of the compromise.

The energy wheel configuration outlined in NASA-Goddard TN D-8185 (Reference 1) sought to maximize energy storage efficiency and low losses with a basic thin rim design. However, there are structural effects which limit the rim energy density in this configuration. Also, rim self loading causes a significant growth in diameter. A Kevlar composite rim, for example, operating at full speed and near ultimate tensile strength, can expand 1.6 to 2% of its diameter. A wheel 50 inches in diameter might expand 1.00 inch, or 0.50 inch on the radius. The effect of this on the magnetic suspension and motor elements can be substantial. If the (stationary) magnetic support structure is continuous, as indicated in NASA Document TN D-8185, it must somehow expand also (both the fixed and the moving elements) to maintain gap width and gap flux density. The alternative is to greatly increase the electromagnetic structures and coil currents to maintain fixed magnetic field strength in the gaps. But in addition, the expansion of the rim requires that the rim metal elements exhibit the same strain (elongation, etc.) as the rim composite structure, or that the metal elements be segmented and mounted elastically to accommodate the difference in strain between the rim composite material and the metal elements. In the first case, the highly strained metal must retain its magnetic properties. In the second case, the metal must be laminated (with the laminations lying in radial planes that contain the wheel axis) and bonded with an elastic adhesive, or the metal must be mounted on an elastic base and made in segmented strips with the long dimension in the circumferential direction.

*A proprietary design

Both solutions introduce losses, as discussed later. In like manner the motor-generator, which is a continuous circumferential structure, must operate with large field-coil gaps due to rim growth and must be made more massive to maintain gap flux density with wheel growth.

Therefore thin-rim, magnetically supported energy wheels pose formidable structural, support and drive problems whose solutions may lead to an energy wheel design of undue complexity, high cost, and low storage efficiency.

The alternative rim-only wheel configurations examined in this study yield cost-effective solutions to the energy storage problem.

D. TRADEOFFS LEADING TO NESTED RING CONFIGURATION

The theoretical performance of a rim material cannot be realized in practice because of the derating factors applicable to fabrication, geometry, and added components.

The rim-mounted magnetic materials necessary for support (laminations, magnets, plus attachment hardware) contribute virtually nothing to the tensile strength of the wheel, but do add mass. Moreover, the mass is added at relatively discrete locations, with the consequent introduction of localized stress concentrations. The addition of a small amount of "dead" weight has a striking impact on performance. Further, the geometry, or distribution, of the added mass is very significant. Therefore, it is a crucial design exercise to minimize the adverse effects of the necessary addition of mass. A generic wheel type described in NASA Document TN D-8185, "Mechanical Capacitor," consists of a magnetically supported rim, driven by a homopolar dc motor. A reproduction of Figure 4 of the TN (with additions) is shown in Fig. A-1. For the properties shown, this would be considered in the class of "thin" rims.

Figure A-1 can be idealized for preliminary analysis as shown in Figure A-2. A brief calculation shows that if the total mass were uniformly distributed within the fiber matrix, and contributed fully to the hoop stress load with the same elastic properties as the fiber, a new specific strength would result, equal to

$$\frac{\sigma_{max}}{\gamma_1} \rightarrow \frac{\sigma_{max}}{(\gamma_1 \Delta R + \gamma_2 \delta)/(\Delta R + \delta)} = \frac{\sigma_{max}}{\gamma_1} \left[\frac{1 + \delta/\Delta R}{1 + \frac{\gamma_2}{\gamma_1} \frac{\delta}{\Delta R}} \right] \triangleq \frac{\sigma_{max}}{\bar{\gamma}}, \qquad \text{(A-1)}$$

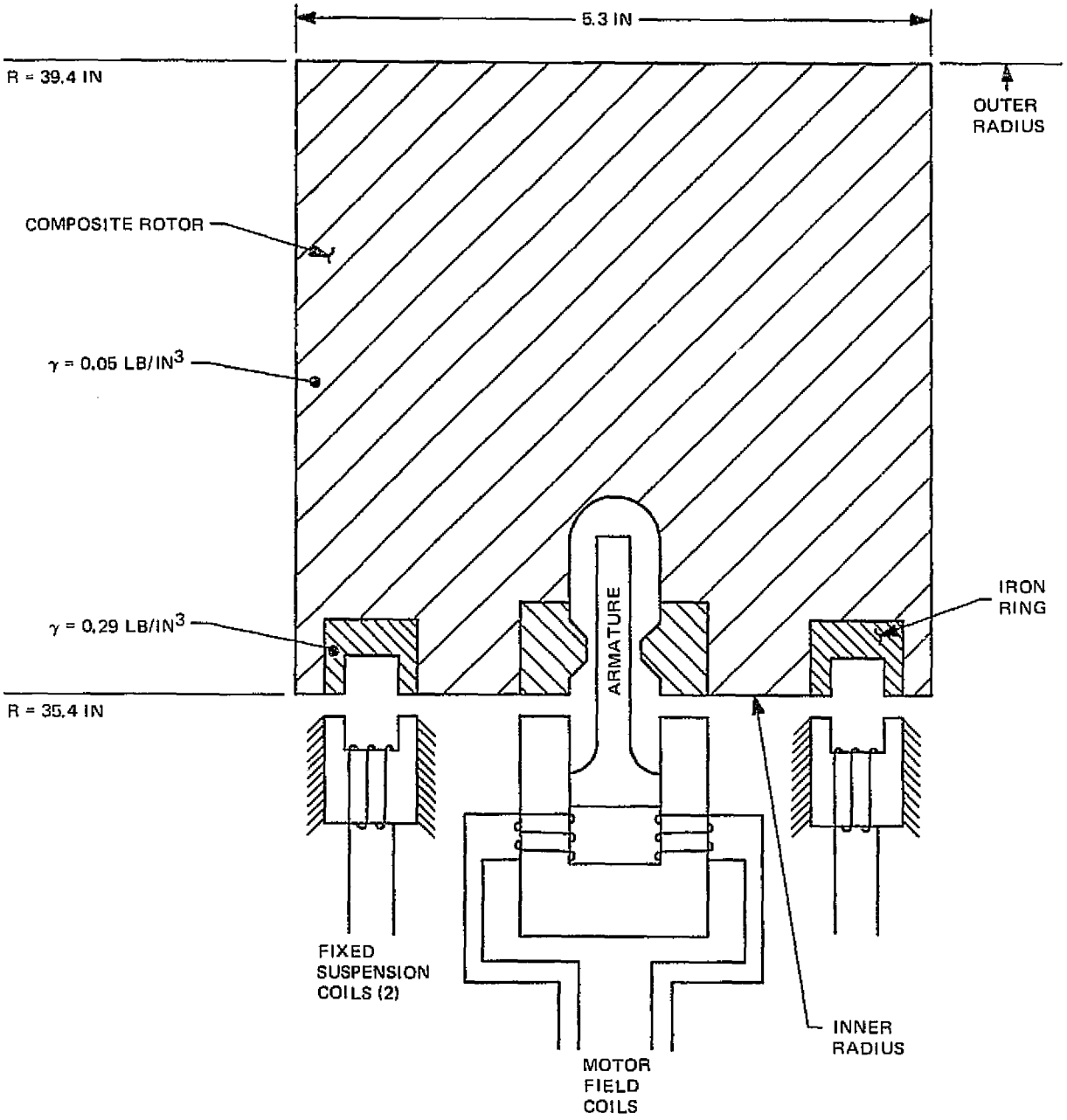

Figure A-1. Cross section of NASA-Goddard rotor.

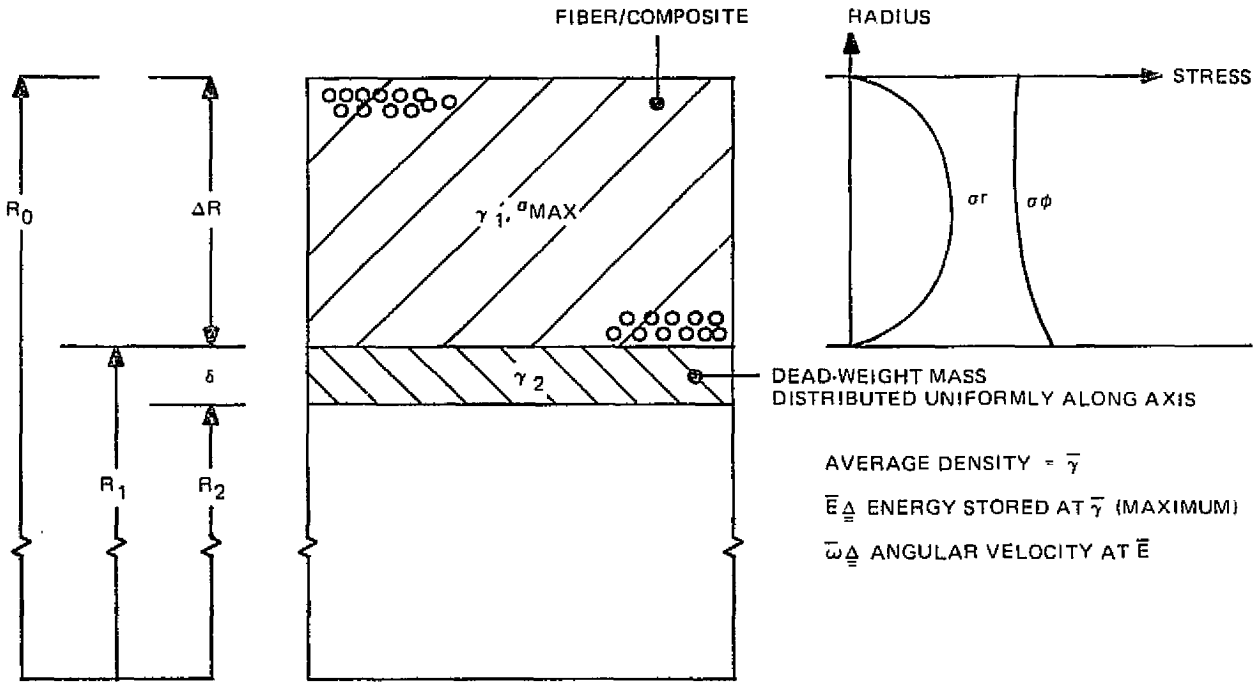

Figure A-2. Effect of stress amplification due to addition of mass.

based on the law of mixtures. (σ_{max}/γ is the basic measure of energy density). For magnetically supported rims of the type shown in Figure A-1, the range of $\delta/\Delta R$ will be typically

$$0.05 \leqslant \delta/\Delta R \leqslant 0.10$$

and the value of γ_2/γ_1 about 6.0. Therefore, the ratio of energy storable for the loaded vs. the unloaded wheel, characterized by $(\bar{\omega}/\omega_{max})^2$, is for the same shape factor

$$0.69 \leqslant \left\{ \frac{\bar{E}}{E} = \left(\frac{\bar{\omega}}{\omega_{max}} \right)^2 = \frac{\bar{\gamma}}{\gamma_1} \right\} \leqslant 0.81 \qquad \text{(A-2)}$$

This result does not appear to be unduly compromising. However, the magnetic elements cannot actually be added according to the above model.

Consider the effect of the added mass of Figure A-2 on stress in the fibers, if the mass does not carry any share of the hoop stress load at all. For this case, the inertial mass force is equivalent to a uniform radial pressure equal to:

$$P = \rho_2 \omega^2 (R_1 - \delta/2)\delta, \quad (\rho = \text{mass density}) \qquad \text{(A-3)}$$

which leads to an additional hoop stress at the inner fibers of the rim of*

$$\sigma_\theta = \frac{P\left(R_o^2 + R_1^2\right)}{\left(R_o^2 - R_1^2\right)} . \tag{A-4}$$

But[1],

$$\sigma_\theta = \frac{\rho_1}{4}\left((3+\upsilon)\,R_0^2 + (1-\upsilon)\,R_1^2\right)\omega^2_{max}, \tag{A-5}$$

for a rotating ring, so that the reduced rotational speed necessary not to exceed $_{max}$ in the fibers is characterized by the sum of Equations A-4 and A-5:

$$\sigma_{max} = \left[\frac{\rho_1}{4}\left((3+\upsilon)\,R_0^2 + (1-\upsilon)\,R_1^2\right) - \frac{\rho_2\,(R_1 - \delta/2)\,(\delta)\,(R_0^2 + R_1^2)}{R_0^2 - R_1^2}\right]\omega^2 \tag{A-6}$$

Again, if $\gamma_2/\gamma_1 = 6$, $\upsilon = 0.36$, $0.05 \leqslant \delta/\Delta R \leqslant 0.10$, and $\Delta R/R_0 = 0.1$, the reduced speed is given by (Equations A-5 and A-6):

$$0.15 \leqslant \left\{\left(\bar{\omega}/\omega_{max}\right) = \frac{\bar{E}}{E}\right\} \leqslant 0.27. \tag{A-7}$$

Some of this loss is recovered because mass has been added (not the same way as implied by Equation A-1, however), which yields additional kinetic energy equal to:

$$\Delta E = \pi \rho_2 \omega^2 (R_1 - \delta/2)^3\ \delta \text{ (per unit axial length).}$$

But the fiber rim has

$$E = \pi \rho_1 \omega^2 \left(\frac{R_0 + R_1}{2}\right)^3 (R_0 - R_1),$$

Roark, R.J., Formulas for Stress & Strain, McGraw Hill, 1965, p. 308.

so that

$$\frac{E + \Delta E}{E} = \frac{8\frac{\rho_2}{\rho_1}\,(R_1 - \delta/2)^3\,\delta}{(R_0 + R_1)^3\,(R_0 - R_1)} + 1 \qquad \text{(A-8)}$$

In our example, then, the effective energy ratio at reduced speed is:

$$0.26 \leqslant \left\{ \frac{\overline{E}}{E} = \left(\frac{E + \Delta E}{E}\right)\left(\frac{\overline{\omega}}{\omega_{max}}\right)^2 \right\} \leqslant 0.34 \qquad \text{(A-9)}$$

which should be compared with (A-7). If the added mass is indeed stressed to values typical of yield for magnetic steel, it can be shown that Equation (A-8) changes little if the mass ratio ρ_2/ρ_1 stays at typical values. Therefore, magnetic elements act as dead weight, for realistic allowable stress for typical magnet steels.

Also, the ratio of radial stress at the interface to fiber tensile strength is (Eqns. A-3 and A-4)

$$\text{RATIO} = \frac{P}{\sigma_{max}} = \frac{\left(\frac{R_1 - \delta/2}{R_0}\right)\left(\frac{\delta}{R_0}\right)}{\frac{1}{4}\frac{\rho_1}{\rho_2}\left((3+\upsilon) + (1-\upsilon)\left(\frac{R_1}{R_0}\right)^2 + \frac{(R_1 - \delta/2)}{R_0}\left(\frac{\delta}{R_0}\right)\left(\frac{R_0^2 + R_1^2}{R_0^2 - R_1^2}\right)\right)} \qquad \text{(A-10)}$$

which, for the above example gives

$$0.022 \leqslant \text{RATIO} \leqslant 0.036 \qquad \text{(A-11)}$$

Because the transverse compressive strength of the fiber-epoxy matrix is usually much less than the hoop strength (typically less than 10%) it is seen that the limiting factor for attaching elements to the rim may well be the lateral compressive strength of the epoxy matrix, which limits the average ratio of element density to rim density. Obviously, discrete elements impose additional problems due to stress risers, such as corners. For the example given, a stress concentration factor of about 2 to 3 would use up the margin of 10%.

Regardless of the method proposed to distribute, shape, and affix the magnetic elements on the single thin rim, the use of elements that do not support some of the hoop stress will significantly derate the energy capacity of a bare rim by as much as 70% for the relative rim proportions given in the examples.

Increasing the value of hoop stress for the material to be attached to the rim does not alter the situation unless the attached material carries its own inherent load without applying radial stresses to the composite. In other words, the radial strain of the magnetic material must match that of the inner fiber of the composite rim. Post* has stated that the condition required is that the elastodensity ratio (E/γ) vary approximately with the cube of the radius. For typical materials, however, the elastodensity ratio of the composite is approximately 4×10^8 in^{-2}, and for iron it is 1×10^8 in^{-2}. Therefore, iron will impose a significant load on the composite because of the implied strain differential.

The addition of mass represented by the motor-generator magnets produces the same effect as that of a dead-weight load. In addition, there is both a shear load and differential normal pressure caused by applied magnetic forces. The effective pressure between the magnetic poles, however, is expected to be of the order of 10 $lb/in.^2$ at best, so that the stresses transmitted to the fiber matrix will be relatively small.

How can the effects of mass loading be reduced without sacrificing specific energy? Consider the abstract situation of Figure A-3, where a thin rim and an inner ring loaded with dead-weight mass are rotating in synchronism. (There is no connection between the two rims, for the moment.)

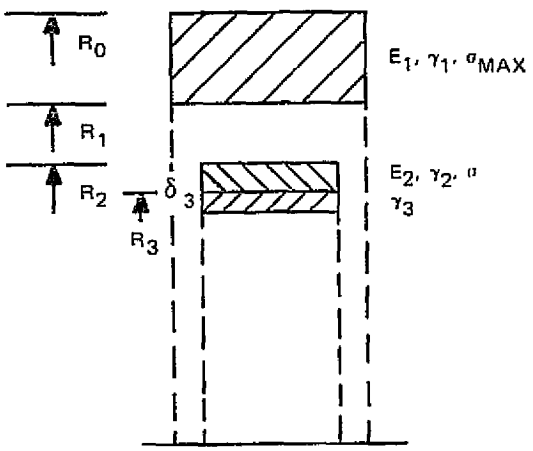

Figure A-3. Multiple-ring rotor.

*Patent 3,859,868; 1975.

The outer rim in this case is fiber composite, and develops its rated specific energy at ω_{max} (say, 60 Wh/lb). Suppose the dead-weight mass is 30% of the fiber composite, by weight, and the inner ring is just large enough to support the dead weight. For simplicity, assume that the inner ring is the same composition as the outer rim, although graphite epoxy is preferred for its significantly smaller strain. Note also that the axial length of the rims are not necessarily the same. What is the efficiency of this model, compared to the previous?

As a specific case, take the axial lengths as indeed equal, and $R_3 = 1/2\ R_1$; the radial pressure is then found as

$$P \approx \rho_3 \omega^2_{max} R_3 \delta_3$$

The allowable stress in the inner ring is, by Equation (A-6):

$$\sigma_{max} \cong \omega^2_{max} \left[\frac{\rho_1}{4} \left((3+\nu) R_2^2 + (1-\nu) R_3^2 \right) + \rho_3 R_3 \delta_3 \right] \frac{(R_2^2 + R_3^2}{(R_2^2 - R_3^2}$$

from which R_2 can be found. For previous material properties,

$$\delta_3 = 2\ (R_0 - R_1) \times 0.05;\ \gamma_3/\gamma_2 = 6;\ \nu = 1/3;\ \text{and}$$

$$\sigma_{max} = \omega^2_{max} \left[\frac{\rho_1}{4} (3+\nu) R_0^2 + (1-\nu) R_1^2 \right]$$

Therefore,

$$1 = \frac{(3+\nu) R_2^2 + (1-\nu) R_3^2 + \frac{4\rho_3}{\rho_1} R_3 \delta_3 \frac{\left(R_2^2 + R_3^2\right)}{R_2^2 - R_3^2}}{(3-\nu) R_0^2 + (1-\nu) R_1^2}$$

If $R_0 = 1.1\ R_1$, substitution of values gives

$$\left(\frac{R_2}{R_3}\right)^4 - 6.296 \left(\frac{R_2}{R_3}\right)^2 + 5.584 = 0$$

From which

$$R_2/R_3 = 1.033, \text{ and } \frac{R_2 - R_3}{R_0 - R_1} = 0.167$$

But, $\delta_3/(R_2 - R_3) = 2/3.3$; so one can see that the original dead weight is being carried by a composite ring that weighs only 28% as much as the dead weight. Alternately, the inner ring is 16.7% of the weight of the outer rim.

The total kinetic energy stored is $\approx 1 + 1/4 \times .3 \times 1.28 = 110\%$ of that of the rim, but the added weight is $1 + .3 \times 1.28 = 138\%$. Therefore, the total derating for this example is 20%! We are thus restored to a value roughly equal to that for the example of uniformly distributed self-supporting mass (Equation (A-2)).

Of course, the matter of connecting the two rings remains. The only requirement for the connecting material is that it provide sufficient strength to overcome shear loads between the rings, support its own inertial weight, and allow for differential radial strain.

If a honeycomb or similar material is considered as a filler between the two rings, the radial specific strength (σ/γ) is the determining design factor. For aluminum honeycomb, the specific strength may be as high as $500/0.0023 = 220,000$, based on radial bond strength of 500 psi. The density would be 4.6% that of the composite; if the annulus were filled in the above example, the added weight of filler would be about 16% of the original rim, and 12% of the combined weight of the two rims. The derating factor calculates out to be roughly $(1 + 0.12 \times 0.75^2)/(1 + 0.12) = 0.95$, for a combined total of 76%. Compared to the 34% of Equation (A-9), this represents a significant improvement. If the original Kevlar composite were rated at 60 Wh/lb, then the total rotor would be rated at 46 Wh/lb.

A second candidate filler is balsa, a well established structural material. The specific strength of balsa is approximately the same as that of honeycomb, and it has the added advantage of providing a continuous end-grain surface for bonding. The derating factor would also be approximately the same.

The final consideration is the method of attaching the filler. Honeycomb is routinely bonded with elastomer, yielding 500 psi average stress across the end faces. If a column of filler is attached between two rings, so that the inner radius is in 500 psi tension and the outer radius is in 500 psi compression, then it is a straightforward matter to determine the allowable radial difference between the rings. This turns out to be a function of the tangential velocity, and it can be shown that

$$\frac{R_i}{R_o} \triangleq \frac{R_{inner}}{R_{outer}} = \text{function} \left\{ \frac{\rho/\rho_0 \, (R_{outer}/R^*)^2}{\sigma_r/\sigma_{max}} \right\}$$

where R* is the equivalent single Kevlar filament radius at ω and σ_{max}, as determined by $\sigma_{max} = \rho_o \omega^2 R^{*2}$, and σ_r is the radial strength of the honeycomb. For the example under discussion,

$$\frac{R_{inner}}{R_{outer}} = \text{function}\left\{ 20.7\ (R_{outer}/R^*)^2 \right.$$

The function is shown in Figure A-4.

Starting from the radius R_1 (Figure A-3), the first ratio R_1/R^* is roughly $\sqrt{0.76}$, as implied by the derated rim, so that $R_1/R_2 \approx 0.88$ from the chart; or, the inner honeycomb radius is limited to 88% of the outer radius. But, we wish to fill to about 50% of the outer honeycomb radius. If a very thin intermediate load carrying ring (1000 psi radial load) is supplied for the honeycomb, as was supplied for the magnets, the honeycomb can be staged (the next honeycomb annulus would get down to 76% of the original; the third down to 65% and, finally, the fourth to 52%). Each of the load carrying rings can be fabricated from Kevlar, and adjusted in size to minimize strain differential. The outer intermediate ring would be about 5% of the weight of the outer rim, with the following rings less than that. The additional derating would be about the same as for the filler itself.

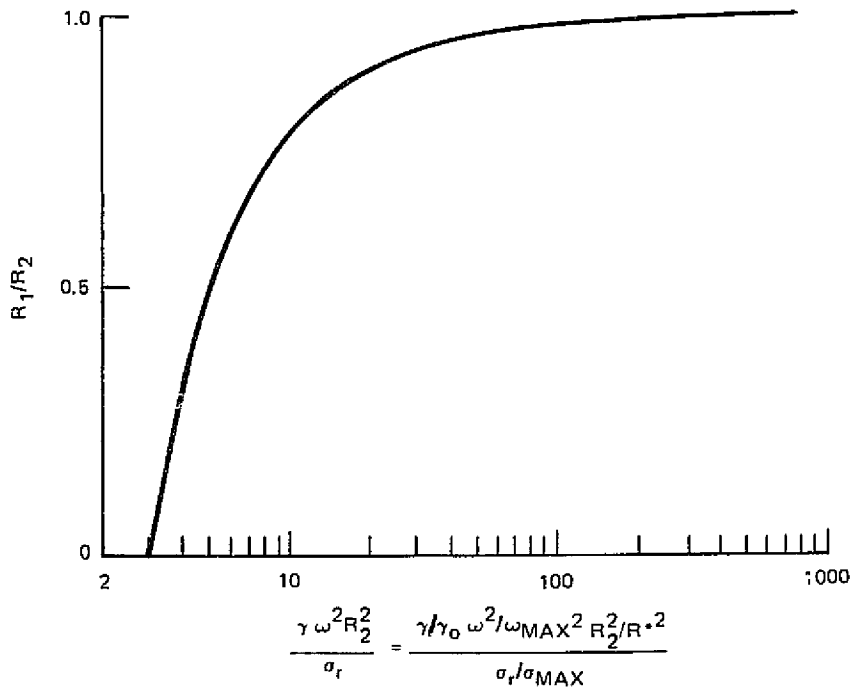

Figure A-4. Allowable radius ratio for filler.

All discussion of the foregoing example is intended solely to illustrate a procedure for minimizing the loss in energy density for the thin-rim wheel that results from the necessary weight of the magnets. A final rim configuration requires many tradeoffs among weight, cost, magnet performance and stress levels. One of the strongest driving factors is system cost, which translates heavily into the maximization of the specific energy of the rim.

E. INTEGRITY OF ASSEMBLY

The tradeoffs described in the preceding section do not address the problems of stress concentration caused by discrete components. Additional derating must be allowed for irreducible stress levels. The design practice of using proper fillets, matching material properties to expected strains to optimize stress distribution, and provision of maximum surface for bonding are a few of the considerations for assuring that the best performance will be attained.

F. VERIFICATION OF STRESSES

The ring design is modeled by a finite element program that takes into account the anisotropic properties of the composite material and the presence of iron in the ring. Although the degree of anisotropy in the composite rim itself is small, computer software handles anisotropic properties as a matter of course. The use of laminations and honeycomb filler implies a high degree of anisotropy locally, which has a significant effect on stress distribution.

Static modelling results in the determination of the stress field in the ring cross section, which is effectively the solution for the entire ring due to symmetry. All of the stress components are available at all points of the section, from which principal stresses and strains are calculated. Effect of centrifugal loading is included.

A sample of a typical stress plot for an energy wheel section is shown in Figure A-5. This rim was analyzed at RCA for a wheel developed for another purpose, using a finite element program with anisotropic axisymmetric elements. The hoop stresses exhibited show a concentration factor of 1.5 at the inside corner of the lamination.

G. VIBRATION MODES

The vibration modes (and frequencies) of the rim determine the speeds at which resonance is likely to occur during operation. Ideally, the natural frequencies of the rim occur outside of the 2:1 range of operational speeds, but if that is not possible, sufficient damping must exist within the rim structure to limit the resonant amplitudes. Even with sufficient damping, however, operation at resonance would represent additional energy loss due to internal friction.

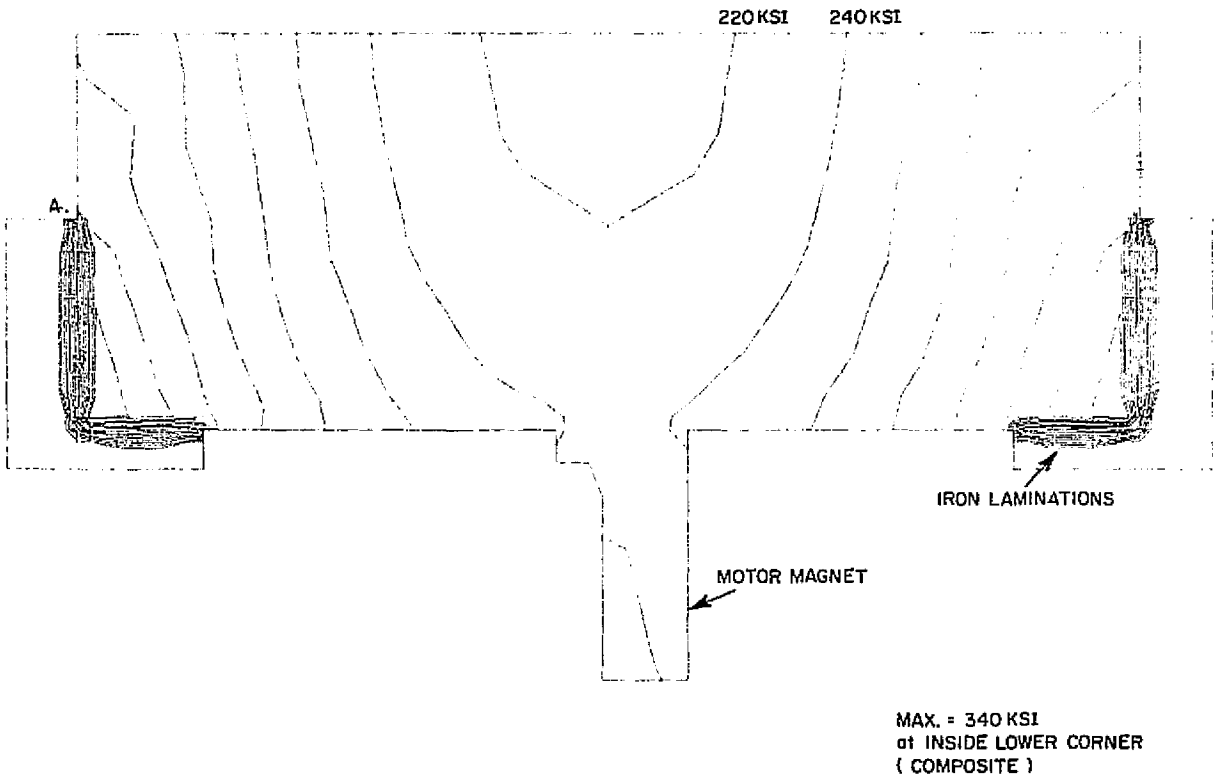

Figure A-5. Hoop stress contours.

For a given mass, the means of raising the lowest natural frequency is by providing the stiffest possible cross section. The nested-ring model provides an inherently stiff section in bending (usually the lowest frequency mode). Also, the increase in tension due to centrifugal loading causes an increase in natural frequency, much as the frequency of a vibrating string increases with tension.

The frequency solution takes into account the same anisotropic material properties as the stress solution.

H. THE POINT DESIGN

The point design is an optimum solution to the problem of maximizing energy density, but only within certain design bounds that are to some extent arbitrary. They are as follows:

The wheel outside diameter was fixed at 48 inches as the baseline dimension. Larger diameters would lead to increased flexibility in the plane of the wheel; smaller diameters lead to higher speeds, posing increased problems for a motor-generator already operating at very high speeds.

The inner diameter was fixed at 24 inches initially and found to be a good compromise dimension. Smaller diameters may lead to a somewhat higher energy density but introduce motor-generator problems that tend to disappear with larger diameters.

As stated earlier, the metal elements on this wheel were assumed to be inert, or non-load bearing, an assumption with important consequences which are discussed later.

The composite material in the inner rim was limited to Ultra High Modulus (UHM) graphite in an epoxy matrix, to minimize the expansion for the benefit of the suspension and motor-generator subsystem.

A uniform cross-section was assumed for all rims. The effect of stress concentrations in the inner rim, due to local loads from the metal elements, was not explicitly determined using finite-element stress analysis. The base material allowable stresses, however, were derated to account for stress concentration by factors that reflect previous analytical experience. The metal was assumed to be uniformly distributed on the inner surface of the inner rim, as shown in Figure A-6. The Mechanical Capacitor energy and power density characteristic, for a family of wheel designs similar to the point design, is shown in Figure A-7 (dashed curve). The power density limitation is seen to be severe compared to the characteristic curves for stressed Kevlar and steel wheels and a Mechanical Capacitor wheel with one-half of the rim metal participating in the wheel structure. The benefit through the use of the metal for structure is significant, but requires both good magnetic and structural performance from the rim metal.

The analysis and design of the Mechanical Capacitor was based on the assumption that the rim metal is structurally inert (zero tensile modulus). The magnetic-structural performance of candidate rim metals must be determined before the full potential of the two wheel configurations can be realized.

The axial length of the wheel was assumed to be constant for each wheel, i.e., constant-thickness cross section.

The effect of variations in rim dimensions, weight of metal on the inner rim and intermediate rim locations were investigated in the computer analysis. Typical computer run summaries are shown in Figures A-8 and A-9.

Table A-1 lists the more satisfactory configurations that were analyzed. These exhibit a significant range of specific energies and iron weights, and support the conclusions of Figure A-10. In all cases design energy capacity is 10 kW hr at design speed. Energy density in Wh/lb is significantly affected by the weight of inert metal placed on the inner rim. In Figure A-10 the relationship is shown for RCA wheels of 20, 24, and 26 inches id (od 48 inches). A similar relationship exists for the NASA wheel.

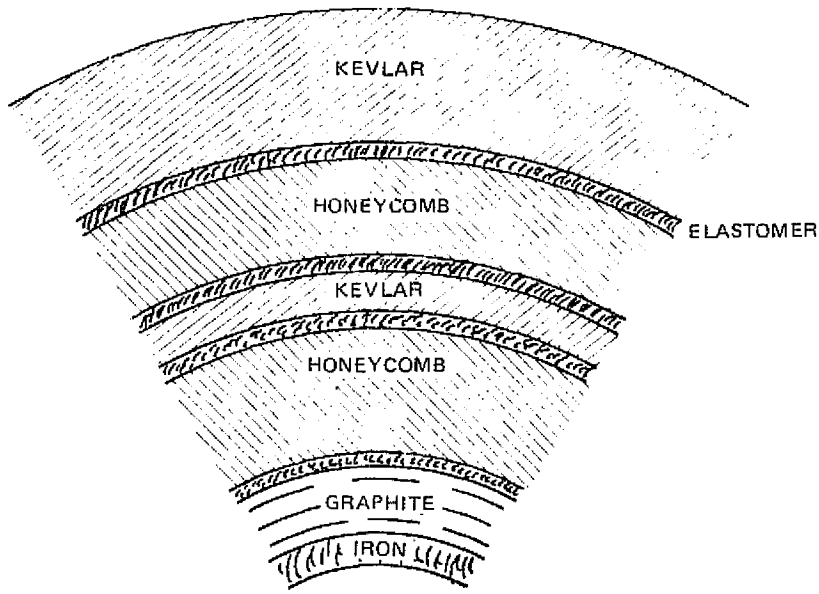

	KEVLAR	ELASTOMER[+]	HONEYCOMB	GRAPHITE	IRON
σ_θ	225 ksi	0–3	0	130	0.3
σ_r	5 ksi	0.5	0.5	5	0.5
$\nu_{r\theta}$	0.28	0–0.35	0	0.28	0
Ξ_θ	10^7 psi	0–10^5	0	25×10^6	5×10^5
E_r	800 ksi	100	50	1700	5×10^5
γ	0.05 lb/in.^{3}	0.036	0.0029	0.056	
w					16 lb. @ 12 in. Mean Radius to 32 lb.

Figure A-6. Inner rim structure.

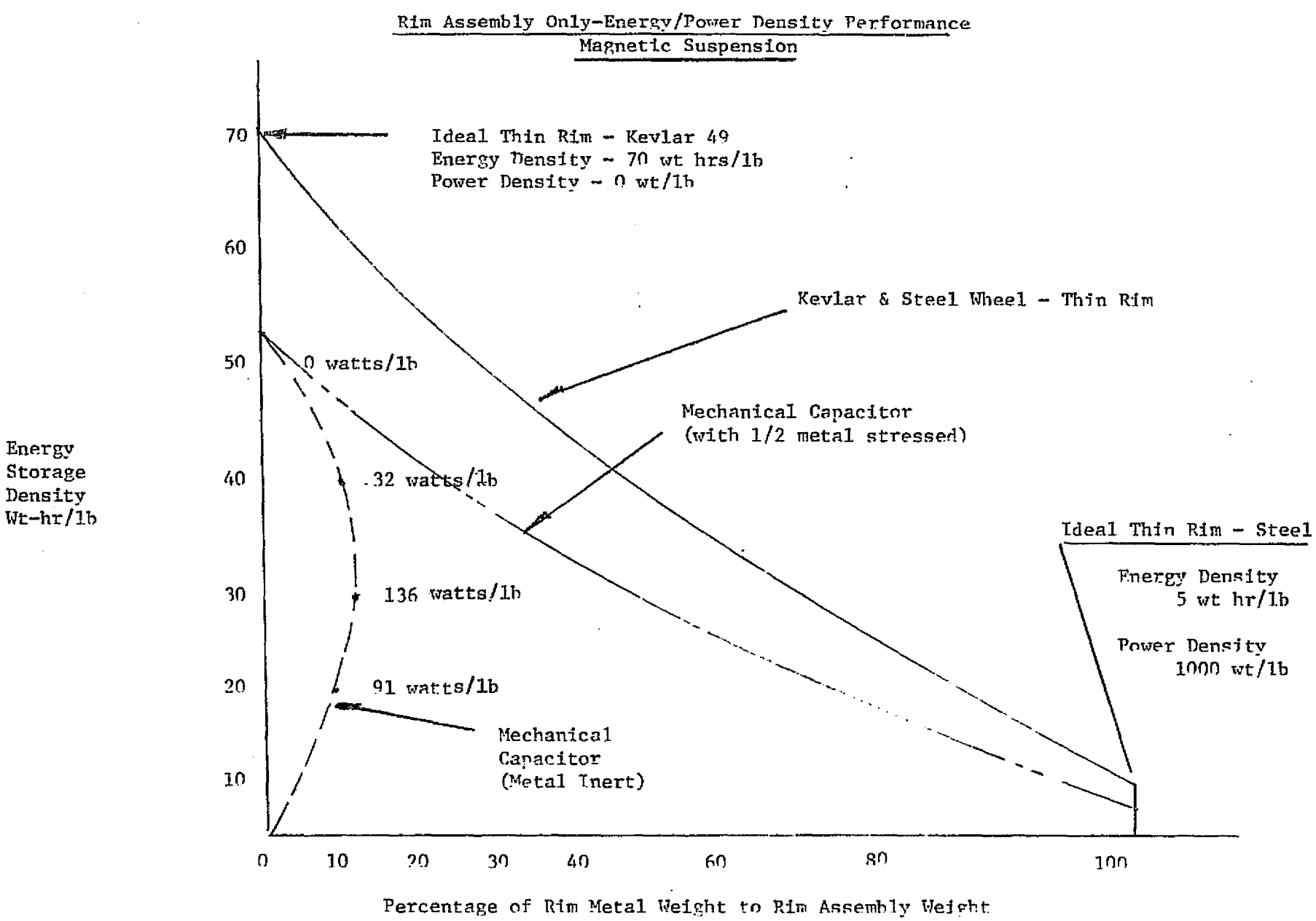

Figure A-7. Energy-power density performance for rim assembly only; magnetic suspension.

STRESS SUMMARY:

RING NO	INNER RADIUS	INNER RADIAL STRESS	INNER TANGENTIAL STRESS	INNER RADIAL STRAIN	INNER RADIAL PRESTRAIN
1	11.000	-.443-10	2.712+03	5.966-02	0.000+00
2	12.500	-.140+05	1.953+05	3.557-02	0.000+00
3	13.500	-.474+04	1.768+05	3.456-02	0.000+00
4	14.650	1.174+03	2.287-03	3.350-02	0.000+00
5	14.850	0.058+02	1.148-02	1.705-01	0.000+00
6	17.000	-.620+03	1.897+05	1.614-01	0.000+00
7	17.400	9.026+02	9.217-03	1.604-01	0.000+00
8	17.500	3.360+02	1.267-02	2.218-01	0.000+00
9	19.500	-.573+03	2.225+05	2.169-01	0.000+00
10	22.000	2.951+03	1.044+05	2.129-01	0.000+00

RING NO	OUTER RADIUS	OUTER RADIAL STRESS	OUTER TANGENTIAL STRESS	OUTER RADIAL STRAIN	OUTER RADIAL PRESTRAIN
1	12.500	-.164+05	-.349+04	3.557-02	0.000+00
2	13.500	-.542+04	1.766+05	3.456-02	0.000+00
3	14.650	1.174+03	1.604+05	3.550-02	0.000+00
4	14.850	1.958+02	1.148-02	1.705-01	0.000+00
5	17.000	-.620+03	0.495-05	1.614-01	0.000+00
6	17.400	9.026+02	1.846+05	1.604-01	0.000+00
7	17.500	3.260+02	1.267-02	2.218-01	0.000+00
8	19.500	-.573+03	1.112-02	2.169-01	0.000+00
9	22.000	2.951+03	1.944+05	2.129-01	0.000+00
10	24.000	-.189-10	1.751+05	2.102-01	0.000+00

Figure A-8. Computer printout, RCA wheel - typical run* (Sheet 1 of 3).

*Analysis by Kirk at University of Maryland

N	AVG PRESSURE	PRESTRESS
1	0.000+00	0.000+00
2	-.151+05	0.000+00
3	-.506+04	0.000+00
4	1.174+03	0.000+00
5	1.958+02	0.000+00
6	-.620+03	0.000+00
7	9.026+02	0.000+00
8	3.260+02	0.000+00
9	-.573+05	0.000+00
10	2.951+03	0.000+00
11	0.000+00	0.000+00

Figure A-8. Computer printout, RCA wheel - typical run* (Sheet 2 of 3).

*Analysis by Kirk at University of Maryland

PROPERTY SUMMARY:

K	RL	RU	T	RHO	NU	ERAD	ETHETA
1	11.000	12.500	3.000	1.200-01	3.000-01	5.000+05	5.000+05
2	12.500	13.500	3.500	6.000-02	2.800-01	2.000+07	7.000+07
3	13.500	14.650	4.000	6.000+02	2.800-01	2.000+07	7.000+07
4	14.650	14.850	4.000	4.000-02	0.000+00	1.000+03	1.000+00
5	14.850	17.000	4.000	3.000-03	0.000+00	5.000+04	1.000+00
6	17.000	17.400	4.000	5.000-02	2.800-01	1.500+06	2.000+07
7	17.400	17.500	4.000	4.000-02	0.000+00	1.000+03	1.000+00
8	17.500	19.500	4.000	3.000+03	0.000+00	5.000+04	1.000+00
9	19.500	22.000	4.000	5.000+02	2.800-01	1.500+06	2.000+07
10	22.000	24.000	4.000	5.000-02	2.800-01	1.500+06	2.000+07

NORMALIZING FACTOR: 2.365+05 PSI
SPECIFIC ENERGY: 4.473+01 WHB/LB @ 17000 RPM
TOTAL IRON: 3.987+01 LB
TOTAL ENERGY: 9.981+00 KWH
TOTAL WEIGHT: 2.232+02 LB

Figure A-8. Computer printout, RCA wheel - typical run* (Sheet 3 of 3).

*Analysis by Kirk at University of Maryland

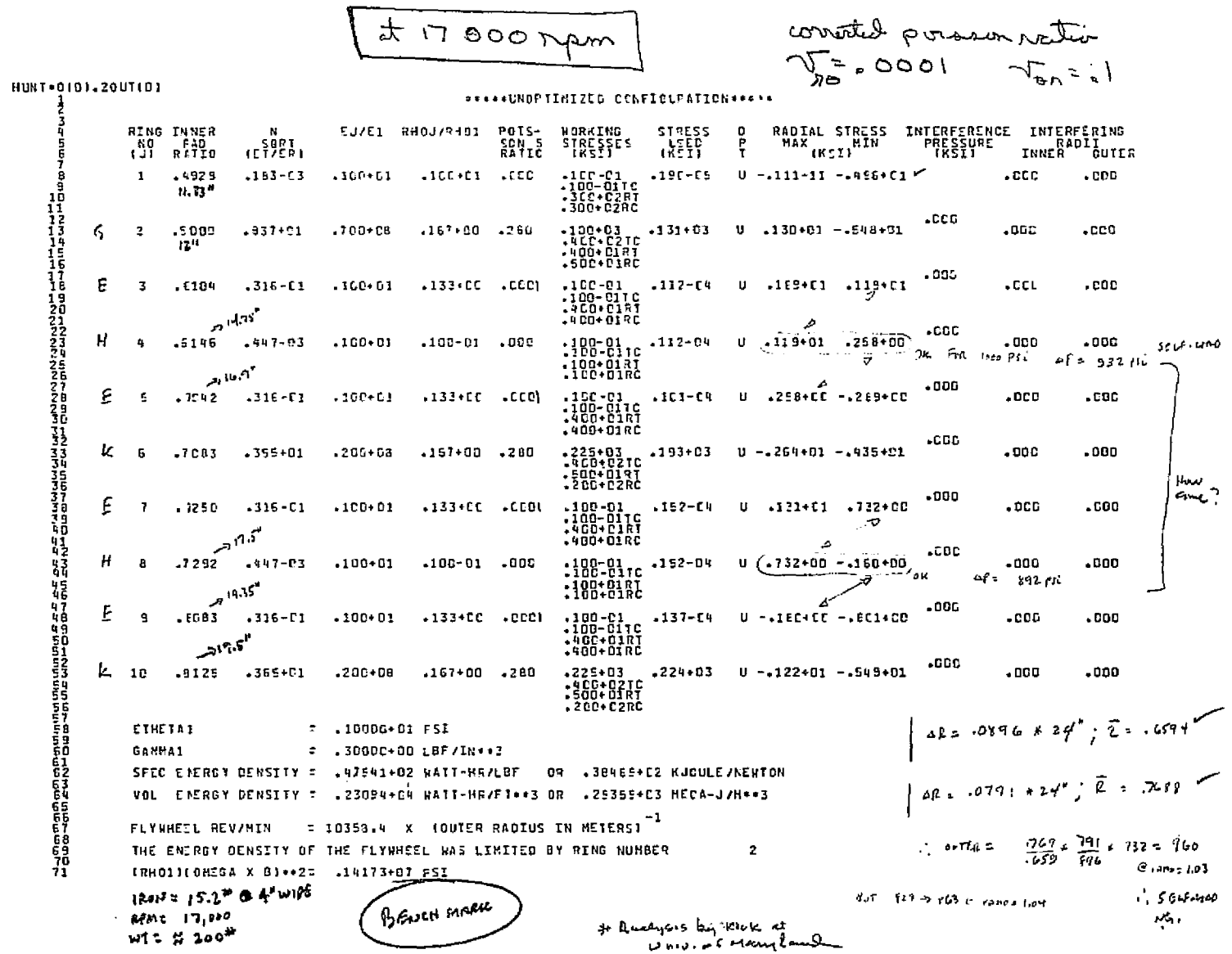

HUNT*D(0).20UT(0)

*****UNOPTIMIZED CONFIGURATION*****

	RING NO (J)	INNER RAD RATIO	N SQRT (E7/ER)	EJ/E1	RHOJ/RHO1	POISSON'S RATIO	WORKING STRESSES (KSI)	STRESS USED (KSI)	OPT	RADIAL STRESS MAX (KSI)	RADIAL STRESS MIN (KSI)	INTERFERENCE PRESSURE (KSI)	INTERFERING RADII INNER	INTERFERING RADII OUTER
	1	.4929	.183-03	.100+01	.100+01	.000	.100-01 .100-01TC .300+02RT .300+02RC	.190-05	U	-.111-11	-.998+01	.000	.000	.000
G	2	.5000	.937+01	.700+08	.167+00	.280	.100+03 .400+02TC .400+01RT .500+01RC	.131+03	U	.130+01	-.548+01	.000	.000	.000
E	3	.6184	.316-01	.100+01	.133+00	.000	.100-01 .100-01TC .400+01RT .400+01RC	.112-04	U	.189+01	.119+01	.000	.000	.000
H	4	.6146	.447-03	.100+01	.100-01	.000	.100-01 .100-01TC .100+01RT .100+01RC	.112-04	U	.119+01	.258+00	.000	.000	.000
E	5	.7042	.316-01	.100+01	.133+00	.000	.100-01 .100-01TC .400+01RT .400+01RC	.101-04	U	.258+00	-.269+00	.000	.000	.000
K	6	.7083	.355+01	.200+08	.167+00	.280	.225+03 .400+02TC .500+01RT .200+02RC	.193+03	U	-.264+01	-.435+01	.000	.000	.000
E	7	.7250	.316-01	.100+01	.133+00	.000	.100-01 .100-01TC .400+01RT .400+01RC	.152-04	U	.121+01	.732+00	.000	.000	.000
H	8	.7292	.447-03	.100+01	.100-01	.000	.100-01 .100-01TC .100+01RT .100+01RC	.152-04	U	.732+00	-.160+00	.000	.000	.000
E	9	.8083	.316-01	.100+01	.133+00	.000	.100-01 .100-01TC .400+01RT .400+01RC	.137-04	U	-.180+00	-.801+00	.000	.000	.000
K	10	.8125	.355+01	.200+08	.167+00	.280	.225+03 .400+02TC .500+01RT .200+02RC	.224+03	U	-.122+01	-.549+01	.000	.000	.000

ETHETA1 = .1000G+01 PSI

GAMMA1 = .3000C+00 LBF/IN**3

SPEC ENERGY DENSITY = .47541+02 WATT-HR/LBF OR .3846E+02 KJOULE/NEWTON

VOL ENERGY DENSITY = .23084+04 WATT-HR/FT**3 OR .2535E+03 MEGA-J/M**3

FLYWHEEL REV/MIN = 10358.4 X (OUTER RADIUS IN METERS)$^{-1}$

THE ENERGY DENSITY OF THE FLYWHEEL WAS LIMITED BY RING NUMBER 2

(RHO1)(OMEGA X B)**2= .14173+07 PSI

Figure A-9. Computer printout, NASA wheel – typical run.* (Sheet 1 of 3)

*Analysis by Kirk at University of Maryland

HUNT=0(01.20UTPLT(0)

1	1 RING	RADIUS	RAD STRESS	TANG STRESS
2	1	.1183+02	-.1106-08	.1098-02
3	1	.1198+02	-.4374+04	.1874-02
4	1	.1200+02	-.4960+04	.1870-02
5	2	.1200+02	-.4960+04	.1295+06
6	2	.1213+02	-.4186+04	.1245+06
7	2	.1220+02	-.3309+04	.1196+06
8	2	.1243+02	-.2686+04	.1153+06
9	2	.1250+02	-.2065+04	.1118+06
10	2	.1273+02	-.1515+04	.1088+06
11	2	.1288+02	-.1020+04	.1062+06
12	2	.1303+02	-.5975+03	.1041+06
13	2	.1318+02	-.2174+03	.1024+06
14	2	.1333+02	.1185+03	.1010+06
15	2	.1348+02	.4144+03	.9985+05
16	2	.1363+02	.6741+03	.9894+05
17	2	.1378+02	.9010+03	.9822+05
18	2	.1393+02	.1098+04	.9768+05
19	2	.1408+02	.1267+04	.9729+05
20	2	.1423+02	.1411+04	.9701+05
21	2	.1438+02	.1532+04	.9683+05
22	2	.1453+02	.1630+04	.9672+05
23	2	.1465+02	.1691+04	.9668+05
24	3	.1465+02	.1691+04	.1371-02
25	3	.1468+02	.1620+04	.5169-02
26	3	.1475+02	.1195+04	.1121-01
27	4	.1475+02	.1195+04	.1122-01
28	4	.1483+02	.1157+04	.1116-01
29	4	.1498+02	.1091+04	.1105-01
30	4	.1514+02	.1025+04	.1094-01
31	4	.1529+02	.9588+03	.1083-01
32	4	.1544+02	.8929+03	.1073-01
33	4	.1559+02	.8272+03	.1063-01
34	4	.1574+02	.7617+03	.1053-01
35	4	.1589+02	.6963+03	.1043-01
36	4	.1604+02	.6311+03	.1033-01
37	4	.1619+02	.5659+03	.1024-01
38	4	.1634+02	.5009+03	.1015-01
39	4	.1649+02	.4359+03	.1005-01
40	4	.1664+02	.3710+03	.9955-02
41	4	.1679+02	.3062+03	.9876-02
42	4	.1690+02	.2575+03	.9811-02
43	5	.1690+02	.2675+03	.9809-02
44	5	.1694+02	.4982+02	.1013-01
45	5	.1700+02	-.2095+03	.9663-02
46	6	.1700+02	-.2095+03	.1933+06
47	6	.1709+02	.9597+02	.1921+06
48	6	.1724+02	.7078+03	.1902+06
49	6	.1739+02	.1275+04	.1884+06
50	6	.1740+02	.1315+04	.1882+06
51	7	.1740+02	.1315+04	.9388-02
52	7	.1750+02	.7318+03	.1522-01
53	8	.1750+02	.7318+03	.1522-01
54	8	.1754+02	.7137+03	.1519-01
55	8	.1769+02	.6428+03	.1506-01
56	8	.1784+02	.5719+03	.1494-01
57	8	.1799+02	.5012+03	.1481-01
58	8	.1814+02	.4306+03	.1469-01
59	8	.1829+02	.3599+03	.1457-01
60	8	.1844+02	.2894+03	.1445-01
61	8	.1859+02	.2189+03	.1434-01
62	8	.1874+02	.1484+03	.1422-01
63	8	.1889+02	.7792+02	.1411-01
64	8	.1904+02	.7460+01	.1400-01
65	8	.1919+02	-.6300+02	.1389-01
66	8	.1934+02	-.1335+03	.1378-01
67	8	.1940+02	-.1602+03	.1374-01
68	9	.1940+02	-.1602+03	.1374-01
69	9	.1949+02	-.7527+03	.1148-01
70	9	.1950+02	-.8008+03	.1110-01
71	10	.1950+02	-.8008+03	.2234+06
72	10	.1964+02	-.3208+03	.2210+06
73	10	.1979+02	.1439+03	.2194+06
74	10	.1994+02	.5683+03	.2174+06
75	10	.2009+02	.9535+03	.2155+06

Figure A-9. Computer printout, NASA wheel - typical run.* (Sheet 2 of 3)

*Analysis by Kirk at University of Maryland

76	10	.2024+02	.1301+04	.2137+06
77	10	.2039+02	.1611+04	.2119+06
78	10	.2054+02	.1886+04	.2102+06
79	10	.2069+02	.2126+04	.2085+06
80	10	.2084+02	.2332+04	.2068+06
81	10	.2099+02	.2506+04	.2052+06
82	10	.2115+02	.2646+04	.2037+06
83	10	.2130+02	.2755+04	.2021+06
84	10	.2145+02	.2834+04	.2006+06
85	10	.2160+02	.2883+04	.1991+06
86	10	.2175+02	.2903+04	.1976+06
87	10	.2190+02	.2893+04	.1961+06
88	10	.2205+02	.2856+04	.1947+06
89	10	.2220+02	.2791+04	.1932+06
90	10	.2235+02	.2698+04	.1918+06
91	10	.2250+02	.2579+04	.1904+06
92	10	.2265+02	.2434+04	.1889+06
93	10	.2280+02	.2262+04	.1875+06
94	10	.2295+02	.2066+04	.1861+06
95	10	.2310+02	.1844+04	.1846+06
96	10	.2325+02	.1597+04	.1832+06
97	10	.2340+02	.1325+04	.1817+06
98	10	.2355+02	.1030+04	.1803+06
99	10	.2370+02	.7101+03	.1788+06
100	10	.2385+02	.3668+03	.1773+06
101	10	.2400+02	.7667-02	.1758+06

BRESUNE

Figure A-9. Computer printout, NASA wheel - typical run.* (Sheet 3 of 3).

*Analysis by Kirk at University of Maryland

TABLE A-1. WHEEL CONFIGURATIONS

Iron Wt. (Lb)	Wheel Wt. (Lb)	ID (in.)	Thickness (in.)	Radial Growth (in.)	Construction	RPM
15.2	500	12	10	0.008	I-G-R-H-R-K-R-H-R-K	11,000
15.2	200	12	4	0.019	I-G-R-H-R-K-R-H-R-K	17,000
16.0	263	13.4	4	0.040	I-G-K (prestress)	15,280
18.8	175	13.5	2.5	0.017	I-K (prestress)	18,900
9.2	526	12.1	3.6	0.035 (est)	I-G-K (prestress)	14,000
22	167	12.1	2.5	0.017	I-K (prestress)	19,600
15	370	12	4/8.5	0.01	I-G-H-K-H-K	12,000
15	209	12	4.1	0.02	I-G-H-K-H-K	17,000
30	308	12	5.5	0.02	I-G-H-K-H-K	14,300
15.2	208	12	4	0.022	I-G-R-H-K-R-H-K	17,000
22.5	330	12	5.7	0.021	I-G-R-H-K-R-H-K	13,800
45	227	12	4	0.12	I-K-R-H-K	17,000
0	203	12.5	4.3	0.02	I-G-R-H-K-R-H-K	17,000
20	270	12.5	5.1	0.031	I-G-R-H-K-R-H-K	15,000
39.9	362	12.5	6.5	0.037	I-G-R-H-K-R-H-K	13,300
0	199	11.5	4.2	0.018	I-G-R-H-K-R-H-K	17,000
20	250	11.5	4.5	0.02	I-G-R-H-K-R-H-K	16,000
40	320	11.5	5.5	0.02	I-G-R-H-K-R-H-K	14,500
0	197	13.5	4.1	0.025	I-G-R-H-K-R-H-K	17,000
39.6	400	13.5	7	0.023	I-G-R-H-K-R-H-K	12,900

Notes: I: Iron
G: Graphite
R: Elastomer
H: Honeycomb
K: Kevlar

Working Stress:
All wheels: 48 in. O.D. 10 kWh
Kevlar = 225 ksi
Honeycomb = 500 psi (1100 ksi)
Graphite = 120 ksi

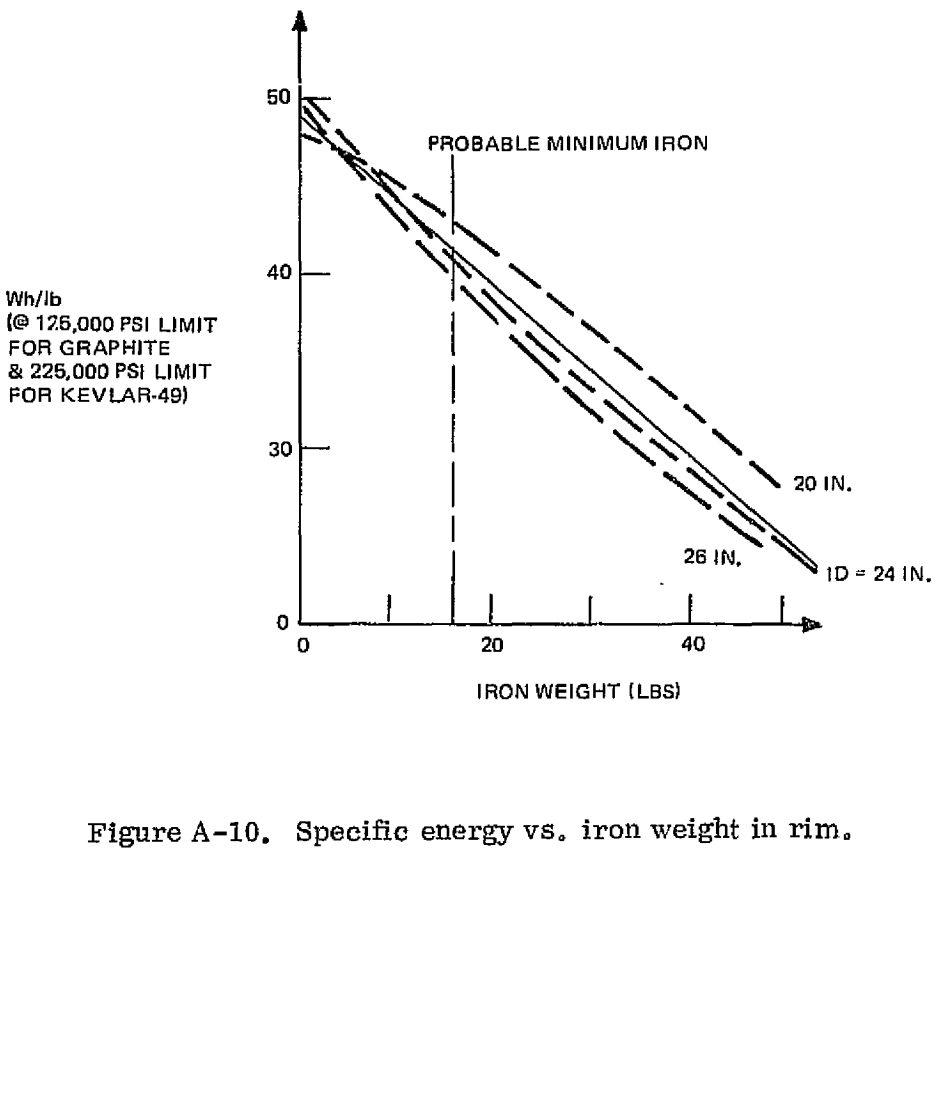

Figure A-10. Specific energy vs. iron weight in rim.

APPENDIX B

SUSPENSION SUBSYSTEM

Appendix B

SUSPENSION SUBSYSTEM

This section presents the design rationale, tradeoffs, servo design, and design details for the suspension subsystem, the self-contained system that supports the rotor from zero to full speed for any specified motor-generator power.

The subsystem design resulted from logical consideration of elementary factors and various tradeoffs.

A. DESIGN RATIONALE

The design rationale has been to achieve the desired performance with low loss and high reliability. To this end, system-level tradeoff studies were conducted, starting the treatment of each topic from a very general viewpoint. Based upon these tradeoff studies and SOW-specified axis bearing stiffness, the five servo loop designs are presented.

Finally, design details of the suspension subsystem are given.

B. TRADEOFFS

1. Basic Bearing Choice

Before pursuing the magnetic bearing design, it is instructive to undertake a general overview.

The ring shaped rotor, conceptually simple and efficient in utilizing stressed fiber, is the basic approach followed in this study. Compromises with this design evolved and comprise a large portion of this report.

The full spectrum of bearings listed below can be considered:

- Roller
- Ball
- Hydrostatic (liquid, gas)
- Magnetic
- Electrostatic

The listing is roughly in order of stiffness or local pressure. Two factors weigh against the use of roller or ball bearings; the high centrifugal stress in the shaftless rim-only design, and the need for very low ambient pressure to reduce windage losses. The latter factor also rules out hydrostatic bearings. Thus, one quickly arrives at the last two alternatives and these are easily separated by a consideration of properties of materials. The maximum flux density allows a magnetostatic pressure that exceeds the electrostatic pressure obtainable with the highest work function material by roughly two orders of magnitude. The electrostatic system is attractive for requiring the least additional rim weight, but the need for very high vacuum, excessively large bearing area, and pure metal surface conditions rule it out.

2. Wheel Orientation

a. General

Safety considerations and site-development costs require mounting the wheel with the spin axis along the local vertical. This is also preferred from the suspension standpoint, since radial magnetic field symmetry is preserved, thereby minimizing hysteresis and eddy-current losses.

The wheel, mounted on the spinning earth, is precessed in inertial space, requiring a steady torque input to achieve the precession. This can be eliminated by utilizing an equatorial mount, with the spin axis parallel to the earth's axis if required.

This effect has been analyzed in an idealized manner and is presented in the following paragraphs, where it is shown that the precession bearing force at the equator for a local vertical mount is manageably small.

b. Gyroscopic Effect

An energy wheel with the spin axis parallel to local zenith provides the most efficient arrangement for bearing the wheel weight. However, with this configuration, the gyroscopic torque due to earth's rate must be considered.

The energy storage is:

$$E = \frac{1}{2} J\omega^2, \qquad \text{(B-1)}$$

where

J = inertia,

ω = wheel speed

or

$$J = \frac{2E}{\omega 2} \tag{B-2}$$

For a tangential stress-limited rim speed,

$$r\omega = V \tag{B-3}$$

Substituting into Equation (2)

$$J = \frac{2Er^2}{V^2} \tag{B-4}$$

It is tacitly assumed that r presents both the radius of gyration and maximum radius; i. e. , a thin shell.

Since

$$H = J\omega \tag{B-5}$$

$$H = \frac{2Er}{V} \qquad (H = \text{momentum}) \tag{B-6}$$

The gyroscopic torque is:

$$\overline{T} = \overline{\omega_o} \times \overline{H} \tag{B-7}$$

where

$\overline{\omega_o}$ = earth's rate.

At the equator, the torque is

$$T = \omega_o H \tag{B-8}$$

And the counteracting bearing torque is

$$T = 2rF$$

where F is bearing force.

Solving for F,

$$F = \frac{E\omega_o}{V} \tag{B-9}$$

The gyroscopic bearing force is independent of rim radius.

The maximum surface speed, V, is related to maximum stress and density by:

$$V = \sqrt{\frac{\sigma_{max}}{\gamma}}\, g \qquad \text{(B-10)}$$

or

$$F = \frac{E\omega_o}{\sqrt{\frac{\sigma_{max}}{\gamma}}\, g} \qquad \text{(B-11)}$$

For

$$E = 3.6 \times 10^7 \text{ joules (10 kW-hr)}$$

$$\omega_o = 7.27 \times 10^{-5} \text{ rad/sec (1 r/24 hrs)}$$

$$\frac{\sigma_{max}}{\gamma} = 1.143 \times 10^5 \text{ m (Kevlar)}$$

$$g = 9.804 \text{ m/s}^2$$

$$F = 2.47 \text{ newtons (0.555 lbf)}$$

Even if the stress were 1/4 and the bearing radius 1/2 the rim radius, the force would be only 9.88 newtons (2.22 lbf).

The East-West torque that must be generated in opposition will cause an I^2R loss and, by virtue of the non-uniform flux density, eddy-current and hysteresis losses as well. These will be quite small, however. Alternatively, a Virtual Zero Power (VZP) control mode may be utilized, allowing the rotor to cock slightly to generate the correction torque without losses.

To calculate this effect, assume that the geometry is such that the force given by Equation (B-9) is doubled. Then the torque is:

$$T = 2\,(rF) = 2\,(2 \times 0.6096 \times 2.47) = 6.02 \text{ N}\cdot\text{m}$$

From the orientation loop study of Paragraph C.1, the spring constant due to the permanent magnets is:

$$4.84 \times 10^5 \text{ N}\cdot\text{m/rad}$$

Therefore, in a VZP mode, the rotor will deflect:

$$\frac{6.02}{4.84 \times 10^5} = 12.4\ \mu\text{rad}$$

At the bearing, the gap change will be a negligibly small 3.8 μm.

Thus, precession torque can be easily taken care of by a conventional displacement loop with small (but uncalculated) losses or by a VZP loop with no losses and slight tilt. Also, the effect decreases with the cosine of latitude.

3. Bearing Angle

The Mechanical Capacitor will be mounted as shown in Figure B-1. The spinning portion of the bearing, a partial cone, was chosen to more easily accommodate the increase in radial displacement with speed. This is readily done by axial movement of the stationary portion of the bearing. This configuration rules out serrated passive bearings. Another factor in this decision was losses from field discontinuties. A conventional active radial, passive axial, arrangement would have required segmented stationary bearings to accommodate the inner wheel radius change with speed. The discontinuties caused by the segmentation would have produced appreciable eddy-current and hysteresis losses.

Having thus chosen the basic geometry of Figure B-1, this analysis addresses the choice of the bearing slant angle.

An attractive system is assumed with ferrite or steel laminations for the rim mounted magnetic keeper. Figure B-2 is a cross-sectional view showing the forces acting. The bias force, F, must be chosen large enough so that in the presence of wheel weight and disturbances, the bearing force does not reach zero. Bearing forces in an attractive system are unidirectional (tensile). Only the magnitude can be changed.

With gravity and a horizontal disturbance force acting, the forces are as shown in Figure B-2(b).

Summing forces and moments:

$$\Sigma Fx \quad F_1 - F_3 + F_2 - F_4 = \frac{W}{\cos \alpha} \tag{B-12}$$

$$\Sigma Fy \quad F_1 + F_3 - F_2 - F_4 = \frac{\pi/2\ F_H}{\sin \alpha} \tag{B-13}$$

$$\Sigma M \quad F_1 + F_3 + F_2 + F_4 = 0 \tag{B-14}$$

(The factor $\pi/2$ in Equation (B-13) is discussed later.)

These three equations (B-12, B-13, B-14) can be solved for the four variables only if a bias value is assigned.

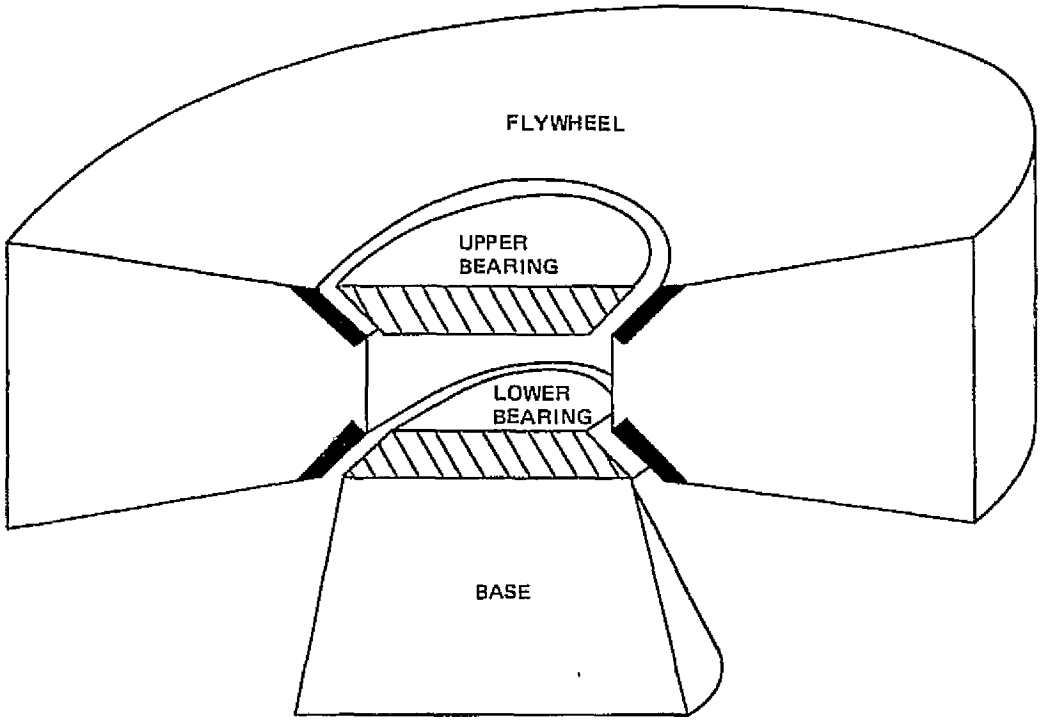

NOTE: TOP FIXED BEARING IS MOVED VERTICALLY TO MAINTAIN CONSTANT GAP AS RADIUS VARIES WITH SPEED AND AXIAL LENGTH WITH POISSON'S RATIO

Figure B-1. Mechanical Capacitor mounting.

The criterion for choosing the angle a is to minimize the difference in the largest and smallest forces. This also minimizes the bias force and minimizes the bearing weight-power product.

It can be seen from Figure B-2 that F_1 will be the maximum force and F_4 the minimum.

Adding Equations (B-12 and B-13):

$$\Delta F = F_1 - F_4 = \frac{1}{2}\left(\frac{W}{\cos a} + \frac{\pi/2\ F_H}{\sin a}\right) \qquad \text{(B-15)}$$

In the presence of both horizontal and vertical external forces, ΔF approaches ∞ as a approaches 0 or $\pi/2$.

Differentiating Equation (B-15) to find the value of a that minimizes ΔF:

$$a = \tan^{-1}\left(\frac{\pi/2\ F_H}{W}\right)^{1/3} \qquad \text{(B-16)}$$

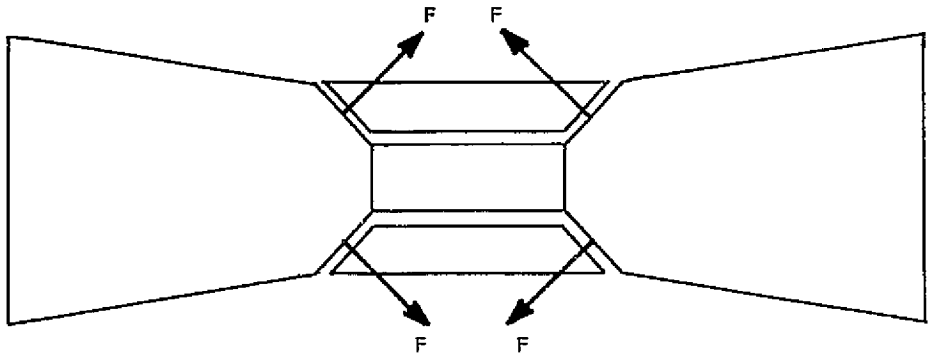

(a) BIAS FORCE, F, WITH GRAVITATIONAL AND OTHER FORCES ZERO.

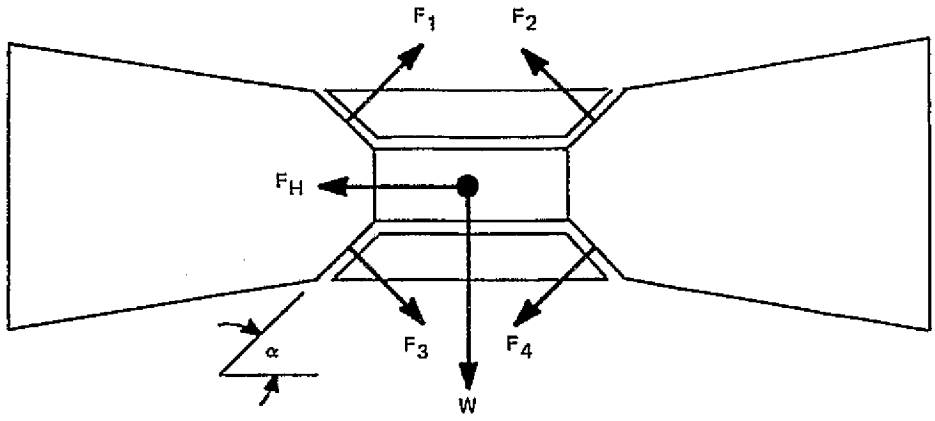

(b) VERTICAL (WEIGHT) AND HORIZONTAL FORCES PRESENT

Figure B-2. Cross-section of bearing.

Substituting back into Equation (B-15), the minimum force difference is:

$$\Delta F_{min} = \frac{W}{2}\left[1 + \left(\frac{\pi/2\ F_H}{W}\right)^{2/3}\right]^{3/2} \qquad \text{(B-17)}$$

If, for example,

$W = 90.8$ Kg (200 lbs)

$F_H = 3.6$ Kg (8 lbs)

$F/W = 0.04$

and from Equation (B-16)

$\alpha = 21.7°$

and from Equation (B-17)

$F_{min} = 45.4\ (1.246) = 56.6$ Kg (124.5 lb)

Thus, a horizontal force which is 4% of the weight causes a 25% increase in the bearing force difference.

Figure B-3 shows the reason for the factor $\pi/2$ in Equation (B-13). As can be seen, a rather ideal bearing arrangement has been chosen. However, for continuous bearing structures with versatile, multiple winding switching, and adequate gap sensing, this configuration can be approached. The analysis is easily modified for different bearing geometry.

The angle α has been chosen as 25 degrees, in lieu of definitive horizontal seismic data, which is a function of geography.

Finally, it should be noted that this angle can be chosen independently of desired axis spring constants (operating actively in a position loop - not VZP), which can be separately controlled by judicious gain assignments for the various control loops.

4. Active or Passive Suspension

The proposed system is active in all five degrees of freedom, requiring a sensor and servo loop for each, although electromagnets are shared.

An active system was chosen for several reasons. For one, it represents a conservative approach with positive control in each loop; this is especially important when motor generator currents are large. The passive bearing performance is a matter of geometry and hence, for a given design, fixed; it lacks flexibility and may be incapable of handling rotor structural model effects.

I. ZERO SIDE FORCE

(a) BEARING FORCE DISTRIBUTION

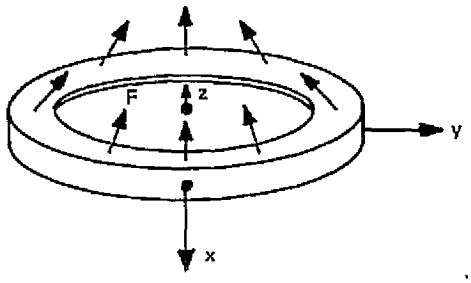

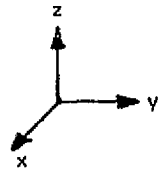

F IS UNIT FORCE (TENSILE PRESSURE), EQUALLY DISTRIBUTED ABOUT CIRCUMFERENCE AND NORMAL TO SURFACE.

(b) TOP VIEW

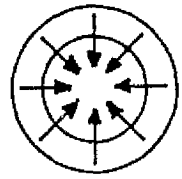

FORCE PROJECTION IN X-Y PLANE RESULTANT = 0

II. FINITE SIDE FORCE

UNIT FORCE, F, IS UNIFORMLY INCREASED TO LEFT OF x AXIS AND UNIFORMLY DECREASED TO THE RIGHT OF THE x AXIS.

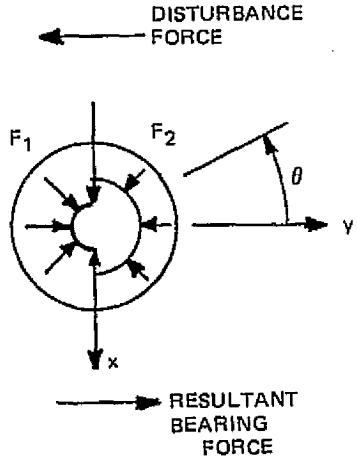

IT IS OBVIOUS THAT THE AVERAGE FORCE IN THE y DIRECTION IS:

$$F_{av} = \frac{1}{\pi}\int_{-\frac{\pi}{2}}^{\frac{\pi}{2}} (F_1 - F_2)\,\mathrm{SIN}\,\alpha\, d\theta = \frac{2}{\pi}(F_1 - F_2)\,\mathrm{SIN}\,\alpha$$

WHERE α IS THE ANGLE BETWEEN THE FORCE AND THE x-y PLANE.

Figure B-3. Side force resolution.

It would be difficult to maintain bearing stiffness with wheel growth, since this changes the geometry. Passive damping is very difficult to achieve, whereas active damping is readily obtained and easily changed by electronic compensation. The stiffness of a passive bearing is fixed and once designed and built cannot be changed; the stiffness of an active loop, which can easily be made to exceed that of a passive passive one by very large factors, is readily adjustable.

For the above reasons, an all-active suspension system was chosen.

5. Sensor Configuration

With 5 degrees of freedom (DOF) (rotation about the spin axis is controlled by the motor), 5 independent measurements must be made to determine the rotor displacement and orientation.

A single sensor failure must not cause bearing failure. Thus, redundancy is needed to detect sensor failure and provide adequate information to avoid bearing failure. This basic design feature has a strong influence on sensor configuration. Two sensor configurations have been examined.

Figure B-4(a) shows 6 sensors placed symmetrically on the lower bearing cone, each directed normal to the surface. In the event of failure of one, 5 independent measurements remain to establish rotor displacement and orientation. This configuration has the advantage of requiring the least number of sensors. However, it is intuitively obvious that the signal processing is complex and sensitivity to displacements in the xy plane is low. This latter fact is of importance only to the extent that sensor noise constrains the gain-bandwidth product.

A second approach, that trades signal processing complexity for additional sensors, is illustrated in Figure B-4(b). Four sensors, symmetrically placed about the cone, are directed normal to the surface, as before. These are used to determine spin axis tilt (2 DOF) and vertical displacement (1 DOF). The 4 sensors thus have one redundant piece of information. Four additional sensors, symmetrically placed about the circumference and directed normal to the circumference in the xy plane, provide xy displacement information. With this arrangement, the radial rotor diameter change with speed comes into play, and an additional sensor is required for this information. Thus, in effect, only one sensor is redundant. Note that in the event of failure of one of these sensors, the operative diametrically opposed set provides the expansion information and hence allows the single quadrature sensor to still provide its axis displacement. The signal processing is obviously simpler and xy sensitivity greater than in the 6-sensor scheme discussed previously; however, two more sensors are required.

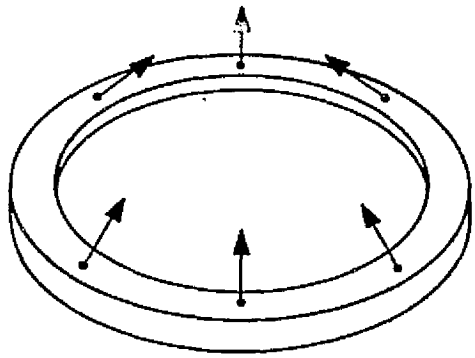

(a) 6 DISPLACEMENT SENSORS EQUALLY SPACED ON BEARING CIRCUMFERENCE, DIRECTED NORMAL TO CONICAL SURFACE

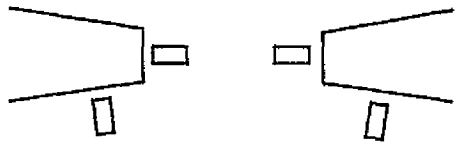

(b) 8 SENSORS
4 EQUALLY SPACED ABOUT CIRCUMFERENCE, DIRECTED NORMAL TO CONICAL SURFACE
4 SPACED THE SAME BUT DIRECTED RADIALLY

Figure B-4. Sensor placement configuration.

The configuration analysis considered the sensor arrangement from a broad DOF basis.

The various signals are processed and steered to finally control the bearing coils as shown in Figure B-5, providing the specified spring constants with adequate bandwidth. This, in essence, is the servo design presented in Paragraph C.

C. SERVO DESIGN

This subject is devoted to the closed loop control of the rotor. The rotor is assumed rigid in the frequency band of interest, applied torques are pure couples, and control forces (resultant force) act through the rotor center of mass. Thus, the only inter-axis effect is due to gyroscopic coupling. It is further assumed that the displacement and orientation error signals are free of axis crosstalk by virtue of ideal processing of the interactive sensor outputs.

For a fully active system, it follows from the assumptions that the three displacement control loops are independent of each other and of the two angular displacement loops; the latter two are coupled by gyroscopic action.

Major effort has been expended on the design of these two coupled loops. This design is independent of the chosen sensor configuration, whether 6 or 8 sensors.

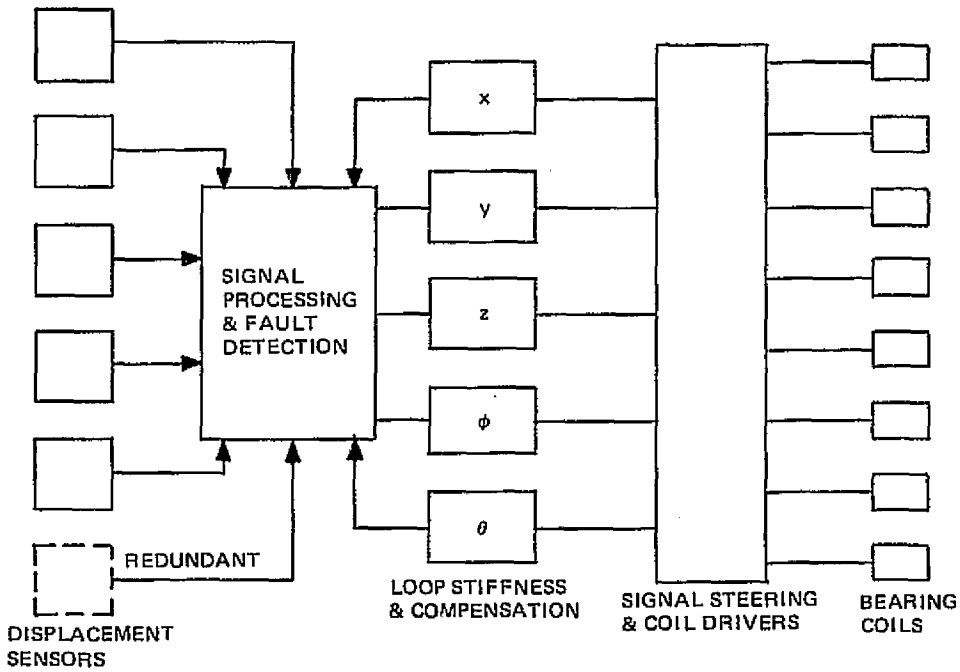

Figure B-5. Suspension system - block diagram.

Although Virtual Zero Power (VZP) control modes are discussed in this section, the following loop designs are all in terms of conventional displacement loops utilizing the surface sensors to measure displacement. VZP control loops can be employed utilizing velocity information derived from the same sensors. Although not investigated, if the sensor SNR is sufficiently high, velocity information over the bandwidth of interest can be obtained by suitable filtering to obtain stable VZP loops.

Figure B-5 is the overall block diagram for the suspension subsystem. Figure B-6 shows the geometry, sign convention, and how the coils are controlled, whereas Figure B-7 details how the error signals are mixed to achieve the desired control.

1. Angular Orientation

A block diagram of the angular orientation loops is shown in Figure B-8. Rotation about the x and y axes is coupled by the gyroscopic terms. A rotor angular displacement about the x-axis may be corrected by applying a torque about that same axis or about the y-axis, the latter method corresponding to processing an instrument gyro, for example. However, since the rotor must be stable in the magnetic bearing at start up (zero speed) as well as in its normal operating range of 50 to 100% speed, direct axis control must be utilized.

For zero rotor speed, Figure B-8 reduces to two identical uncoupled loops as shown in Figure B-9. The starting point for the design is evaluation of the negative spring constant due to the bias permanent magnets. In the Electromagnetic Design Subsection (Paragraph D), a vertical negative spring constant of 1.042×10^7 N/m (59,500 lb/in.) has been designed. In a Virtual Zero Power mode, twice the rotor weight - 1779 N (400 lb) will cause the rotor to rise:

$$\frac{1779}{1.042 \times 10^7} = 1.707 \times 10^{-4} \text{ m (6.7 mils).}$$

The lineal vertical spring constant must be converted to an angular spring constant. Consider Figure B-10, where a displacement θ will produce a negative torque that tends to increase θ. The bias permanent magnet is continuously distributed on the bearing circumference.

The lineal vertical spring constant per unit of circumference is:

$$K'_m = \frac{K_m}{2\ R}$$

where Km is the total rotor vertical spring constant.

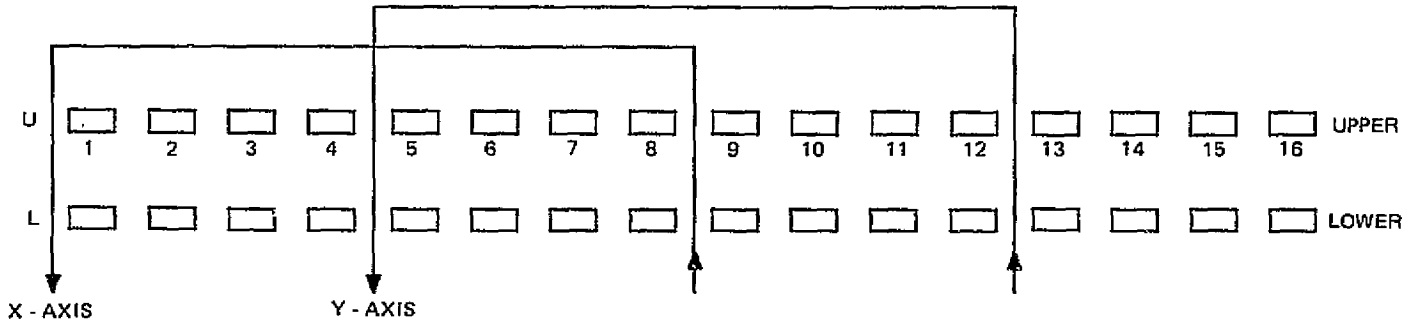

FORCE DIRECTION	BEARING ELEMENTS	
	INCREASE	DECREASE
x	(U+L) (13-4)	(U+L) (5-12)
y	(U+L) (1-8)	(U+L) (9-16)
z	U (1-16)	L (1-16)
TORQUE DIRECTION		
x ↷	L (9-16) U (1-9)	U (9-16) L (1-9)
y ↷	L (13-4) U (5-12)	U (13-4) L (5-12)

U = UPPER
L = LOWER

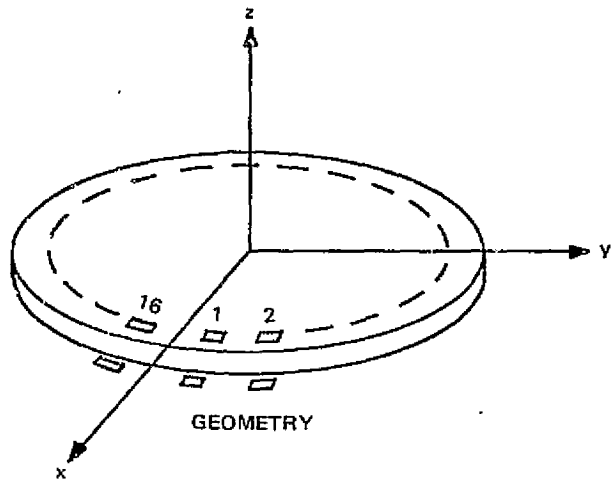

Figure B-6. Magnetic bearing control method.

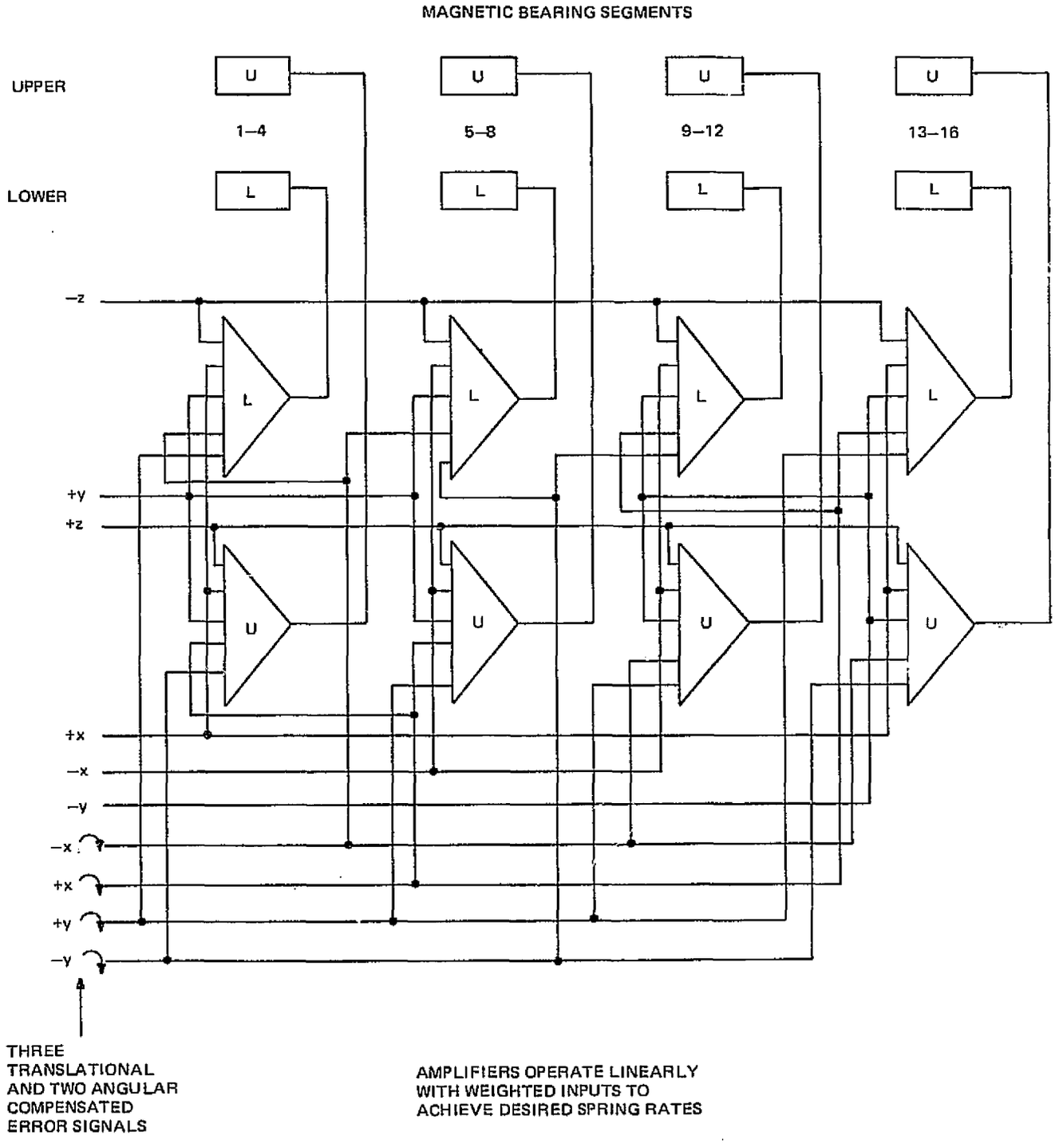

Figure B-7. Magnetic bearing amplifier and electromagnet arrangement.

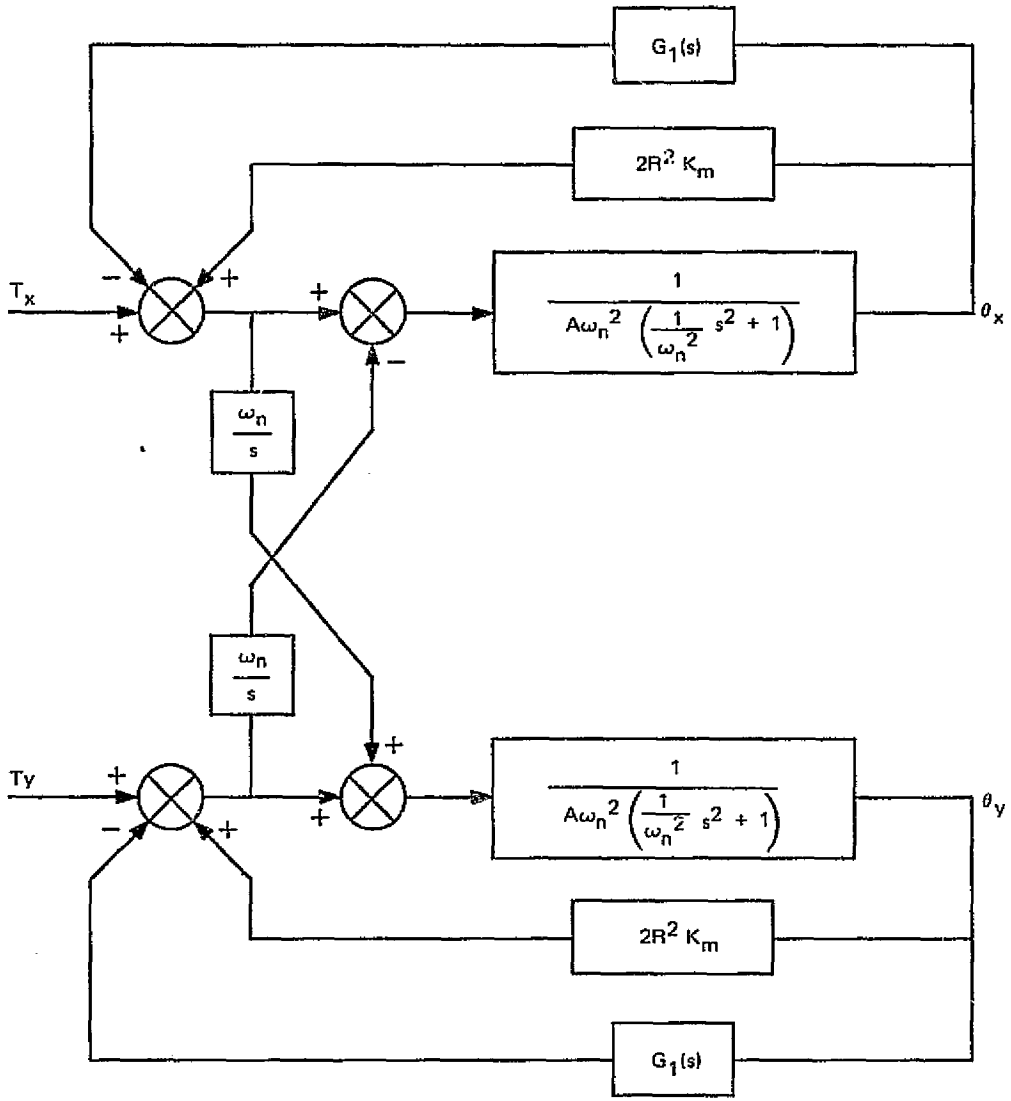

G_1 = GAIN AND COMPENSATION
R = BEARING RADIUS
K_m = PERMANENT MAGNET SPRING CONSTANT
A = ROTOR TRANSVERSE MOMENT OF INERTIA
ω_n = NUTATION FREQUENCY RADIANS/SEC. = 2 x ROTATIONAL FREQUENCY FOR WHEEL CONFIGURATION
T_x = TORQUE DISTURBANCE ABOUT x AXIS
θ_x = ANGULAR DISPLACEMENT ABOUT x AXIS

Figure B-8. Angular orientation control block diagram.

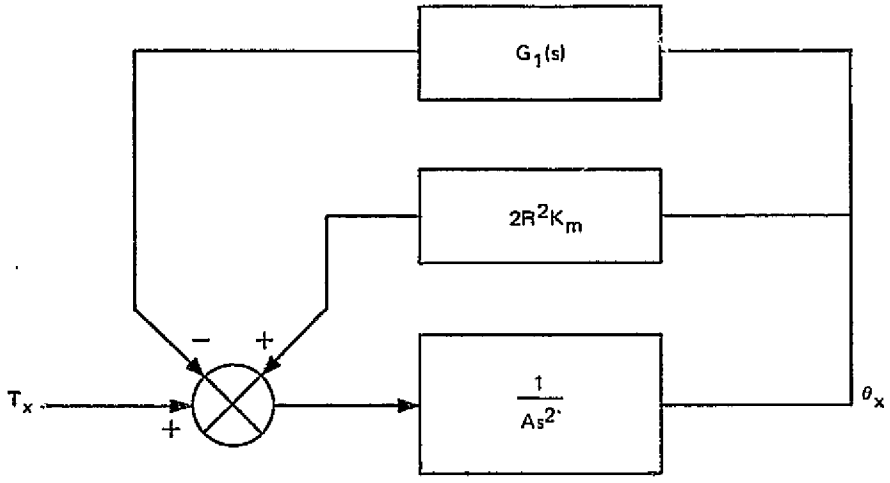

NOTE:

1. DERIVED FROM FIGURE B-8 BY LETTING $\omega_n = 0$
2. G_1 MUST BE DESIGNED TO PROVIDE ADEQUATE BEARING STIFFNESS AND STABILITY.

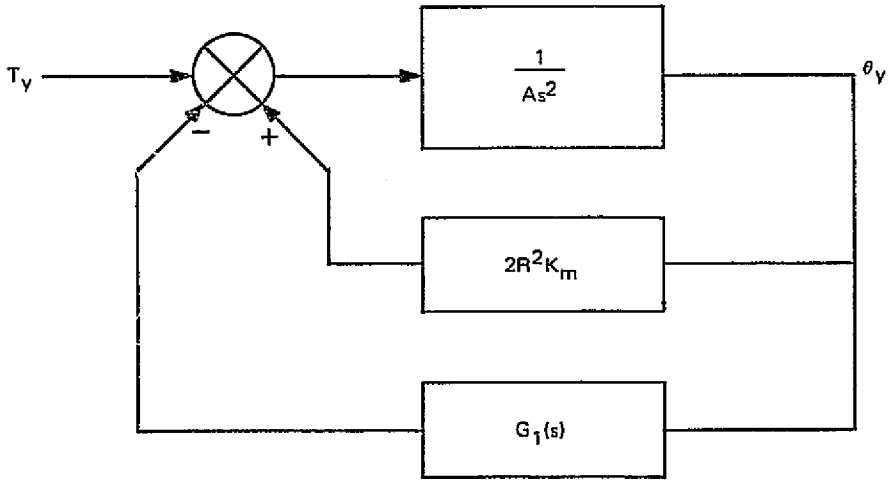

Figure B-9. Angular orientation control block diagram for zero rotor velocity.

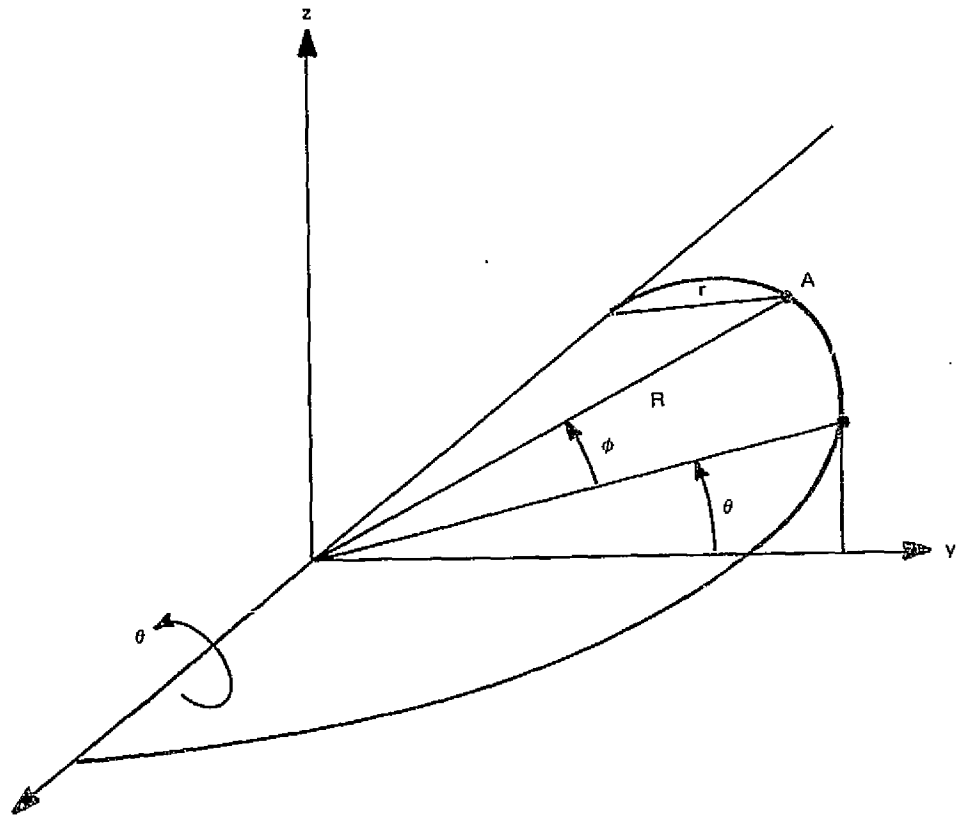

NOTES:

1. θ IS SPIN AXIS TILT ABOUT x AXIS
2. GAP CHANGE AT POINT A IS $r\theta$
3. DIFFERENTIAL FORCE $dF = (r\theta)\, K'_m\, R d\phi$

   $dT = r^2\, \theta\, K'_m R d\phi$
4. INTEGRATING FOR THE WHOLE ROTOR:

$$T = \frac{R}{2} K_m \theta$$

Figure B-10. Determination of tilt axis spring constant due to bias permanent magnets.

The vertical deflection at point A (perpendicular to the plane of the paper) is $r\theta$ and the differential force is:

$$dF = (r\theta)\, K_m' R d\phi$$

The torque is:

$$dT = r^2 \theta K_m' R d\phi$$

Since $r = R \cos\phi$

$$T = 4R^3 K_m' \theta \int_0^{\pi/2} \cos^2\phi d\phi \quad \text{(whole rotor)}$$

The result is

$$\frac{T}{\theta} = \frac{R}{2} K_m$$

For

$R = 0.3048$ m (12 in.)

$K_m = 1.042 \times 10^7$ N/m (59,500 lb/in.)

$\frac{R^2}{2} K_m = 4.863 \times 10^5$ Nm/rad (4.284×10^6 in. lb/rad)

With the negative angular spring rate determined, the identical x and y loops (for zero speed) can be designed as shown in Figure B-11, where the destabilizing positive feedback loop is counteracted by providing greater negative feedback with lead compensation for stable crossover.

$$G(s) = \frac{k_1 - a}{A} \times \frac{\frac{k_1 \tau_1 - a\tau_2}{k_1 - a} s + 1}{s^2 (\tau_2 s + 1)}$$

where

$$a = \frac{R^2}{2} K_m$$

In order to obtain a decade of lead compensation,

$$\frac{\tau_1}{\tau_2} = 10 - 9\frac{a}{k_1}$$

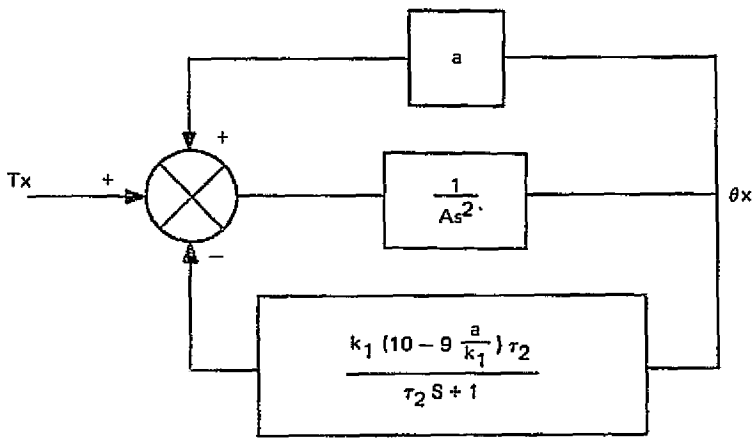

a. BLOCK DIAGRAM FOR EACH LOOP AT ZERO SPEED.

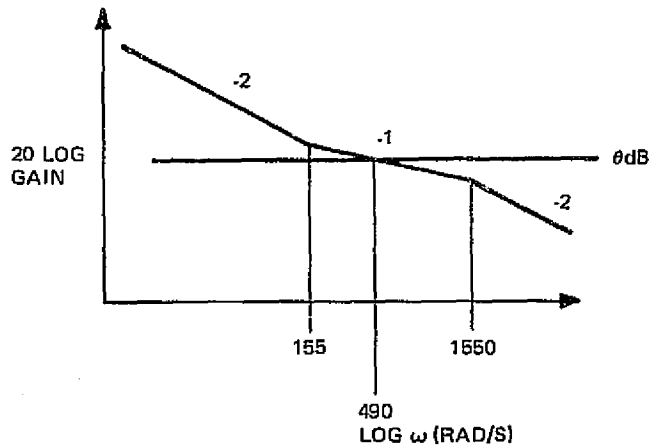

NOTES:

a = 4.863×10^5 Nm/RAD (4.284×10^6 IN. LB/RAD)
k_1 = 3a
A = 1.315m kgs^2 (114 IN. LBs^2)
τ_2 = 0.6452×10^{-3} S.

PHASE
MARGIN = 55°

b. BODE PLOT.

Figure B-11. Angular orientation control loop.

The active gain, k_1, must be large enough to overcome the destabilizing force gradient of the bearing permanent magnets, and any motor induced gradient as well (the motor destabilizing effect is predominantly radial) and still provide adequate static stiffness.

However, large values of gain, k_1, lead to large bandwidths and narrow linear range of bearing force versus displacement. The large bandwidth can be overcome by adding lag compensation, but at this point the added analytical complexity would obscure the underlying principles.

For $k_1 = 3a$, and choosing the lead break at 155 rad/s, the crossover is 490 rad/s with a phase margin of 55°. The Bode plot is shown in Figure B-11. The crossover frequency (79 Hz) seems high and could be reduced by additional lag compensation on a second design iteration.

The torsional (tilt) spring constant is simply $3a - a = 2a$

$2a = 9.726 \times 10^5$ Nm/rad (8.568×10^6 in. lb/rad)

Stability as a function of rotor speed is now considered. The x and y axis rotation loops have been identically compensated as described previously.

The open loop transfer function of the x axis loop with the y axis reflected into it via the gyroscopic coupling terms is shown in Figure B-12, where the block diagram reduction from the two coupled loops is shown. It is assumed that the y-axis external torque disturbance is zero.

The y-axis closed loop response is given by

$$\frac{G_7}{1 + G_7}$$

$$G_7 = \frac{2a}{A\omega_n^2} \times \frac{10\,\tau_2\, s + 1}{(\tau_2\, s + 1)\left(\frac{1}{\omega_n^2}\, s^2 + 1\right)}$$

$a = 4.863 \times 10^5$ Nm/rad (4.284×10^6 in. lb/rad)

$A = 1.315$ M Kg sec^2 (114 in. lb s^2)

$T_2 = 0.6452 \times 10^{-3}$ s.

ω_n = nutation frequency, rad/sec. = 1151.9

= 2 x rotor angular velocity

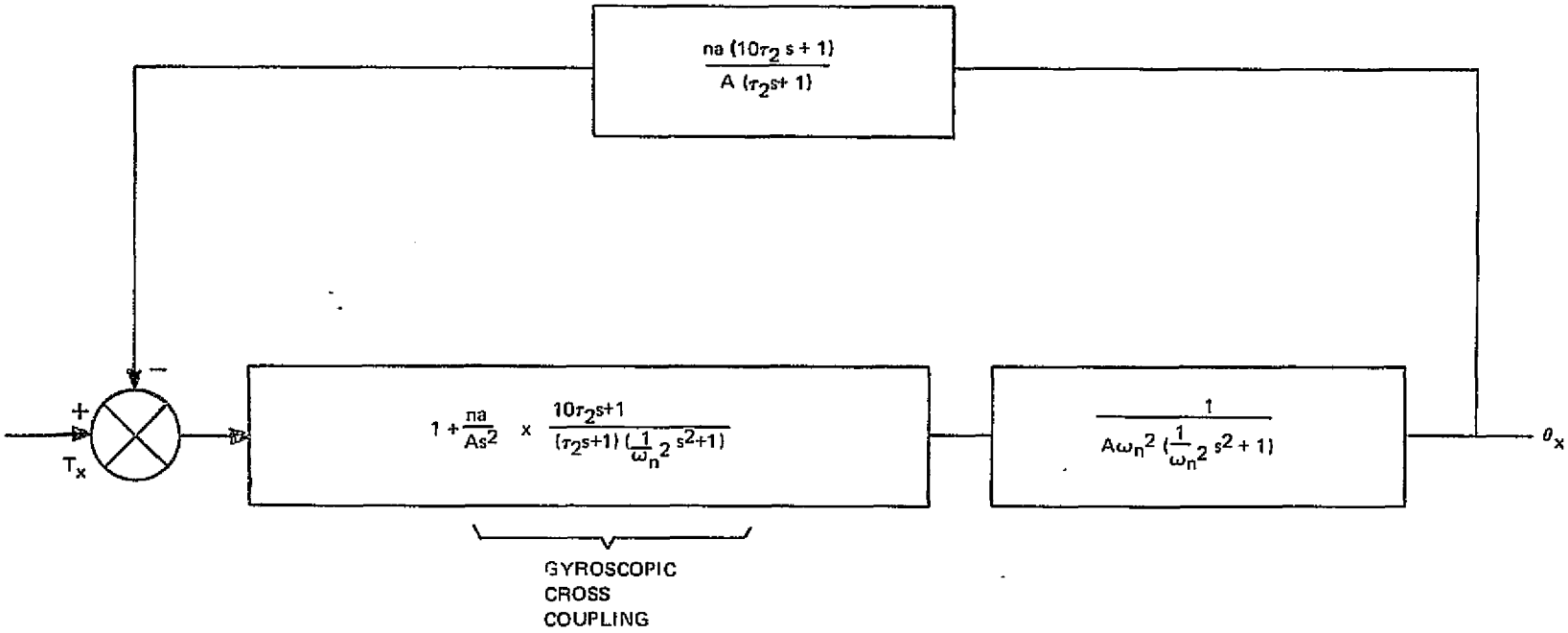

a = NEG. SPRING RATE (PM)
n = TOTAL STABLE GAIN NORMALIZED TO a; $n \geq 1$
A = ROTOR TRANSVERSE INERTIA
τ_2 = COMPENSATION LAG T.C.
$10\tau_2$ = COMPENSATION LEAD T.C.
ω_n = NUTATION FREQUENCY (TWICE ROTATIONAL FREQUENCY)

Figure B-12. Angular orientation control with y loop reflected into x loop.

A Routhe's test performed on the closed loop function,

$$1 + \left[1 + \frac{\omega_n^2}{s^2} \times \frac{G_7}{1 + G_7} \right] G_7$$

proved that it was stable for all finite values of ω_n.

The characteristic equation (in LaPlace transform notation) of the coupled loops is:

$$b^2 c^3 s^8 + 2\,bc^3 s^7 + c^2 [2\,b^2 (10\,d + 1) + c]\, s^6 + 2\,bc^2 (11\,d + 2)\, s^5 +$$

$$c\,[b^2 (10\,d + 1)^2 + 2\,c\,(d + 1)] s^4 + 2\,bc\,(10\,d^2 + 11\,d + 1)\, s^3 + [d^2 (100\,b^2 + c) +$$

$$c\,(2\,d + 1)]\, s^2 + 20\,d^2 b^2 s + d^2 = 0$$

The complex frequency, s, in the above equation has been transformed by a factor of 10^3 to obtain more convenient coefficient values.

Then

$$b = 10^3\, \tau_2 = 0.6452$$

$$d = \frac{10^{-6} \times 2a}{A\omega_n^2} = \frac{0.075158}{\omega_n^2}$$

$$c = \frac{1}{\omega_n^2}$$

Table B-1 shows the coefficients of this eighth order equation arranged in a Routhe array above the double line. The terms below that line have been developed according to the Routhe procedure.

For the closed-loop system represented by the above characteristic equation to be stable, all terms in the first column must have the same sign. The constants d and b are positive and c, inversely proportional to speed squared, is also positive.

By inspection, only the last term, R61, could be negative. When the design values for a and b given above are substituted into R61, the result is:

$$\frac{R61}{C^3} = 0.74755\, C^3 + 2.2919\, C^2 + 0.0045614\, C + 1$$

Thus

$$R61 > 0 \text{ for } C \geq 0$$

Therefore, the coupled orientation loops are stable for all rotor speeds.

TABLE B-1. ROUTHE STABILITY DEVELOPMENT

b^2c^3 R11	$c^2\ [2G^2\ (10d+1) + c]$ R12	$c\ [b^2(10d+1)^2 + 2c(d+1)]$ R13	$d^2\ (100b^2+c) + c(2d+1)$ R14	d^2 R15
$2bc^3$ R21	$2Gc^2\ (11d+2)$ R22	$2bc\ (10d^2+11d+1)$ R23	$20\ d^2b^2$ R24	
$c^2(9db^2+c)$ R31	$c[9db^2(10d+1) + 2c(d+1)]$ R32	$d^2(90b^2+c) + c(2d+1)$ R33	d^2 R34	
$c^2[b^2(10d+1) + c]$ R41	$c[b^2(10d^2+d+1) + c(d+1)]$ R42	$d(10db^2+c)$ R43		
$c[9d^2b^4(90d+19) + b^2c\ (91d^2+21d+1) + c^2(d+1)]$ R51	$90d^2b^4(9d+1) + b^2c\ (10d^3+92d^2+12d+1) + c^2(d^2+d+1)$ R52			
$9db^6(900d^3-620d^2-81d+9) + db^4c(1620d^2-458d-9) + b^2c^2(81d^2+20d+1) + c^3$ R61				

The closed-loop response (rated speed) yields a complex pole frequency 5% higher than the nutation frequency with a damping factor, δ, of 0.0178.

A potential problem with an all-active suspension is achieving nutation damping without resorting to a large bandwidth which has the disadvantages of lessening stability in the presence of structural modes and causing the bearing servo to waste power in attempting to correct for once-around disturbances.

A study of Figure B-8 shows that the steady state θ_x response to T_x at zero speed as well as at high speed is solely determined by the bearing gain. This is true because in each case integration exists in the forward loop, such that the steady-state net torque applied on the x-axis must be zero.

First cut, angular orientation loops have been designed that provide adequate stiffness and stability for all speeds. Design iterations are needed to perhaps lower the bandwidth and increase nutation damping, although these are most likely contradictory. Excessive nutational motion causes bearing losses, and might reduce machine efficiency or increase its weight if a portion of the air gap must be budgeted for it.

2. Axial Displacement Loop

The axial displacement loop, which is much simpler than the gyroscopically coupled angular orientation loops, must by specification "be capable of supporting twice the weight of the rotating assembly at 1g."

The permanent magnet vertical component of force gradient has been designed to be 1.042×10^{-7} N/m (59,500 lbs. per in.). In a Virtual Zero Power (VZP) mode, the rotor (at specified twice-weight - 1779 N (400 lb) - would rise 1.707×10^{-4} m (6.7 mils), an appropriately small value compared to the total gap.

Statically stabilizing active feedback must provide at least twice this value to achieve the same stiffness in the conventional manner (displacement sensing).

The block diagram is shown in Figure B-13. The active loop static gain is chosen to be twice the permanent magnet force gradient. Large values of gain entail high bandwidth and complex compensation and reduce the bearing dynamic displacement range as well.

The open-loop transfer function is:

$$G(s) = \frac{k_1 - K_m}{m} \times \frac{\frac{k_1 \tau_1 - \tau_2 K_m}{k_1 - K_m} s + 1}{s^2 (\tau_2 s + 1)} \qquad \text{(B-18)}$$

$k_1 = 2$ Km (by choice)

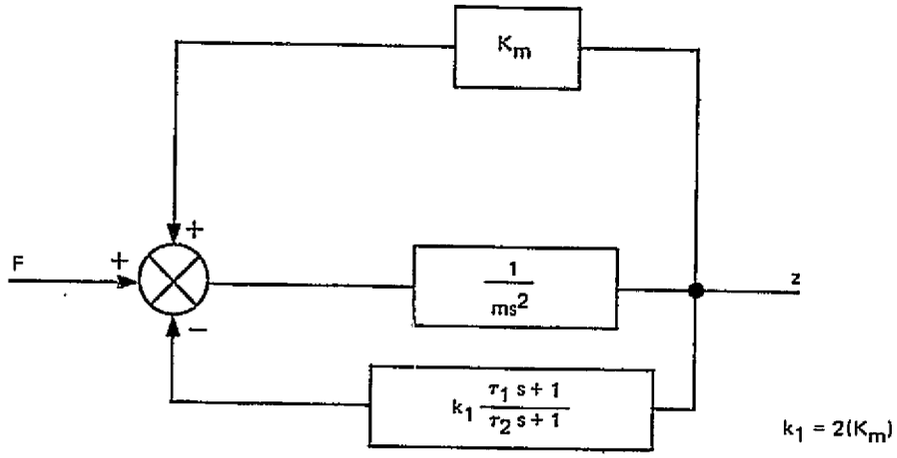

$K_m = 1.042 \times 10^7$ N/m (59,500 lb/in.)

$$m = \frac{w}{g} = \frac{889.6\ N}{9.807\ m/s^2} = 90.7 \frac{Ns^2}{m} \left(0.9067 \frac{lb\ s^2}{in.}\right)$$

(a) AXIAL LOOP BLOCK DIAGRAM

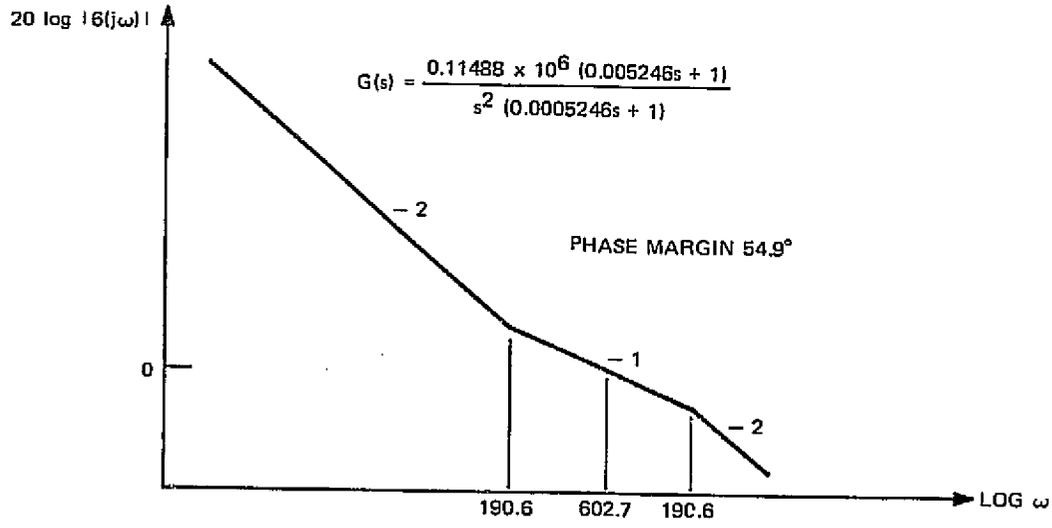

(b) BODE DIAGRAM

Figure B-13. Axial displacement loop data.

In order to obtain a decade of lead compensation:

$$\frac{k_1\tau_1 - \tau_2 K_m}{k_1 - K_m} = 10\ \tau_2$$

and for

$$k_1 = 2\ K_m$$

$$\tau_1 = 11/2\ \tau_2$$

$$G(s) = 0.11488 \times 10^6 \frac{10\tau_2\ s + 1}{s^2\ (\tau_2\ s + 1)}$$

Gain = 101.2 dB.

The Bode plot for this function is sketched in Figure B-13. The crossover frequency is 603 rad/s (96 Hz) with a phase margin of 54.9 degrees.

3. Radial Displacement Loops

These are identical control loops in the x and y directions. By specification, the radial stiffness must be at least 280,160 N/m (1600 lb/in.) and the damping at least 60% of critical.

The x (or y) component of negative spring constant due to the permanent magnets can be determined from the geometry of Figure B-14.

If K'_m is the circumferential spring constant (in the surface normal direction per unit angle, the normal force is a function of lateral displacement.

$$F_n = K'_m\ x \sin\alpha \cos\phi$$

The x component is:

$$dF_x = \sin\alpha \cos\phi\ dF_n$$

or

$$dF_x = K'_m\ x \sin^2\alpha \cos^2\phi\, d\phi$$

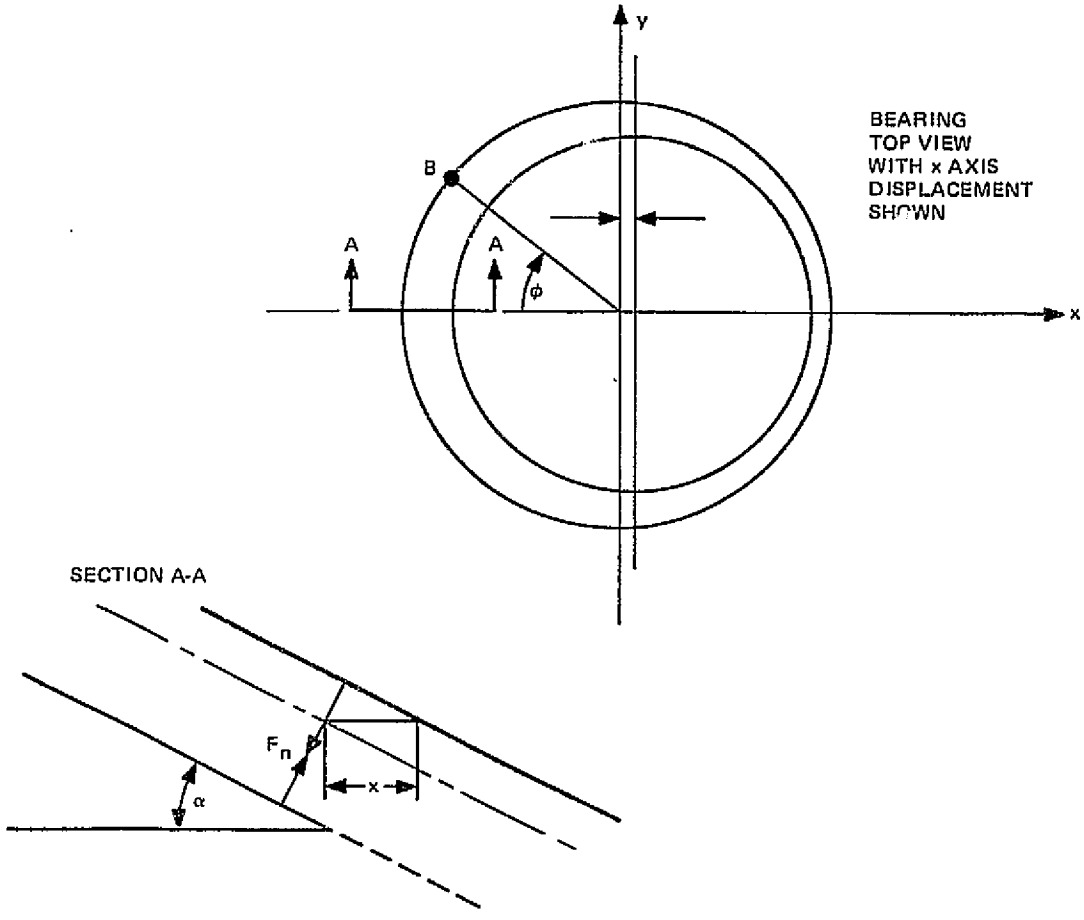

NOTES:

F_n = CHANGE IN NORMAL FORCE BETWEEN TWO BEARING SURFACES DUE TO LATERAL x DISPLACEMENT

K_m' = CIRCUMFERENTIAL SPRING CONSTANT IN THE SURFACE NORMAL DIRECTION

F_x = x COMPONENT OF NORMAL FORCE

ϕ = ANGLE THAT RADIUS TO POINT B (ON CIRCUMFERENCE) MAKES WITH x-AXIS

α = BEARING CONE ANGLE

Figure B-14. Derivation of lateral negative spring constant due to permanent magnets.

For all four quadrants, the total x-direction force is:

$$F_x = 4 K_m' x \sin^2 a \int_0^{\pi/2} \cos^2\phi d\phi$$

$$F_x = K_m' x \sin^2 a$$

Since

$$K_m' = \frac{K}{2\pi}$$

$$\frac{F_x}{x} = \frac{K_m}{2} \sin^2 a$$

For

$$\frac{K_m}{a} = 1.042 \times 10^7 \text{ N/m } (59,500 \text{ lb/in.})$$

$$a = 25°$$

$$\frac{F_x}{x} = 9.305 \times 10^5 \text{ N/m } (5313.5 \text{ lb/in.})$$

An additional spring constant must be added to account for the motor-generator permanent-magnet field, the value of which has yet to be determined.

The negative spring constant given exceeds the specified value so that adequate performance would result if VZP control were employed.

For a normal active displacement-measuring system, gain and compensation is designed to provide a stable loop that meets the spring constant and damping specifications. This loop is more easily designed to have a lower bandwidth than the other loops because of the smaller permanent-magnet spring constant.

The negative spring constant value due to the motor and the axes on which it appears depends upon the motor configuration finally chosen. At this point, it is assumed that the radial force gradient is half the bearing value.

Then the total negative spring constant is:

$$9.305 \times 10^5 (1.5) = 1.396 \times 10^6 \text{ N/m } (7970 \text{ lb/in.})$$

The x-axis displacement loop is identical in form to the axial loop described previously. Thus,

$$G(s) = \frac{k_1 - K_m}{m} x \frac{\frac{k_1 \tau_1 - \tau_2 K_m}{k_1 - K_m} s + 1}{s^2 (\tau_2 s + 1)}$$

Let $k_1 = 2 K_m$.

For a decade of lead compensation:

$$\frac{k_1 \tau_1 - \tau_2 K_m}{k_1 - K_m} = 10 \tau_2$$

$$K_m = 1.396 \times 10^6 \text{ N/m}$$

$$m = \frac{W}{2} = 90.7 \frac{\text{N sec}^2}{\text{M}} \quad (0.9067 \frac{\text{lb/s}}{\text{in.}})$$

$$G(s) = 15390^* \frac{10 \tau_2 s + 1}{s^2 (\tau_2 s + 1)}$$

$$\tau_2 = \frac{1}{\omega_2} = \frac{1}{697.6} = 1.433 \text{ ms.}$$

The crossover frequency is 220.6 rad/s (35.1 Hz) and the phase margin is 54.9 degrees. The closed-loop dominant quadratic pole has a damping factor of 0.96, well above the specified minimum value of 0.6.

The block diagram and Bode plot for these two identical radial displacement loops has the same form as given in Figure B-13 for the axial loop. Only the numerical values differ.

4. Summary

The servo parameters are summarized in Table B-2 for all loops. Determination of rotor vibrational modes in a hardware design may require different compensation to obtain bearing stiffness and response. The rather high crossover frequency (96 Hz) of the axial loop may need reduction, for example.

D. ELECTROMAGNETIC DESIGN

The wheel suspension is shown in sketch SK 2294234, sheets 1 and 2. Suspension is continuous around the inner rim of the wheel. The design vertical load (from the S.O.W) is twice the wheel weight. Horizontal inertial loading is not specified, but

*(83.75 dB)

TABLE B-2. SERVO LOOP PARAMETERS

Parameter	Angular Orientation (2 coupled loops)	Axial	Radial (2 uncoupled loops)
Perm Mag. Spring Constant	-4.863×10^5 Nm/rad	-1.042×10^7 N/m	-9.305×10^5 N/m
Motor Field Spring Constant	0	0	-4.653×10^5 N/m
Total Spring Constant, Active and Passive	9.726×10^5 Nm/rad	$+1.042 \times 10^7$ N/m	$+1.396 \times 10^6$ N/m
Loop Gain dB	97.5 (1)	101.2	83.75
Crossover Frequency rad/s	490 (1)	603	221
Phase Margin Deg.	55 (1)	54.9	54.9
Closed Loop Damping Factor	0.0178 (2)	0.96	0.96

(1) at zero speed

(2) at rated speed

is small in a horizontally disposed wheel, hence the bearing angle is small (refer to the subsection on Bearing Angle, Paragraph B. 3). Further, it is desired to have a small angle to minimize gap growth due to wheel growth with speed. Also, the inner rim is made of ultra-high-modulus graphite fiber ($E = 70 \times 10^6$ lb/in.^{2}) to reduce wheel diameter dilation.

The combination, then, of angle suspension and high-modulus fibers avoids the need for the axial adjustment of the magnetic bearing support structure originally proposed.

1. VZP Suspension

VZP or virtual zero suspension, a concept originated by NASA and proved in earlier magnetic suspension development programs, is assumed in the present wheel. The principle is as follows (Figure B-15):

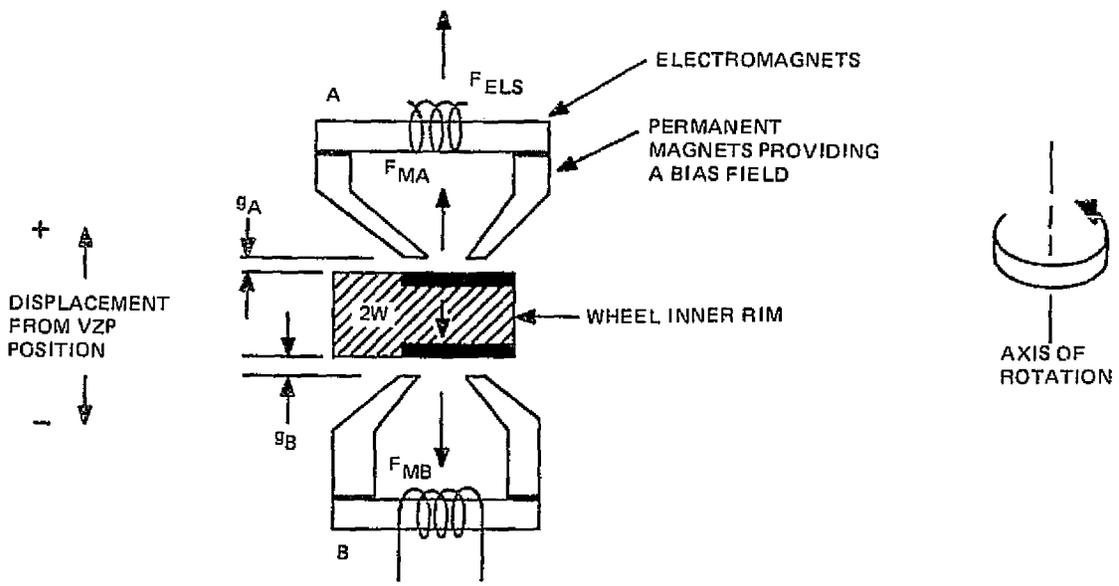

Figure B-15. VZP suspension.

If the two bias field magnets A and B are of equal strength, and gap g_A is greater than gap g_B, the magnet force F_{MA} will be larger than F_{MB}. If the unequal gaps are properly chosen, $F_{MA} - F_{MB} = 2$ W, and the wheel will be supported in a vertical position at a position of neutral stability without electromagnet-coil current. Displacements of the wheel from this position can be countered by varying electromagnet coil currents I_A and I_B in response to the control of the servo suspension loops.

Some basic assumptions have been made to limit the design study and to assign values to design variables, detailed in following paragraphs.

2. Gaps

The nominal gap is assumed to be ±0.030 in. and the allowed total wheel displacement is assumed to be 0.020 in. at the maximum wheel axial or radial excursion. The bias-magnet net attractive force is then at a maximum and is destabilizing. The electromagnet net servo force, F_{ELS}, must be: $F_{ELS} = -2\ W - F_{MB} + F_{MA}$ when the wheel is displaced downward to the full allowed displacement from the VZP position.

The mean diameter of suspension is assumed to be 26 in., based on the preliminary structural design of the wheel. The suspension system is not significantly affected by changes in diameter.

3. Electromagnets

The electromagnets are assumed to have a configuration arrived at during a 1975 IR&D program at RCA concerned with magnetic bearings, and for which there are simulation and test data for use in the current analyses. This configuration contains biased samarium cobalt ($SmCo_5$) magnets. Other configurations can be substituted, if they contain biased magnets, but will not change significantly the results of this design study.

4. Soft Magnetic Metals

Thin laminated glassy metals or compacted forms of carbonyl iron powder are assumed. Both exhibit low eddy current and hysteresis losses. The loss calculations are for glassy metals.

Suspension Electromagnet Sizing

The electromagnet is an assembly with a three-dimensional field structure. The energy contained in the external field, other than in the working gaps, is not

available and must be accounted for. The computation of the fields requires more effort than analogue modeling using Teledeltos paper and electric probes - a technique that is fast, inexpensive, and yields reasonable accuracy. The IR&D electromagnet configuration is shown in Figure B-16 and is scaled up, with minor changes, for the mechanical capacitor. The IR&D electromagnet was built and tested for the biased magnet force at 0.040 in. gap and for electromagnet force as a function of coil current. The test results (shown in Table B-3) are used in this study to determine force displacement curves for sizing purposes.

5. Capability of RCA Test Electromagnet

The residual bias attractive force at an 0.040 in. gap equals 6.5 lbs; a force displacement curve can be constructed from this value.

Gap area = 1.6 in.^{2} (10.32 cm^2)

Magnet area = 4 in.^{2} (25.8 cm^2)

$$R = \frac{L}{\mu A} = \frac{MMF}{\phi}$$

where

R = magnetic reluctance

μ = permeability

A = magnetic element cross section, in.^{2}

MMF= Magnetomotive force

ϕ = magnetic flux

Assume gaps of: 0, 0.02, 0.04, 0.06 and 0.08 in.

Determine: (1) Analogue model force curve for biased magnet.

(2) Test model forces for biased magnet

The test derived force vs. displacement for one 5-in. long electromagnet and the difference between two opposed electromagnets are plotted in Figure B-17. The test results will be used in this analysis because they reflect the effects of all fabrication factors that tend to reduce the ideal performance and yield conservative values.

At the maximum excursion of 0.020 in., the maximum destabilizing force due to the permanent magnets alone in the two opposed electromagnets is 27 - 4.5 = 22.5 per 5-in. length of electromagnet or 4.625 lb/in.

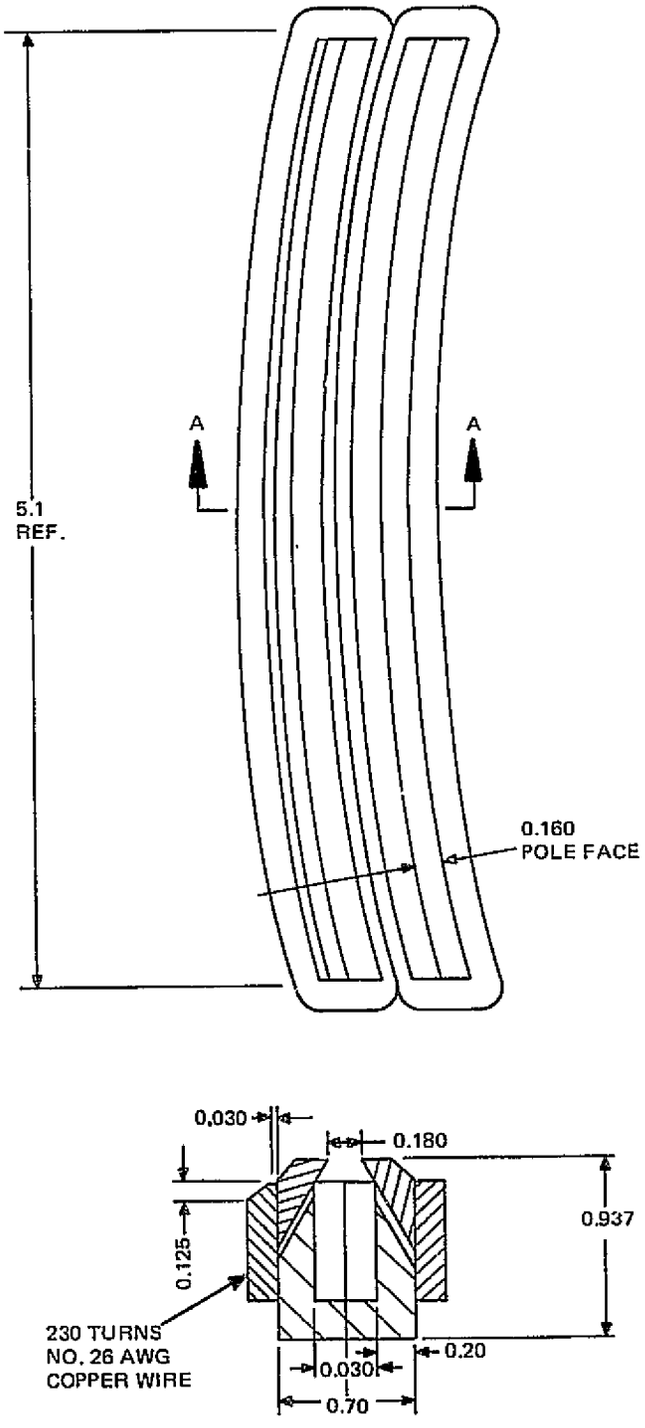

NOTE: ALL DIMENSIONS IN INCHES

Figure B-16. Biased electromagnet.

TABLE B-3. TEST ELECTROMAGNET AND ANALOGUE MODEL FORCE AND GAP FIELDS

	Gap, in./cm			
	0/0	0.02/0.051	.04/0.10	0.06/0.015
R, gap	0	0.005	0.0096	0.0145
R, magnet	.1016/.2616	→	→	→
R, * total	0.0039	0.0089	0.01350	0.0184
B, Kilogauss	11.26	5.70	3.68	2.70K***
(Analogue model) Force, lbs = .577 B^2A	117.04	29.99	12.37	6.73
B (Derived from test) Kilogauss	8.15	4.12	2.65	1.95
Force in lbs Derived from test	61.48	15.71	6.5**	3.52

*Reluctance of the soft metal elements of the circuit are assumed to be zero.

**Single test value from test electromagnet.

***Measured on analogue model

6. Electromagnets for Mechanical Capacitor

Assume: Suspension ring diameter of 26 in.

Wheel weight of 200 lbs

Specification weight of 2 x 200 or 400 lbs

a. Case A - VZP Position

For a 25-degree suspension angle and an assumed upper gap of 0.010 in.,

net passive force = $\frac{2W}{\text{Cos } 25^\circ}$ = 442 lbs

Force (lbs/in.) = $\frac{442}{\pi \times 26}$ = 5.41

The test electromagnet can be scaled up by a factor of 5.41/4.625 or 1.16 to provide the forces.

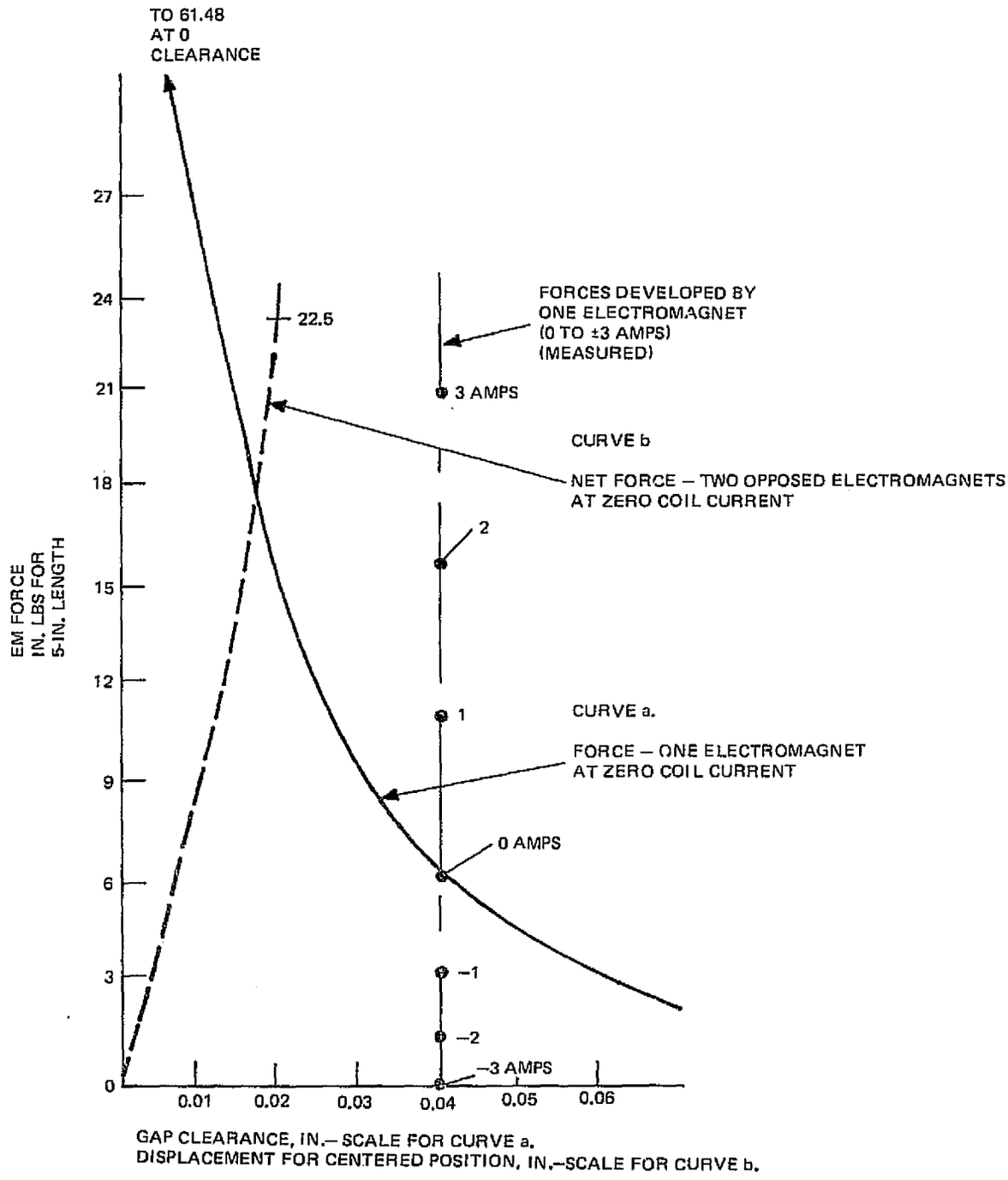

Figure B-17. Electromagnet passive and active forces.

b. Case B - Maximum Negative (Downward) Displacement of Wheel

Upper gap = 0.05 in. (approximately)

Lower gap = 0.01 in. (approximately)

The powered electromagnets must be able to apply a force equal to electromagnet zero current unbalance force + 2 W. From Figure B-17, a single electromagnet sensitivity is equal to approximately 4.83 lb/amp.

At 0.05 in. gap, assuming the EM force vs. current varies as the passive magnet force curve, the sensitivity equals 4.5/6.5 x 4.83 or 3.34 lbs/amp. With a full +3 amps in the upper electromagnet (EM) coil and -3 amps in the lower EM coil, the maximum net force equals:

$$4.5 \text{ (EM)} + 3 \times 3.34 \text{ (EM)} + 3 \times 0 \text{ (EM)}^* = 2.9 \text{ lb/in.}$$

Hence, the electromagnets must be increased in size by a factor of $\frac{5.41}{2.9} = 1.87$.

The second case, B, is the more severe and therefore designs the EMS which appear in sketch SK 2294234.

7. Spring Stiffness

The negative spring stiffness due to the bias magnets above is the slope of curve b in Figure B-17 and is $\frac{-23.5}{0.02}$ or 1175 lb/in. per 5-in. length of EM.

For an EM pair 1.87 larger, the comparable value is -2147 lb/in. per 5-in. length of EM.

For the whole ring, the negative spring stiffness is:

$$\frac{-2197 \times \pi D}{5} = -35,890 \text{ lb/in.}^2$$

*EMs are 100% modulated. Hence, lower magnet is "turned off."

Appendix C

MOTOR-GENERATOR SUBSYSTEM

Appendix C

MOTOR-GENERATOR SUBSYSTEM

The principal design objectives are maximum efficiency and minimum weight, particularly on the wheel. Lesser objectives are low manufacturing cost and a minimum effect of motor-generator forces on suspension-system power expenditure.

Four configurations were analyzed to determine the relative advantages of each (Figure C-1). Configurations 1 and 4 were originally considered by NASA. Later, Configurations 2 and 3 were added, with variants as noted. Thus seven configurations have been considered.

Motor Configuration 1 was first developed in another NASA program. This is a dc torquer, with switched windings to reverse current in the stator windings with rotor (wheel) rotation. The motor can be designed with small air gaps and is relatively insensitive to wheel expansion with speed. It is unstable axially because of the attractive forces between the rim magnets and the stator core.

Configuration 2 has two variants; in one the magnetic circuit is radially directed and in the other the magnetic circuit is circumferentially directed. The stator is an ironless armature. The magnetic gap size is dependent on the amount of copper in the gap. The gaps grow large if the input output power requirements are severe.

Configuration 3 (see Figure C-2), a Lundell claw type motor, has a three-dimensional magnetic circuit and four air gaps. It has the merit of maintaining constant direction of magnetic induction and near-constant induction in the circuit elements, thus minimizing eddy-current and hysteresis losses. Also, with field control, the generator output voltage can be controlled, thus relieving the power conversion unit of this function.

Configuration 4, a NASA concept, is a homopolar-type motor also (like 3), but has three air gaps instead of four. It, however, has long end windings on the ironless armature. The field is controllable, hence generator output voltage can be controlled.

Some general design rules followed in the preliminary analyses of the motors are:

1. Design for maximum magnetic gap field
2. Maximize number of poles to reduce interpole iron

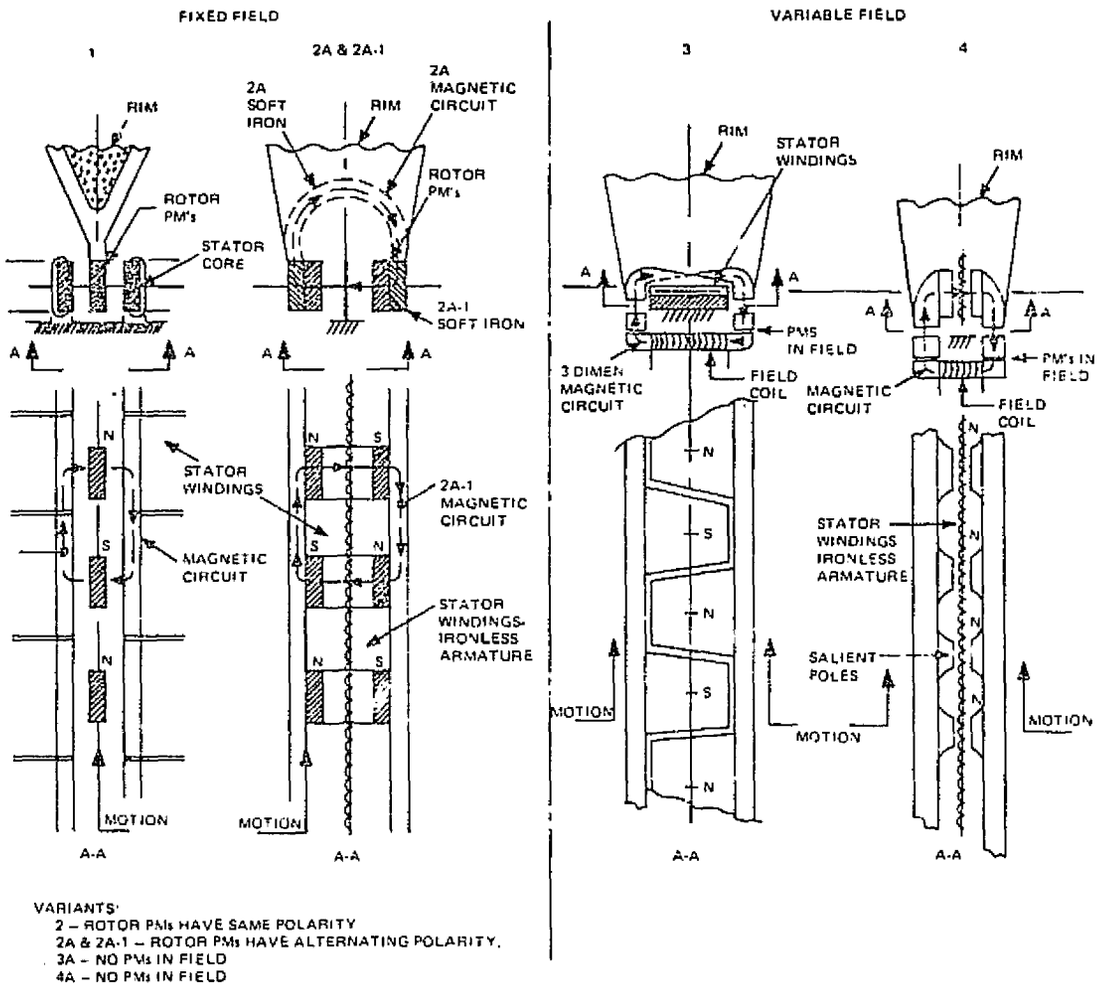

Figure C-1. Mechanical Capacitor m-g configurations.

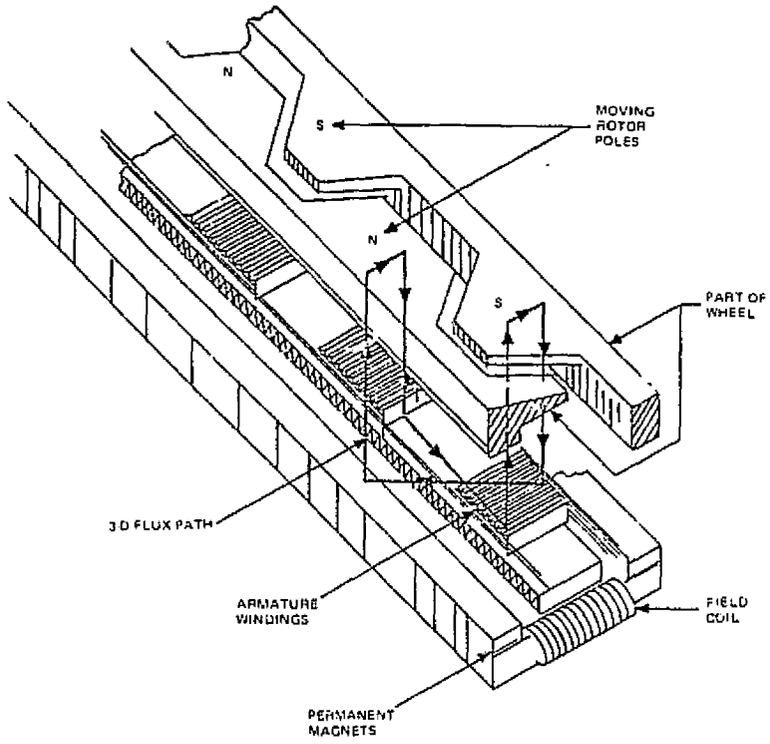

Figure C-2. Mechanical Capacitor m-g configuration No. 3.

3. Maximize motor diameter (special rule for a shaftless motor)

4. Minimize losses, after applying the foregoing rules, by seeking the best trade-off between I^2R (copper losses) and hysteresis and eddy-current losses.

A qualitative comparison of the m-g configurations appears in Table C-1. The best choice based on the design objectives, appears to be configuration 2-A-1.

A. MOTOR-GENERATOR DESIGN REQUIREMENTS

The following characteristics are extracted from the Statement of Work.

Rated Speed - 17,000 rpm

Rated Power - 17.54 kW (before assumed generator losses)

Speed Range - 17,000 to 8500 rpm (1/2 speed)

Rated Power to be available over speed range

TABLE C-1. M-G CONFIGURATIONS (COMPARISONS)

	1	2A-1	3	4
Rotor Weight	Lowest 1	2-3	3	4
Air Gap, in. (Complete Circuit)	Smallest 1 0.12	1 0.14 (min.)	2 0.234	3 0.314
Flux Density (For some length mags. or equiv. electromags)	Highest 1	2	4	3
I^2R Losses	Lowest 1 Armature Coils-Long End Turns	2	3 (I^2R for field is added)	4 Armature Coils - Long End Turns (I^2R for field is added)
Magnetic Losses		Lowest		
-Running	3	1	2	2
-Coasting	3	1	2	2
Crosstalk (Between M/G and Bearing				
-Powered	Yes (axial)	No	Yes (Radial)	Yes (Radial)
-Coasting	Yes (axial)	No	Yes	Yes
Mfg. Cost		Lowest		
	2	1	4	3

Notes:

Wheel growth with m-g dia. of 22 in.
$E = 70 \times 10^6$ lbs/in^2
Maximum Strain = 0.017 in. on radius.

1. Operation* as Motor (Charge period)

   1/2 to rated speed in 8 hours.

   Power delivered to wheel - 1.25 kW maximum.

   Internal losses $\leqq$ 80 watts

2. Operation as Generator Under No Load (Coast Period)

   Zero power input and output

   Coast for 6 hours.

   Internal losses $\leqq$ 45 watts

3. Intermittent Operation as Generator at 10% Rated Power (Intermittent Generation Periods)

   At less than 1.75 kW power (before generator losses) from rated speed to 60% rated speed during 9-hour period with average internal power loss $\leqq$ 80 watts.

4. Generator Operation at Rated Power for Period of 0.063 Hour Some Time During Last Hour of 24-Hour Cycle

   Speed Range - 60% to 50% rated speed.

5. One Time Requirement

   Motor drive shall be capable of taking wheel to 50% overspeed (150% rated speed).

6. Overload

   Generator shall be capable of surviving a short-time overload of 300% for 1 second without damage.

7. Commutation and Rectification

   (For information only)

   Circuitry losses $\leqq$ 50 watts charging, $\leqq$ 40 watts discharging (for Modes 1. and 3. preceding)

8. M-G Vacuum Operation

   All operations will be in a hard vacuum.

*Note: The time to accelerate the wheel from 100 to 150% rated speed is not specified.

9. Other Requirements

a. M-G system to operate from 110/220 V (±10%) 60 Hz, 3 ϕ input, and deliver power in the same form.

b. Mean time between failure - 50,000 hours.

c. No overspeed possibility shall exist.

d. Design shall minimize weight of rotating parts, losses during operation (particularly coasting losses), and manufacturing costs.

10. Configurations

Four configurations are to be considered and roughly sized. The preferred configuration shall be designed sufficiently to delineate materials, processes, components, and physical features, etc. to permit manufacturing cost estimates.

11. Nominal M-G Diameter

The torque circle diameter is assumed to be 22 inches.

12. Maximum Torque

The maximum torque, at 1/2 rated speed and in the generator mode, developing 17.54 kW is 22.44 lb-ft. The maximum torque force is 24.48 lbs.

B. MOTOR GENERATOR DESIGN CALCULATIONS

The following analyses are made assuming the motors to be dc torquers rather than brushless ac motors. The results of the analyses are valid and yield loss estimates and performance data in close agreement with the alternative approach which was finally adopted.

The motor-generator power and energy profiles are summarized in Figure C-3.

1. Motor-generator configuration 1
(Refer to Figure C-4)

From the S.O.W., the specified generator load is 15 kW, at rated speed down to 1/2 rated speed.

Assume generator efficiency	-	95%
Power conversion efficiency	-	90%
Maximum rpm	-	11,000 rpm*

*Later changed to 17,000 rpm. The number of poles was reduced by the speed ratio 11,000/17,000, thus maintaining frequency, etc.

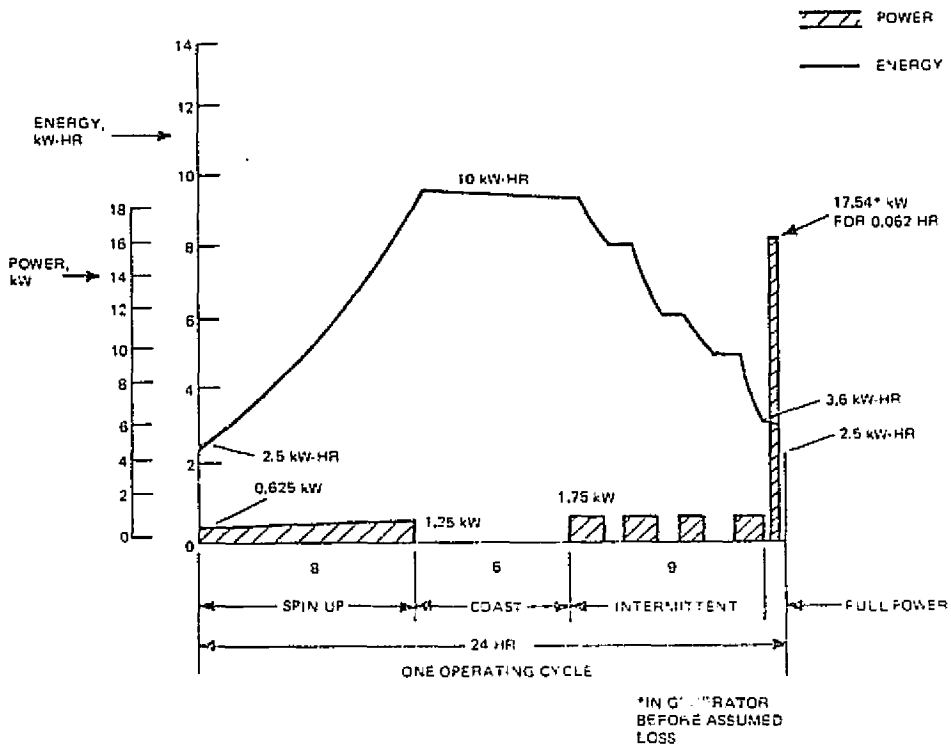

Figure C-3. Mechanical Capacitor power and energy profiles, 24-hour cycle.

Power generated before losses:

$$P = \frac{15}{0.90 \times 0.95} = 17.54 \text{ kW}$$

$$\text{Torque} = \frac{7.04\ W}{\text{rpm}} = \frac{7.04 \times 17,540}{11,000} = 11.22 \text{ lb-ft}$$

Assume Torque couple at 22 in. diameter:

$$\text{Torque Force} = \frac{11.22 \times 12}{11} = 12.24 \text{ lbs}$$

At half speed, torque force = 2 x 12.24 = 24.48 lbs

a. Magnetic Circuit Design Assumptions

Maximum airgaps = 0.030 and 0.040 in.

Magnet area = 1, 2, 3 in^2 (1 x 1, 1.41 x 1.41, 1.73 x 1.73 in.)

Magnet thickness (length) = 0.10, 0.20, 0.30 in.

Magnets - $SmCO_5$ with B_r = 8000 gauss

Armature Core - Metglas 2605 with B_s = 10,000 gauss (for loss equation, see Table C-2)

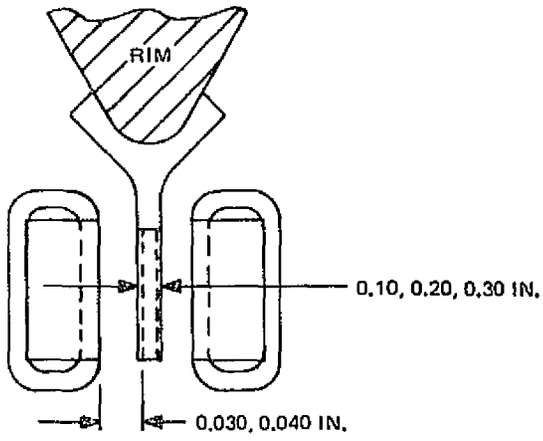

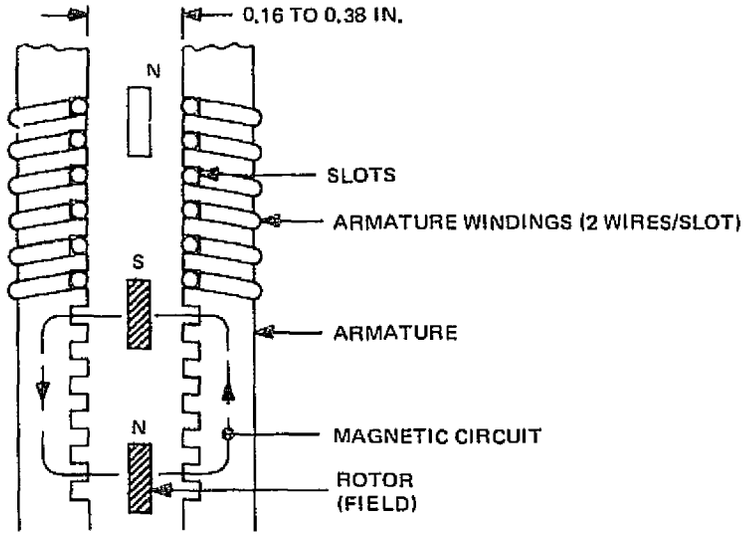

EQUIVALENT CIRCUIT:

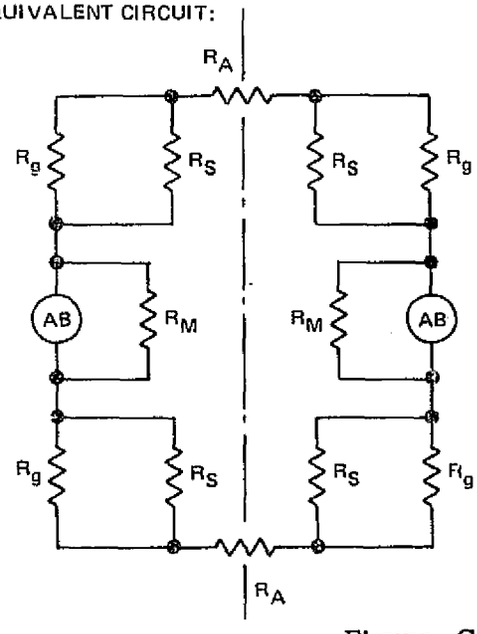

C-4(a)

NOTE:
1. R IS THE RELUCTANCE OF THE ARMATURE, GAP, MAGNET, AND STRAY PATHS (WITH APPROPRIATE SUBSCRIPTS)
2. ASSUME R_A IS $<<$ THAN R_M, R_g, AND R_S (STRAY), SINCE THE PERMEABILITY IS AT LEAST THREE ORDERS HIGHER. THE PERMEABILITIES OF M, g, AND S ARE 1.

Figure C-4. M-G configuration 1.

TABLE C-2. MECHANICAL CAPACITOR; SOFT MAGNETIC METALS FOR ENERGY WHEEL BEARINGS

Material (2 mils thick)	Watts/kg Hysteresis and Eddy Current Loss at Frequency and Induction Noted		
	60 Hz 13,000 Gauss	10^3 Hz 1000 Gauss	10^4 Hz 1000 Gauss
50% silicon iron	1.5	0.26	7.0
50% nickel iron	0.77	0.22	5.5
2605 Metglas*	0.53	0.10	2.9

*The resistivity is 125μohm cm.

In general, at the higher frequencies, Metglas 2605 losses vary from those shown as:

$$\left(\frac{B_1}{B_O}\right)^{1.6}\left(\frac{f_1}{f_O}\right)^{1.4}\left(\frac{t_1/\rho_o}{t_o/\rho_o}\right)$$

where B is the magnetic induction, f is the frequency, and t and ρ the thickness and resistivity, respectively.

The magnetic intrinsinc flux is: $B_r A_M$ where A_M is the magnet cross section.

The flux density in the gap is:

$$\frac{B_r A_M \times A_g}{A_g}\left[\frac{1}{\frac{L_g}{A_g}+\frac{L_S}{A_S}+\frac{L_M}{A_M}}\right]$$

Assume A_S as follows (Figure C-5):

$$A_S = 4L_M - 4L_M^2$$

$$L_S = L_M$$

$$A_M = A_g$$

$$B_r = 8000 \text{ gauss}$$

Then, the gap flux density, H_g, is as follows:

A_g	L_M	L_g	H_g, oersteds
1	0.1	0.060/0.080	4240/3930
1	0.2	0.060/0.080	5380/4830
1	0.3	0.060/0.080	5710/5180
2	0.1	0.060/0.080	2070/1660
2	0.2	0.060/0.080	3050/2580
2	0.3	0.060/0.080	3520/3060
3	0.1	0.060/0.080	1123/880
3	0.2	0.060/0.080	1820/1460
3	0.3	0.060/0.080	2300/1800

The plotted values of H_g are shown in Figure C-6.

Based on the plot of Figure C-6, a 0.3-in. long, 1-inch square magnet is the preliminary selection.

Flux density is = 5700 oersted/gauss in the 0.030 in. gaps.

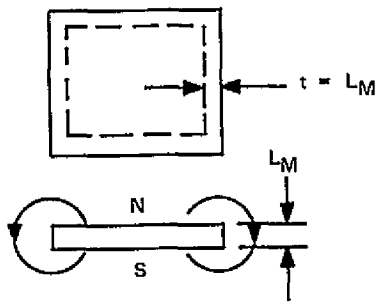

Figure C-5. Magnet area for stray flux.

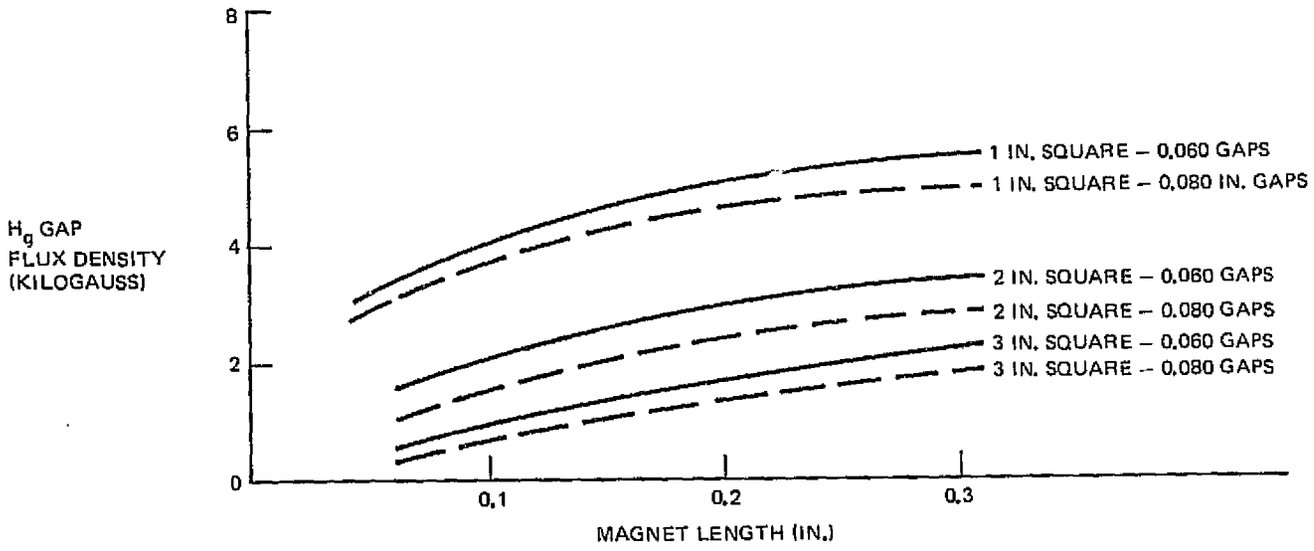

Figure C-6. Gap flux density

b. Motor-generator design assumptions

- Pole diameter = 22 in.; circumference = $\pi D \cong 70$ in.
- Armature coils on both sides (Figure C-1)
- 1 in. square $SmCo_5$ magnets, 0.30 in. long, on rotor
- Magnet spacing - 2.5 in., or 28 poles
- All armature coils active
- Coil length (circumferential) - 1.25 in., with 1.25 in. between coils
- Torque force as function of magnet travel:
  (assume coil is fully effective, when opposite magnets) - Figure C-7

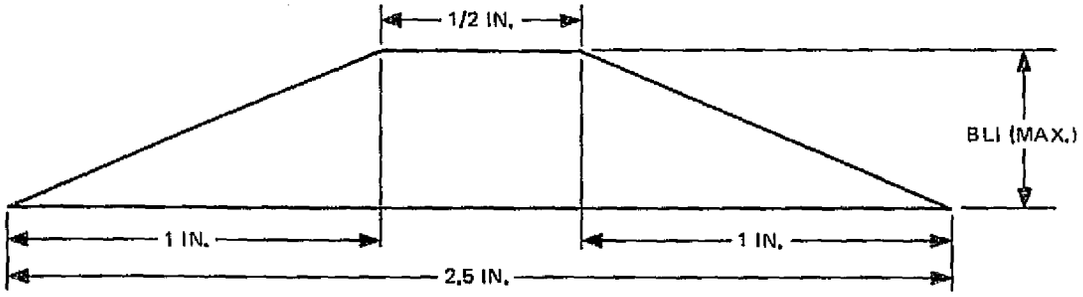

Figure C-7. Torque force variation.

- No. 16 AWG wire, 0.060 in. dia., carrying 8 amperes maximum
- Slots 0.060 in. wide with 0.060 teeth

Gap flux density = 0.85 x 5700 = 4845 oersteds/gauss = 0.4845 webers/m^2

Torque force per coil, P = 0.5 BLI (Units - newtons, webers/m^2, meters, amperes)

$$\text{Torque force for all coils} = \frac{24.48}{0.225} = 108.8 \text{ newtons}$$

$$108.8 = 0.5 \times 0.4845 \times L \times 8$$

$$L = 56.14 \text{ m}$$

$$L/\text{coil} = 56.14/4^* \times 28 = 0.501 \text{ m} = 19.73 \text{ in}$$

$$\text{Active length per coil} = \frac{\text{Coil length}}{\text{Wire spacing}} \times \text{core height} + \text{wire dia.}$$

$$19.73 = \frac{1.25}{0.120} (H + 0.060)$$

$$H = 1.83 \text{ in.}$$

Average EMF/coil at rated and 1/2 rated speed:

$$\text{EMF} = 0.5 \text{ BLV}$$

$$= 0.5 \times 0.4845 \times \frac{19.73}{39.37} \left(\frac{22\pi}{39.37} \times \frac{11,000}{60} \right)$$

$$= 39.06 \text{ V}$$

$$= 19.55 \text{ V at } 5500 \text{ rpm}$$

Assume 4 coils in series and 28 parallel paths.

Voltage per path = 4 x 39.06 $\cong$ 160 V at 11,000 rpm

$\cong$ 80 V at 5500 rpm

Generated power $\cong$ 17.54 kVA

Assume:

- 10,000 gauss saturation flux density in core (1.0 weber/m^2)
- Reluctance of armature $\ll$ Magnet and air gap reluctance

*(4 coils/pole - 2 in each set of slots)

Core has two fluxes: (a) due to permanent magnets, (b) due to armature coils (Figure C-8).

(a) Flux density = 4845 oersted/gauss in gap

$$= 0.48 \text{ webers/m}^2$$

(b) Flux density due to coil is:

$$= F/R$$

$F = NI = 20 \times 8 = 160$ ampere turns (2 coils)

Assume $R_s = (2 R_g + R_M)$

$F = 80$ ampere turns/gap branch of circuit

$$2 R_g + R_M = \frac{L_g}{\mu_o A_g} + \frac{L_M}{\mu_o A_M}$$

$$= \frac{1}{4\pi \times 10^{-7}} \left[\frac{0.36 \times .0254}{(1 \times 1.61)\, 0.0254^2} \right]$$

$$= 0.700 \times 10^7$$

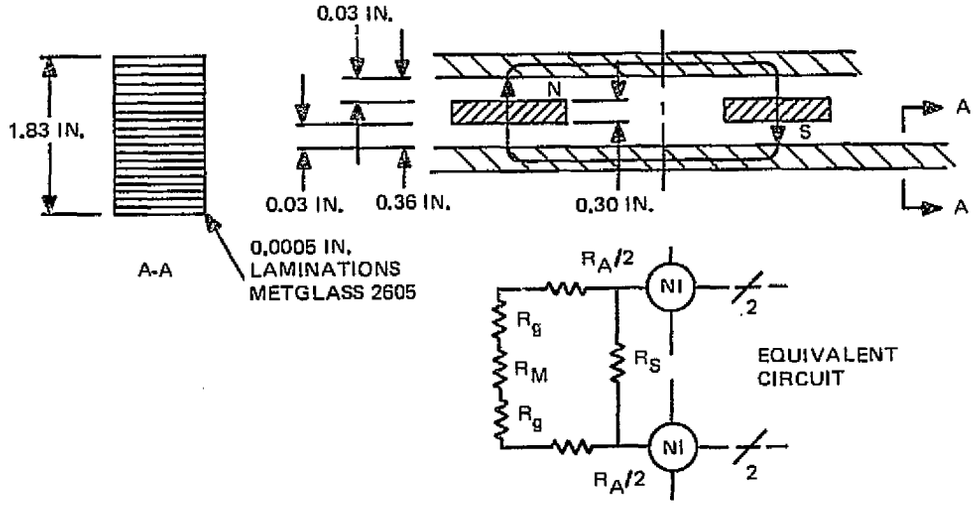

Figure C-8. Magnet core sizing.

$$\phi = \frac{F}{R} = \frac{80}{0.700 \times 10^{7}} = 0.114 \times 10^{-4} \text{ weber}$$

for 1.0 weber/m^2 (saturation value for core) and 0.45 weber/m^2

Core area:

$$\frac{\left[0.114 \times 10^{-4}\right]}{A} + 0.48 = 1.0$$

$$0.114 \times 10^{-4} = 0.52A$$

$$A = 0.219 \times 10^{-4} \text{ in.}^2$$

$$A = 0.219 \times 10^{-4} \times 39.37^2$$

$$= 0.708 \text{ in.}^2$$

$$\text{width} = \frac{0.708}{1.83} = 0.387 \text{ in.}$$

c. Motor Losses, Spin-up

Stored energy in wheel = 10 kW-hr

$$= 26.55 \times 10^{6} \text{ ft-lbs}$$

Assume wheel moment of inertia, $I = 333 \times 1.96^2 = 1290$ lb-ft^2

Kinetic energy at 11,000 rpm

$$KE = 1/2\, I\omega^2$$

$$= \frac{1290}{2 \times 32.2} \times \left(\frac{11,000}{60} \times 6.28\right)^2$$

$$= 20.031 \times 1.32556 \times 10^{6}$$

$$= 26.55 \times 10^{6} \text{ ft-lbs}$$

Torque required for spin-up from 5,500 to 11,000 rpm in eight hours

$$T = \frac{I \times \text{rpm change}}{308 \times \text{time}} \qquad \text{(ft-lb-s units)}$$

$$T = \frac{1290 \times 5500}{308 \times 480 \times 60} = 0.799 \text{ lb-ft}$$

Torque force = $0.799 \times \frac{12}{11} = 0.873$ lb

Power input at full rated speed:

$$HP = \frac{T \times N}{63025} \qquad \text{where T is in in.-lb}$$

$= 0.799 \times 12 \times 11,000/63025 = 1.674$, or 1.25 kW

Assume stator coils are on 100% of time

Current = $0.8725 \times 8/24.48 = 0.285$ ampere

Coil resistance = 4.016 ohms/1000 ft

Coil Length = 56.14 m = 184.2 ft

Total coil length = $184.2 \times 4.67/1.83 = 470$ ft

I^2R loss = $0.285^2 \times \frac{470}{1000} \times 4.016 = 0.153$ W

d. Iron Losses

Stator core weight = 2 x HxW x number of conductors x circumference x density

$W = 1.83 \times 0.387 \times 2 \times 22 \times \pi \times 0.20$

$W = 19.58$ lbs

Assume saturation of cores at 10,000 gauss/in.^{2}.

Hysteresis and eddy current loss = $\frac{W}{2.2}\left(\frac{B_1}{B_o}\right)^{1.6} \times \left(\frac{f_1}{f_o}\right)^{1.4} \times \left(\frac{t_1 \rho_1}{t_o \rho_o}\right)$

where subscript 'o' test values are given in Table C-1

For Metglas 2605, loss in W/kg is 0.1 at 1000 gauss flux density, 1000 Hz, and 0.002 in. laminations.

Assume 0.0005 in. laminations,

Motor loss = $L = \frac{19.58}{2.2} \times 0.1 \times (10)^{1.6} \times (2.566)^{1.4} \times \frac{0.0005}{0.002}$

$= 33$ W

at 1/2 rated speed, loss is $33 \times (.5)^{1.4} = 12.5$ W

Total loss = 12.65 to 33 W
(1/2 to full speed)

e. Motor Losses, Coasting

Core losses persist and I^2R loss goes to zero. Hence, loss = 33 W (versus 45 W in S. O. W.)

f. Generator Losses Under Full Load and at 60% Rated Speed

$$I^2R \text{ loss} = (6.4)^2 \times \frac{470}{1000} \times 4.016 = 77.3 \text{ W}$$

Hysteresis and eddy-current losses from before = 33 W

$$\text{At reduced speed loss} = 33 \times \left(\frac{60}{100}\right)^{1.4} = 16.2 \text{ W}$$

Total = 94 W

g. One Half Rated Speed

$$I^2R \text{ loss} = 8^2 \times \frac{470}{1000} \times 4.016 = 120.80$$

Hysteresis and eddy current loss =

$$L = \frac{19.55}{2.2} \times 0.1 \times 10^{1.6} \times \frac{(1283)}{1000}^{1.4} \times \frac{0.0005}{0.002}$$

$$= 12.55 \text{ W}$$

Total Loss = 12.55 + 120.6 = 133.35 W

h. Intermittent Operations

At 60% rated speed and 10% maximum load, the torque load is 1.87 lbs.

$$I = \frac{1.87}{22.44} \times 8 = 0.66$$

$$I^2R = (0.66)^2 \times 1.89 = 0.83 \text{ W}$$

$$\text{Hysteresis and eddy current} = 12.55 \times \left(\frac{60}{50}\right)^{1.4} = 16.20$$

At 100% rated speed, losses are 0.30 and 33 W, respectively.

2. Configurations 2A and 2A-1

Note: Configuration 2 is not considered since it utilizes long end turns.

a. Gap size

Wire size in the gap is a principal determinant of gap dimension. The gap can be minimized by using rectangular wire of varying width to satisfy current requirements.

If a coil is built as shown in Figure C-9, then wires in gap can be held to 0.030 in. thick by adjusting the width to carry the full assumed or rated current.

From Anaconda Co. catalogue: (Figure C-10)

Minimum rectangular wire thickness = 0.030 in. (assume 0.040 in. with insulation)

Minimum area = 2509 sq. mils

Corner radius = 0.016 in.

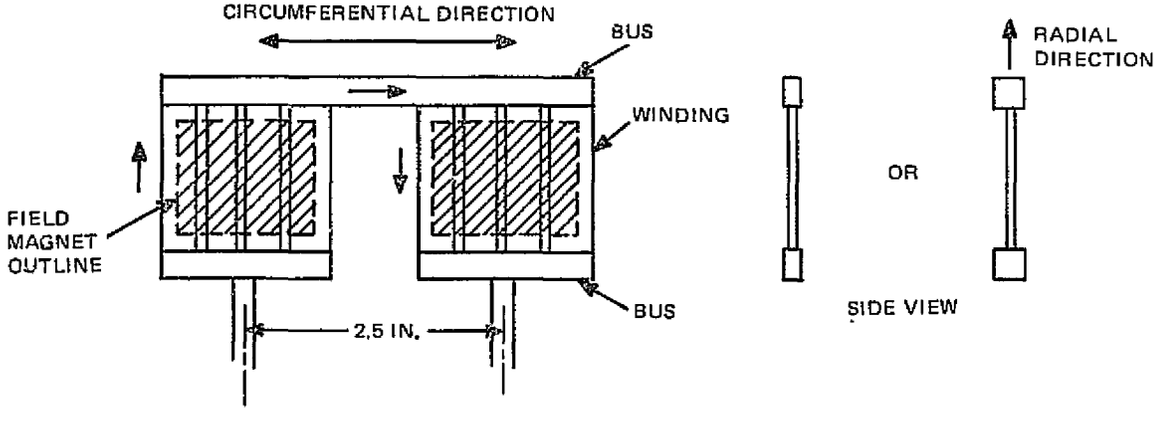

Figure C-9. Coil construction.

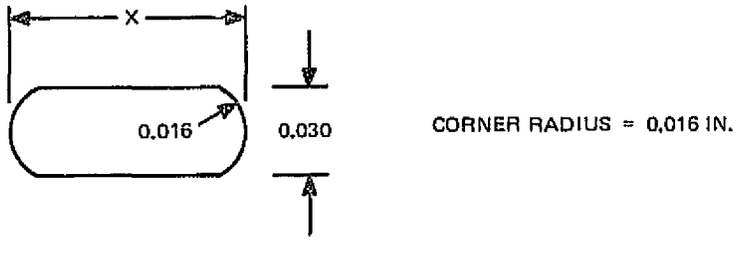

Figure C-10. Anaconda wire shape.

Resistance, ohms/1000 ft $= \frac{8146}{A}$ (Anaconda formula)

	Width - W, in.			
	0.050	0.060	0.070	0.080
Area, sq. mils	1500-220	1800-220	2100-220	2400-220
	1280	1580	1880	2180
R, ohms per 1000 ft	6.36	5.16	4.33	3.74

- Assume: higher current capacity, compared to round wire, of 30%

  Maximum air gap is: (2 x 0.030) + 0.080* = 0.14 in.

  Assume: same size magnets, poles, coil height, etc. as in configuration No. 1

Assume a toroid magnetic circuit as in Figure C-11.

$$H_g = \frac{A_g/L_g}{A_g/L_g + A_S/L_S + A_M/L_M} \cdot \frac{A_M}{A_g} \cdot B$$

Assume magnet lengths of 0.1, 0.2, 0.3 in.

Assume $R_S = 0.66\, R_g$

Also: $A_M = A_g$

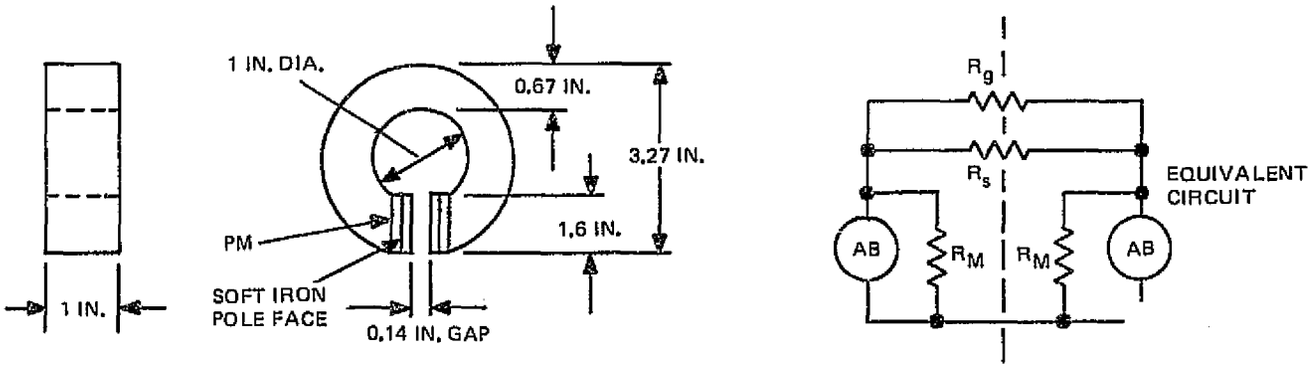

Figure C-11. Toroid magnetic circuit configuration.

*2 coils superimposed per pair of poles

A_g	L_g	A_g/L_g	A_S/L_S	A_M	L_M	A_M/L_M	$1/2 \times \frac{A_M}{A_g} \cdot B = H_g$
1.6	$\frac{0.14}{2}$	22.6	15.1	1.6	0.1	16	3389
1.6	$\frac{0.14}{2}$	22.6	15.1	1.6	0.2	8	3979
1.6	$\frac{0.14}{2}$	22.6	15.1	1.6	0.3	5.3	4227

Use same magnets as for configuration 1 (0.30 in. long) $\therefore$ gap flux density $\cong$ 4200 gauss.

Assume:

Pole diameter = 22 in., circum $\cong$ 70 in.

Rectangular coils (Figure C-12 and Figure C-13)

Magnet Spacing - 2.5 in. or 28 poles

All armatures coils active, rect. wire equivalent to No. 16 gauge (0.051 dia.)

Coil length (circumferential) - 1.25 in. with 1.25 in. between coils

Avg. torque force = 0.5P, where P is the torque force

Maximum current = 8 x 1.3 = 10.4 amps

Generator maximum torque force = $\frac{24.48}{2.25}$ = 108.8 newtons

Total coil length = P/0.5BI

$$= \frac{108.8}{0.5 \times 0.42 \times 10.4} = 49.8 \text{ meters}$$

Length/pole $\frac{49.8}{28}$ = 1.779 meters = 70 in.

Assume 2 thicknesses of coil (2 coils), total thickness is 0.080 in.

Width of conductors is chosen to equal area of 16 gauge round wire

$$0.051^2 \times 0.7854 = (0.04 \times W) - 220 \times 10^{-6}$$

$$W = 0.057 \text{ in.}$$

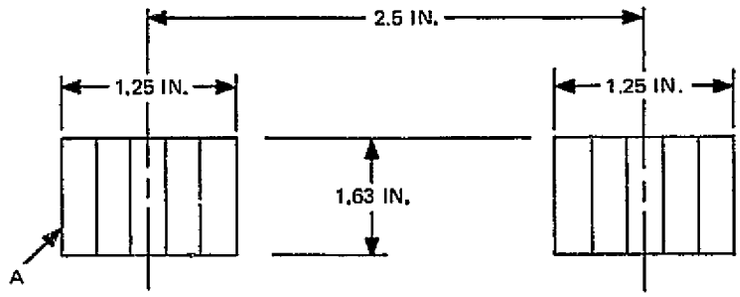

Figure C-12. Coil arrangement.

No of individual conductors, A, $= \frac{70}{2 \times 1.63} = 2,147 \cong 22$

Distance between conductors $= \frac{1.25 - 22.00 \times .057}{21} \cong 0$

Generator voltage at rated speed:

$$V = 0.5\ BLV$$

$$\text{Avg. EMF per coil} = 0.5 \times 0.42 \times \frac{1.63 \times 2}{39.37} (321.86)\ \text{(Mks units)}$$

$$= 5.60\ \text{V per coil}$$

If 28 sets are in series, $V = 28 \times 5.60 = 156.8$

If 56 sets are in series, $V = 313.6$

Weight of poles $= 28\ [\{\text{Avg. OD}^2 - (\text{I. D.})^2\}\ D^2/4 \times \text{Width} \times \text{Density}]$

$$= 28\ [\{(2.52)^2 - 1^2\}\ 0.7854 \times 1 \times 0.28]$$

$$= 32.95\ \text{lb}$$

Note that this is a heavy configuration.

Consider Configuration 2A-1 of Figure C-1

Assume soft iron induction density is 10,000 gauss

$$\text{Area} = \frac{4227 \times 1.6 \times 1}{10,000} = 0.681\ \text{in}^2$$

Assume 22 in. diameter

Weight of rotor metal = magnets + soft iron weight

$= 5[illegible] \times 0.29 \times 0.3 \times 1.6 + 22 \times \pi \times 0.681 \times 2 \times 0.29$

$= 7.8 + 27.3$

$= 35.1$ lb

which is heavy also. The alternative is to utilize the keeper metal as shown in Sketch SK2294234 as one of two inner rim motor - suspension configurations. In this case, motor-generator weight can be shared with the suspension system, at some risk of cross-talk forces.

b. Losses for Each Phase of Operation

(1) Spin-Up

Assume constant current and variable voltage, hence low power increasing to maximum power at rated speed.

I^2R loss in armature wire;

$$I = \frac{10.4 \times 0.799}{22.44} = 0.37 \text{ ampere}$$

$R = 5.52$ ohms/2000 ft

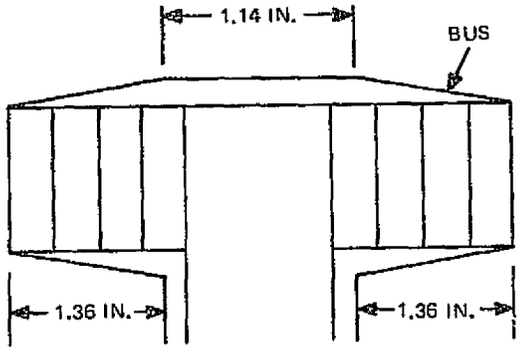

Figure C-13. Coil arrangement.

$$R = \frac{49.8 \times 2 \times 5.52 \times 3.28}{1000} = 1.80 \text{ ohms}$$

$I^2R = 0.37^2 \times 1.80 = 0.246$ W

Maximum magnet drag can be ignored.

(2) Coast

With the armature coils open-circuited, losses should be approximately zero.

(3) Estimate of Armature Field ON Losses

Problem: determine induction in magnets due to armature field. The field moves relative to the magnets and is switched (commutated) when displaced one pole space. Switching is done in the interpole space.

The pole edges see the field varying approximately as shown in Figure C-14.

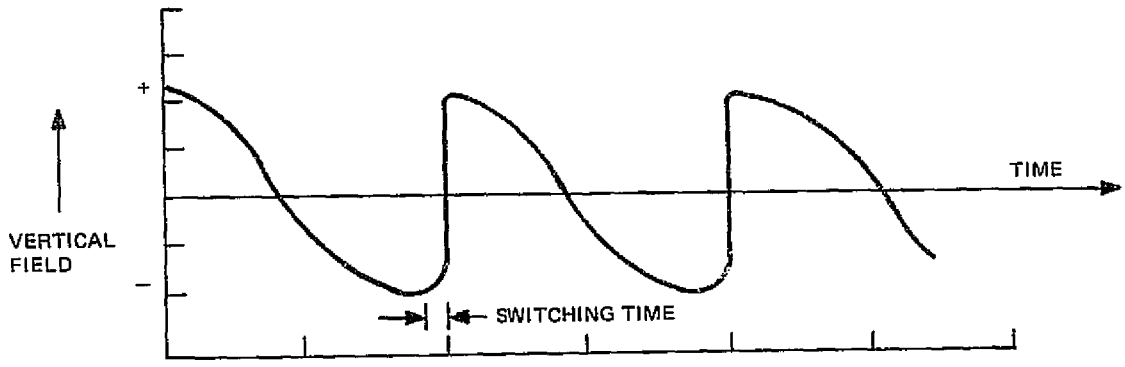

Figure C-14. Armature field variation.

Several assumptions have to be made:

- The whole armature field flux passes through the magnets (Figure C-15)
- The field is two dimensional (actually it is not)
- Magnetic effects are not time dependent (no lag)
- The usual expressions for losses apply

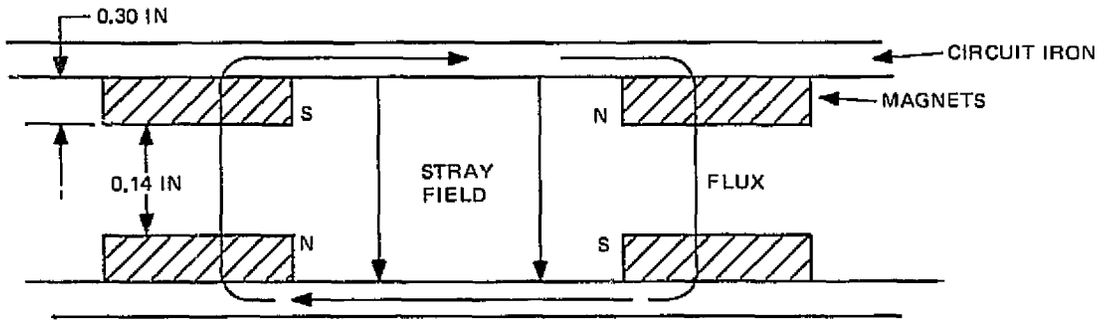

Figure C-15. Magnetic circuit.

$$MMF = NI = \phi R = \frac{\phi l}{\mu A}$$

Assume $l = (0.3 + 0.14 + 0.3)\ 2.2 = 1.628$ in.

In CGS units

$$I = \frac{0.795\ NI \times \mu A}{l}$$

$$= BA$$

$$B = \frac{0.7957}{l}\ \mu NI = \frac{0.7957}{l}\ NI$$

where

l is in cm

B in gauss

I in amperes

As a generator, $NI = 48 \times 10.4 = 499.2$ ampere turns

Hence $B = \frac{0.7957 \times 10.4 \times 48}{1.628 \times 2.54} = 96.1$ gauss

using another check for NI.

From C. S. Siskind, 'Direct Current Machinery, McGraw Hill Book Co., Inc., 1952, page 85:

$$\text{Ampere Turn per pole} = (ZI_a/2aP) \times 0.757$$

$$= \frac{48 \times 28}{28} \times \frac{20.4}{2}$$

where

Z/P = conductors under one pole

$I_a/a = \frac{\text{total current}}{\text{parallel paths}}$

Hence the demagnetizing or magnetizing field from the coils is small. Also the hysteresis loss will be negligible and can be ignored.

The maximum frequency $= \frac{11,000 \times 28}{60} = 5133$ Hz

Magnet resistivity = 50 μ ohm-cm

From: P. R. Bardell, 'Magnetic Materials in the Electrical Industry', New York Philosophical Library, 1055, page 123:

$$\text{watts loss/cm}^3 = \frac{\pi^2 f^2 B_m{}^2 t^2 10^{-16}}{6p}$$

$$= \frac{\pi^2 (5133)^2 \times (96)^2 \times (2.54)^2 \times 10^{-16}}{6 \times 50}$$

$$= 5.15 \times 10^{-6}$$

where

$f = 5133$

$B_m = 96$ gauss

$t = 2.54$ cm

$p = 50$ ohm-cm

The total magnet volume = 128 cm^3

Hence the loss is: $5.15 \times 10^{-6} \times 1.28 \times 10^2 = .00066$ W

(4) Lower Power Intermittent Operation

(a) Assume 60% rated speed, or 6600 rpm

Power out = 1.75 kW max (10% rated max. load)

$T = \frac{7.04 \times W}{rpm} = \frac{7.04 \times 1750}{6600} = 1.87$ lb ft

From coasting case, I = 0.74 for 1.3 lb ft.

Hence $I^2R = (0.74 \times \frac{1.87}{1.6})^2 \times 1.8 = 1.34$ W

Maximum magnet losses may be ignored

Hence total loss is = 1.34 W

(b) At 100% rated speed, the corresponding loss is $\left(\frac{60}{100}\right)^2 \times 1.34 \cong 0.48$W

(5) High Power at 50% Rated Speed

$I^2R = 10.4^2 \times 1.80 = 194.7$ W

Magnet drag loss ≃ 0

Total loss = 194.7 W

3. Motor Configuration 4 (NASA)

(Includes permanent magnets and field coils, Figures C-16 and C-17.)

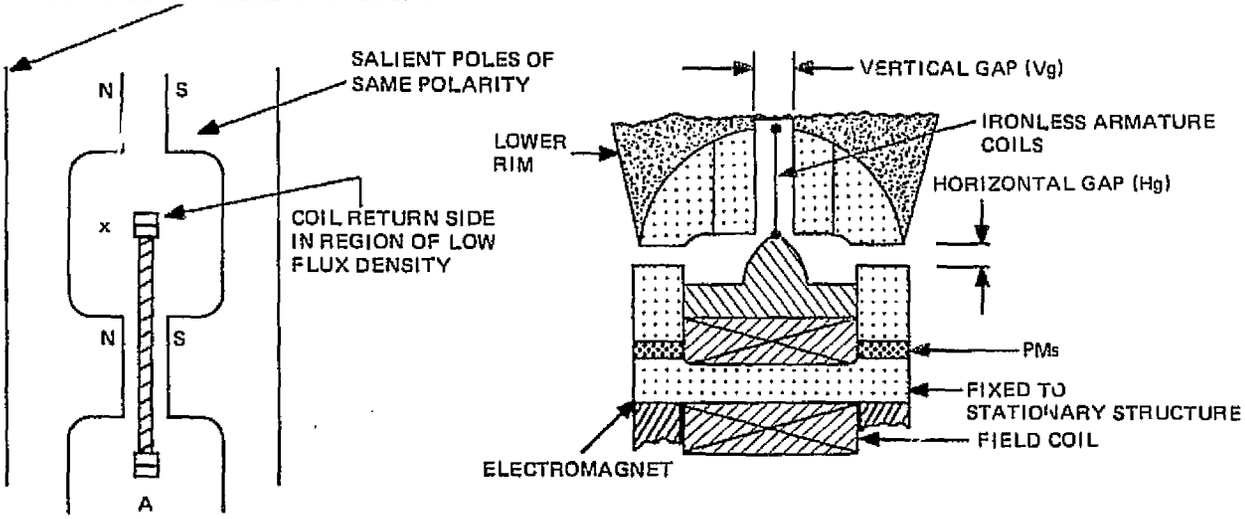

Figure C-16. Motor Configuration 4.

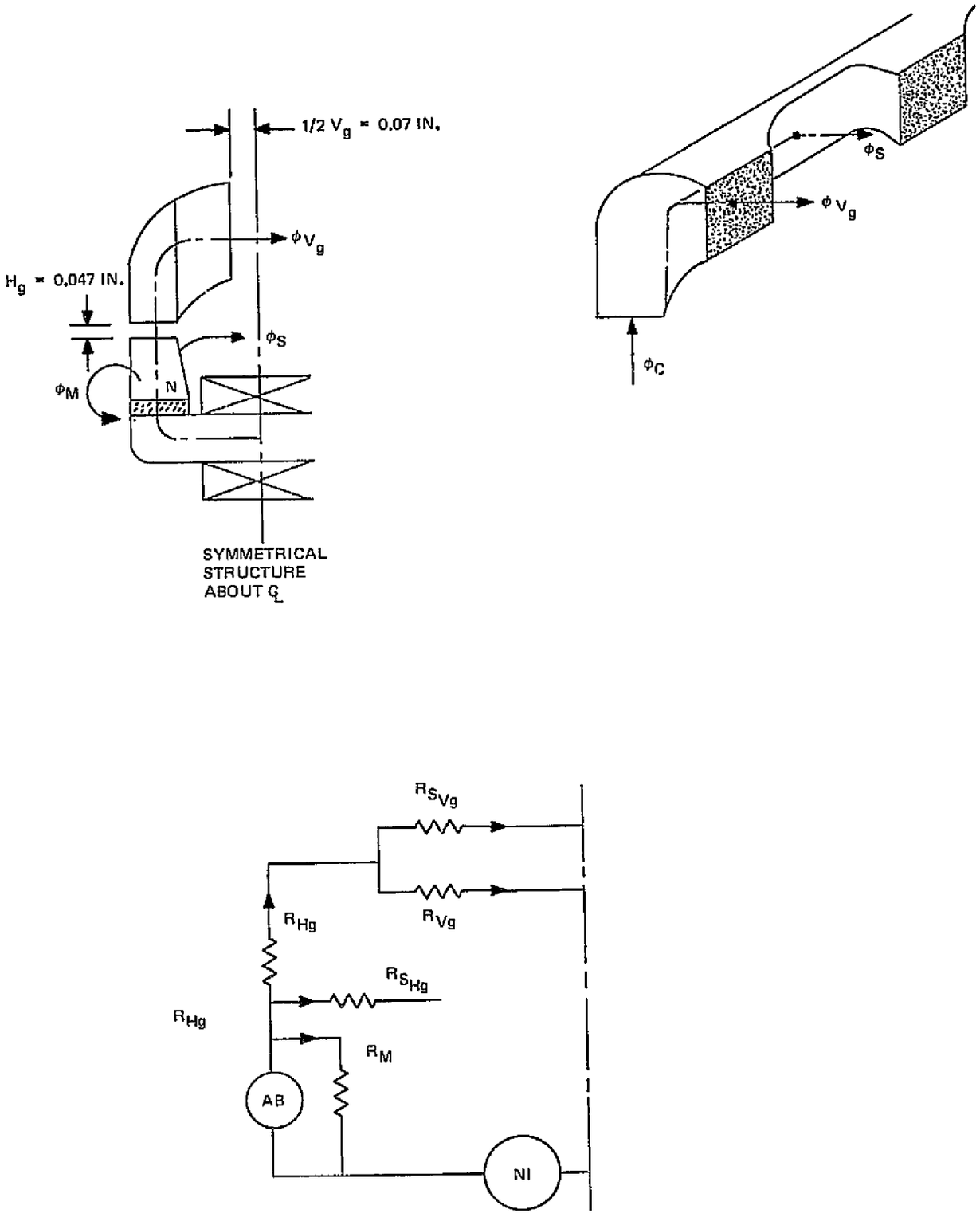

Figure C-17. Magnetic circuit and equivalent circuit.

Assume:

- Same permanent magnets as for motor-generator configuration 1 and 2A-1
- Magnet dimensions - 0.3 x 1 x 1.83 in. (approx)
- Gap H_g = .030 to 0.017 (wheel dilated) = 0.047 in.
- Gap V_g = .060 + 0.08 = 0.14 in. ($^1/2$ gap = 0.07 in.)
- Number of poles = 28
  Pitch = 2.5 in.
  All poles active

At the vertical gap, the parallel circuit reluctance is:

$$\frac{1}{R_c} = \frac{1}{R_{v_q}} + \frac{1}{R_{vg}} = \frac{2\,Rvg}{(Rvg)^2} = 2\left(\frac{0.07}{1.83}\right)\Big/\left(\frac{.07}{1.83}\right)^2 = 52.4$$

$R_c = 0.019$

$R_{H_g} = \frac{0.047}{1.83} = 0.0256$

$R_c + R_{H_g} = 0.0446 \qquad G = 22.42$

$$H_bH_g = \frac{\frac{1}{Rc}}{\frac{1}{R_c} + \frac{0.2}{R_c} + \frac{1}{R_M}} \times \frac{A_M}{A_G} \cdot B_s \qquad H_bH_g = \text{flux density in horiz. gap}$$

$$H_bH_g = \frac{22.42}{22.42 + (0.2 \times 22.46) + 6} \times 8000 = 5452 \text{ gauss}$$

$$H_{bV_g} = \frac{5452}{2} = 2726 \text{ gauss}$$

a. Field Coil

Assume 2 to 1 variation in field

Modulation of permanent magnet field in the vertical gap is:

$\pm 2726/3$ W $\cong$ 908 gauss

From 3638 gauss at 1/2 rated speed to 1818 gauss at rated speed

$NI = \phi R$

Magnet intrinsic flux = $8000 \times 1.83 \times 2.54^2 = 94451$ maxwells

R of whole magnet circuit:

$$\frac{1}{R_{V_g}} = \frac{1}{\frac{0.07}{1.83 \times 2.54}} + \frac{1}{\frac{0.07}{1.83 \times 2.54}} = 132.8$$

$$R_{V_g} = 0.0075$$

$$R_{H_g} = \frac{0.047}{1.83 \times 2.54} = 0.010$$

$$R_M = \frac{0.3}{1.83 \times 2.54} = 0.0645$$

$$R_s = 4 \times 0.010 = 0.040 \qquad \frac{1}{R_T} = \frac{1}{R_{V_g} + R_{H_g}} + \frac{1}{R_s} + \frac{1}{R_M}$$

$$\frac{1}{R_T} = \frac{1}{0.0175} + \frac{1}{0.040} + \frac{1}{0.0645} = 97.6$$

$$R_T = 0.0102$$

R_T (whole circuit) = 0.0204

$\phi R = 94451/3 \times 0.0204 = 642.2$ gilberts = 807 AT

Assume field coil serves two poles.

AT = 1614 ampere turns; use No. 36 AWG wire

b. Conductors, Armature

Assume conductors are made sufficiently large to take more current to offset smaller field (1700 gauss) at rated speed.

Conductor thickness = $0.030 \times \frac{3829}{1818} = 0.0632$ in.

Assume same width - as in motor configuration 2, or 0.057 in.

Area = 3380 mils, $R = \frac{8146}{3380} = 2.41$ ohms/1000 ft

At rated speed of 11,000 rpm, torque force $= \frac{108.8}{2} = 54.4$ newtons

Assume wire current capacity = 143 sq mils/ampere;

I = 23.6 amperes

Torque force = 0.5 BLI

$$54.4 = 0.5 \times 0.18 \times L \times 23.6$$

$$L = 25.6 \text{ meters}$$

Length of conductor in armature/per pole

$$= \frac{25.6 \times 39.37}{28} = 35.995 \cong 36 \text{ in.}$$

c. Back EMF

$$\text{EMF} = 0.5 \text{ BLV} = 0.5 \times 0.18 \times \frac{1.50 \times 24}{39.37} \times 321.86 = 26.48 \text{ V/Coil}$$

with 4 coils in series, V ≅ 106 in 7 parallel paths

Power = 0.7 x 23.6 x 106 = 17,503 W

= 17.5 kW

At 1/2 rated speed, B = 3638 gauss and the torque force = 108.8 newtons.

So the current and voltage remain the same.

d. Weight of Motor on Rim (Figure C-18)

Ass. , 10,000 gauss working induction

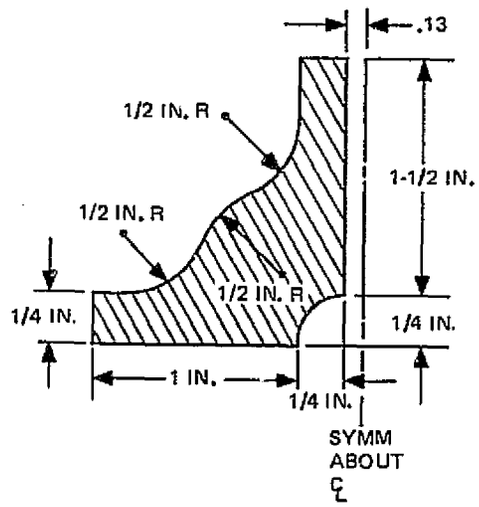

Figure C-18. Rim metal configuration.

Maximum induction at salient poles = 5452/0.5 x 1 ≅ 11,000 gauss

Approximate weight of metal:

$$\text{Weight} \cong (.25 \times 1.5 \times 28 \times .29 \times 2) + (.25 \times 1 + .5^2 \times \frac{.7854}{2}) \times 22\pi \times 29 \times 2$$

$$= 20.03$$

Increase weight to $\frac{11,000}{10,000}$ x 20.03, or 22.03 lbs to reduce induction to 10,000 gauss.

e. Losses at Rated Speed and Power

(1) Losses-Conductors, Armature I^2R

Rated speed = 11,000 rpm, maximum power = 17.54 kW

Conductor length = $28 \times 24 \times \frac{1.5}{12} \times 4 = 336$ ft.

$R = \frac{336}{1000} \times 2.41 = 0.809$ ohms

$I^2R = (23.6)^2 \times 0.809 = 451$ W

(2) Field Coil I^2R Loss

AT = 1614 ampere turns per 2 poles

AT produces 1/3 flux of magnets, or $2 (8000 \times 1.83 \times 2.54^2) =$ 188,900 maxwell;

Coil cross-section, assuming 10,000 gauss induction =

$$\frac{\text{Magnet cross-section x 2}}{3} \times \frac{8000}{10,000} = 1.83 \times \frac{2}{3} = 0.976 \text{ in.}^2 \cong 1.00 \text{ in.}^2$$

Assume round coil, $D = \frac{1.00}{0.7854}$, D = 1.12 in.

Assume No. 16 AWG wire at 6 amperes maximum current

R = 4.094 ohms/1000 ft

Total wire turns = $\frac{AT}{A} = \frac{1614 \times 14}{6} = 3766$

$$\text{Length} = \frac{(1.12 + 0.25)\pi \times 3766}{12} = 1351 \text{ ft}$$

$R = 4.094 \times 1.351 = 5.53$ ohms

$I^2R = 6^2 \times 5.53 \cong 200$ W

(3) Eddy Current and Hysteresis Losses

From a previous analysis (Configuration 2A-1) losses in the present configuration can be assumed to be zero.

(4) Eddy Current and Hysteresis Losses in Iron on Rotor Due to Bias Magnets

If it is assumed the permanent magnet variations result in a horizontal gap flux variation of ± 5% and this carries through the rotating metal, the average induction is 4000 gauss, and the variation is sinusoidal with a half wave of 1.25 in.

From the Metglas data for .002 in. laminations:

$$\text{Loss/kg} = 0.1 \times W \times \left(\frac{B_1}{B_0}\right)^{1.6} \times \left(\frac{f_1}{f_0}\right)^{1.4} \times 1$$

$$= 0.1 \times \frac{22.03}{2.2} \times \left(\frac{4}{1}\right)^{1.6} \times \left(\frac{11000 \times 28}{10000 \times 60}\right)^{1.4}$$

$$= 91.5 \text{ W}$$

For 0.0005 in. laminations, the loss $= \frac{91.5}{4} = 22.9$ W

The total loss $= 451 + 200 + 22.9 = 673.9$

At 60% speed, the loss is estimated to be 6.21 W, and at 50% speed, the loss is estimated to be 12.33W

f. Loss at 1/2 Rated Speed and Power

The loss will be slightly less than at rated speed due to the somewhat smaller eddy-current and hysteresis losses.

g. Low Power Intermittent Operation

Maximum speed is assumed to be 11,000 rpm and the voltage constant. The field coils will adjust the vertical gap flux to yield constant voltage out of the generator. The speed range is from 100% to 60% rated speed.

Hence, $BLV_{100\%} = BLV_{60\%}$, and B at the lower speed is 1.66 x $B_{100\%}$

$B_{100\%}$ = 1818 gauss

$B_{60\%}$ = 1818 x 1.66 = 3018, of which 3018 - 2726 = 292 is supplied by the coils.

Hence from the full power case, field coil power is $200 \times \frac{292}{908} = 64.3$ W

From motor configuration 2 analysis

Maximum power out = 1.75 kW

At 60% rated speed, $T_{(lb\ ft)} = 1.87$; Torque force = $1.87 \times \frac{12}{11} = 2.04$

= 9.06 newtons

9.06 = 0.5 BLI

= 0.5 x .302 x 25.6 x I

I = 2.34 amperes

$I^2R = 2.34^2 \times 0.809 = 4.42$W

Total Loss = 6.21 + 64.3 + 4.42 = 74.93 W

h. Spin Up to Rated Speed

Assume constant acceleration. Field and/or current can be varied. If the coil field is inactive, only the bias field exists.

B = 2726 gauss

Torque force = 0.8725 lbs, or 3.88 newtons

Torque force = 0.5 BLI

3.88 = 0.5 x 0.2726 x 25.6 x I

I = 1.13 amperes

$I^2R = 1.13^2 \times .810 = 1.034$ W

Total loss = 22.9 + 1.0 = 23.9 W

Assume bias is augmented by field coils:

B = 3636, Coil loss = 200 W

∴ Use of field coils is costly and must be compared with the loss in the power converter.

C-3

i. Coast

The loss will be largely from iron-hysteresis and eddy-currents due to variations in the magnetic induction in the iron. The loss is conservatively estimated to be 22.9 watts as shown in the rated power case.

j. 100% Rated Speed - Intermittent Power Case

$$T = \frac{7.04 \times 1750}{11,000} = 1.12 \text{ lb ft}$$

$$\text{Torque force} = 1.12 \times \frac{12}{11} = 5.43 \text{ newtons}$$

B is 1818 gauss (field coil fully On) = 0.18 weber/m^2

$$0.5\,BLI = 5.43 = 0.5 \times 0.182 \times 25.6 \times I$$

$$I = 2.34 \text{ amperes}$$

$$I^2R = 2.34^2 \times 0.809 = 4.43 \text{ W}$$

Field coil power (from full power case) = 200 W

Total loss = 4.4 + 200 + 22.9 = 227.3 watts

4. Motor-Generator Configuration 3

Assume use of bias magnets and field coils to obtain constant voltage and control with variation in speed.

Assume total air gap in magnetic circuit = 2 x 0.047 + 2 (0.03 + 0.08)* = 0.314 in. = 0.157 in. (half Circuit).

The circuit is three dimensional (as in Figure C-19). Assume the stray flux is as in the motor configuration 4.

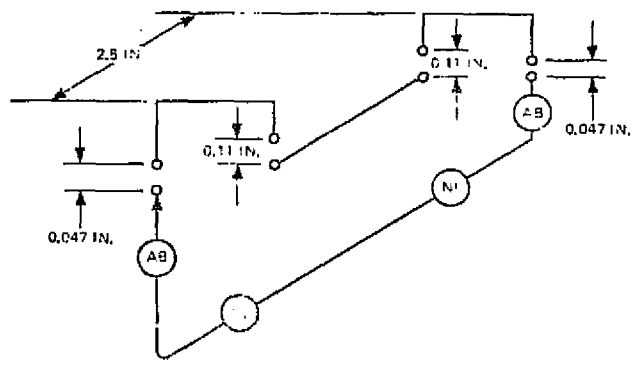

Figure C-19. Three dimensional magnetic circuit.

* assumed armature wire thickness

Assume the moving poles to have the planform as in Figure C-20.

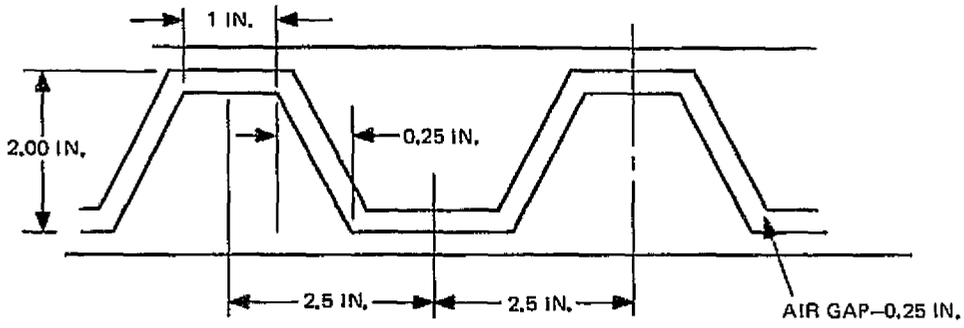

Figure C-20. Moving pole configuration.

Use the same size permanent magnets as in the other configurations (0.3 x 1 x 1.83 in., approximately).

Also assume alternating polarity. Both sides of the armature coils are active in the field of the alternating polarity poles.

The only advantage over Configuration 4 is the smaller gap at the pole face.

Use the same procedure for determining the pole gap field as in motor configuration 4. Also assume 28 poles and pole pitch of 2.5 in.

The magnetic circuit and the equivalent circuit is shown in Figure C-21.

H_{g-2} Reluctance:

$$\frac{1}{R_T} = \frac{1}{R_{s-2}} + \frac{1}{R_{g-2}} = \frac{2\,R_{g-2}}{(R_{g-2})^2}$$

$$= \frac{2\,(0.11)}{\left(\frac{0.11}{1.83}\right)^2} = \frac{\frac{1.83}{0.12}}{0.0036} = 33.33$$

$(R_T = 0.03)$

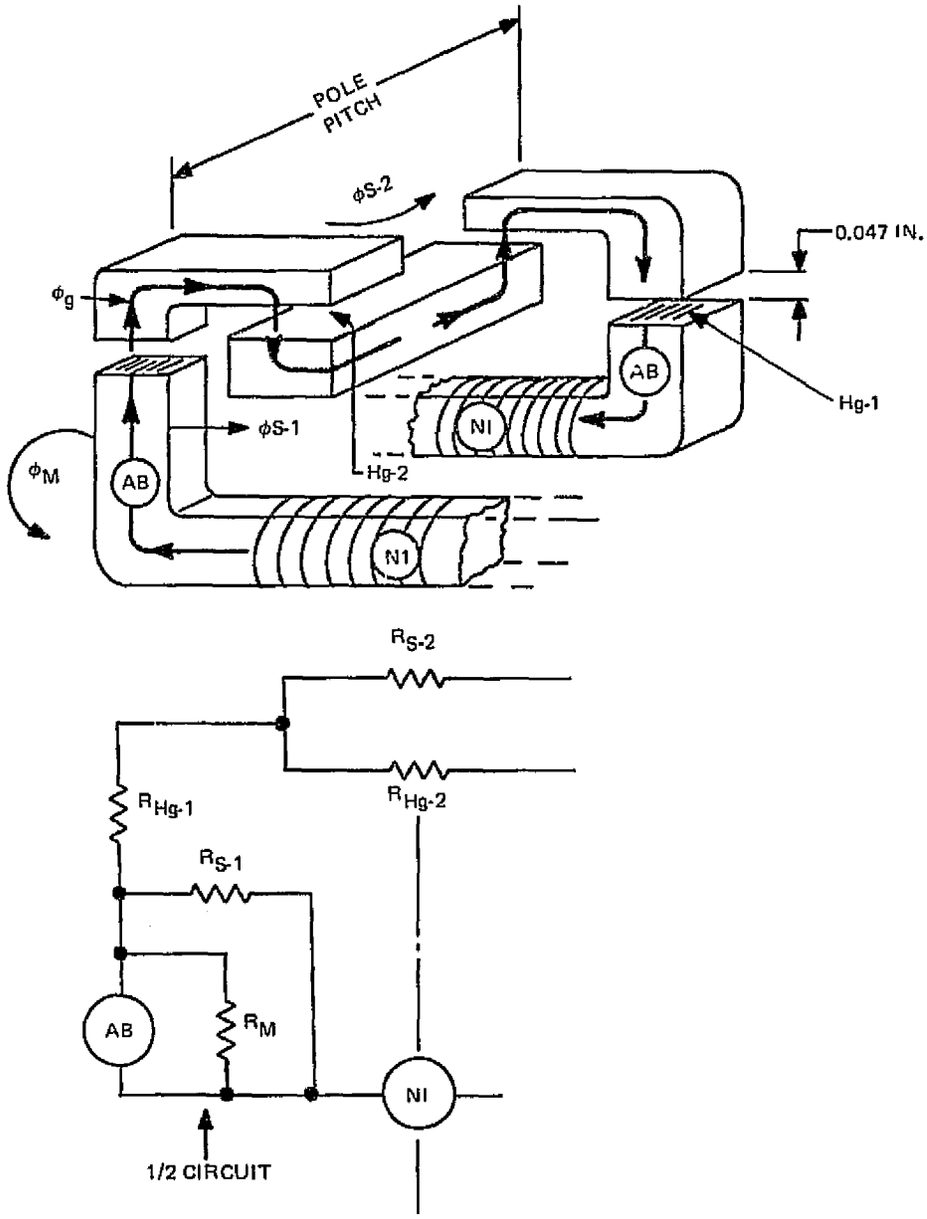

Figure C-21. Magnetic circuit, Configuration 3A.

$$R_{g-1} = \frac{0.047}{1.83} = 0.0256$$

$$R_{g-1} + R_T = 0.0556, \; G_{g-1} + G_T = 17.99$$

$$R_M = \frac{0.3}{1.8} = 0.167, \; G_M = 6$$

$Hb_{g-1} = H_{g-1}$ flux density

$$Hb_{g-1} = \frac{\frac{1}{R_{g-1} + R_T}}{\left(\frac{1}{R_{g-1} + R_T}\right) + .2\left(\frac{1}{R_{g-1} + R_T}\right) + \left(\frac{1}{R_M}\right)} \times \frac{A_M}{A_q} \quad B_s$$

$$= \frac{17.99}{1.2\,(17.99) + 6} \times 8000$$

$$= \frac{17.99}{27.59} \times 8000 = 5216 \text{ gauss}$$

$Hb_{g-2} =$ 5216/2 = 2608 gauss

a. Field Coil

Assume 2 to 1 variation in field (to maintain voltage with constant armature current over a 2 to 1 speed range. Field must vary 2608/3 = ± 869 gauss or 3477 to 1738 gauss (1/2 speed) (rated speed).

$NI = \phi R$

Magnet intrinsic flux = 94451 maxwells

R of magnetic circuit:

$$\frac{1}{R_{gap\ 2}} = \frac{1}{\frac{0.11}{1.83 \times 2.54}} + \frac{1}{\frac{0.11}{1.83 \times 2.54}} = 84.50$$

$$R_{gap\ 2} = 0.0118$$

$$R_{gap\ 1} = 0.010$$

$$R_{gap\ 1} + R_{gap\ 2} = 0.0218$$

$$R_{Mag} = 0.0645$$

$$R_{s-1} = 0.040$$

$$\frac{1}{R_{total}} = \frac{1}{0.0218} + \frac{1}{0.040} + \frac{1}{0.0645}$$

$$\frac{1}{R_{total}} = 45.87 + 25 + 15.5 = 86.37$$

$$R_{total} = 0.0115$$

$$R = \frac{99451}{3} \times 0.0115 = 381.2 \text{ gilberts} = 479 \text{ AT}$$

(1 field coil per pole or 28 in all; use No. 36 wire)

b. Armature Conductors (Rectangular - 0.057 In. Wide)

$$\text{Thickness} = 0.030 \times \frac{3829}{1738} = 0.066 \text{ in.}$$

Area = 3540 sq mils

$$R = \frac{8146}{3540} = 2.30 \text{ ohms per 1000 ft.}$$

At rated speed torque force = 54.4 newtons

$$\text{Wire current capacity} = \frac{3540}{143} = 24.76 \text{ amperes}$$

Torque force = 0.5 BLI

$$54.4 = 0.5 \times 0.1738 \times L \times 24.76$$

$$L = 25.28 \text{ meters}$$

$$\text{Height of conductors in armature} = \frac{25.28 \times 39.37}{28} = 35.545 \text{ in.}$$

Back EMF = 0.5 BLV

$$= 0.5 \times 0.174 \times \frac{35.545}{39.37} \times 321.86$$

$$= 25.28 \text{ V}$$

With 4 coils in series, V ≅101, with 7 parallel paths

Power = 24.76 x 7 x 101 = 17.505 kW

At 1/2 rated speed: B = 3.477 kg

T_{force} = 108.8 newtons

Hence, I and V remain the same.

c. Losses

Assume conductors carrying maximum current of 24.76 amperes.

Conductor size = 0.057 x 0.066 in., rectangular

R = 2.30 ohms/1000 ft

I = 24.76 amperes

$$L = 25.28 \times \frac{39.37}{12} = 82.94 \times (2)^{*} = 165.88 \text{ ft}$$

$$I^2R = 24.76^2 \times \left(\frac{82.94 \times 2 \times 2.30}{1000}\right) = 233.78 \text{ watts}$$

(1) Field Coil

Power loss is approximately the same as for motor 4, approximately 200 watts.

(2) Eddy Currents and Hysteresis

Use same values as for motor 4.

(3) Spin-Up

Current = 1.13 amperes (from motor 4)

$I^2R = 1.13^2 \times 0.38 = 0.485 \cong 0.5$ watt

Hysteresis loss = 12.8 to 22.9 watts

Total losses = 23.4 watts

*full coil length

(4) Intermittent Operation at 60% Rated Speed

Assume coil loss same as for motor 4, or 64.3 watts

Torque force = 9.06 = 0.5 BLI

$$= 0.5 \times 0.302 \times 25.28 \times I$$

$$I = 2.37 \text{ amperes}$$

$$I^2R = 2.37^2 \times 0.3815 = 2.14 \text{ watts}$$

The foregoing losses for the four motor-generator configurations are summarized in Table 2-4.

d. Motor Weight

Assume 10,000 gauss flux density in the rim metal (see Figure C-22).

$$\text{Rim weight} \cong 22 \times \pi \ (1 \times 0.25 + 0.44 \times 0.625) \times 2 \times 0.29 + 28 \ \frac{(0.625 + 0.25)}{2} \times$$

$$1.25 \times 0.29 \times 2$$

$$\cong 31 \text{ lbs.}$$

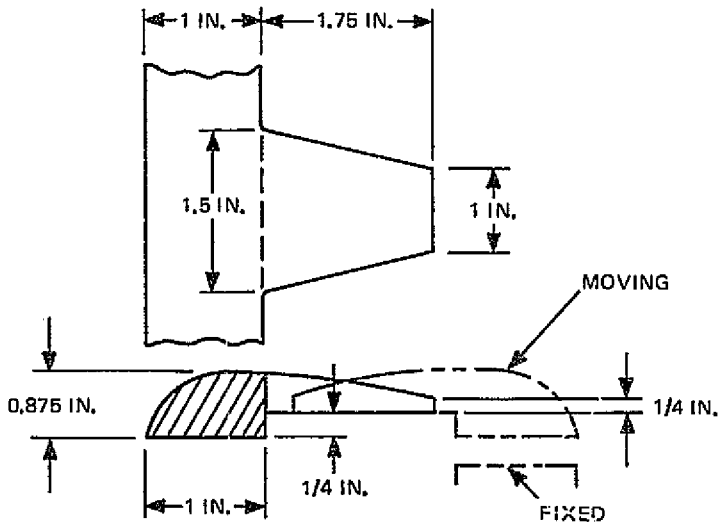

Figure C-22. Rim motor metal.

Table C-3 contains a list of design values derived from the foregoing analysis. A decision was made later to go to a three-phase arrangement rather than a torquer arrangement. The values shown are for the latter configuration. The items marked with a bullet are still pertinent and the losses are unaffected.

TABLE C-3. M-G DATA

	Configuration			
	1	2A-1	3	4
• Number of Poles	28	28	28	28
• Pole Span, in.	2.5	2.5	2.5	2.5
• Stack Height, in.	1.8	1.6	1.5	1.5
• Torque Force Arm, in. x 2	22	22	22	22
• Magnet Size, in.	0.3 Lg x 1 x 1.8	0.3 x 1 x 1.6	0.3 x 1 x 1.83	0.3 x 1 x 1.5
• Number of Magnets/ Circuit	1	2	2	2
• Gap-in. (complete circuit)	0.12	.14/217	0.314	0.234
• Gap Field, B, gauss	4845	4200	2608	2726
Wire Size, in. Armature	0.051 round	0.040 x .057 rect.	0.066 x 0.057 rect.	0.062 x 0.057 rect.
Field	--	--	0.051 round	0.051 round
Conductor Length, ft.	470	326	166	336
• Copper Volume, cu in.	11.52	5.83	9.90	13.36
• Weight-Moving Parts, lb.	4.65	35.10	31.04	22.03
Maximum Current	8	10.4	24.76	23.6
• Current Density Amps/in.^{2}	3950	6980	6980	6980
Coils in Series	4	28	4	4
Number of Parallel Paths	28	-	7	7

C. TECHNICAL NOTE C-1 (INLAND MOTORS DESIGN SHEETS AND CRITIQUE)

The Inland Motor Division of the Kollmorgen Corporation reviewed the RCA preliminary designs and performed some preliminary analysis of two motor configurations, 1 and 2. Their contributions follow in pages C-42 through C-63.

D. ARMATURE COIL DESIGN

The ironless armature can be designed as shown in the typical coil layout in Figure C-23, or by concentrating the individual strands into twisted bundles (litz wires) as partly shown in Sketch SK 2294234. The first construction poses problems in providing clearance for the coil ends at the inner rim and is wasteful of wire (hence I^2R loss). Also, to minimize eddy current loss in the wire, the number of coils becomes impractically large. An unconventional armature design has been selected for the point design.

From Section II (Technical Note 2-1), the armature coil eddy current upper bound loss has been calculated. This is based on the use of litz wires. Actual losses are expected to be a small fraction of the calculated value.

Litz Wire Diameter

AWG No. 10 wire diameter is 0.1019 in.

The Litz equivalent is AWG No. 36 in 413 strands

Area of No. 10 is 0.00816 $in.^2$

Area of one Litz strand is 0.000373 $in.^2$

Area of 413 strands is 0.0154 $in.^2$

Assume 80% pack factor

Total area = 0.01015 $in.^2$

Assume round shape

Litz wire diameter = 0.157 in.

Coil Winding

The coils per phase per pole = 2

The coil pitch is 2/3 (throw 1-5)

The coil winding arrangement is shown in Figure C-24.

TORQUE MOTOR DESIGN SHEETS

MOTOR CONFIGURATION 1

Customer: RCA
Dwg. No.:
Date: 1-25-77

I Assumptions =

No. Poles = P = 24

No. Teeth = 112

Pole Span = 0.425

Stack Height = 1.0

Stator O. D. = —

Stator I. D. = } 22 mean Dia., Δ = 0.030

Rotor O. D. =

Rotor I. D. =

Stator Casing (If Req'd) =

Max. Current Input = 6 amps / path - 24 paths

II To find magnet operating point:

M_W = Magnet Width = 1.0

M_t = Magnet Radial Thickness = $\frac{\text{Stator O. D.} - \text{Stator I. D.} - .030}{2}$ = $\frac{1.0 - .97}{2}$

M_A = Magnet Area = $M_W M_t$ = $0.5(1) = .5 \text{ in.}^2$

Assume a flux/pole: $\phi = \frac{M_A \times 60{,}000 \times 2}{1.5}$ = —

W_p = Width of Pole Constriction = $\frac{\phi}{110{,}00\ M_W}$ = —

M_L = Magnet Length = $\frac{(\text{Stator I. D.} + .030)\pi}{P} - W_p$ = .3

Pole Arc = $\frac{(\text{Stator I. D.})\pi}{P}$ x Pole Span = 1.0

K_s = Carter's Coefficient = $\dfrac{(5g + W_s)\ S_p}{(5g + W_s)\ SP - W_s^2}$ = say 1.1

Permeance/Pole = $\dfrac{\text{(Pole Arc)(Stack Height)}}{K_s\ g}$ = $\dfrac{1\,(1)}{1.1\ (.062)}$ = 14.5

$u_1 = \dfrac{4\ M_a}{M_L} = \dfrac{\text{Permeance}}{\text{Permeance}} = \dfrac{30.5\ (.5)}{4\ (.5)}$ = 4.57

To find u when motor is energized:

Current per path = $\dfrac{\text{Max. Current Input}}{2}$ = 8.4 / 1.41 = 5.95

Assumed turns/coil = 10

T_p = No. Teeth/Pole = $\dfrac{\text{No. Teeth x Pole Span}}{P}$ $\dfrac{112\ (.455)}{2\ \#}$ = 1.61

C_m = Demagnetizing ampere - turns per pole

$C_m = \dfrac{\text{(Turns/coil)(Current per Path)(No. Teeth)}}{P}$ x Pole Span $10(\#)(1.62) = 129.6$

Demag. Oersteds = $\dfrac{C_m}{2.02 \times M_L}$ $\dfrac{129.6}{2.02}$ $\div$) = 214.3 - Very Low

Bgap = $\dfrac{\phi}{\text{(Pole Arc)(Stack Height)}}$ =

GAP A.T. = .313 $B_g K_s$ =

Tot. Drop While Energized = GAP A.T. + Total Demagnetizing A.T./Pole =

Note: Operating density obtained from curve of magnet material selected

Magnet Chosen = _____

Operating Density = 6.5 K Gauss x 6.45 = _____

(1) ϕ_M = Magnet Flux/Pole = Operating Density x 2 M_A = 2(.5) 4.37 = 4.37 lines

ϕ_B = Flux/Pole in bridge = 2 x 130,000 x B_t x M_W = _____ where B_t = Bridge Thickness

(2) ϕ_A = Air Gap Flux/Pole = $\frac{(1) - (2)}{\text{Leakage Factor}}$ = 4.25 = 4.25 x 10^5 lines

III To find slot dimensions:

Lam. Material Used = No. of Slots =

B = Flux Density Used =

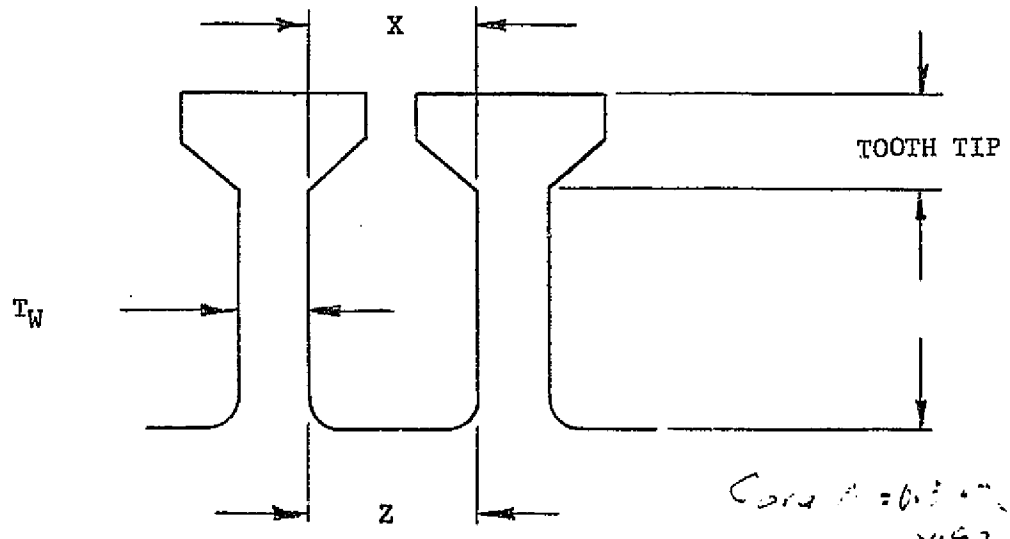

Core Area = 6.5 x 2.5 = 16.25 in²

.493 = 1.317 in²

Yoke Thickness = $\frac{\phi}{2\ B\ (\text{Stack Height})\ .93}$ = $B_{core} = \frac{2.54\phi}{1.317} = 2.0 \times kL$

$t_w = \frac{\phi}{B\ T_p\ (\text{Stack Height})\ .93}$ =

$$X = \frac{[\text{Rotor O. D.} - 2(\text{Tooth Tip})]\,\pi}{\text{No. Teeth}} - t_w =$$

$$Y = \frac{\text{Rotor O. D.} - 2(\text{Tooth Tip}) - \text{Rotor I. D.} - 2\,(\text{Yoke})}{2} =$$

$$Z = \frac{[\text{Rotor O. D.} - 2(\text{Tooth Tip}) - 2y]\,\pi}{\text{No. Teeth}} - t_w =$$

$$A_{slot} = \frac{(x+z)y}{2} =$$

IV| To determine torque sensitivity:

$A_{wire} = K_F\,(A_{slot}) =$ where K_F = Fill Factor

Size wire chosen = #16

$$\text{No. Conductors/Slot} = \frac{A_{wire}}{\pi/4\,(\text{Wire Dia})^2} =$$

$$\text{No. Turns/Coil} = \frac{\text{No. Conductors/Slot}}{2} = 12$$

Z = Tot. Conductors = (No. Conductors/Slot)(No. Slots) = 2(12)(112) = 2688

$T_s = 22.5 \times 10^{-8}\; Z\,\phi\,\frac{P}{a}$ oz.-in./amp. $22.5(10^{-8})(2.24)(40540)\frac{2^4}{2\times}$ = 20.43 oz-in/A

$= \frac{20.43}{192}$ lb ft/A = 0.1064 lb ft/A, $K_b = 1.3(.1064) = 0.1443$ V/rad/s

T_s = Volts @ 11,000 rpm = 0.1443 (11000) = 16.62 Volts

V| To find resistance: $\frac{16.62}{2} = 8.31$ Volts @ 550 rpm

$$\text{LMT} = 2(\text{Stack Height}) + 2(\text{End Bundle}) + 2\pi\,[\text{Rotor O.D.} - (y + 2(\text{Tooth Tip}))] \times \frac{\text{Teeth Linked}}{\text{Total Teeth}}$$

LMT $\cong$ 2 [1.772 + 0.3π + 1] = 8.16"

$$R = \frac{(LMT)(No.\ Teeth)(No.\ Turns/Coil)(Wire\ Resistance\ in\ ohms/ft.)}{48}$$

$R_M = R \times K_{BR}$ where K_{BR} = Shorting Factor due to Brushes

$ft/path = \frac{8.568}{12}\left(\frac{12\ T}{coil}\right)\left(4\ \frac{Coil}{path}\right) = 29.56\ ft$

$Resistance = \frac{29.56(0.00493)}{2} = 0.00432\ ohms$

at 1/2 speed:

$I^2R = [8(28)^2(0.00432)] = 216.76$ watts @ half speed

Generator Losses (11,000 RPM) $= 83(224) = 18592$

$- 217$ (base)

18375

$Efficiency = \frac{18375}{18592}(100) = 98.8\%$

at full speed:

$I^2R \approx [4(28)^2(0.00432)] = 54.2$ watts

FEATURES

Well-Balanced Magnetic Properties

HICOREX is made to have a residual flux density (Br) value approximately equal to the coercive force (BHC) value. Because of this balance, HICOREX performs ideally even when magnetized in single pieces before installation into equipment. Moreover, thinner magnets can be made from HICOREX than any other magenetic material.

Excellent Stability

The coercive force of HICOREX is 10 times that of Alnico magnets. HICOREX resists demagnetizing forces remarkably well, and its properties are little affected by vibrations encountered under ordinary circumstances.
HICOREX also offers excellent resistance to corrosion and oxidation. Because of these superior properties, HICOREX can be used with the same confidence and ease as Alnico magnets.

MAGNETIC PROPERTIES OF HICOREX

Grade	Residual Induction Br (KG)	Coercive Force BHC(KOe)	Maximum Energy Product (BH)max.MGOe
HICOREX 10	6.0~6.6	6.0~6.6	9~11
" 12	6.6~7.2	6.6~7.2	11~13
" 14	7.2~7.7	7.2~7.7	13~15
" 16	7.7~8.2	7.7~8.0	15~17
" 18	8.2~8.7	8.0~8.5	17~19
" 20	8.7~9.2	8.5~9.0	19~21

Recoil permeability,	μ rec	1.0~1.1
Curie point,	Tc	710°C
Irreversible loss	(0°C~250°C)	3~7%
Reversible temperature coefficient	(0°C~200°C)	−0.03~−0.05%/°C
Hardness	Hv	460
Density	gr/cm³	7.3~8.3

HICOREX 20

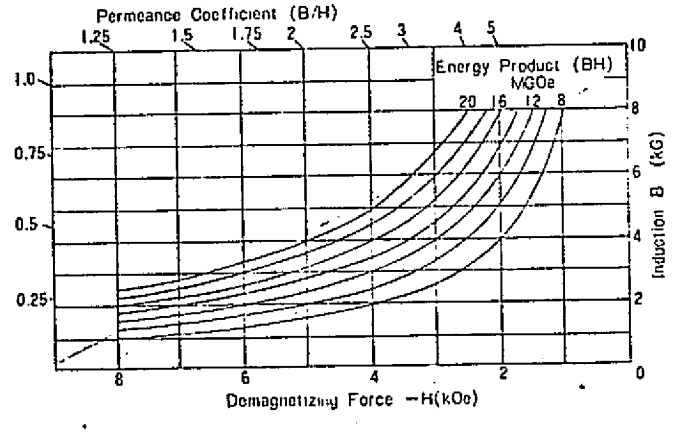

HICOREX 18

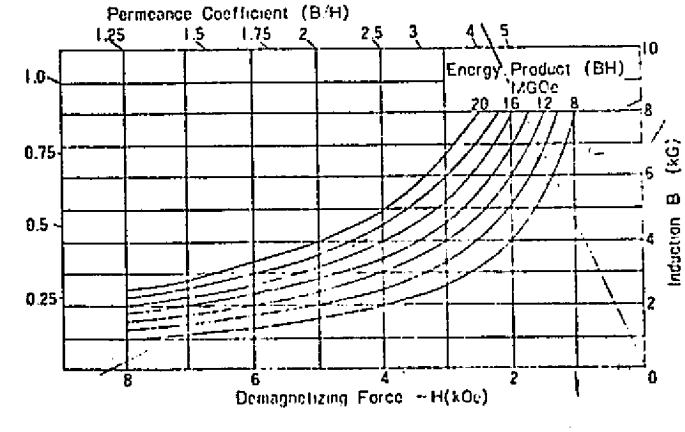

HICOREX 90
(BH)max BH = 18 MILLION MIN
(BH)R BR =
HC (BH)R HC = 6500 @ BR = 2000

TORQUE MOTOR DESIGN SHEETS

Motor Configuration 2A-1

Assume 1. 2 Ø winding

2. Sufficient iron in Stator to Carry flux

Customer: RCA
Dwg. No.:
Date: 1-25-77

I | Assumptions =

No. Poles = P = 28

No. Teeth = 112

Pole Span = 1.648 = $\frac{1.6}{\frac{\pi(22)}{28}}$

Stack Height = 1.25"

Stator O. D. = —

Stator I. D. = } 22.000 Mean Dia Δ = 0.030 + 0.250 inch/pole, Δ = 0.280 in

Rotor O. D. = } 0.2

Rotor I. D. =

Stator Casing (If Req'd) =

Max. Current Input =

II | To find magnet operating point:

M_W = Magnet Width = 1.00

M_t = Magnet Radial Thickness = $\frac{\text{Stator O. D.} - \text{Stator I. D.} - 0.030}{2}$ = $\frac{1}{2}$*(1.0) = 0.4

M_A = Magnet Area = $M_W M_t$ = 0.4 (1.1) = 0.18 in.^{2}

* To fit equation for μ_1 only 2

Assume a flux/pole: ϕ = $\frac{M_A \times 60{,}000 \times 2}{1.5}$ = /

W_p = Width of Pole Constriction = $\frac{\phi}{110{,}00\ M_W}$ = /

M_L = Magnet Length = $\frac{(\text{Stator I. D.} + .030)\pi}{P}$ - W_p = 2*(0.3) = .6 x 2

* To fit equation μ_1 only 2

Pole Arc = $\frac{(\text{Stator I. D.})\pi}{P}$ x Pole Span = 1.6 in

K_s = Carter's Coefficient = $\frac{(5g + W_s)\ S_p}{(5g + W_s)\ SP - W_s^2}$ = Say 1.0

Permeance/Pole = $\frac{\text{(Pole Arc)(Stack Height)}}{K_s\ g}$ = $\frac{1(1.6)}{1(.155)}$ = 10.3

$\mu_1 = \frac{\text{Permeance}}{\frac{4\ M_a}{M_L}}$ = _____ =

To find μ when motor is energized:

Current per path = $\frac{\text{Max. Current Input}}{2}$ =

Assumed turns/coil =

T_p = No. Teeth/Pole = $\frac{\text{No. Teeth x Pole Span}}{P}$ $\frac{112}{28}$ = 2.0

C_m = Demagnetizing ampere - turns per pole

$C_m = \frac{\text{(Turns/coil)(Current per Path)(No. Teeth)}}{P}$ x Pole Span 1(65.3)2.0 = 130

Demag. Oersteds = $\frac{C_m}{2.02 \times M_L}$ = $\frac{130}{2.02(.6)}$ = 140 oe (Say 500)

Bgap = $\frac{\phi}{\text{(Pole Arc)(Stack Height)}}$ =

GAP A.T. = .313 $B_g K_s$ =

Tot. Drop While Energized = GAP A.T. + Total Demagnetizing A.T./Pole =

Note: Operating density obtained from curve of magnet material selected

Magnet Chosen = Hiperm 49

Operating Density = 5.0 Gauss x 6.45 = 32250 maxwells/in^2

(1) ϕ_M = Magnet Flux/Pole = Operating Density x 2 M_A = $\frac{2(5.0)(3225.0)}{?}$ = 51600 max

ϕ_B = Flux/Pole in bridge = 2 x 130,000 x B_t x M_W = ? where B_t = Bridge Thickness

(2) ϕ_A = Air Gap Flux/Pole = $\frac{(1) - (2)}{\text{Leakage Factor}}$ = $\frac{51600}{1.05}$ - 49142 lines/pole

$B_g = \frac{49142}{1.0}$ = 23.7 kl/in^2

III To find slot dimensions:

Lam. Material Used = No. of Slots =

B = Flux Density Used =

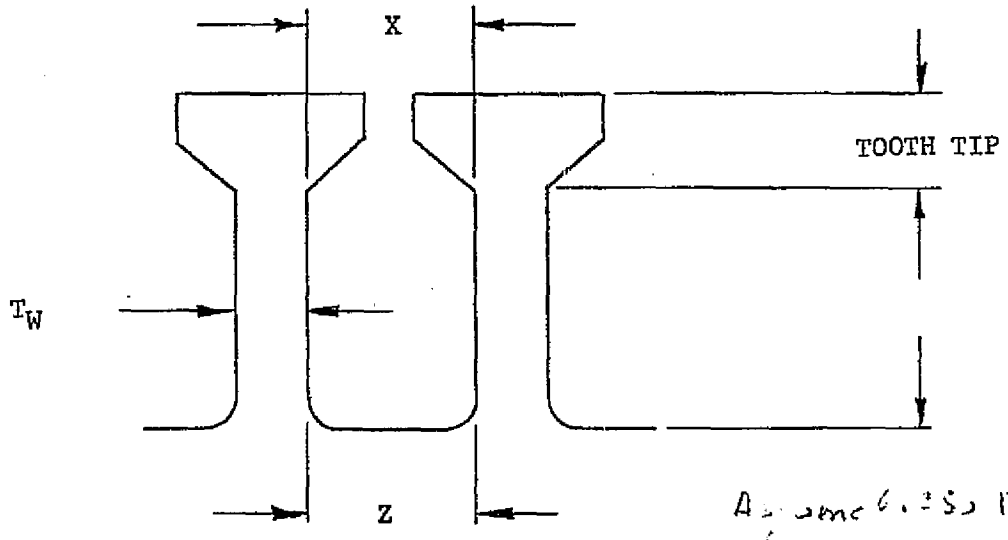

Assume 6.25 plate on bottom of magnet OD = 23 in ID = 21 in

Yoke Thickness = $\frac{\phi}{2\ B\ (\text{Stack Height})\ .93}$ =

$B = \frac{51600}{(.25)(1)(2)}$ = 103.2 kl/in^2

t_w = $\frac{\phi}{B\ T_p\ (\text{Stack Height})\ .93}$ =

Weight = .28 $(3.14/2)(23^2 - 21^2)(25)(1/2)$

= 9.7 lbs

$$X = \frac{[\text{Rotor O. D.} - 2(\text{Tooth Tip})]\,\pi}{\text{No. Teeth}} - t_w =$$

$$Y = \frac{\text{Rotor O. D.} - 2(\text{Tooth Tip}) - \text{Rotor I. D.} - 2\,(\text{Yoke})}{2} =$$

$$Z = \frac{[\text{Rotor O. D.} - 2(\text{Tooth Tip}) - 2y]\,\pi}{\text{No. Teeth}} - t_w =$$

$$A_{slot} = \frac{(x+z)y}{2} =$$

IV| To determine torque sensitivity:

$A_{wire} = K_F\,(A_{slot}) =$ where K_F = Fill Factor

Size wire chosen = #10

$$\text{No. Conductors/Slot} = \frac{A_{wire}}{\pi/4\,(\text{Wire Dia})^2} =$$

$$\text{No. Turns/Coil} = \frac{\text{No. Conductors/Slot}}{2} = 1 \text{ on } \tfrac{2}{3} \text{ pitch}$$

$C = 16(.212) = 5.3$

$K_w = .924(.944) = .872$

K_w = Distribution x chord factor

Z = Tot. Conductors = (No. Conductors/Slot)(No. Slots) = $CK_w = 47.8$

$$T_s = 22.5 \times 10^{-8}\; Z\,\phi\,\frac{P}{a} \text{ oz.-in./amp.} = 71\,(P)^2\phi I\left(\frac{CK_w}{2P}\right)\left(\frac{I}{I}\right)10^{-8}$$

$$= 71\,(28)^2(48140)\,\frac{47.8}{2\times 28} \times 10^{-8} = 23.38 \text{ oz in/A} = .121 \text{ Lb/ft/A}$$

~~T_s~~ $K_B = 1.352\,(.1216) = .1649$ V/rad/s

Back gen. volts @ 11,000 = $(11000/4.55) = 190$ volts

V| To find resistance:

$$LMT = 2(\text{Stack Height}) + 2(\text{End Bundle}) + 2\pi\left[\text{Rotor O.D.} - (y + 2(\text{Tooth Tip}))\right] \times \frac{\text{Teeth Linked}}{\text{Total Teeth}}$$

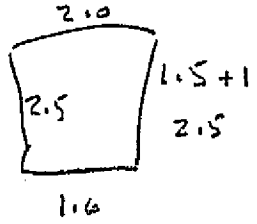

LMT = ft/phase = $(2 + 2.5 + 2.5 + 1.6)\,21 = 20$ ft

Res/phase @ 21°C = $\left(.00010 \times 4_x \left(\frac{12}{20}\right)\right) = .0234$ ohms

$$R = \frac{(LMT)(\text{No. Teeth})(\text{No. Turns/Coil})(\text{Wire Resistance in ohms/ft.})}{48}$$

$R_M = R \times K_{BR}$ where K_{BR} = Shorting Factor due to Brushes

Peak Watts Output = 17540

Watts/phase = $\frac{17540}{2}$ = 8770

RMS Volts = $\frac{160.707}{2}$ = 134.3

RMS Amps = $\frac{8770}{134.3}$ = 65.3 amps

CM = 10400 $CM/A = \frac{10400}{65.3}$ = 159

Watts loss = $I^2(R)(2) = (65.3)^2(.12)(2)$ = 1711 watts

FEATURES

Well-Balanced Magnetic Properties

HICOREX is made to have a residual flux density (Br) value approximately equal to the coercive force (BHC) value. Because of this balance, HICOREX performs ideally even when magnetized in single pieces before installation into equipment. Moreover, thinner magnets can be made from HICOREX than any other magenetic material.

Excellent Stability

The coercive force of HICOREX is 10 times that of Alnico magnets. HICOREX resists demagnetizing forces remarkably well, and its properties are little affected by vibrations encountered under ordinary circumstances.
HICOREX also offers excellent resistance to corrosion and oxidation. Because of these superior properties, HICOREX can be used with the same confidence and ease as Alnico magnets.

MAGNETIC PROPERTIES OF HICOREX

Grade	Residual Induction Br (KG)	Coercive Force BHC (KOe)	Maximum Energy Product (BH)max MGOe
HICOREX 10	6.0~6.6	6.0~6.6	9~11
" 12	6.6~7.2	6.6~7.2	11~13
" 14	7.2~7.7	7.2~7.7	13~15
" 16	7.7~8.2	7.7~8.0	15~17
" 18	8.2~8.7	8.0~8.5	17~19
" 20	8.7~9.2	8.5~9.0	19~21

Recoil permeability,	μ rec	1.0~1.1
Curie point,	Tc	710°C
Irreversible loss	(0°C~250°C) H_c 0.5	3~7
Reversible temperature coefficient	(0°C~200°C)	−0.03~−0.05%/°C
Hardness	Hv	460
Density	gr/cm³	7.3~8.3

HICOREX 20

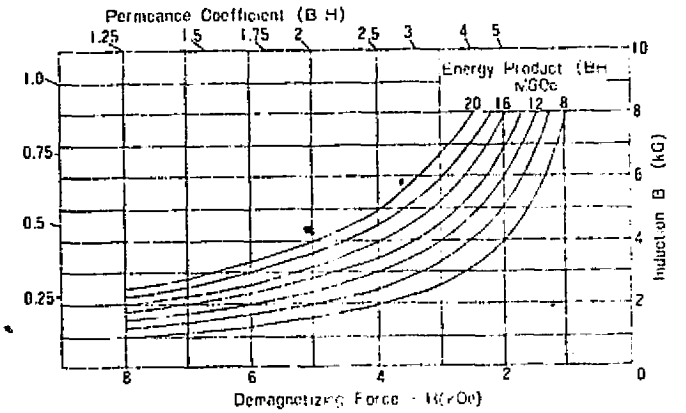

ORIGINAL PAGE IS
OF POOR QUALITY

HICOREX 18

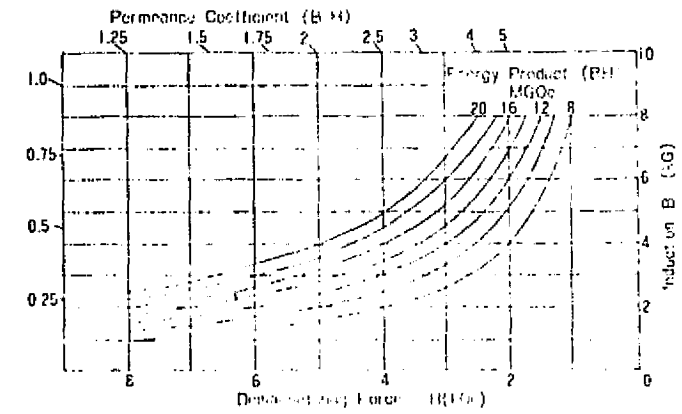

Ref.
↓ HICOREX 90
(typ.) BH = 18 MGOe (min.)
(typ.) Br =
Hc (typ.) Hc=6.5kOe @ Br=20kG

TORQUE MOTOR DESIGN SHEETS

Motor Configuration 24-1

Customer: RCA
Dwg. No.:
Date: 1-25-77

Assume: 1. Delta Connected 3 ϕ winding
2. Sufficient iron in Stator & Carrier for flux.

I | Assumptions =

No. Poles = P = 24

No. Teeth = 144 (2 Coils/Phase/Pole)

Pole Span = .648 = 1.6/3.14(23)/24

Stack Height = 1.25

Stator O. D. =

Stator I. D. =

Rotor O. D. = } 22.00 Mean Dia., Δ = 2 (.03) + .250 = .310

Rotor I. D. =

Stator Casing (If Req'd) =

Max. Current Input =

II | To find magnet operating point:

M_W = Magnet Width = 1.00

M_t = Magnet Radial Thickness = $\frac{\text{Stator O. D.} - \text{Stator I. D.} - .030}{2}$ = $\frac{1}{2}$ (1.6) = .8

M_A = Magnet Area = $M_W M_t$ = (1.0)(.8) = .8 in²

* To find equation for μ, on Pg 2

Assume a flux/pole: $\phi = \frac{M_A \times 60{,}000 \times 2}{1.5}$ = /

W_p = Width of Pole Constriction = $\frac{\phi}{110{,}00\ M_W}$ = /

M_L = Magnet Length = $\frac{(\text{Stator I. D.} + .030)\pi}{P} - W_p$ = (2)(.8)(.83) = 1.2 in.

2 magnets/pole in series

Pole Arc = $\frac{(\text{Stator I. D.})\pi}{P}$ x Pole Span = 1.6 in.

K_s = Carter's Coefficient = $\dfrac{(5g + W_s)\ S_p}{(5g + W_s)\ SP - W_s^2}$ = Say 1.0

Permeance/Pole = $\dfrac{\text{(Pole Arc)(Stack Height)}}{K_s\ g}$ = $\dfrac{1\ (1.6)}{(0.3)}$ = 5.16

$\mu_1 = \dfrac{\text{Permeance}}{\dfrac{4\ M_a}{M_L}} = \dfrac{5.1\ (1.2)}{4\ (1.8)} = 1.935$

To find u when motor is energized: Max Rms line amps

Current per path = $\dfrac{\text{Max. Current Input}}{2} = \dfrac{77}{.707}\ \dfrac{1}{2}) = 54.5$

Assumed turns/coil = 1

T_p = No. Teeth/Pole = $\dfrac{\text{No. Teeth x Pole Span}}{P}$ = $\dfrac{1\pi(6.644)}{24} = 3.888$ use 4.0

C_m = Demagnetizing ampere - turns per pole

$C_m = \dfrac{\text{(Turns/coil)(Current per Path)(No. Teeth)}}{P}$ x Pole Span = $\dfrac{1\ (54.5)(4}{24} = C_m$

Demag. Oersteds = $\dfrac{C_m}{2.02 \times M_L}$ $\dfrac{218}{2.02\ (1.2)}$ = 90 ok, say 500

Bgap = $\dfrac{\phi}{\text{(Pole Arc)(Stack Height)}}$ =

GAP A.T. = .313 $B_g K_s$ =

Tot. Drop While Energized = GAP A.T. + Total Demagnetizing A.T./Pole =

Note: Operating density obtained from curve of magnet material selected

Magnet Chosen = Hicorex 9,

Operating Density = 5.0 Gauss x 6.45 = 32250 Gauss/in.²

(1) ϕ_M = Magnet Flux/Pole = Operating Density x 2 M_A = 2 (0.8) 32250 = 51600

ϕ_B = Flux/Pole in bridge = 2 x 130,000 x B_t x M_W = — where B_t = Bridge Thickness

(2) ϕ_A = Air Gap Flux/Pole = $\frac{(1) - (2)}{\text{Leakage Factor}}$ = $\frac{51600}{1.05}$ = 47143 lines/pole

$B_g = \frac{47143}{1.6} = 30.7$ kg/in

III To find slot dimensions:

Lam. Material Used = No. of Slots =

B = Flux Density Used =

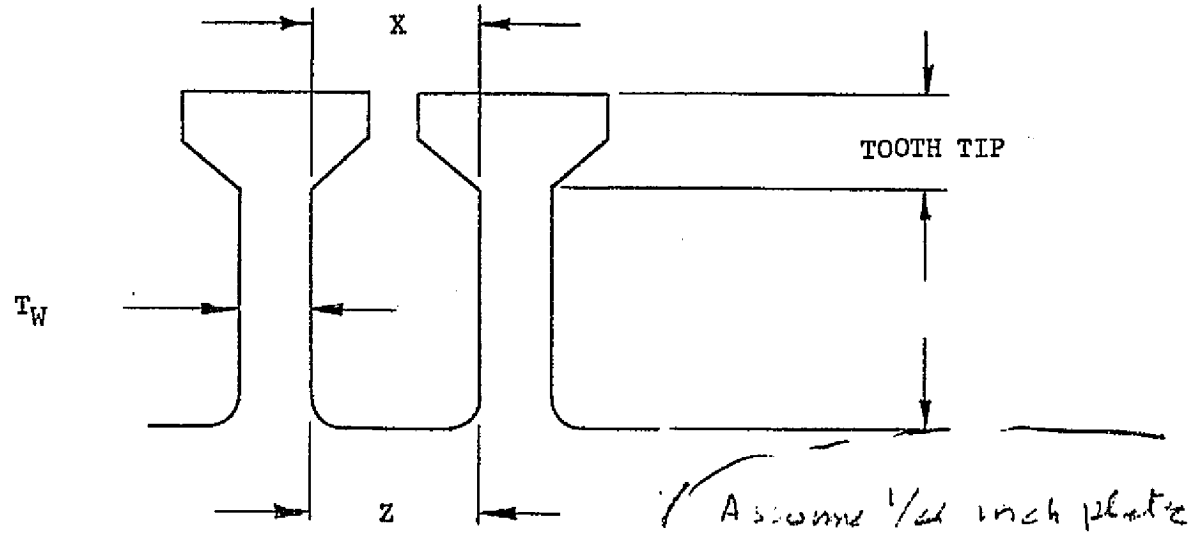

Yoke Thickness = $\frac{\phi}{2\ B\ (\text{Stack Height})\ .93}$ =

$t_w = \frac{\phi}{B\ T_p\ (\text{Stack Height})\ .93}$ =

Assume 1/4 inch plate on back of magnets
O.D. = 23, I.D. = 21 in.
$B = \frac{51600}{2(1)(.25)} = 103.2$ kl/in²
Weight = .28 lb./in³ × $\frac{3.14}{4}(23^2 - 21^2)(.25)$
= 9.7 lbs.

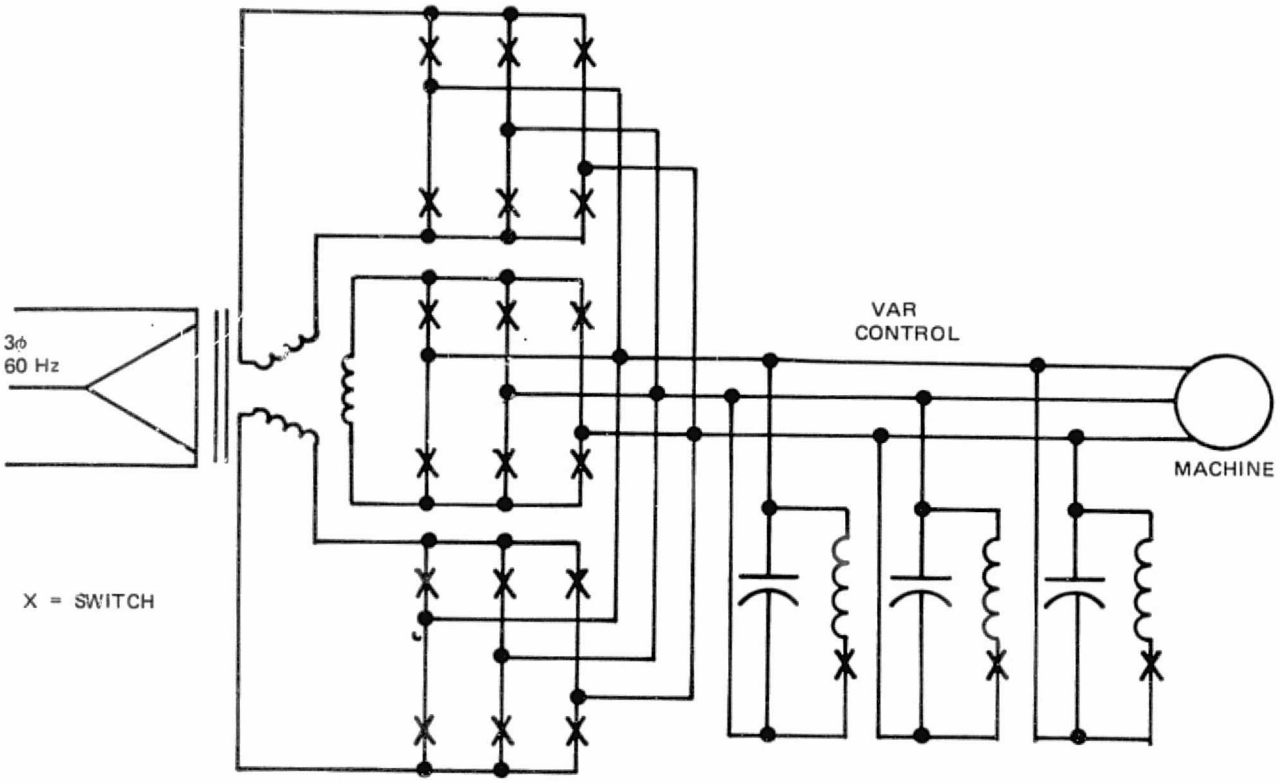

(a) Elemental schematic of NCC.

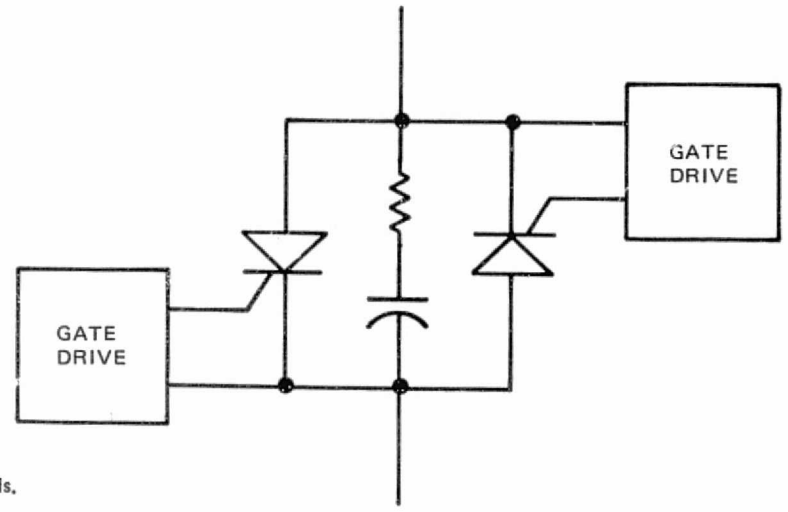

(b) Switch details.

Figure D-2. NCC diagrams.

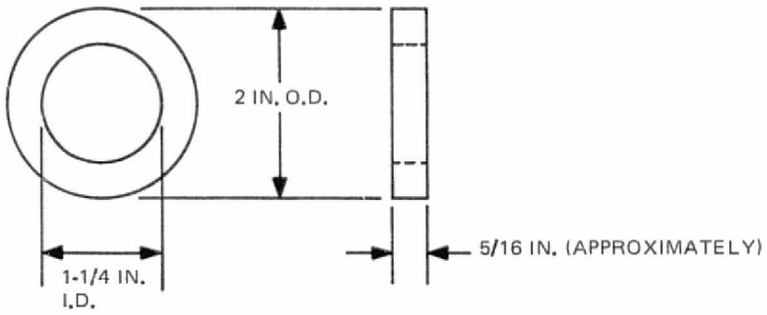

Figure F-1. Core dimensions.

Five powder grades were prepared, but only three cores made from these were sound and suitable for testing. The weights of these are:

Grade	Wt, grams
E_{cr}	97.6
C	96.2
L	94.4

Figure F-2 shows the powder, compacting mold and a finished core with a simulated winding to show the method of winding.

Figure F-2. Toroid coil components.

K_s = Carter's Coefficient = $\dfrac{(5g + W_s)\ S_p}{(5g + W_s)\ SP - W_s^2}$ = [illegible]

Permeance/Pole = $\dfrac{\text{(Pole Arc)(Stack Height)}}{K_s\ g}$ = [illegible]

$u_1 = \dfrac{\text{Permeance}}{\dfrac{4\ M_a}{M_L}}$ = [illegible]

To find u when motor is energized:

Current per path = $\dfrac{\text{Max. Current Input}}{2}$ = [illegible]

Assumed turns/coil = 10

T_p = No. Teeth/Pole = $\dfrac{\text{No. Teeth x Pole Span}}{P}$ [illegible]

C_m = Demagnetizing ampere - turns per pole

$C_m = \dfrac{\text{(Turns/coil)(Current per Path)(No. Teeth)}}{P}$ x Pole Span [illegible]

Demag. Oersteds = $\dfrac{C_m}{2.02 \times M_L}$ [illegible]

Bgap = $\dfrac{\phi}{\text{(Pole Arc)(Stack Height)}}$ =

GAP A.T. = .313 $B_g K_s$ =

Tot. Drop While Energized = GAP A.T. + Total Demagnetizing A.T./Pole =

Note: Operating density obtained from curve of magnet material selected

Magnet Chosen = _____

Operating Density = 6.5 K Gauss x 6.45 = [illegible]

(1) ϕ_M = Magnet Flux/Pole = Operating Density x 2 M_A = 2(.5) [illegible] = [illegible]

ϕ_B = Flux/Pole in bridge = 2 x 130,000 x B_t x M_W = _____ where B_t = Bridge Thickness

(2) ϕ_A = Air Gap Flux/Pole = $\frac{(1) - (2)}{\text{Leakage Factor}}$ = [illegible]

III To find slot dimensions:

Lam. Material Used = No. of Slots =

B = Flux Density Used =

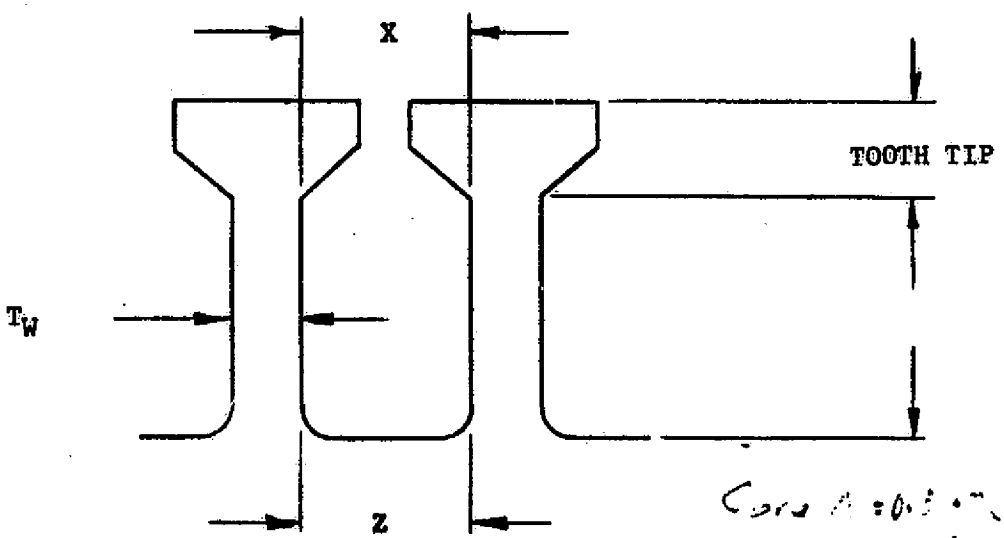

Core [illegible]

x.93 = 1.317 [illegible]

Yoke Thickness = $\frac{\phi}{2\ B\ (\text{Stack Height})\ .93}$ = $B_{core} = \frac{2.548}{1.317} = 20.\times$ KL

$t_w = \frac{\phi}{B\ T_p\ (\text{Stack Height})\ .93}$ =

$$X = \frac{[\text{Rotor O. D.} - 2(\text{Tooth Tip})]\,\pi}{\text{No. Teeth}} - t_w =$$

$$Y = \frac{\text{Rotor O. D.} - 2(\text{Tooth Tip}) - \text{Rotor I. D.} - 2\,(\text{Yoke})}{2} =$$

$$Z = \frac{[\text{Rotor O. D.} - 2(\text{Tooth Tip}) - 2y]\,\pi}{\text{No. Teeth}} - t_w =$$

$$A_{slot} = \frac{(x+z)y}{2} =$$

IV] To determine torque sensitivity:

$A_{wire} = K_F\,(A_{slot}) =$ where K_F = Fill Factor

Size wire chosen = #16

$$\text{No. Conductors/Slot} = \frac{A_{wire}}{\pi/4\,(\text{Wire Dia})^2} =$$

$$\text{No. Turns/Coil} = \frac{\text{No. Conductors/Slot}}{2} = 15$$

Z = Tot. Conductors = (No. Conductors/Slot)(No. Slots) = 24(15)(112) = 4224

$T_s = 22.5 \times 10^{-8}\; Z\,\phi\,\frac{P}{a}$ oz.-in./amp. $22.5(10^{-8})(2.24)(.40543)\frac{2\times}{2\times}$ oz-in/A $= 20.43$ lb ft/A $= 0.1064$ lb ft/A, $K_b = 1.35 \times .1064) = 0.1443$ V/rad/s

T_s = Volts @ 11,000 rpm $= 0.1443(11000) = 16.62$ Volts

V] To find resistance: $\frac{166.2}{2} = 83.1$ Volts @ 5500 rpm $\frac{8.55}{}$

$$\text{LMT} = 2(\text{Stack Height}) + 2(\text{End Bundle}) + 2\pi\,[\text{Rotor O.D.} - (y + 2(\text{Tooth Tip}))] \times \frac{\text{Teeth Linked}}{\text{Total Teeth}}$$

LMT $\doteq 2\,[1.22 \times 0.3\pi^2]\,2 =$

$$R = \frac{(LMT)(No.\ Teeth)(No.\ Turns/Coil)(Wire\ Resistance\ in\ ohms/ft.)}{48}$$

$R_M = R \times K_{BR}$ where K_{BR} = Shorting Factor due to Brushes

$ft/path = \frac{8.868}{12}\left(12\frac{T}{coil}\right)\left(4\ coil/path\right) = 29.56\ ft$

$Resistance = \frac{29.56(0.000491)}{2} = 0.00432\ ohms$

at ½ Speed:

$I^2R = [8(28)^2(0.00432)] = 216.74$ wts each brush

Generated Losses (11,200 RPM) $= 88(224) = 19692$

$- 217$ (brush)

19475

$Efficiency = \frac{19475}{19692}(100) = 98.9\%$

at full Speed:

$I^2R \approx [4(28)^2(0.00432)] = 54.2$ wts

FEATURES

Well-Balanced Magnetic Properties

HICOREX is made to have a residual flux density (Br) value approximately equal to the coercive force (bHC) value. Because of this balance, HICOREX performs ideally even when magnetized in single pieces before installation into equipment. Moreover, thinner magnets can be made from HICOREX than any other magenetic material.

Excellent Stability

The coercive force of HICOREX is 10 times that of Alnico magnets. HICOREX resists demagnetizing forces remarkably well, and its properties are little affected by vibrations encountered under ordinary circumstances.
HICOREX also offers excellent resistance to corrosion and oxidation. Because of these superior properties, HICOREX can be used with the same confidence and ease as Alnico magnets.

MAGNETIC PROPERTIES OF HICOREX

Grade	Residual Induction Br (KG)	Coercive Force bHC (KOe)	Maximum Energy Product (BH)max (MGOe)
HICOREX 10	6.0~6.6	6.0~6.6	9~11
" 12	6.6~7.2	6.6~7.2	11~13
" 14	7.2~7.7	7.2~7.7	13~15
" 16	7.7~8.2	7.7~8.0	15~17
" 18	8.2~8.7	8.0~8.5	17~19
" 20	8.7~9.2	8.5~9.0	19~21

Recoil permeability,	μ rec	1.0~1.1
Curie point,	Tc	710°C
Irreversible loss	(0°C ~ 250°C)	3~7%
Reversible temperature coefficient	(0°C ~ 200°C)	−0.03~−0.05%/°C
Hardness	Hv	460
Density	gr/cm³	7.3~8.3

HICOREX 20

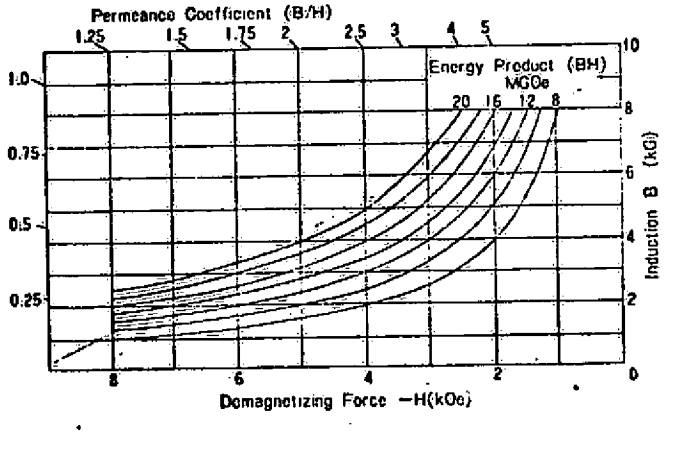

HICOREX 18

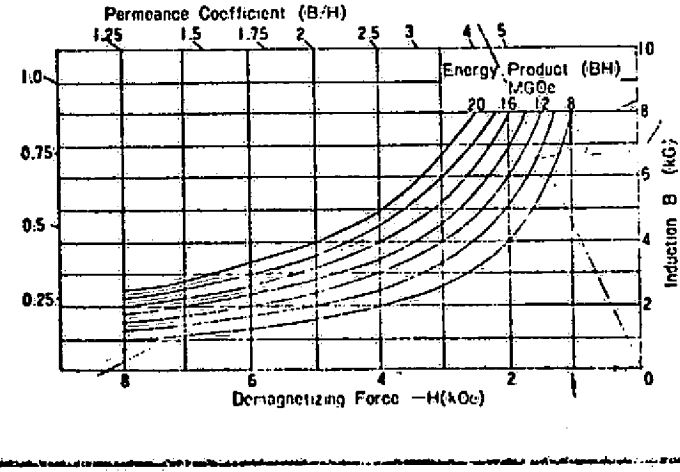

HICOREX 90
(BH)max BH = 18 MILLION MIN
(BH)R BR −
HC (BH) HC = 6500 @ BR = 2000

TORQUE MOTOR DESIGN SHEETS

Motor Configuration 2A-1

Assume 1. 2 ϕ winding

2. Sufficient iron in Stator to Carry flux

Customer: RCA
Dwg. No.:
Date: 1-25-77

I Assumptions =

No. Poles = P = 28

No. Teeth = 112

Pole Span = 3.648 = $\frac{1.6}{\frac{3.14(22)}{28}}$

Stack Height = 1.25"

Stator O. D. = —

Stator I. D. = } 22.000 Mean Dia Δ = 0.030 + 0.250 / 0.2 inch/pole

Rotor O. D. = } Δ = 6.1250 × 2

Rotor I. D. =

Stator Casing (If Req'd) =

Max. Current Input =

II To find magnet operating point:

M_w = Magnet Width = 1.00

M_t = Magnet Radial Thickness = $\frac{\text{Stator O. D.} - \text{Stator I. D.} - 0.030}{2}$ = $\frac{1}{2}$*(1.6) = 0.8 ×

M_A = Magnet Area = $M_w M_t$ = 0.8 (1.1) = 0.8 in.²

× To f.f equation for μ_1 only 2

Assume a flux/pole: ϕ = $\frac{M_A \times 60{,}000 \times 2}{1.5}$ = /

W_p = Width of Pole Constriction = $\frac{\phi}{110{,}00\ M_w}$ = /

M_L = Magnet Length = $\frac{(\text{Stator I. D.} + .030)\pi}{P}$ - W_p = 2*(0.3) = .6 × 2

* To f.f equation μ_1 only 2

Pole Arc = $\frac{(\text{Stator I. D.})\pi}{P}$ x Pole Span = 1.6 in

K_s = Carter's Coefficient = $\dfrac{(5g + W_s)\ S_p}{(5g + W_s)\ SP - W_s^2}$ = Say 1.0

Permeance/Pole = $\dfrac{\text{(Pole Arc)(Stack Height)}}{K_s\ g}$ = $\dfrac{1(1.6)}{1(.153)}$ = 10.4

$\mu_1 = \dfrac{4\ M_a}{M_L} = \dfrac{\text{Permeance}}{\qquad\qquad} =$

To find μ when motor is energized:

Current per path = $\dfrac{\text{Max. Current Input}}{2}$ =

Assumed turns/coil =

T_p = No. Teeth/Pole = $\dfrac{\text{No. Teeth x Pole Span}}{P}$ $\dfrac{112}{24}$ = 2.33

C_m = Demagnetizing ampere - turns per pole

$C_m = \dfrac{\text{(Turns/coil)(Current per Path)(No. Teeth)}}{P}$ x Pole Span 1(65.3) = 65.3

Demag. Oersteds = $\dfrac{C_m}{2.02 \times M_L}$ = $\dfrac{173}{2.02(.6)}$ = 143 oe (Say 500)

Bgap = $\dfrac{\phi}{\text{(Pole Arc)(Stack Height)}}$ =

GAP A.T. = .313 $B_g K_s$ =

Tot. Drop While Energized = GAP A.T. + Total Demagnetizing A.T./Pole =

Note: Operating density obtained from curve of magnet material selected

Magnet Chosen = Hiner 9

Operating Density = 5.0 Gauss x 6.45 = 32250 maxwell/in²

(1) ϕ_M = Magnet Flux/Pole = Operating Density x 2 M_A = 2(2)(32250) = 516000 max

ϕ_B = Flux/Pole in bridge = 2 x 130,000 x B_t x M_W = ? where B_t = Bridge Thickness

(2) ϕ_A = Air Gap Flux/Pole = $\frac{(1) - (2)}{\text{Leakage Factor}}$ = $\frac{516000}{1.05}$ = 491428 lines/pole

$B_g = \frac{491428}{17.8}$ = 27.7 kl/in²

III To find slot dimensions:

Lam. Material Used = No. of Slots =

B = Flux Density Used =

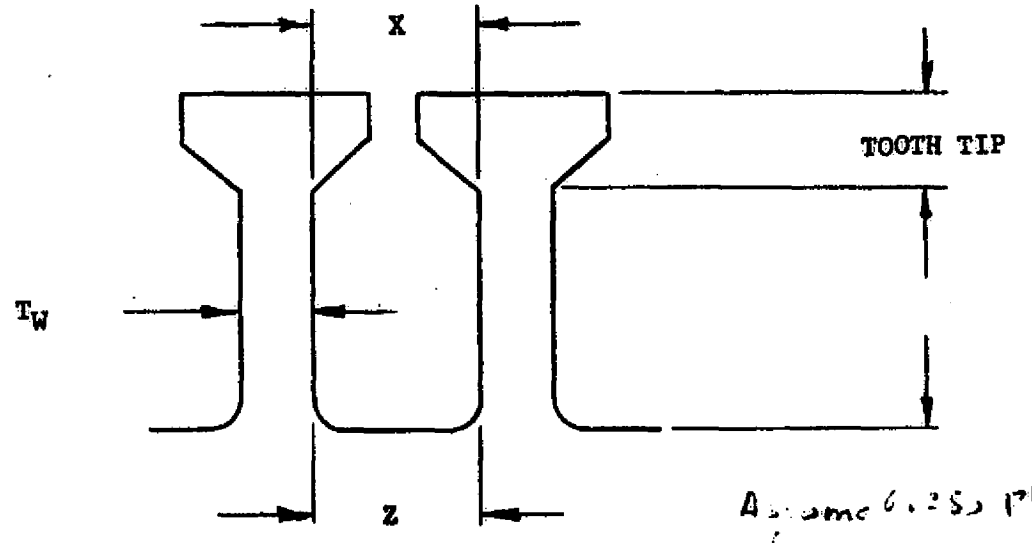

Assume 6.25 plate on back of magnet OD = 23 in ID = 21 in

Yoke Thickness = $\frac{\phi}{2\ B\ (\text{Stack Height})\ .93}$ =

$B = \frac{516000}{(.25)(1)(2)}$ = 103.2 kl/in²

$t_w = \frac{\phi}{B\ T_p\ (\text{Stack Height})\ .93}$ =

Wt = .28 (3.14)(23² − 21²)(25)(2)

= 9.7 lbs

$$X = \frac{[\text{Rotor O. D.} - 2(\text{Tooth Tip})]\,\pi}{\text{No. Teeth}} - t_w =$$

$$Y = \frac{\text{Rotor O. D.} - 2(\text{Tooth Tip}) - \text{Rotor I. D.} - 2\,(\text{Yoke})}{2} =$$

$$Z = \frac{[\text{Rotor O. D.} - 2(\text{Tooth Tip}) - 2y]\,\pi}{\text{No. Teeth}} - t_w =$$

$$A_{slot} = \frac{(x+z)y}{2} =$$

IV | To determine torque sensitivity:

$A_{wire} = K_F\,(A_{slot}) =$ where K_F = Fill Factor

Size wire chosen = #10

$$\text{No. Conductors/Slot} = \frac{A_{wire}}{\pi/4\,(\text{Wire Dia})^2} =$$

$$\text{No. Turns/Coil} = \frac{\text{No. Conductors/Slot}}{2} = 1 \text{ on } \tfrac{2}{3} \text{ pitch}$$

$C = 16(.21/2\pi) = 5.$

$K_w = .924/944) = .955$

K_w = Distribution factor × chord factor

Z = Tot. Conductors = (No. Conductors/Slot)(No. Slots) = $C K_w = 47.8$

$$T_s = 22.5 \times 10^{-8}\; Z\,\phi\,\frac{P}{a} \text{ oz.-in./amp.} = 71\,(P)^2\phi\left(\frac{C K_w}{2P}\right)\left(\frac{I}{T}\right)10^{-8}$$

$$= 71\,(28)^2(48140)\,\frac{47.8}{2 \times 28} \times 10^{-8} = 23.38 \text{ oz-in/A} = .121 \text{ Lb/ft/A}$$

$K_B = 1.352(.1216) = .1649$ V/rad/s

Back gen. volts @ 11,000 = (11000/955) = 190 volts

V | To find resistance:

$$LMT = 2(\text{Stack Height}) + 2(\text{End Bundle}) + 2\pi\,[\text{Rotor O.D.} - (y + 2(\text{Tooth Tip}))] \times \frac{\text{Teeth Linked}}{\text{Total Teeth}}$$

LMT

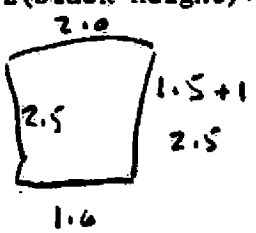

LMT = ft/phase = (2 + 2.5 + 2.5 + 1.6)/21 = 20 ft

Res/phase @ 21°C = $\left(.00010154\left(\frac{12}{20}\right)\right)$ = .0204 ohms

$$R = \frac{(LMT)(No.\ Teeth)(No.\ Turns/Coil)(Wire\ Resistance\ in\ ohms/ft.)}{48}$$

$R_M = R \times K_{BR}$ where K_{BR} = Shorting Factor due to Brushes

Peak Watts Output = 17540

Watts / phase = $\frac{17540}{2} = 8770$

RMS Volts = $100 \times 0.707 = 134.3$

RMS Amps = $\frac{8770}{134.3} = 65.3$ amps

CM = 10400 $CM/A = \frac{10400}{65.3} = 159$

Watts loss = $I^2(R)(2) = (65.3)^2(.12\ \Omega)(2) = 1022$ watts

FEATURES

Well-Balanced Magnetic Properties

HICOREX is made to have a residual flux density (Br) value approximately equal to the coercive force (BHC) value. Because of this balance, HICOREX performs ideally even when magnetized in single pieces before installation into equipment. Moreover, thinner magnets can be made from HICOREX than any other magenetic material.

Excellent Stability

The coercive force of HICOREX is 10 times that of Alnico magnets. HICOREX resists demagnetizing forces remarkably well, and its properties are little affected by vibrations encountered under ordinary circumstances.
HICOREX also offers excellent resistance to corrosion and oxidation. Because of these superior properties, HICOREX can be used with the same confidence and ease as Alnico magnets.

MAGNETIC PROPERTIES OF HICOREX

Grade	Residual Induction Br (KG)	Coercive Force BHC (KOe)	Maximum Energy Product (BH)max (MGOe
HICOREX 10	6.0~6.6	6.0~6.6	9~11
" 12	6.6~7.2	6.6~7.2	11~13
" 14	7.2~7.7	7.2~7.7	13~15
" 16	7.7~8.2	7.7~8.0	15~17
" 18	8.2~8.7	8.0~8.5	17~19
" 20	8.7~9.2	8.5~9.0	19~21

Recoil permeability,	μ rec	1.0~1.1
Curie point,	Tc	710°C
Irreversible loss	(0°C ~ 250°C) H_d 0.5	3~7%
Reversible temperature coefficient	(0°C ~200°C)	−0.03 ~ −0.05%/°C
Hardness	Hv	460
Density	gr/cm³	7.3~8.3

HICOREX 20

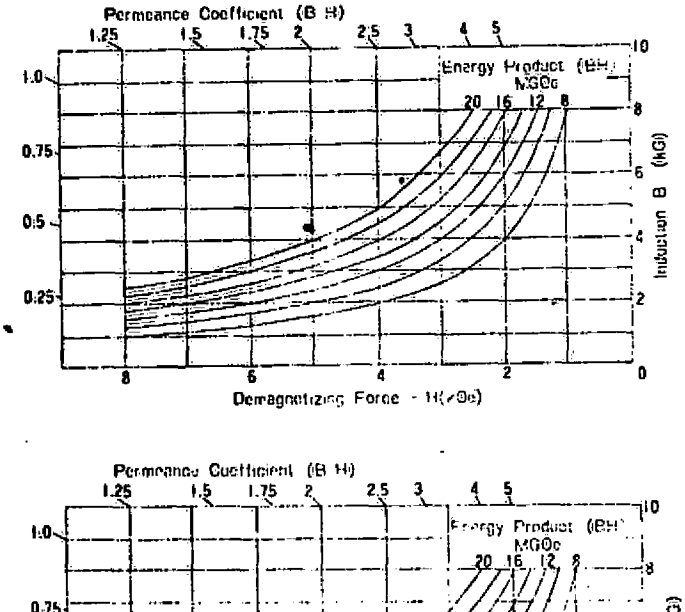

ORIGINAL PAGE IS
OF POOR QUALITY

HICOREX 18

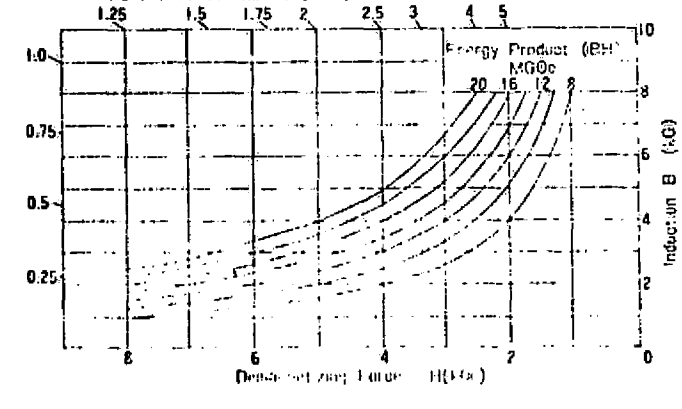

HICOREX 90
(BH) BH = 18 MGOe
(BR) BR =
HC (BHC) HC = 6500 Oe

TORQUE MOTOR DESIGN SHEETS

Motor Configuration 24-1

Customer: RCA
Dwg. No.:
Date: 1-25-77

Assume: 1. Delta connected 3 ϕ winding
2. Sufficient iron in Stator & Carrier to carry flux.

I | Assumptions =

No. Poles = P = 28

No. Teeth = 168 (2 Coils/phase/pole)

Pole Span = .648 = 1.6/3.14(28)/2

Stack Height = 1.25

Stator O. D. =

Stator I. D. =

Rotor O. D. = } 22.00 Mean Dia., Δ = 2 (.03) + .250 = .310

Rotor I. D. =

Stator Casing (If Req'd) =

Max. Current Input =

II | To find magnet operating point:

M_w = Magnet Width = 1.00

M_t = Magnet Radial Thickness = $\frac{\text{Stator O. D.} - \text{Stator I. D.} - .030}{2}$ = $\frac{1}{2}$ (1.6) = .8 *

M_A = Magnet Area = $M_w M_t$ = (1)(.8) = .8 in²

Assume a flux/pole: $\phi = \frac{M_A \times 60{,}000 \times 2}{1.5}$ = /

W_p = Width of Pole Constriction = $\frac{\phi}{110{,}00\ M_w}$ = /

M_L = Magnet Length = $\frac{(\text{Stator I. D.} + .030)\pi}{P} - W_p$ = (2)(2)(.63) = 1.2 in.

Pole Arc = $\frac{(\text{Stator I. D.})\pi}{P}$ x Pole Span = 1.6 in.

* To find equation for M_t on pg 2

2 magnets/pole in series

K_s = Carter's Coefficient = $\dfrac{(5g + W_s)\ S_p}{(5g + W_s)\ SP - W_s^2}$ = Say 1.3

Permeance/Pole = $\dfrac{\text{(Pole Arc)(Stack Height)}}{K_s\ g}$ = $\dfrac{1\ (1.6)}{(0.3)}$ = 5.16

$\mu_1 = \dfrac{\text{Permeance}}{\dfrac{4\ M_a}{M_L}} = \dfrac{5.16\ (1.2)}{4\ (.8)} = 1.935$

To find u when motor is energized: Max Rms line amps

Current per path = $\dfrac{\text{Max. Current Input}}{2} = \dfrac{77}{.707}\ \dfrac{1}{2}) = 54.5$

Assumed turns/coil = 1

T_p = No. Teeth/Pole = $\dfrac{\text{No. Teeth x Pole Span}}{P} = \dfrac{(69.64)1}{24} = 3.488$ use 4.3

C_m = Demagnetizing ampere - turns per pole

$C_m = \dfrac{\text{(Turns/coil)(Current per Path)(No. Teeth)}}{P}$ x Pole Span = $\dfrac{1\ (54.5)(4}{24} = C_m$

Demag. Oersteds = $\dfrac{C_m}{2.02 \times M_L}$ $\dfrac{218}{2.02\ (1.2)}$ = 90 OK, Say 500

Bgap = $\dfrac{\phi}{\text{(Pole Arc)(Stack Height)}}$ =

GAP A.T. = .313 $B_g K_s$ =

Tot. Drop While Energized = GAP A.T. + Total Demagnetizing A.T./Pole =

Note: Operating density obtained from curve of magnet material selected

Magnet Chosen = Hiconex 9

Operating Density = 5.0 Gauss x 6.45 = 32250 Gauss/in²

(1) ϕ_M = Magnet Flux/Pole = Operating Density x 2 M_A = 20.8 | 32250 = 51000

ϕ_B = Flux/Pole in bridge = 2 x 130,000 x B_t x M_W = — where B_t = Bridge Thickness

(2) ϕ_A = Air Gap Flux/Pole = $\frac{(1) - (2)}{\text{Leakage Factor}}$ = $\frac{51000}{1.05}$ = 47143 lines/pole

$B_g = \frac{47143}{1.6}$ = 30.7 kl/in²

III To find slot dimensions:

Lam. Material Used = No. of Slots =

B = Flux Density Used =

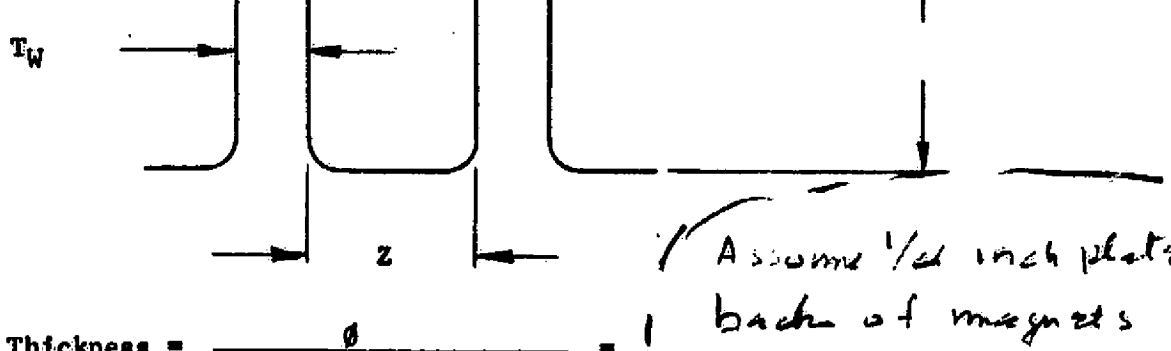

Yoke Thickness = $\frac{\phi}{2\ B\ (\text{Stack Height})\ .93}$ =

$t_w = \frac{\phi}{B\ T_p\ (\text{Stack Height})\ .93}$ =

Assume 1/2 inch plate in back of magnets
O.D. = 23, I.D. = 21 in.
$B = \frac{51000}{2(1)(.25)} = 103.2$ kl/in²
wgt = .28 lb/in³ × $\frac{\pi}{4}(.5)(23^2 - 21^2)$
= 9.7 lbs

$$X = \frac{[\text{Rotor O. D.} - 2(\text{Tooth Tip})]\ \pi}{\text{No. Teeth}} - t_w =$$

Slot [illegible] 3.14 (18)/169 = 0.355 in [illegible]

$$Y = \frac{\text{Rotor O. D.} - 2(\text{Tooth Tip}) - \text{Rotor I. D.} - 2\ (\text{Yoke})}{2} =$$ for two (2) [illegible]

$$Z = \frac{[\text{Rotor O. D.} - 2(\text{Tooth Tip}) - 2y]\ \pi}{\text{No. Teeth}} - t_w =$$

$$A_{slot} = \frac{(x+z)y}{2} =$$

IV To determine torque sensitivity:

$A_{wire} = K_F\ (A_{slot}) =$ where K_F = Fill Factor

Size wire chosen = #10

$$\text{No. Conductors/Slot} = \frac{A_{wire}}{\pi/4\ (\text{Wire Dia})^2} =$$

C = [illegible]

K_w = [illegible] = 0.94

$$\text{No. Turns/Coil} = \frac{\text{No. Conductors/Slot}}{2} =$$ 1 on 2/3 pitch

Z = Tot. Conductors = (No. Conductors/Slot)(No. Slots) = $C K_w$ = 112 (0.94) = 93.64

T_s = ~~22.5 x 10^{-8} Z ϕ $\frac{P}{a}$ oz. in./amp.~~ $= 71 (P)^2 \phi (\frac{C K_w}{2P}) \frac{I}{I} (10^{-8})$

$= 71 (28)^2 \times 4414 \times (93.64) 10^{-8} / 2(28) = 45.76$ oz-in/A = [illegible] lb-ft/A

$T_s = K_{12}$ = 1.356 (.2383) = .3232 V/R/S

Peak Gen. Volts @ 11,000 RPM = .3232 (11,000) = 372 Volts peak or [illegible] .707 (372) = 263 Volts

V To find resistance:

$$\text{LMT} = 2(\text{Stack Height}) + 2(\text{End Bundle}) + 2\pi\ [\text{Rotor O.D.} - (y + 2(\text{Tooth Tip}))] \times \frac{\text{Teeth Linked}}{\text{Total Teeth}}$$

LMT

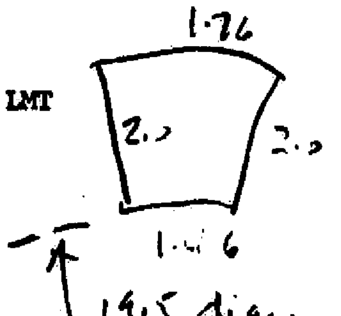

$$\text{LMT} = \frac{(1.76 + 2 + 1.46 + 2)(2)(28)}{12}$$ = [illegible] use 35 ft

Res/phase = [illegible] 35 = 0.03 [illegible] ohm (25°C)

ORIGINAL PAGE IS OF POOR QUALITY

$$R = \frac{(IMT)(\text{No. Teeth})(\text{No. Turns/Coil})(\text{Wire Resistance in ohms/ft.})}{48}$$

$R_M = R \times K_{BR}$ where K_{BR} = Shorting Factor due to Brushes

Real watts output = 17540 watts.

Watts/phase = $\frac{17540}{3}$ = 5847 watts/phase.

Phase current = $\frac{5847}{263 \text{ Volts RMS}}$ = 22.23 Amps RMS

Conductor $\frac{\text{amps}}{\text{in}^2}$ = $\frac{22.23}{(0.102)^2\left(\frac{314}{4}\right)}$ = $\frac{22.23}{.5021712}$ = 2720 OK

I^2R loss (25°C) = $(22.23)^2(.0356)(3)$ = 52.8 Watts.

Line Current = 22.23$(\sqrt{3})$ = 38.5 Amps RMS

at 11501 RPM
2567 Hz

Volts (L-L) = 263 Volts RMS
Amps (line) = 38.5 Amps RMS
= 52.8 Watts
TOTAL Watts loss
TOTAL Output Watts = 17538 Watts.

at 5500 RPM
1283 Hz

Volts (L-L) = 131 Volts RMS
Amps (line) = 77 Amps RMS
TOTAL Watts loss = 211 Watts.
TOTAL Output Watts = 17470 Watts.

ORIGINAL PAGE IS
OF POOR QUALITY

FEATURES

Well-Balanced Magnetic Properties

HICOREX is made to have a residual flux density (Br) value approximately equal to the coercive force (BHC) value. Because of this balance, HICOREX performs ideally even when magnetized in single pieces before installation into equipment. Moreover, thinner magnets can be made from HICOREX than any other magenetic material.

Excellent Stability

The coercive force of HICOREX is 10 times that of Alnico magnets. HICOREX resists demagnetizing forces remarkably well, and its properties are little affected by vibrations encountered under ordinary circumstances.
HICOREX also offers excellent resistance to corrosion and oxidation. Because of these superior properties, HICOREX can be used with the same confidence and ease as Alnico magnets.

MAGNETIC PROPERTIES OF HICOREX

Grade	Residual Induction Br (KG)	Coercive Force BHC(KOe)	Maximum Energy Product (BH)max(MGOe)
HICOREX 10	6.0~6.6	6.0~6.6	9~11
" 12	6.6~7.2	6.6~7.2	11~13
" 14	7.2~7.7	7.2~7.7	13~15
" 16	7.7~8.2	7.7~8.0	15~17
" 18	8.2~8.7	8.0~8.5	17~19
" 20	8.7~9.2	8.5~9.0	19~21

Recoil permeability,	μ rec	1.0~1.1
Curie point,	Tc	710°C
Irreversible loss	(0°C~250°C)1%0.5	3~7%
Reversible temperature coefficient	(0°C~200°C)	−0.03~−0.05%/°C
Hardness	Hv	460
Density	gr/cm³	7.3~8.3

HICOREX 20

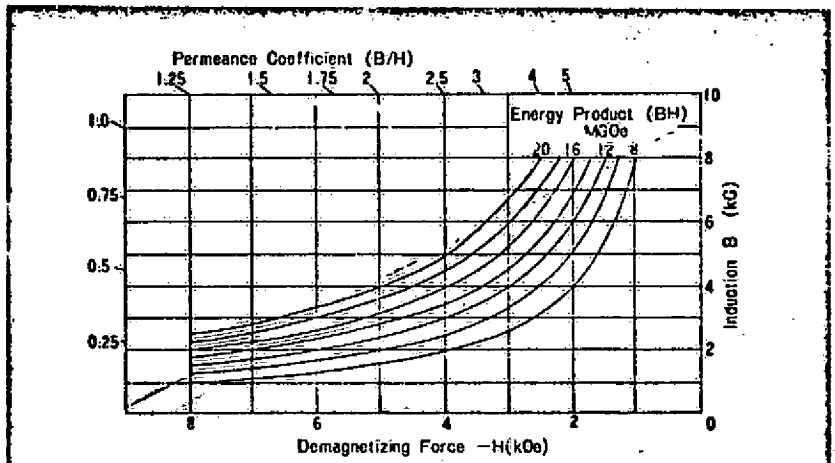

HICOREX 18

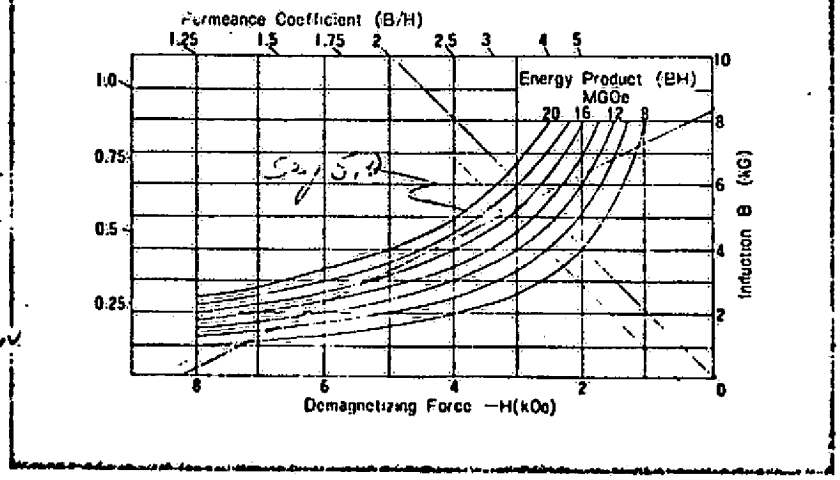

Ref. ↓ HICOREX 90
(BH)max BH = 18 MILLION MIN.
(BH)R BR −
HC (BH)D HC = 6500 Oe = 8000

MOTOR/GENERATOR DESIGN REVIEW

OBJECTIVES:

purpose of the consultation

The ~~object of the subject Purchase Order~~ was for Inland Motor Division, Kollmorgen Corporation, to review the four motor/generator design configurations supplied by RCA to compare the configurations for losses and manufacturing costs and to recommend changes, if any.

DISCUSSION:

The four designs, as defined below, were reviewed with regard to performance, ease of manufacture and costs.

Configuration 1: This design has 28 poles with two radial gaps, one on each side of the axially oriented magnets which are on the rotating member. The windings are in slots in radially laminated iron. Although the desired performance can be achieved, this configuration would be ranked second choice because:

1. The difficulty of obtaining uniform radial slots. If machined after the laminated core is rolled, the inter-lamination burrs would cause excessive eddy current losses. If punched before being rolled, the slot spacing must uniformly increase as the diameter increases.
2. The utilization of copper is low since each turn around the iron is one conductor having a long end turn. This increases the resistance.

3. The iron in the wound member will have considerable hysteresis and eddy current losses at a frequency of 2567 Hertz at 11000 RPM.
4. The manufacture cost would be ranked second.

Configuration 2a: This design has 28 poles with two magnets per pole, one on each side of an ironless, radial, armature winding which is stationary. This design has twice the magnet volume as Configuration 1 and the adjacent axial poles have alternating polarities. The most efficient magnetic circuit requires an iron ring at each end of the unit as return paths for the flux.

This configuration is the preferred or first choice because:

1. The costs would be the lowest.
2. The design does not deviate too far from well established construction concepts.
3. The absence of iron in the wound member eliminates the hysteresis and eddy current losses.
4. The unit would be the smallest volume and have the lowest total weight.
5. The inductance would be minimum because of the lack of iron in the wound member and the permanent magnets at the air gap surfaces.

Configuration 3a: This design has both magnets and windings plus a control field coil on the stationary member. The rotating member has a Lundell type pole arrangement which requires flux paths across two additional air gaps at the ends of the unit. The armature windings are placed in slots in an axially

laminated iron core. This configuration would be ranked last or fourth choice because:

1. The manufacturing cost would be ranked fourth.
2. The inductance would be the highest of the four designs because of soft iron on both sides of the air gap.
3. The hysteresis and eddy currents would be highest of the four designs because of iron on both sides of the air gap. Also the pole pieces cannot be laminated.
4. The magnetic circuit would be less effective because of the many parallel leakage paths for the flux.
5. The unit would be the largest and heaviest.

Configuration 4: This design is similar to the one in 3a except the armature winding is radial and is ironless and the axial poles are of the same polarity on the same side of the armature winding. This configuration would be ranked the third choice because:

1. The cost would be ranked third.
2. The utilization of copper would be low because when one side of the coil is under a pole the other side is between poles.
3. The inductance would be ranked second lowest.
4. There would be some hysteresis and eddy current losses in the pole faces which cannot be laminated.

RECOMMENDATIONS:

The recommended configuration is a modification of 2a as defined below.

Poles - 28 (alternate polarity - 56 magnets spaced 28 on each side of the air gap and having 1/4" thick iron ring as flux return path.)

Magnet size - 1" x 1.6" x 0.3"
(located 1" radially, 1.6" circumferentially, 0.3" axially.)

Magnet material - Samarium Cobalt
18 million energy product.

Armature - Ironless, windings are radial, supported by epoxy.

Winding type - 3 phase-Delta connected

Equivalent slots - 168

Coils/phase/pole - 2

Coil Pitch - 2/3 (throw 1-5)

Turns/coil - 1

Wire size - #10 AWG or equivalent

Air gap length - 0.310 inch (Can be reduced to .217 in)

Mechanical clearance each side of armature - .030 inch.

Mean armature diameter - 22 inches.

Calculations were made resulting in the following performance:

As a Motor:

DC Resistance per phase @ 25°C = 0.0356 ohms.
DC Resistance line to line of Delta = 0.0237 ohms.
Torque sensitivity, K_T, = 0.238 lb.ft./amp.
Back EMF constant, K_B, = 0.323 Volts/Rad/Sec.

When the Delta winding is excited line to line for electronic commutation (3 point commutation) :

Pulse rate at 11000 RPM = 15400 Pulses/second.
Pulse Voltage to overcome Back EMF at 11000 RPM = 372 volts.

As a Generator:

Output - Balanced, sinusoidal, three phase Delta.

at 11000 RPM:

Frequency = 2567 Hertz
Total generated volts, line to line, = 263 volts RMS
Total generated watts = 17540 watts
Line Current = 38.5 amps. RMS
Total internal I^2R losses = 53 watts

at 5500 RPM

Frequency = 1283 Hertz
Total generated volts, line to line, = 131 volts RMS
Total generated watts = 17470 watts
Line Current = 77 amps. RMS
Total internal I^2R losses = 211 watts

A copy of the calculation is attached.

ESTIMATED COSTS:

A firm and accurate cost estimate is impossible at this early stage of the study program. However, it is estimated that the cost will be in the range of $1200 to $1700 each in quantities of 1000 and 10000. This estimate does not include tooling, the extent of which will affect the unit cost.

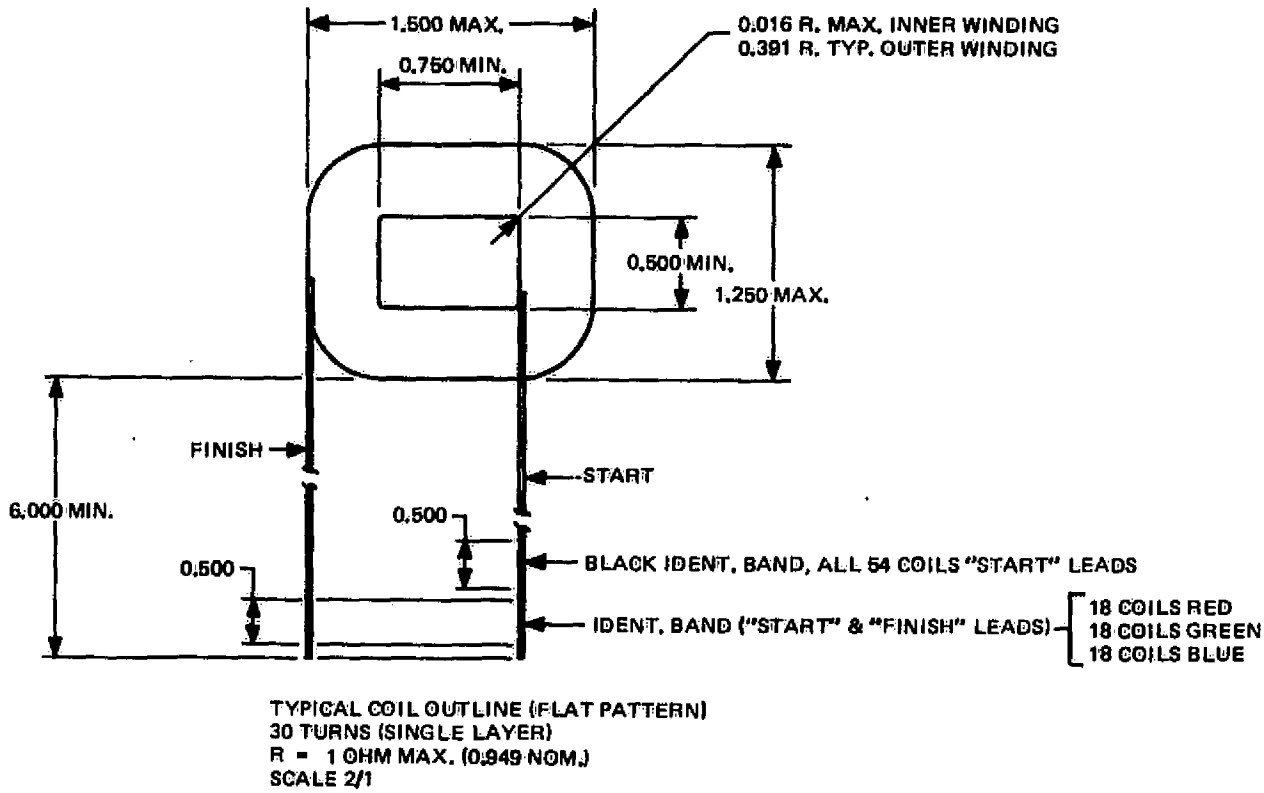

Figure C-23. Typical ironless armature coil.

E. EFFECT ON MOTOR-GENERATOR WEIGHT OF CHANGE IN WHEEL INSIDE DIAMETER

$$\text{Motor torque} = P_r = \frac{63025 \times HP}{N}$$

$$\text{Tangential force} = \frac{P_r}{R} = \frac{63025 \times HP}{NR}$$

If the radius R is reduced to R_1, N will increase to achieve the same energy storage density and stress which is: $K R^2 N^2$.

$$\text{So } K R^2 N^2 = K R_1^2 N_1^2$$

$$\text{If } R_1 = 2R$$

$$N_1 = \frac{N}{2}$$

Also, if the wheel motor diameter increases, $P_r R = BLIR = \text{Torque}$

If the wheel speed is constant and the torque is constant

$$PR = P_1 R_1 \qquad \text{(C-1)}$$

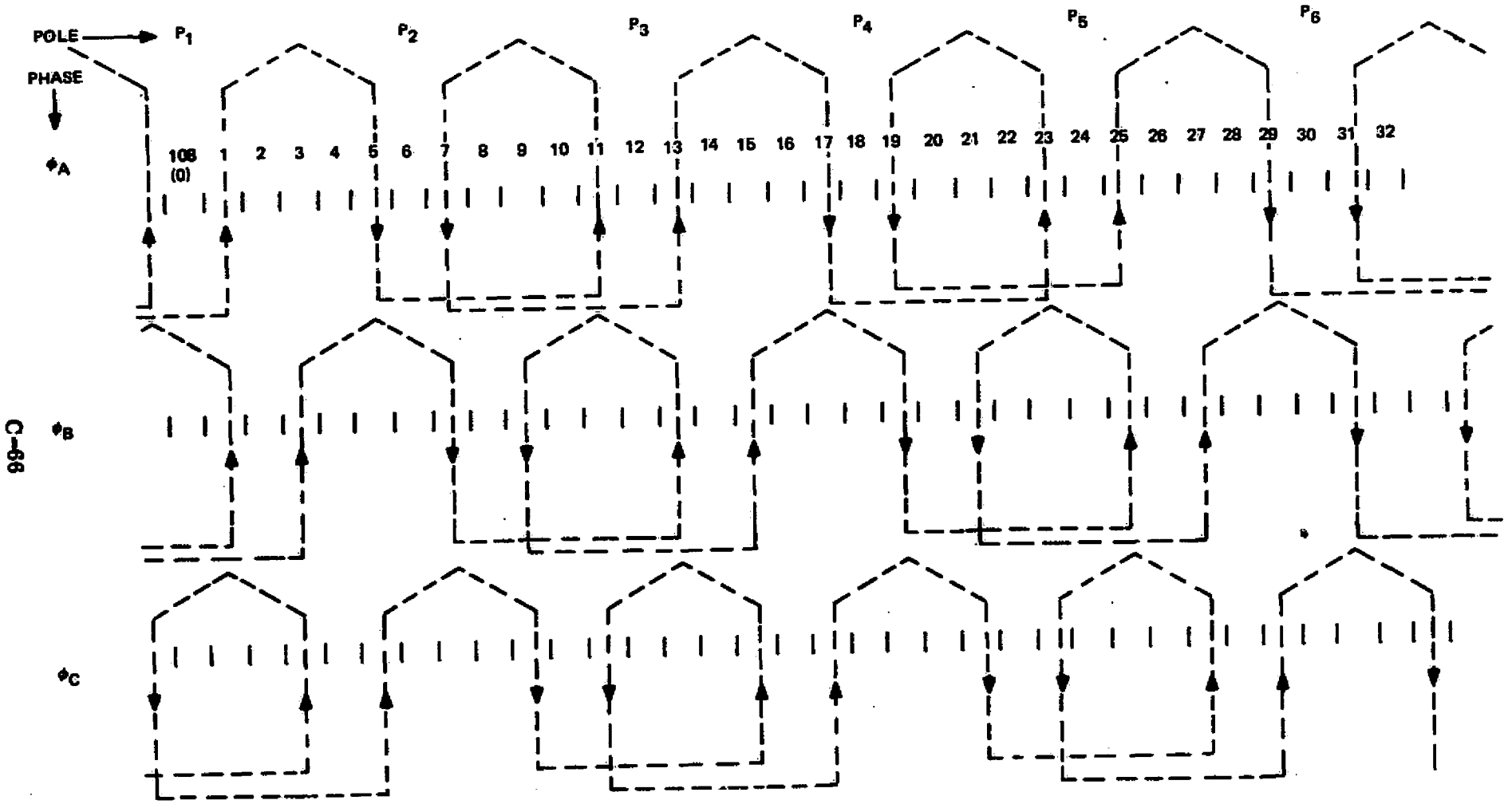

Figure C-24. Coil winding data.
(3D - 2/3 (1 - 5 throw) delta connected)

and

$$BLIR = B_1 L_1 I_1 R_1$$

but

$B = B_1$ if the air gap is held constant

so,

$$LIR = L_1 I_1 R_1 \qquad \text{(C-2)}$$

if

$I_1 = I_0$ by design

$$L_i = L\frac{R}{R_1} \qquad \text{(C-3)}$$

if

$L = L_1$ by design (C-4)

$$I_1 = I\frac{R}{R_1}$$

The motor-generator soft iron weight can be traded for copper weight. Also motor-generator weight can be changed by changing the number of poles. Therefore, design decisions can mask the effect of a change in motor diameter on motor rim weight.

Lacking a rigorous weight model, the gross effect of motor-generator design changes has been estimated for the case where motor diameter increases 50%, as shown in Table C-4. The fixed and variable parameters are noted at the top of the table.

The conclusion is that motor-generator weight can be increased or decreased with increased diameter, depending on design values chosen for the motor design parameters.

TABLE C-4. MOTOR-GENERATOR WEIGHT, CONFIGURATION 2A-1

Fixed - Wheel Speed
Flux Density
Torque

Variable - M-G Diameter, D
No. of Poles, N
Conductor Length, L
Current, I

N, L, I, D } Point Design

$N_1 > N$, $N_2 < N$, L_1, I_1, D_1 } Assumed

Poles	L & I		WT Model $WT_1 = WT \times$ Factor Below	Normalized Weight for: $D_1/D = 1.5$, $N_1/N = 1.5$, and $N_2/N = 0.667$
N	$L_1 = L$	Soft Iron	D_1/D	1.5
		PMS	1	1
	$I_1 = I$	Soft Iron	1	1
		PMS	D/D_1	.667
N_1 ($N_1 > N$)	$L_1 = L$	Soft Iron	$N/N_1 \times D_1/D$	1
		PMS	N_1/N	1.5
	$I_1 = I$	Soft Iron	N/N_1	.667
		PMS	D/D_1	.667
N_2 ($N_2 < N$)	$L_1 = L$	Soft Iron	$N/N_2 \times D_1/D$	1
		PMS	N/N_2	1.5
	$I_1 = I$	Soft Iron	N/N_2	1.5
		PMS	D/D_1	.667

Appendix D

POWER CONDITIONING SUBSYSTEM

Appendix D

POWER CONDITIONING SUBSYSTEM

The subsystem requirements were refined during the study to include the following assumptions and statements:

- 3Ø, 110/220W supply and load.
- Supply has infinite tolerance for converter reactive volt-ampere demand and converter injected harmonics.
- Parallel tie-line operation.
- Motor harmonic impedances high.
- No filtering between converter and m-g.

Motor configuration 2A-1 (Figure 1-8) was used for the analysis.

The Westinghouse R&D Center Systems Analysis group consulted on the subsystem design and cost estimate.

From a technical viewpoint, there are a number of ways to approach the problem posed. The most elegant, conceptually, would use a direct frequency changer, or cycloconverter, between the high-frequency machine and the 60-Hz supply. The two most attractive versions of this basic approach would be

(1) The use of a naturally commutated cycloconverter (NCC) with thyristors as the active devices, or

(2) The use of an unrestricted frequency changer (UFC) with transistors as the active devices.

The NCC has at least one serious technical deficiency—it draws, inevitably, a lagging quadrature component of input current regardless of loading, and draws that current from its commutating source which, in this application, would be the high-frequency machine. Providing controlled compensation to offset the NCC's lagging quadrature current demand is technically feasible, but both adds to the cost and reduces the efficiency of the approach.

Both the NCC and the UFC suffer, however, from major economic disadvantages in low-power applications. The simplest realization of an NCC, a 3-pulse version, would use 18 active devices. Because of both input-current and output-voltage waveform considerations, at least a 6-pulse realization, using 36 active devices, would be needed. Since each device (thyristor) has associated with it, as in any power conversion application, a heat sink, snubber network, gate drive and control circuitry, and supporting hardware, the cost of such an equipment would be considerably higher than that of approaches using fewer active devices even when those approaches require more expensive devices. This might be offset, wholly or in part, if an isolation transformer were not required. However, the machine voltage range is such as to mandate the use of such a component in order to interface successfully with a 208- or 220-volt, 3-phase, 60-Hz source.

A 3-pulse UFC need use only 9 transistors, but would need 36 associated high-speed diodes; alternatively, 18 transistors and 18 diodes could be employed. It is possible, but unlikely, that the input current and output voltage waveforms of a 3-pulse UFC might be acceptable in the application. More likely, a 6-pulse version would again be needed, and it would use twice as many devices, both transistors and diodes. Once more, the economic disadvantages compared to approaches needing fewer devices are quite serious, especially in view of the fact that the transformer at the 60-Hz input cannot be eliminated.

Both frequency changer approaches should give quite high efficiency. Since they are single stage power processing, they are inherently more efficient than alternatives using double-conversion techniques. They are shown in block diagram form in Figure D-1. Figure D-2(a) shows an elemental schematic arrangement, 6 pulse, for the NCC with Figure D-2(b) showing some details of the switches. Figure D-3(a) depicts an elemental 6 pulse UFC schematic, with Figure D-3(b) showing details of the switch arrangement for the UFC.

Both of these conceptually attractive approaches are not, at the power level predicated in this application, worth pursuing because of their economic problems.

All other approaches would use double conversion with a dc link, i.e., as depicted in the block diagram of Figure D-4, an ac-dc/dc-ac converter coupling the 60-Hz supply to a dc link and a second ac-dc/dc-ac converter coupling the dc link to the high-frequency machine.

Within this format lie a number of technically viable combinations. Each of the converters can, in principle be either current- or voltage-fed (with reference to the dc link). Thus, conceptually, four possible arrangements exist, to wit:

(1) Current-fed and current-fed

(2) Current-fed and voltage-fed

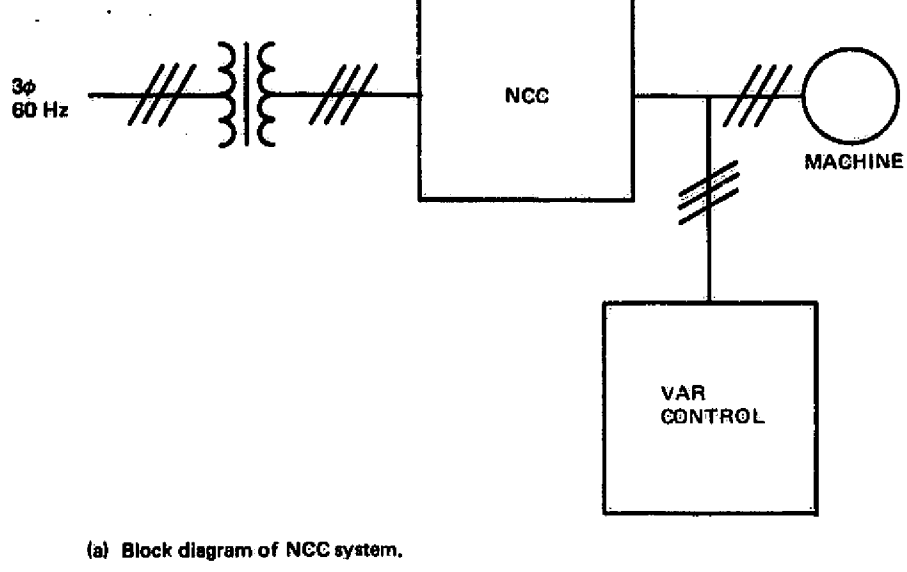

(a) Block diagram of NCC system.

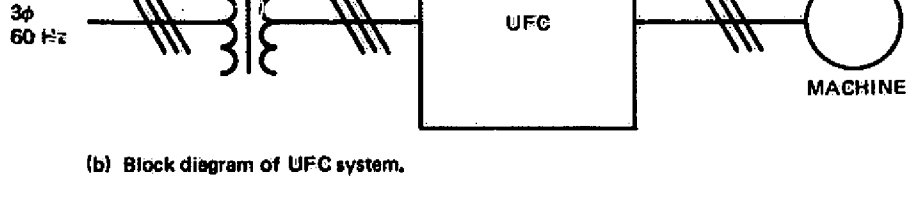

(b) Block diagram of UFC system.

Figure D-1. Frequency changer systems, block diagrams.

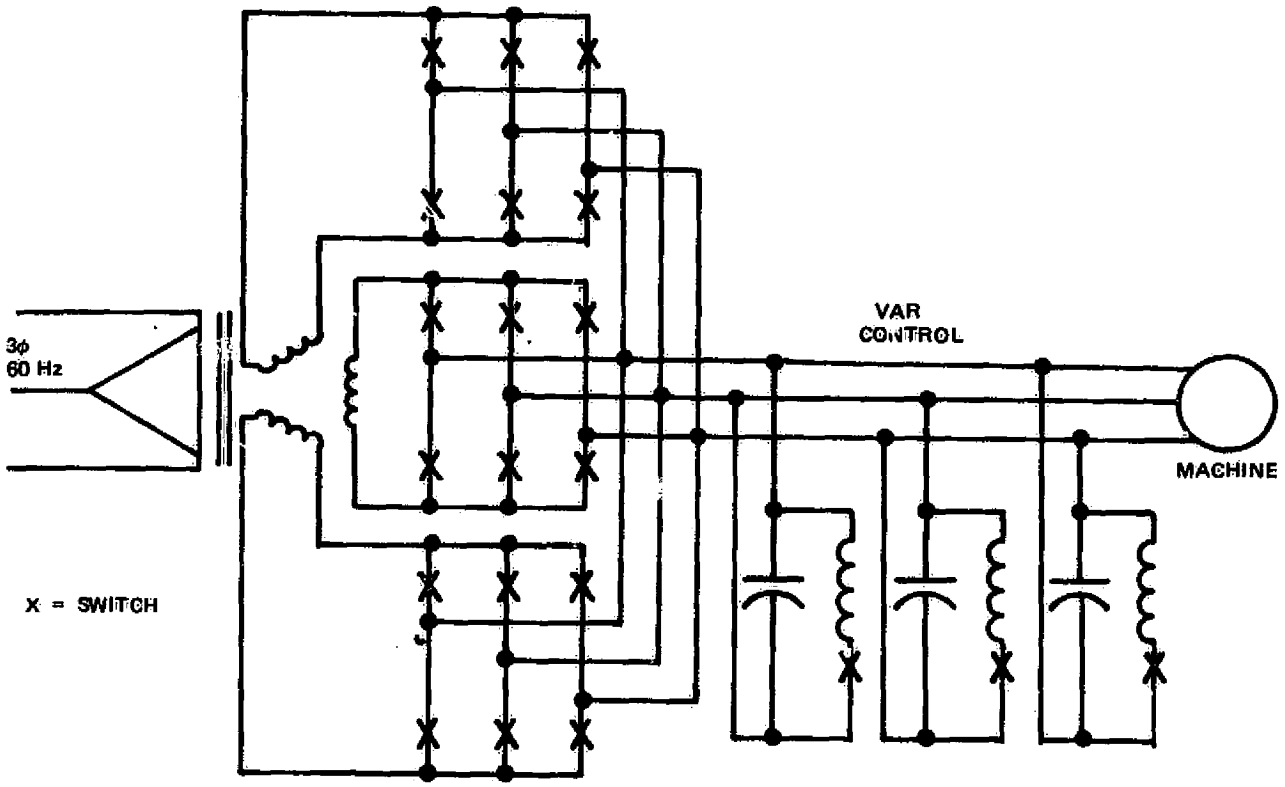

(a) Elemental schematic of NCC.

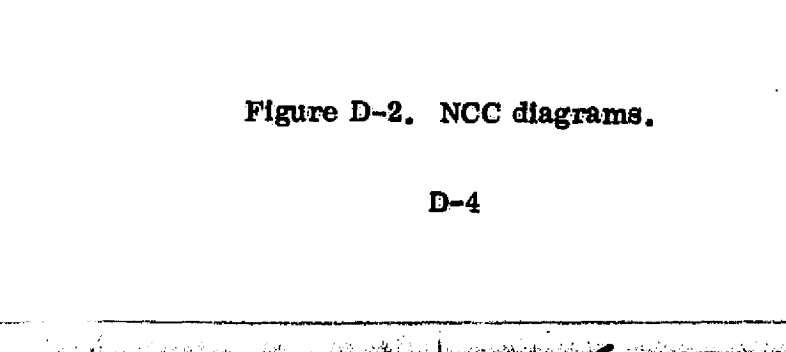

(b) Switch details.

Figure D-2. NCC diagrams.

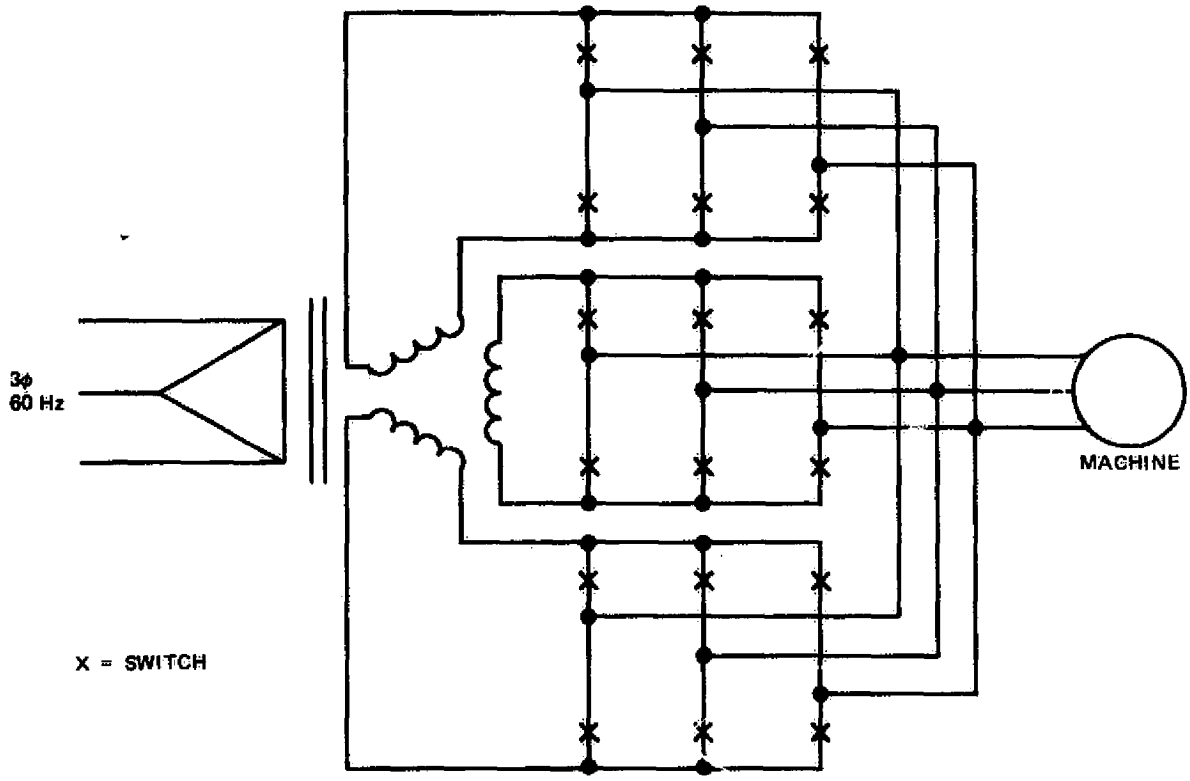

(a) Elemental schematic of UFC

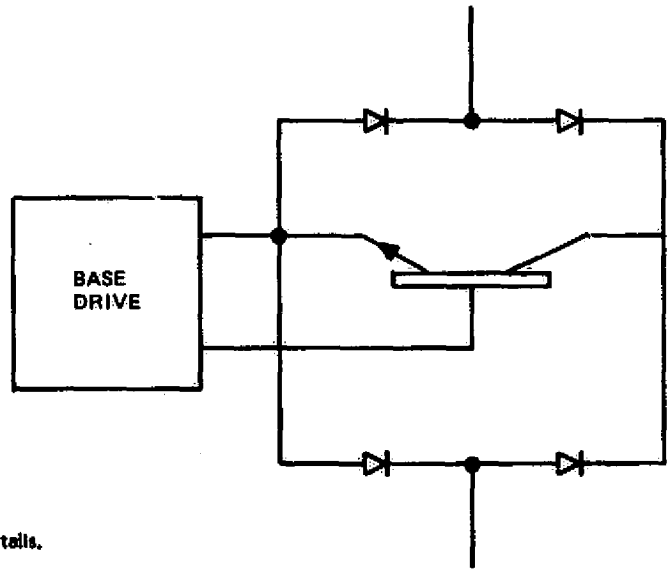

(b) Switch details.

Figure D-3. UFC diagram.

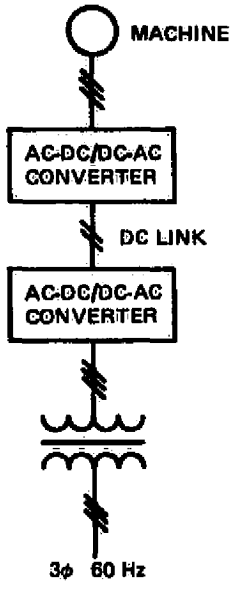

Figure D-4. Block diagram of double-conversion system.

(3) Voltage-fed and voltage-fed

(4) Voltage-fed and current-fed.

To establish the best configuration, the problem can be approached as comprising two separate and essentially independent converters. The use of current-fed converters ("adjustable current inverters", or ACI's) to drive, at variable speed, synchronous ac machines has recently gained some popularity (so called "brushless dc drives"); however, the combination of frequency, speed range, and machine type encountered here make it unlikely that the current-fed approach can fit the bill for the machine converter. A voltage-fed approach, on the other hand, is eminently suited to the task, being superior in performance (by far) and, probably, but little if any more expensive when all application requirements are accounted for.

Voltage-fed converters can, of course, use either thyristors or transistors as their controllable active devices (inverse parallel connected diodes are required in both cases). Thyristors need additional force-commutating circuitry. At the operating frequencies predicated here, the cost of this will more than offset the higher cost of transistors in the main switch positions (despite the fact that parallel-connected transistors are needed with the present state of the art, and likely will continue to be for some time; however single thyristors are available that will comfortably handle the combined current and voltage requirements). Further, the losses of a thyristor self-commutated

converter operating in this frequency range are substantially higher than those of a transistor version — again due, in large part, to the force commutating circuitry needed.

It can be concluded that the most efficient and economical machine converter will prove to be a transistor voltage-fed scheme for which a 6-pulse elemental schematic is shown in Figure D-5(a). Figure D-5(b) shows switch details as they would be using transistors presently available; for the 1980-85 time frame, higher current devices may become available, reducing the number required in parallel to 2 for the machine without field control (i.e., with variable voltage over the operating speed range), and perhaps to one only for a machine with field control.

The output line-to-line voltage wave of such a converter is 6-pulse in character, i.e., contains only harmonics of order $6k \pm 1$, k any integer, with amplitudes relative to the fundamental of $1/(6k \pm 1)$. The sequences of these harmonics depend on their order, every $6k - 1$ component being negative sequence and every $6k + 1$ component being positive sequence. Thus the lowest order harmonic (the 5th) has 20% relative amplitude and any current it causes to flow in the machine will generate negative (or counter) torque. The 7th harmonic, with approximately 14% relative voltage amplitude, is positive sequence so any current it causes to flow will create aiding torque.

It is assumed that machine harmonic impedances are sufficiently high that a 6-pulse voltage wave excitation will create no problems for either the machine or the converter. (Substantial harmonic currents, if they would flow, must be considered in the converter design). Thus, the conceptual design allows for no filtering between converter and machine.

Voltage-fed converters, as the name implies, require a dc voltage source with a very low impedance to the ripple current they generate, as an inescapable result of their mode of operation, at their dc terminals. As depicted in Figure D-5(a), this requirement is usually met by using a suitable bypass capacitor at the dc terminals.

For accelerating the machine from rest to half speed, at initial start up, such a converter can be operated in a "pulse patterned" (or "pulse-width-modulated") mode to provide the lower voltage, lower frequency excitation required without needing to reduce the dc link voltage below the value obtaining at half speed, full conduction. This feature is widely employed in voltage-fed converter ac machine devices currently on the market, and while it does complicate the control somewhat, it presents no major technical or economic difficulties.

For the 60-Hz supply interface, the converter choice is largely dictated by whether the application calls for parallel tie operation only (i.e., with the utility or other 60-Hz generating system always present) or whether operation into passive load alone is predicated. In the latter event, a self-commutated converter is mandated and at the power level obtaining, a voltage-fed converter would be far the most economical and efficient

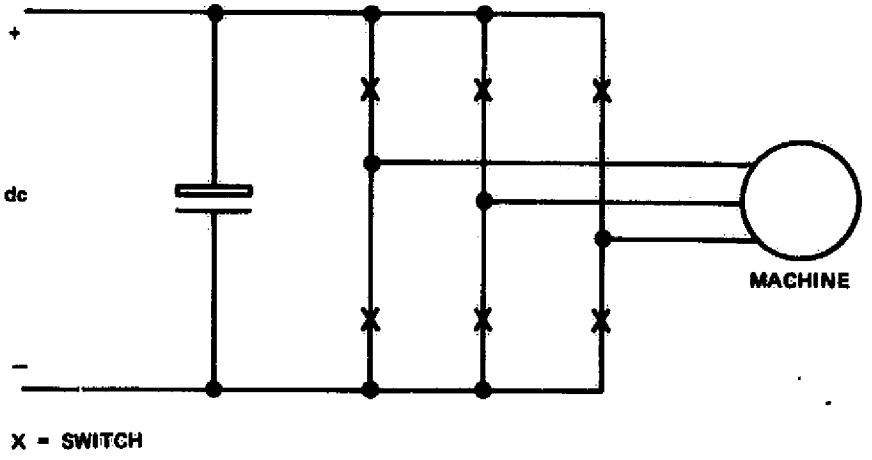

a. Elemental schematic diagram of voltage-fed converter.

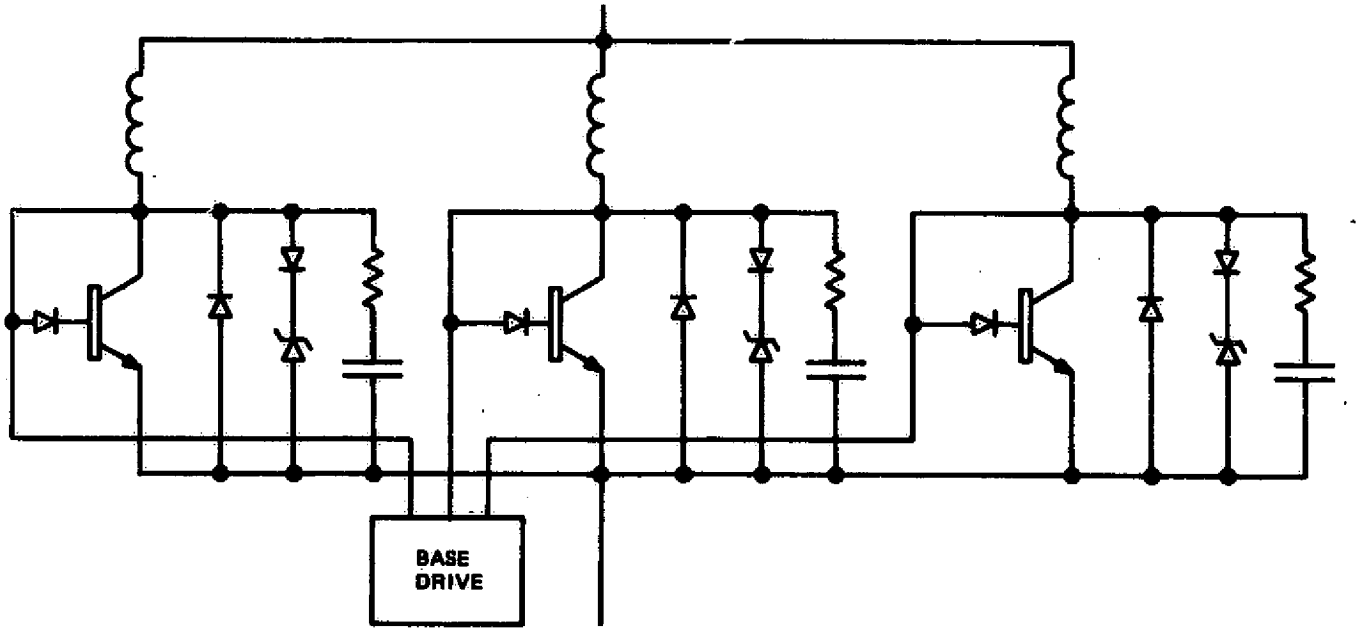

b. Switch details.

Figure D-5. Voltage-fed converter diagrams.

solution at this interface too, albeit using thyristors and auxiliary force commutating circuits rather than transistors, the frequency being low enough (60 Hz) to make thyristors superior from an economic standpoint and not dramatically inferior in efficiency.

However, only the parallel tie case is considered, and only to a 3-phase, 60-Hz system of 208 or 220 volts line-to-line. Also, it is assumed that this source has infinite tolerance for both converter reactive volt-ampere demand and converter injected harmonics. In this case, a simple 6-pulse current-fed converter, with electromechanical dc reversing switches to permit change of operation from rectification to inversion, is by far the most economical and efficient solution. Depicted in elemental schematic form in Figure D-6(a), this converter uses thyristors as its active switching elements. The requirement to maintain continuous dc current flow despite the not-inconsiderable ripple voltage generated at the dc terminals of this converter mandates the use of a sizable reactor in the dc link. The further requirement for operation over a quite wide range of dc currents necessitates that the reactor be a "swinging choke" (i.e., exhibit an inductance approximately inversely proportional to the dc current level over the operating range) for economic reasons.

A major drawback of this converter approach is, of course, its inevitable lagging quadrature current demand on the 60-Hz supply and the impact that this has on the rating requirement (and hence size, weight, cost, and losses) of the isolation transformer. Thus, as is seen below, a system with a field-controlled high-frequency machine, and hence an essentially invariant dc link voltage, enjoys substantial benefits in both cost and efficiency at the 60-Hz converter interface.

If this conversion scheme, depicted in full elemental schematic in Figure D-7, is simply designed to handle the maximum machine power, on a continuous basis, preliminary estimates for costs and losses are as follows:

	Cost	Losses at Full Machine Power
Variable dc link version –		
at full speed/voltage	$11,400	2410 watts
at half speed/voltage		3020 watts
Fixed dc link version	$8,270	2520 watts

An obvious disadvantage of such designs is that during charging operation, at machine powers of 625 to 1250 watts, and during intermittent low power discharge at power levels returned to the 60-Hz system of less than 2 kW, the efficiency will be very low, probably in the range 40 to 60%. Consider only the isolation transformer; for the variable voltage unit, this component must be rated at approximately 50 kVA and for fixed voltage at approximately 25 kVA (lower ratings are permissible if we

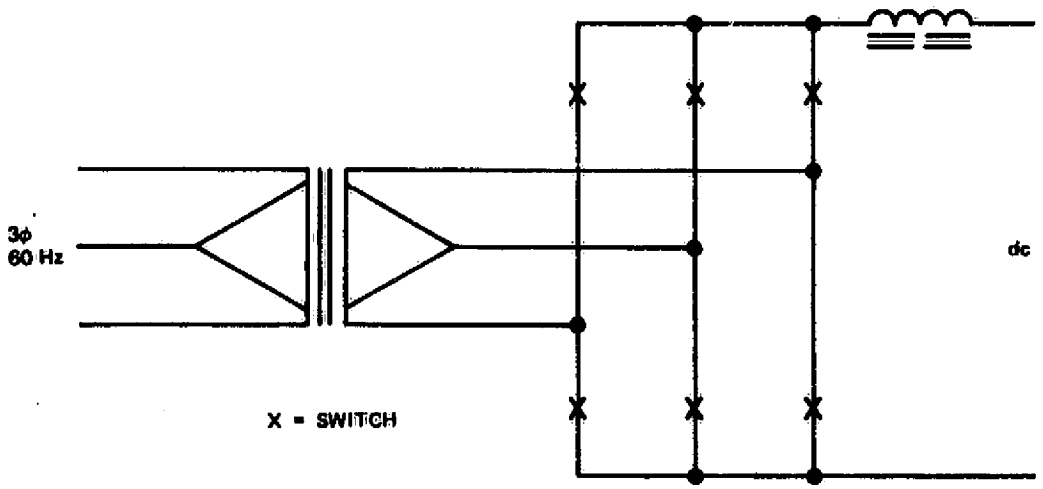

a. Elemental schematic diagram of current-fed converter.

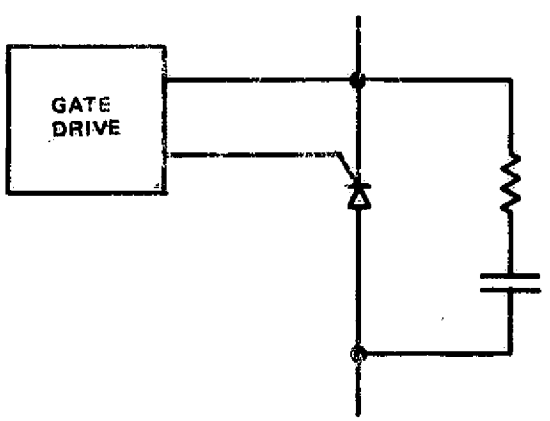

b. Switch details.

Figure D-6. Current-fed converter diagrams.

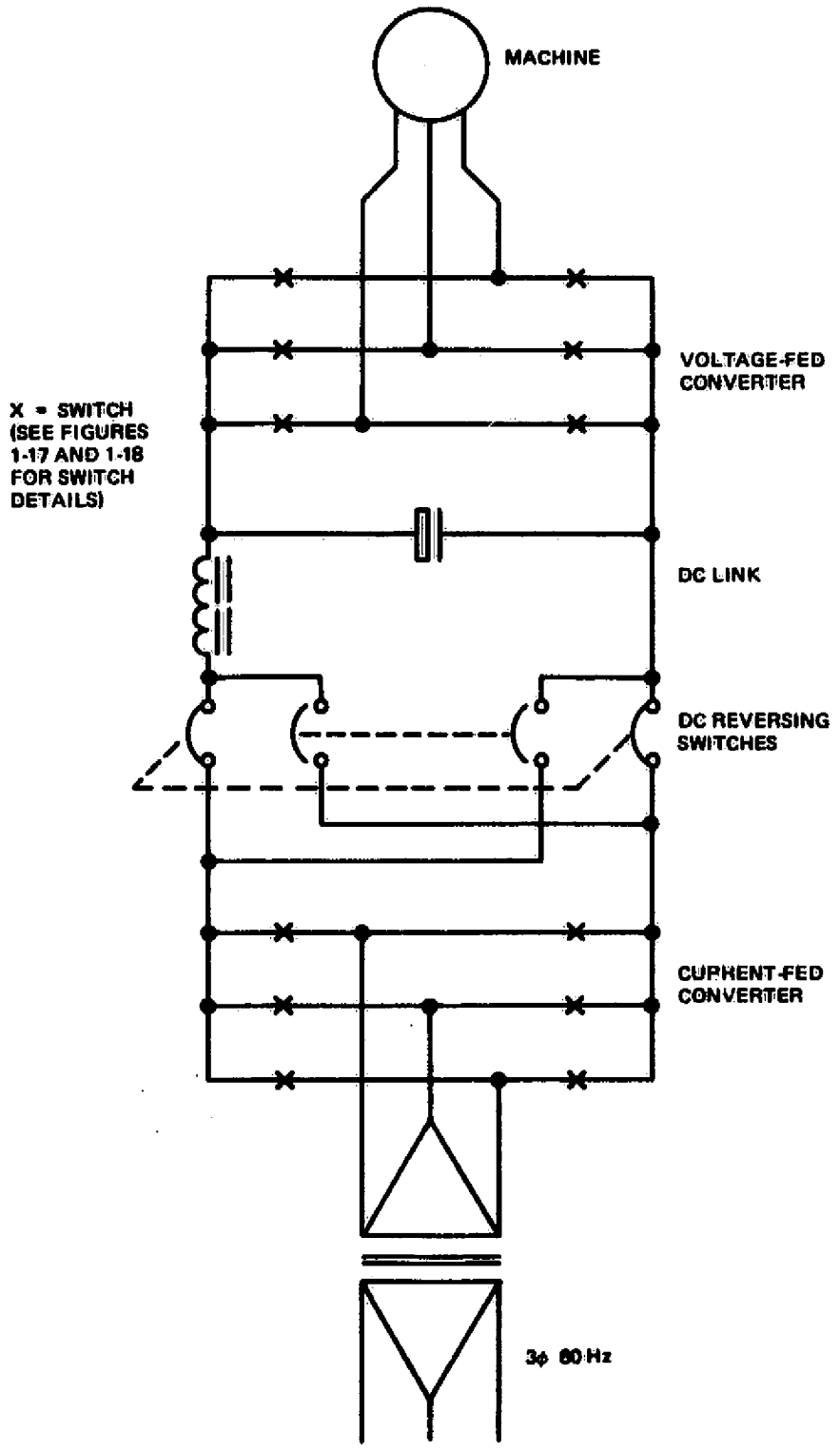

Figure D-7. Schematic diagram of double-powered conversion system.

take advantage of the thermal overload capability of the transformer for the short-term full-power discharge, but would result in substantial increases in transformer losses at both full and part loads). We can compute transformer losses to be as follows:

	Variable Voltage at Full Voltage	Variable Voltage at 1/2 Voltage	Fixed Voltage
Full Load	500 watts	1000 watts	500 watts
10% Load	335 watts	340 watts	173 watts
5% Load	334 watts	335 watts	168 watts

Thus due to the transformer alone and presuming "full load" is 15 kW, at 1.5 kW or 10% load, the efficiency is but 81.5% for the variable-voltage version and 89.7% for the fixed-voltage version. At 750 watts, or 5% load, the transformer efficiency reduces to 69.1% for the variable-voltage and 81.7% for the fixed-voltage scheme.

Since both converter and the dc link components have some loss contributions that exhibit similar behavior, the overall efficiency suffers radically at reduced load.

This behavor can be circumvented, at additional cost, by establishing 2 power conversion "channels", one designed to handle quite modest power levels and therefore exhibiting good efficiency thereat, and the other to provide the conversion capacity for full-power operation. Time and effort limitations of the present study preclude the exploration of this option, in any of all its possible ramifications.

Appendix E

VACUUM HOUSING AND MOUNT

Appendix E

VACUUM HOUSING AND MOUNT

A. DESIGN CONSIDERATIONS

Two primary considerations are involved in the design of the vacuum housing: vacuum seal and environmental protection for the wheel, and isolation from the foundation.

A vacuum environment must be provided to eliminate windage loss at the rotational speeds to be used. Without a reduced-pressure environment, it would not be possible to even reach an operating speed of 17,000 rpm for a 4-foot-diameter wheel with the rated energy storage of 10 Kw-hr. A vacuum of 10^{-4} torr or better is desired to reduce windage losses to a negligible level, compared to other system losses (electrical).

On the other hand, only those components that rotate should be exposed to the vacuum, since electrical components are better cooled if exposed to a controlled atmosphere. Also, outgassing and other reactions to a hard vacuum are avoided. Maintenance and test procedures are simplified as well.

Isolation from the foundation has two advantages, depending on the installation. First, the isolation protects the wheel from external disturbances which, while they may not cause failure of the system, will cause additional power loss through the suspension as a function of frequency and amplitude. Secondly, the isolation protects the environment from vibrations caused by the wheel.

With respect to vibration caused by the system, however, it can be noted that unless the wheel runs very quietly and without vibration, the losses due to the suspension servo attempting to accommodate the wheel motion will be unacceptably large. It therefore seems to be a rational point of view to assume that system-induced vibration will be negligible and will not be a problem except for the rare event of destructive failure.

The possibility of destructive failure, on the other hand, makes it very probable that the system will be installed in a protection pit, with a substantial foundation embedded in the ground. Therefore, the method of mounting the system need consider only vibrations transmitted from the ground to the system.

Ground induced vibrations are of two kinds: vehicle/machinery induced and earth-induced (earthquake). The frequency spectra of these events are within overlapping decades, but it is difficult to provide a shock mounted system in a simple way. The requirement imposed by the relatively low frequencies of an earthquake (1 to 10 Hz) spectrum is that a passive mount have its natural frequency at approximately 0.3 Hz. Such isolators tend to be constructed as air bellows springs and are usually servoed. A fully passive system could be constructed with a pendulum leveling device, but tends to be bulky.

Typical ground measurements, even for earthquake motions, show peak accelerations below 0.25 g. Vehicle/machinery motions are less than 10% of that value. Most damage to structures results because the structure amplifies the ground motion by resonance near the principal driving frequencies. The Mechanical Capacitor, on the other hand, can be constructed to have resonances that are much higher than the 1 to 10 Hz driving frequencies expected at its mounts. Because the wheel suspension system is adequate to handle 2-g inputs, and is servoed for several hundred Hz bandwidth, there is actually little need to shock mount the system for earthquake inputs. Other inputs are most easily accounted for by providing a heavy concrete slab on elastomer pads to afford ground isolation at 1 Hz or above.

The Mechanical Capacitor vacuum cover can then be mounted to the concrete slab with isolator mounts at a nominal value, say 10 Hz, primarily to accommodate expansion, rather than additional vibration isolation.

B. SYSTEM CONFIGURATION

The mechanical capacitor system is shown in sketch SK2294234. The housing material is fiberglass/epoxy, to eliminate magnetic interaction between the moving motor fields and a metallic case. The fiberglass cover is reinforced with attached ribs and supported by a central core that supports most of the compressive load produced by the vacuum.

The central core also acts as a non-evacuated but sealed chamber for housing the electronics. The only non-rotating parts exposed to the vacuum are thus the motor and suspension coils and supporting structure. An access port over the central core allows maintenance and test to be performed while the wheel is operating, if desired.

In order to maintain a hard vacuum, a make up pump is included with the installation. The pump is a standard OEM laboratory vacuum pump, with an expected long life. It can be used for initial pump-down, and with automatic pressure detection, can be used intermittently to maintain the vacuum over the life of the system. Leakage of the case will be well below the pumping capacity.

APPENDIX F

INVESTIGATION OF LOW-LOSS MAGNETIC MATERIALS

Appendix F

INVESTIGATION OF LOW LOSS MAGNETIC MATERIALS

A. CORE MATERIAL INVESTIGATION

The high-speed energy wheel contains soft magnetic materials in the magnetic suspension and motor-generator subsystems. The high relative velocity between the moving and stationary elements of the magnetic circuits in both subsystems leads to rapid magnetic field changes and the potential for high hysteresis and eddy-current losses, or 'friction' (see Section II).

NASA suggested the use of powdered iron as a candidate low-loss material. The following notes describe the investigation and test program that was undertaken as a subtask of the study.

Many kinds of soft ferromagnetic metals have been used for years for the purpose of reducing magnetic losses in transformers, motors, inductors, and other equipment. A number of candidate materials are listed in Table F-1. The values shown are representative only; one must refer to the manufacturers data for more detailed data. However, the data for two candidate materials are not in the literature for different reasons. Carbonyl iron has been used mainly in high-frequency, low-induction-level applications and the Metglass alloys are a new development for which data for specific applications are not fully available. However, both kinds of metals are of interest because of their potentially superior low-loss performance in power devices operating in the frequency range encountered in the energy wheel.

The Allied Chemical Corporation has been developing Metglas alloys for use in power transformers and other devices. These are produced in thin strip form and have a glassy structure. They are suitable for laminated magnetic structures. One alloy, Metglas 2605, shown in Table F-2, exhibits lower losses than existing transformer irons. Further, the Metglas alloys may be used as load bearing structural elements.

However, the extensive use of thin laminations may lead to fabrication difficulties and high production costs. Soft magnetic parts made from powders may be an alternative approach.

TABLE F-1. SOFT MAGNETIC MATERIALS

	Si Iron (Laminated)	Ni Iron (Laminated)	Ferrite (Powder)	Carbonyl Iron (Powder)	Met-glas (Laminated)	Molybdenum Permalloy (Powder)
Initial Permeability, μo	to 1.5K	to 100K	to 10K	?	?	14-125
Maximum Permeability μm	High 6-40K	High 25-100K	High to 15K	13-58	High	Low 130
Maximum Saturation Induction, Bs	Med-High to 10K	High to 18K	Med. to 5.2K	?	High to 15K	Med. to 7K
Resistivity, μohm-cm	Low 50-60	Low 7-80	High to 10^{10}	High 10^{10}	Low 100-150	High 10^{6}
Hysterisis at high inductions	High	High	Med.	**	Med-High	Very Low*
Eddy Current at high inductions and frequencies						

*Approximately equal to 4-79 permalloy and superpermalloy.
**Must be verified by tests.

TABLE F-2. SOFT MAGNETIC METALS FOR ENERGY WHEEL

Material (2 Mils Thick)	Watts/kg Hysteresis and Eddy-Current Loss at Frequency and Field Noted		
	60 Hz 13,000 Gauss	10^3 Hz 1000 Gauss	10^4 Hz 1000 Gauss
50% Silicon Iron	1.5	0.26	7.0
50% Nickel Iron	0.77	0.22	5.5
2605 Metglas*	0.53	0.10	2.9
*The resistivity is 125 μohm cm.			

In general, at the higher frequencies, METGLAS 2605 losses vary from those shown as:

$$\left(\frac{B_1}{B_0}\right)^{1.6} \cdot \left(\frac{f_1}{f_0}\right)^{1.4} \cdot \left(\frac{t_1/\rho_o}{t_o/\rho_o}\right)$$

where B is the induction field, f is the frequency and t and ρ the thickness and resistivity, respectively.

Of these, carbonyl irons have potential for use in energy wheels. Accordingly, a limited investigation of several electronic grades produced by GAF Corporation was undertaken.

Through the cooperation of the GAF Corporation, RCA prepared several types of carbonyl iron powders in the GAF quality control laboratory to ensure proper powder preparation. The powders were then compressed and bonded into toroid core test specimens suitable for magnetic loss measurements. Paragraph B, from a GAF specification, describes the preparation of cores for several iron powder grades.

The prepared powders were pressed at 33,000 psi, cured at RCA, and wound for loss measurements. The specimen dimensions are as shown in Figure F-1.

The cores are wound with 100 turns each of 24 gauge enameled wire for the primary and secondary.

The cores were tested through the cooperation of the Allied Chemical Corporation Research Center. Table F-3 contains the test results. Unfortunately the capability of the test set-up did not allow for high inductions at high frequencies and changes to the test equipment are not feasible at present. The results at a low frequency, (60 Hz) show no measurable loss. Losses were not detected below the frequency of 50 kHz. However, the induction was low (to 20 gauss). More measurements must be run at inductions up to 10,000 gauss on a follow on program.

Table F-3 lists the test results and Figure F-3 illustrates the B vs H hysteresis curves for the C grade material.

TABLE F-3. CARBONYL POWDER TEST RESULTS

Sample	E	L	C
Weight (g)	97.6	94.4	96.2
Approx. ρ (g/cm)	4	3.5	3.5
l_m (cm)	14.96	14.96	14.96
$N_1 = N_2$	100	100	100
A (cm^2)	1.63	1.8	1.84
N_2A (cm^2)	16.3	180	184
dc Hc (O_e)	~0	5.25	6.3
dc μ_o	13.8	31	20
Br (gauss)	~ 0	163	125
60 Hz loss (W/kg)	~ 0	~ 0	~ 0
loss 50 kHz (watts/kg)	0.72 at 110 gauss	0.77 at 30 gauss	0.8 at 13.5 gauss
	0.24 at 6.5 gauss	0.32 at 125 gauss	0.25 at 7.5 gauss
Hc at 50 kHz (O_e)	0.29 at 11 gauss	0.18 at 20 gauss	0.27 at 13.5 gauss
	0.18 at 6.5 gauss	0.14 at 12.5 gauss	0.20 at 7.5 gauss
μ_o at 50 kHz	11	22.1	16.6

l_m = mean length of toroid

N_1, N_2 = primary, secondary windings

A = area of toroid cross section

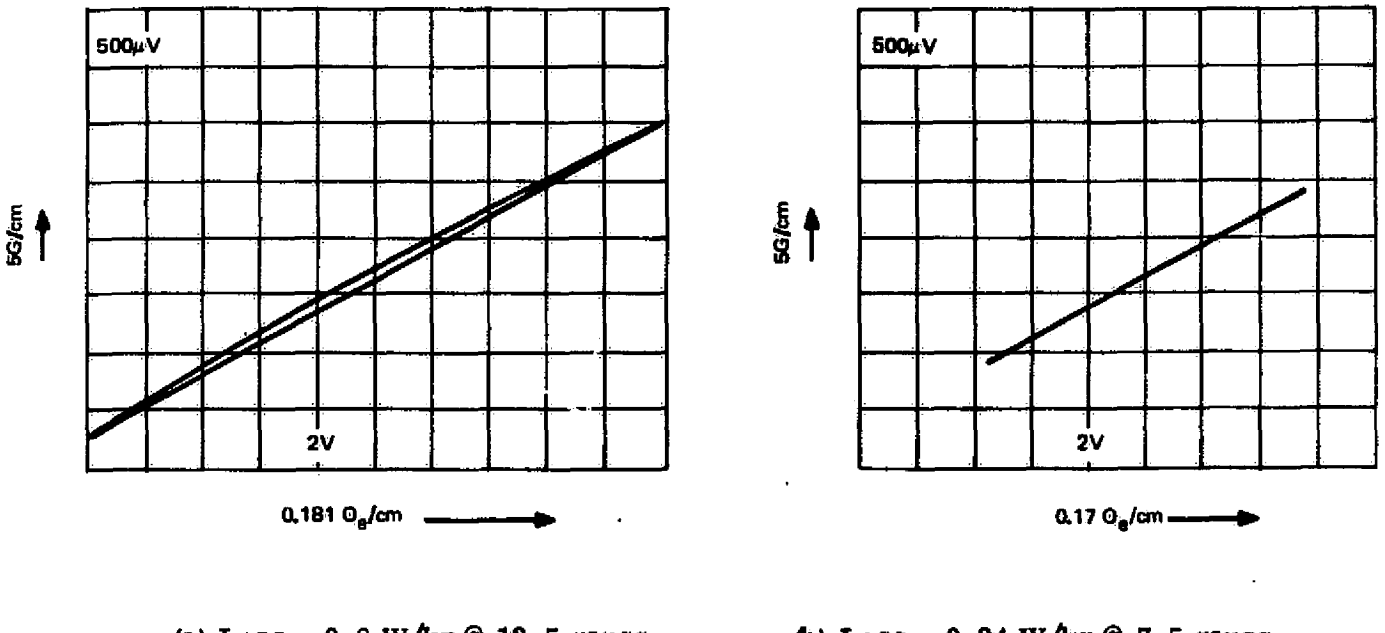

(a) Loss = 0.8 W/kg @ 13.5 gauss. (b) Loss = 0.24 W/kg @ 7.5 gauss.

Figure F-3. Hysteresis curves for C grade carbonyl powder cores at 50 kHz.

Other powdered metals, including hydrogen-reduced iron and molybdenum permalloy, should be measured also.

B. CORE FABRICATION (GAF SPECIFICATION)

The fabrication of cores is done in three steps.

(1) The powder is insulated.

(2) The binder is applied.

(3) Using this "press" powder, cores are formed.

The manufacturing program consists of basically three groups of powders: (1) the unreduced grades E, TH, SF, J and W; (2) the reduced grades C, HP, L and MR; and (3) the reduced but preinsulated powders GQ4 and GS6.

Accordingly different methods for the quality control have been established.

C. INSULATION

For the following grades of powders it is necessary that the iron particles are insulated:

E, TH, SF, J, W, C, HP, and L

MR is basically a 50-50 mixture of HP and L for which special procedure for testing was developed.

In the case of GQ4 and GS6, the antisintering agent acts as an insulation and no additional insulation was found to be necessary.

In every case where insulation is required the procedure is the following:

50 g of powder are placed into an evaporating dish of 6-inch diameter. Next 0.5 cc of 60-percent orthophosphoric acid is diluted with 15 cc of acetone and added to the powder. The dish is placed on a mortar grinder situated under a hood. A 250 watt infrared bulb is placed so that the radiation heats the mixture, while agitation continues for 2 cycles of 7.5 minutes. After the first cycle, some wet lumps remain and are broken up manually with a pestle. At the end, the powder is completely dry and dusty, and the particles are now covered with a thin layer of high-resistance iron orthophosphate.

D. BINDER APPLICATION

For the standard core test on unreduced powder grades, 2.5 grams of Durite are dissolved in 15 cc of acetone and added to the insulated powder. It is next thoroughly mixed and agitated with a stainless steel spatula until all the acetone is evaporated. Evaporation is assisted by a 250 watt infrared bulb mounted above an evaporating dish. The almost-dry mass is pressed through a 20 mesh sieve. Finally, 0.1 gram of atomized Acrawax is added and mixed in.

For the reduced powder grades C, HP, L, and GS6, the procedure is the same except that 0.5 gram of Durite and 0.25 of Acrawax are used.

For GQ4, 0.3 gram of Durite and 0.25 gram of Acrawax are used.

For MR, 1.75 gram of Bakelite laquer is dissolved in 15 cc of acetone and added to 50 grams of powder. The procedure is then the same as previously.

E. PRESSING OF CORES

After the binder is applied, the powder is ready to be pressed into cores. The powder in this stage is called "press powder".

For the unreduced powder grades, 6.0 grams of press powder is weighed out and poured in the die No. 2. This is a cylindrical die of 2-inch diameter, 3-inch length, and a Lore of 0.368-inch. The two plungers are so dimensioned that the length of the core is 0.770 inch. A pressure of 6 tons is then applied to the plungers,

which will be flush with the die at that pressure, simulating conditions in rotary presses as used by our customers and resulting in isodense cores.

For the powders SF, J, and W, it was found necessary to test side press cores in addition to the cylindrical cores to be able to determine the characteristics of these powders under isobaric conditions.

For these cores, 4.5 grams of press powder is weighed out and poured into die No. 4, a rectangular die. The cavity is 1.504-inch long, 0.196-inch wide and 1.5-inch deep. The plungers are made to fit the cavity, but each plunger extends about 1 inch over the die, thus the pressure on the core can be controlled. A pressure of 9 tons is used for unreduced powder grades.

For the reduced powder grades (except MR), 6.5 grams of press powder are compressed in die No. 4 under a force of 1[illegible] ons.

For the MR Grade, 6.4 grams of press powder are compressed in die No. 4 under a force of 18 tons. All cores are then cured for 30 minutes at 170°C to set the binder.

APPENDIX G

An Interference Assembled Multi-Ring Flywheel

FINAL REPORT

to

RCA Corporation
Advanced Technology Laboratories
Camden, New Jersey 08120

by

Dr. James A. Kirk
Engineering Consultant

and

Mr. Richard A. Huntington
Engineering Consultant

3605 Jefferson St.
Hyattsville, Maryland 20782

Introduction

Energy storage in rotating flywheels is an area that a number of investigators [1-12] are currently studying. Most of the current work involves maximizing the stored energy density (energy per unit of flywheel weight), by selecting rotor designs which can take advantage of the large values of specific strength of fiber reinforced composite materials. Because these materials exhibit anisotropic elastic properties, full utilization of their strength requires designs which predominantly stress the composite material in the fiber direction. One design which is suggested to satisfy this constraint is the multirim flywheel proposed by S. F. Post and R. F. Post[9] and D. W. Rabenhorst[7]. In these designs a number of concentric rings (not all of the same material) are bonded together and connected to a central shaft (usually by some type of spoke arrangement) to provide for the input and output of power.

Kirk, Studer, and Evans[13,14,15] of the Goddard Space Flight Center, have suggested a rotor design which eliminates the need to couple to a central power shaft. Their design utilizes a thin (overall ID/OD > .9) magnetically suspended rotating pierced disk, which also serves as the rotating element of a motor/generator system. All energy input and output is electrical and there is no mechanical contact between any rotating and stationary components. Their rotor consists of an iron ring which is joined to a circumferentially wound continuous filament ring (Kevlar-49). Kirk and Huntington[16] have performed a stress analysis on the 2 ring design and have shown that the presence of the iron ring will cause minimum derating of stored energy density if an interference assembly is used between the two rings. Additional work by Kirk and Huntington[18] has shown that if the iron

is segmented in the circumferential direction (in essence a dead weight) there is virtually no derating of the stored energy density. One problem with the Goddard design is its low volumetric energy density (stored energy per unit of swept volume). However, the analysis presented in this paper will show the volumetric energy density can be substantially improved with little effect on the stored energy weight density.

The purpose of this paper is to present an analysis of the stress distribution in a constant thickness, orthotropic, multi-ring flywheel. This configuration differs from the multi-ring design by Post[9] in that elastomeric rings bonded between adjacent structural rings are not necessary, although their presence can be analyzed. Also an outline and demonstration of an energy density maximization procedure, which utilizes an interference assembly of the flywheel rings, is presented. It will be shown that by proper selection of the interference fit of each ring it is possible to redistribute the tangential and radial stresses throughout the rotor, so that there is an increase in both energy weight density and volumetric energy density.

Stress Analysis

Shown in Figure 1 is a schematic of the multiring flywheel rotor which is considered in this paper. The rotor is modeled as n concentric, constant thickness rings. Each ring can be considered as either isotropic or orthotropic, with the orientation of the orthotropic directions being radial and tangential.

For convenience in performing the stress analysis, nondimensional expressions for the radial and tangential stress are useful. Kirk and Huntington[16] have developed these equations, and with slight modification, they are shown in equations (1A) and (1B). Note that when N=1 (isotropic ring) these equations reduce to the standard isotropic plane stress equations for a rotating pierced disk[17].

$$\sigma^*_{rj} = \frac{\sigma_{rj}}{\rho_1\omega^2b^2} - \frac{(3+\nu_{r\theta j})}{9-N_j^2}\frac{\rho_j}{\rho_1}\left(\frac{r}{b}\right)^2 + A_j\left(\frac{r}{b}\right)^{N_j-1} + B_j\left(\frac{r}{b}\right)^{-N_j-1} \qquad (1A)$$

$$\sigma^*_{\theta j} = \frac{\sigma_{\theta j}}{\rho_1\omega^2b^2} - \frac{(N_j^2+3\nu_{r\theta j})}{9-N_j^2}\frac{\rho_j}{\rho_1}\left(\frac{r}{b}\right)^2 + A_jN_j\left(\frac{r}{b}\right)^{N_j-1} - B_jN_j\left(\frac{r}{b}\right)^{-N_j-1} \qquad (1B)$$

where j = ring number (1, 2, 3, ... n)

$N_j = \sqrt{E_\theta/E_r}$

$\rho_1\omega^2b^2$ = nondimensional factor

A_j, B_j = constants evaluated with boundary conditions

The boundary conditions which are applied to equations (1A) and (1B) state the following:

a. The radial stresses at the free surface are zero.

b. The radial stress is continuous across the ringe boundaries.

c. The radial displacements at the ring boundaries is continuous.

d. For a solid disk (inner radius equals zero) the magnitude of the radial as well as tangential stress must be finite.

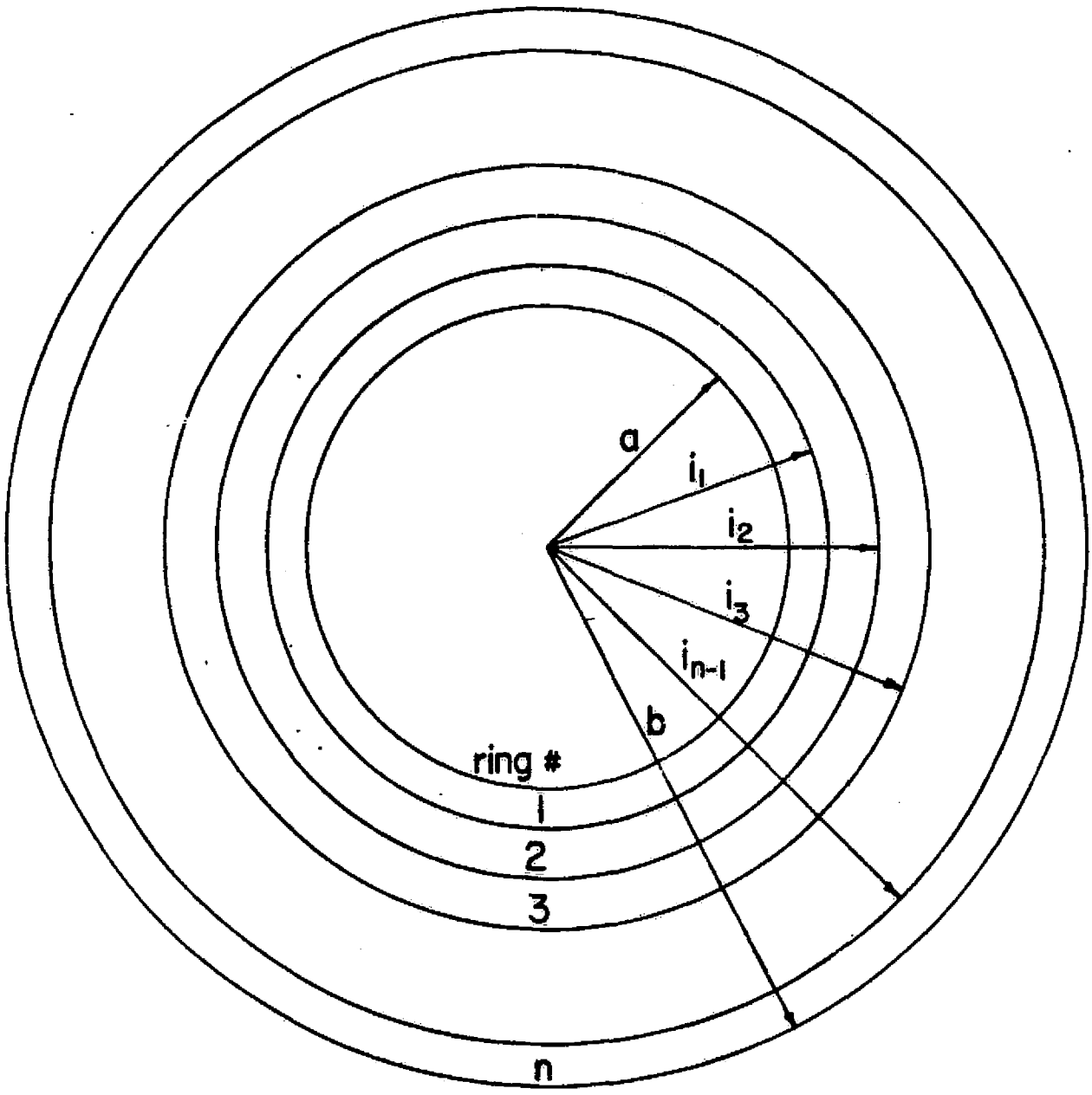

Figure 1. Multi-ring flywheel rotor configuration

Applying the boundary conditions provides the complete solution for the nondimensional radial and tangential centrifugal stresses throughout the entire flywheel. These stress expressions are dependent on 5 nondimensional variables for each ring. These are:

a. a/b or i_k/b, which specifies the ratio of the inner radius of the ring to the outer radius of the flywheel.

b. N_j, material parameter ($N_j = \sqrt{E_{\theta j}/E_{rj}}$)

c. $E_{\theta j}/E_{\theta 1}$, material ratio of the tangential modulus of elasticity of ring j to that of ring 1

d. ρ_j/ρ_1, material ratio of the density of ring j to that of ring 1

e. $\nu_{r\theta j}$, Poisson's ratio

Specification of each of these variables for each ring will allow the nondimensional radial and tangential stress distributions to be obtained. However, it is also necessary to provide the working stresses for each ring and the weight density of ring 1, so that a complete analysis, including energy storage capability, can be performed.

Figures 2 and 3 show typical plots of nondimensional tangential and radial stress with r/b. The plots are for a flywheel rotor composed of five rings of Kevlar-49/Epoxy. However, the boundaries of the rings are not apparent, since the materials in the rings have identical properties. The boundaries will become apparent after the application of the maximization procedure, which will be discussed in the next section.

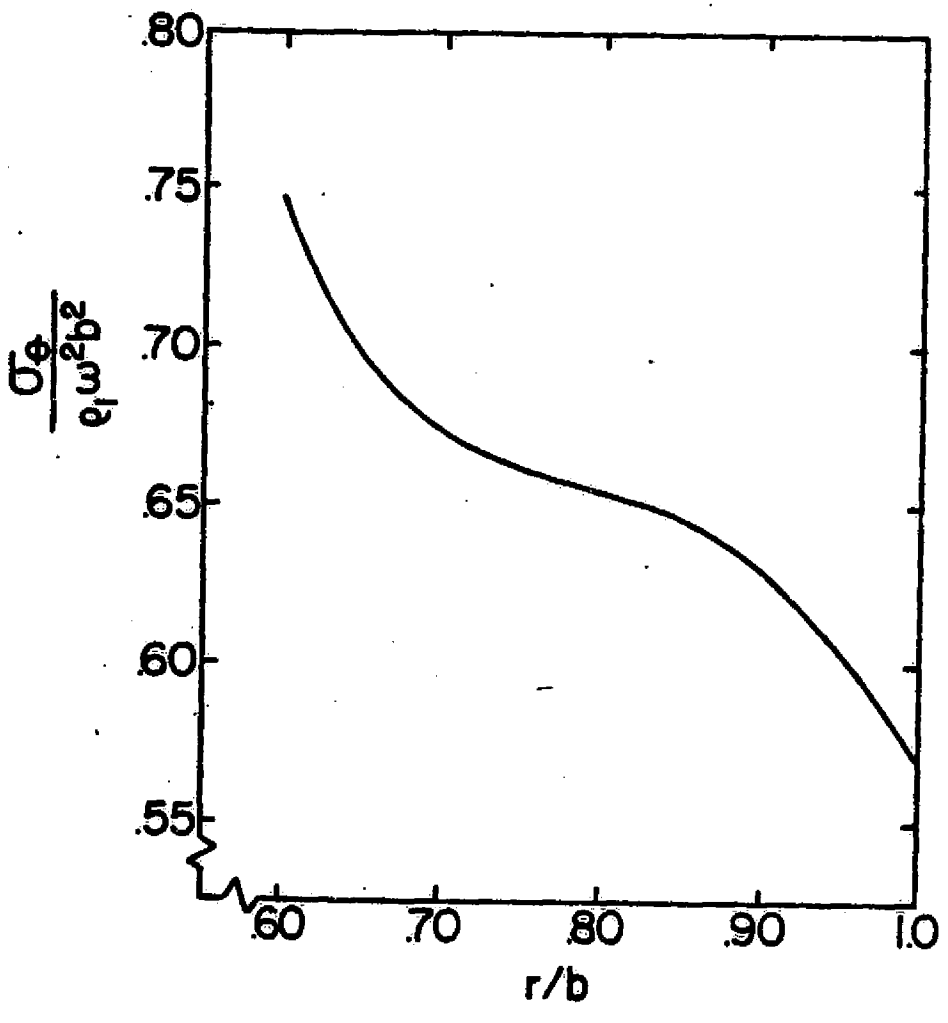

Figure 2. Non-dimensional tangential stress distribution of five non-dimensional assembled Kevlar rings (ID/OD = .6)

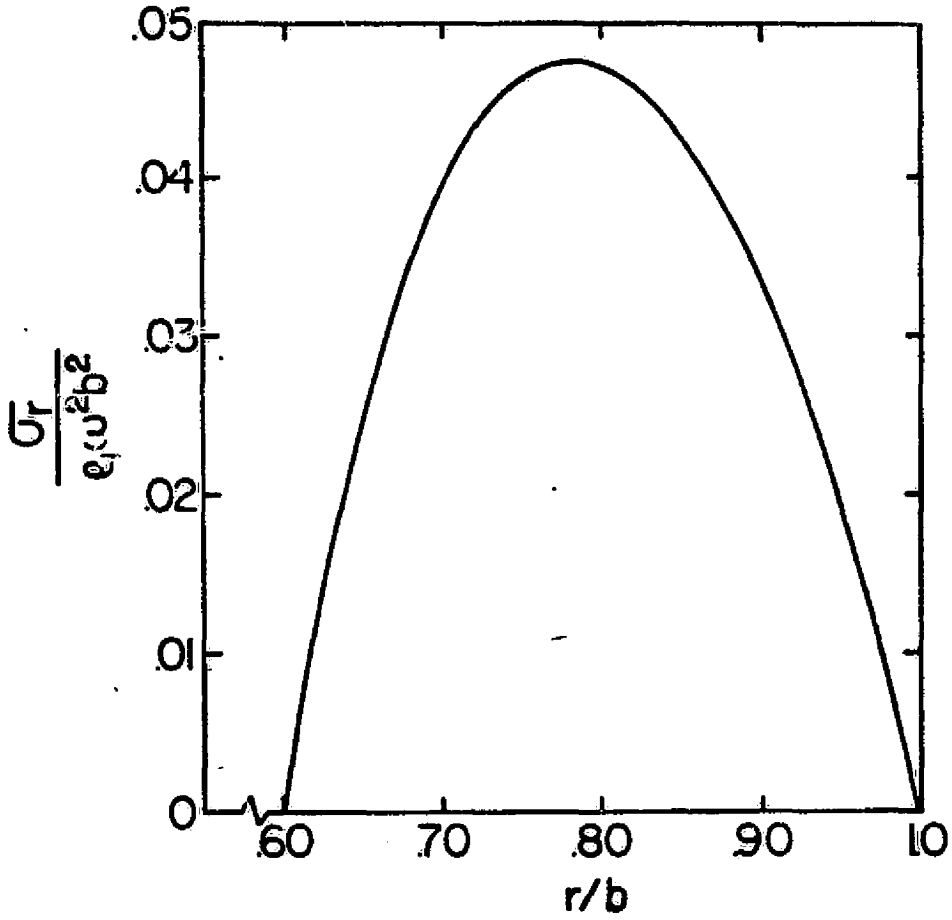

Figure 3. Non-dimensional radial stress distribution of five non-interference assembled Kevlar rings (ID/OD = .6)

Maximization of Energy Density

Two measures of energy storage are commonly used to characterize flywheel rotors. The first is specific energy density (SED or E_w) and is the total stored kinetic energy per unit weight of the flywheel rotor. The second is volumetric energy density (VED or E_v) and is the total stored kinetic energy per unit swept volume of the rotor. The expressions for E_w and E_v are derived in Appendix A and are as follows:

$$E_w = \frac{1}{4\gamma_1}(\beta)\ \frac{\left\{(\frac{i_1}{b})^4 - (\frac{a}{b})^4 + \frac{\rho_2}{\rho_1}[(\frac{i_2}{b})^4 - (\frac{i_1}{b})^4] + \ldots + \frac{\rho_n}{\rho_1}[1 - (\frac{i_{n-1}}{b})^4]\right\}}{\left\{(\frac{i_1}{b})^2 - (\frac{a}{b})^2 + \frac{\rho_2}{\rho_1}[(\frac{i_2}{b})^2 - (\frac{i_1}{b})^2] + \ldots + \frac{\rho_n}{\rho_1}[1 - (\frac{i_{n-1}}{b})^2]\right\}} \qquad (2)$$

$$E_v = \frac{1}{4}(\beta)\left\{(\frac{i_1}{b})^4 - (\frac{a}{b})^4 + \frac{\rho_2}{\rho_1}[(\frac{i_2}{b})^4 - (\frac{i_1}{b})^4] + \ldots + \frac{\rho_n}{\rho_1}[1 - (\frac{i_{n-1}}{b})^4]\right\} \qquad (3)$$

In these equations γ_1 is the weight density of ring 1 and β is the smallest ratio of working stress to normalized centrifugal stress for all rings in the flywheel. Its value is determined as shown in Appendix A.

To improve the energy density of the multiring flywheel, it is desirable to increase β by redistributing the stresses throughout the entire multiring flywheel. In practice, this can be accomplished by interference assembly between the individual rings of the flywheel.

The nondimensional interference stress equations are derived in Appendix B and are as follows:

$$Qr1 = (\frac{i_k}{b})^{N_j+1}(\frac{i_j}{b})^{-2N_j}(\frac{r}{b})^{N_j-1} - (\frac{i_k}{b})^{N_j+1}(\frac{r}{b})^{-N_j-1} \qquad Q\theta 1 = (\frac{i_k}{b})^{N_j+1}(\frac{i_j}{b})^{-2N_j}(\frac{r}{b})^{N_j-1} + (\frac{i_k}{b})^{N_j+1}(\frac{r}{b})^{-N_j-1}$$

$$Qr2 = (\frac{i_k}{b})^{2N_j}(\frac{i_j}{b})^{-N_j+1}(\frac{r}{b})^{-N_j-1} - (\frac{i_j}{b})^{-N_j+1}(\frac{r}{b})^{N_j-1} \qquad Q\theta 2 = (\frac{i_k}{b})^{2N_j}(\frac{i_j}{b})^{-N_j+1}(\frac{r}{b})^{-N_j-1} + (\frac{i_j}{b})^{-N_j+1}(\frac{r}{b})^{N_j-1}$$

(4a)

$$\sigma^{*}_{rsj} = \frac{P^{*}_{K}\{Qr1\} + P^{*}_{j}\{Qr2\}}{\left[\left(\frac{i_k}{i_j}\right)^{2N_j} - 1\right]}$$

(4b)

$$\sigma^{*}_{\theta sj} = \frac{P^{*}_{K}\{Q\theta 1\} - P^{*}_{j} N_j \{Q\theta 2\}}{\left[\left(\frac{i_k}{i_j}\right)^{2N_j} - 1\right]}$$

where $j = 1,2,3, \ldots n$

$K = j-1$

$\frac{i_o}{b} = \frac{a}{b}$; $\frac{i_n}{b} = 1$; $P^{*}_{o} = P^{*}_{n} = 0$

In Eqs. 4a and 4b, P^{*}_{K} and P^{*}_{j} are nondimensional inner and outer pressures caused by the interference fit. The other parameters are material and geometric constants.

It was recognized that filamentary wound composites are best used under uniaxial stress conditions. Ideally, it would be desirable if the multiring flywheel could produce a circumferential stress field which is uniaxial. To approach this condition it is necessary to redistribute the tangential stresses throughout the flywheel so each ring reaches its design limit at the same rotational speed. This can be accomplished by requiring that the maximum tangential stresses in each ring be equal to the design limit stress at the same rotational speed. Practically, this condition may be accomplished by choosing interference pressures (between rings) to force this condition to occur.

By adding Eq. 8 to Eq. 1b (by superposition) the combined stress distribution of rotation and interference assembly in the circumferential direction can be found, with the inner and outer pressure as yet unspecified. To achieve the condition described above the following requirement can be imposed on the combined stress distribution in 2 adjacent ring (rings i and j, i = j-1);

$$\frac{(\sigma^*_{\theta j} + \sigma^*_{\theta sj})_{max}}{(\sigma^*_{\theta i} + \sigma^*_{\theta si})_{max}} = \frac{\sigma_{w\theta Tj}}{\sigma_{w\theta Ti}} \qquad (5)$$

where $(\sigma^*_{\theta j} + \sigma^*_{\theta sj})_{max}$ is the maximum value of combined tangential stress and $\sigma_{w\theta Tj}$ is the tangential design stress in the j^{th} ring.

It was decided to adopt a more conservative design criterion than equation (8), based upon both tangential and radial stress at a point in any ring (i.e. maximum strain criterion ref. 18). This new equation is derived in Appendix C (equation C-4) and is given as:

$$\frac{\sigma_{\theta wTj}}{\sigma_{\theta wTi}} = \frac{[\sigma^*_{\theta j} + \sigma^*_{\theta sj} - \nu_{r\theta j}(\sigma^*_{rj} + \sigma^*_{rsj})]_{max}}{[\sigma^*_{\theta i} + \sigma^*_{\theta si} - \nu_{r\theta i}(\sigma^*_{rj} + \sigma^*_{rsj})]_{max}} \qquad (6)$$

If equations (1), (4), and (6) are applied to every pair of adjacent rings, a set of n-1 linear simultaneous equations, in n-1 unknown interference pressures, is obtained. These equations are shown in Appendix C (equation C-5). The solution of this equation set provides the interference pressures which will bring each ring to the tangential design limit at the same rotational speed. In general, it is necessary to first guess the radial location used in equations (1) and (4) to obtain the maximum combined stress for use in the bracketed expression in equation (6). This first guess is the inner radius of each ring. Using this guess, the interference pressures are obtained and the bracketed quantity in equation (6) is re-evaluated (for each ring) to find the new radial position where the maximum occurs. This new maximum radial position is used to recompute interference pressures and the

iteration is repeated until the new interference pressures are within 1% of those computed in the previous step. Four to five iterations is generally all that is needed.

There are three additional constraints which must be placed on the final values of interfacial pressure which are obtained from the analysis described above.

1. The pressures must not cause any tensile radial stresses with the flywheel at rest.

$$\sigma_{rsj} \leq 0 \tag{7}$$

2. The pressures must not cause the radial and tangential stresses at any point, in any ring, to exceed the design limit.

$$\sigma_{\theta sj} - \nu_{r\theta j}\, \sigma_{rsj} \leq \sigma_{\theta wcj} \tag{8}$$

$$\sigma_{rsj} - \frac{\nu_{r\theta i}}{N^2}\, \sigma_{\theta sj} \leq \sigma_{rwcj} \tag{9}$$

3. The pressures must not cause buckling of any of the rings. This constraint is developed in Appendix D and the constraint is as follows:

$$P^*_{kB} \leq \frac{-2}{FS} \frac{E_\theta}{\rho_1 \omega^2 b^2} \left[\frac{i_k/b - i_j/b}{i_k/b + i_j/b}\right] - P^*_j \tag{10}$$

These constraints are applied from the inner ring outward. For example, the interface pressure from the simultaneous equations at the ring 1 - ring 2 interface is used to test if the constraints in equations (7) thru (10) are satisfied. If they are not, this pressure is reduced to meet the limiting constraint. Pressure P_1 (or P^*_1) is then fixed at the new value and the linear interference equations (Appendix C, equation C-5) are reduced by eliminating the first row and column and re-evaluating for the remaining interference pressures. The new P_2 (or P^*_2) is then tested

against the constraints (equations (7) thru (10) and reduced to meet the limiting constraint - if needed. Pressure P_2 (or P_2^*) is then fixed at this value and the linear interference equations are re-evaluated for the remaining pressures. This process is repeated for all pressures giving a final interference pressure set which satisfies all constraints. In practice, this procedure was used at each step of the iteration process described previously (i.e. radial location finder). The end result produces a set of interference pressures which satisfy all constraints.

These interference pressures are then put in equations (4A) and (4B) and combined with equations (1A) and (1B) to obtain the combined stresses distribution for the complete flywheel. The amount of actual radial interference for each ring can be easily calculated given the interference pressures (see ref. 19 for details).

Figures 4 and 5 show the effect of interference assembly on the radial and tangential stress distributions. It can be seen that the stresses have been redistributed, in effect decreasing overall variations and approaching a constant stress disk (in the circumferential direction).

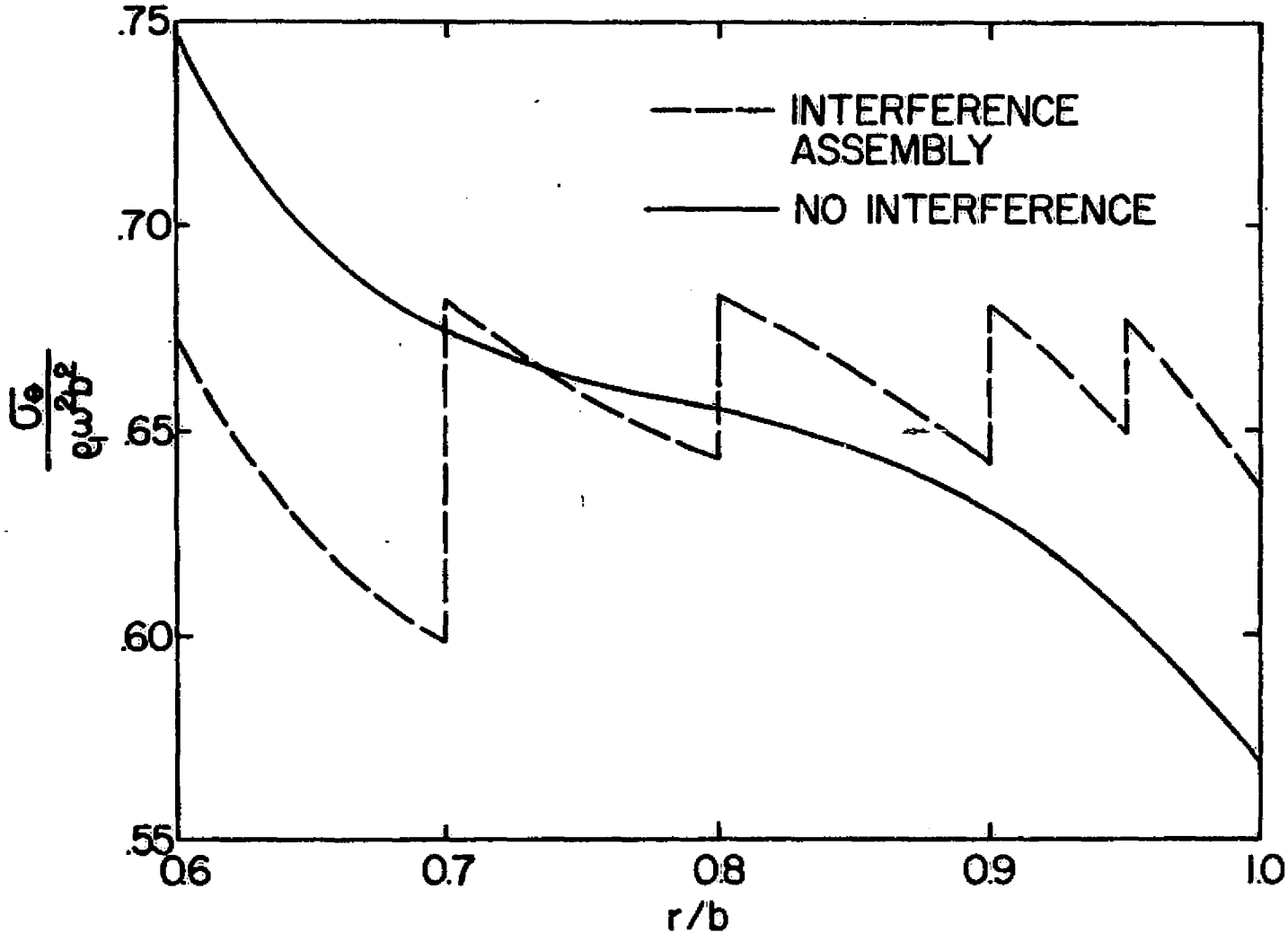

Figure 4. Comparison of non-dimensional tangential stress distributions of five ring Kevlar rotor before and after interference assembly (ID/OD = .6)

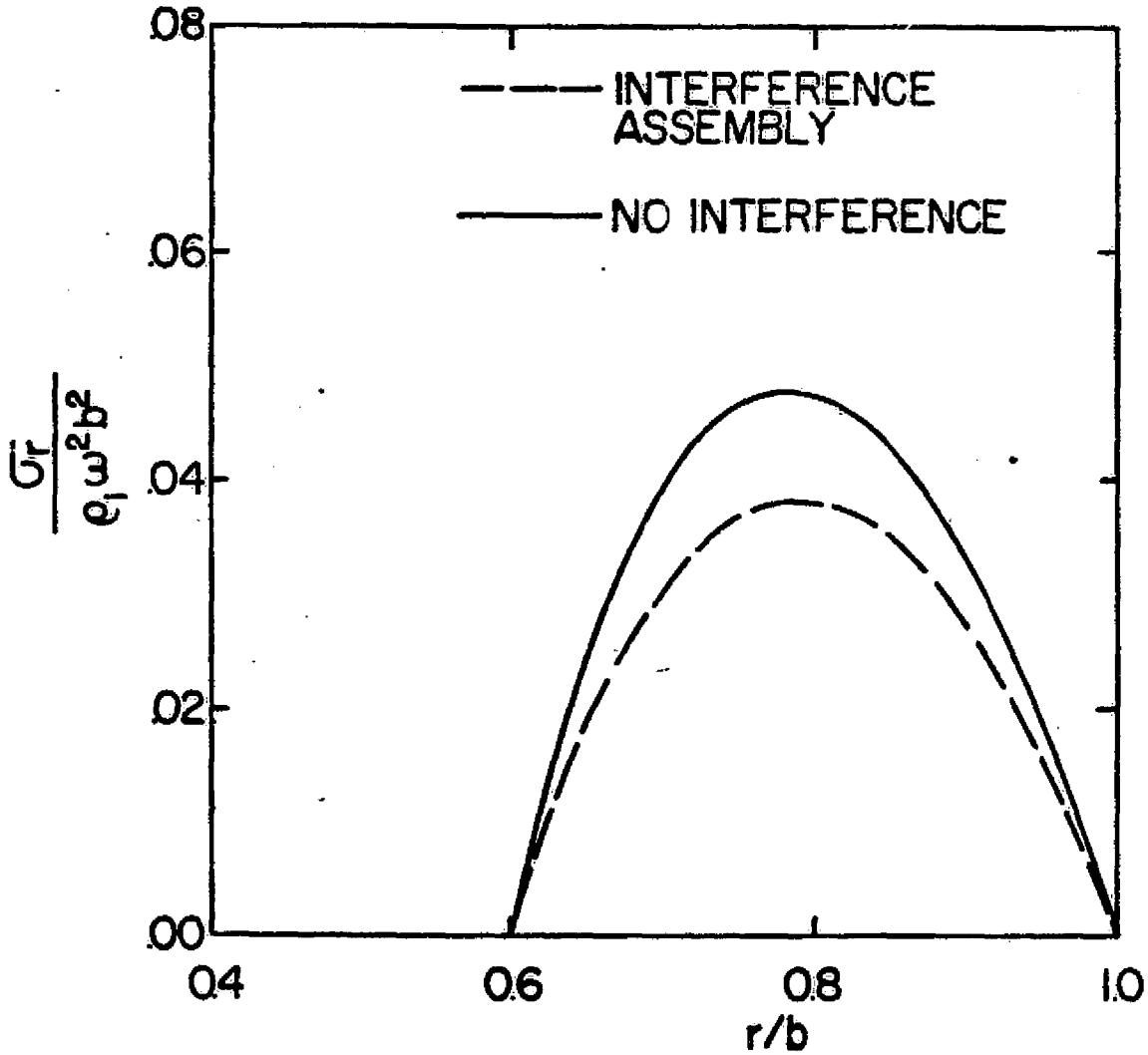

Figure 5. Comparison of non-dimensional radial stress distributions of five ring Kevlar rotor before and after interference assembly (ID/OD = .6)

Results and Discussion

The energy density maximization procedure discussed in the preceding sections has been programmed on a computer to determine the stress distributions and energy densities of a constant thickness spokeless pierced disk or solid disk rotor with up to ten rings. The model is assumed to be in plane stress and the materials may be modelled as isotropic or specially orthotropic (elastic properties). This section of the paper will present and discuss four example flywheel configurations which were analyzed with the program.

The examples considered are described in Table I. The first configuration (single ring) is included only for comparison to the other three, since the maximization procedure cannot be applied. The last two are included because a similar rotor design (with an iron core for the purpose of magnetic suspension and motor/generator energy transfer) is a subject of current interest.*

Shown in Table II are the material properties of the unidirectional composite and segmented iron used in the example configurations. The composite considered is assumed to be circumferentially wound so that the fiber direction corresponds to the tangential (θ) direction and the cross-fiber to the radial (r) direction. The segmented iron is assembled with the other rings to act only as a "dead weight" lending no tangential strength or stiffness to the rotor.

Shown in Figures 6 and 7 are comparisons of SED and VED for the four examples, with and without interference assembly. Significant gains in energy storage capacity are seen for each of the three maximized configurations. However, none of these equal the SED of the single ring, although large gains in VED are found.

The interference assembly not only improved the tangential stress carrying ability of these flywheel, but also helps to control tensile radial stresses.

* NASA Contract NAS5-23650 awarded to Advanced Technology Laboratory, RCA, Camden, N.J.

TABLE I

Description of Example Configurations

Conf. #	ID/OD	# of Rings	Ring Materials (inner to outermost)
1	.9	1	Kevlar-49/Epoxy
2	.6	5	all Kevlar-49/Epoxy
3	.55	6	Iron-Kevlar-49/Epoxy(remaining 5 rings)
4	.55	6	Iron-Carbon/Epoxy-Kevlar-49/Epoxy (remaining 4)

TABLE 2

Material Properties

Material	Modulus of Elasticity E_θ 10^9 Pa (10^6 psi)	Modulus of Elasticity E_r 10^9 Pa (10^6 psi)	N $(\sqrt{E\theta/Er})$	Mass Density 10^3 kg/m^3 (lb/in^3)	Working Strengths Tangential Tensile MPa (ksi)	Tangential Comp MPa (ksi)	Radial Tensile MPa (ksi)	Radial Comp MPa (ksi)
Kevlar	103. (15.)	7. (1.)	3.87	1.38 (.05)	1550. (225.)	276. (40.)	34.5 (5.)	138. (20.)
Carbon	131. (19.)	6.2 (.9)	4.59	2.08 (0.75)	1380 (200.)	1100. (160.)	41. (6.)	138. (20.)
Iron	0.0	207. (30.)	0.0	7.91 (.286)	0.0	0.0	207. 30.	207. 30.

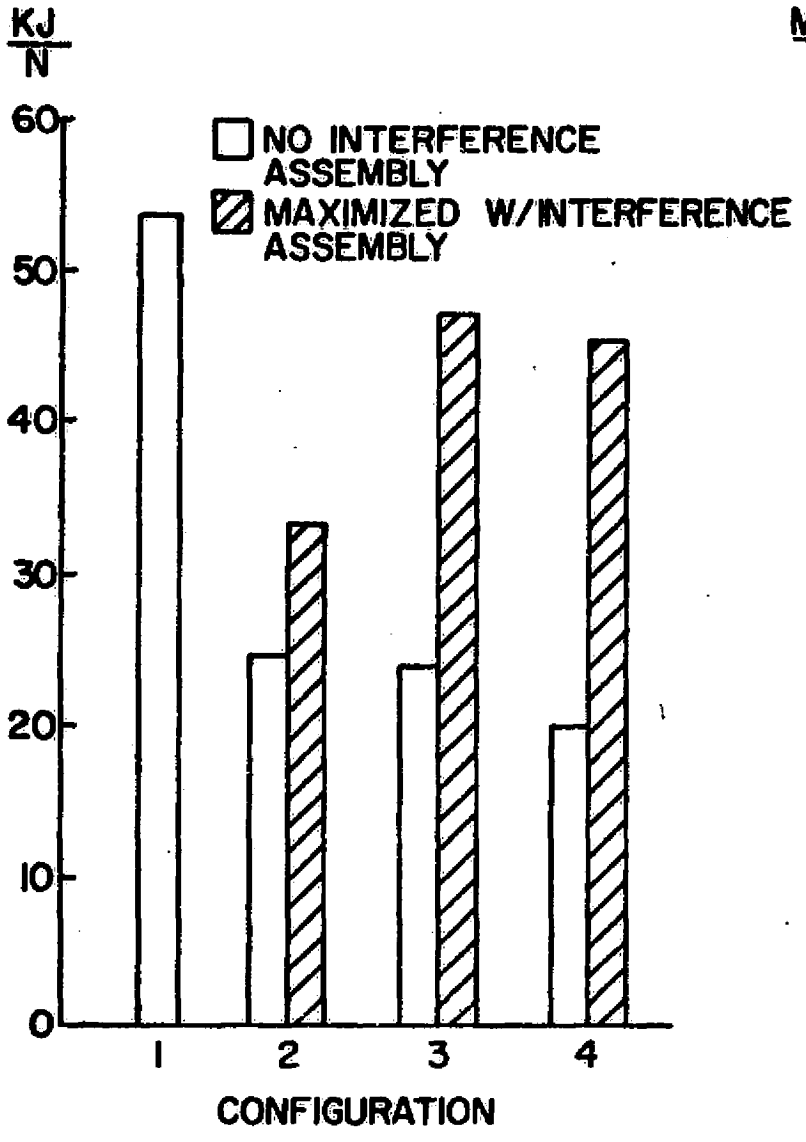

Figure 6. Comparison of specific energy density of four example configurations before and after maximization

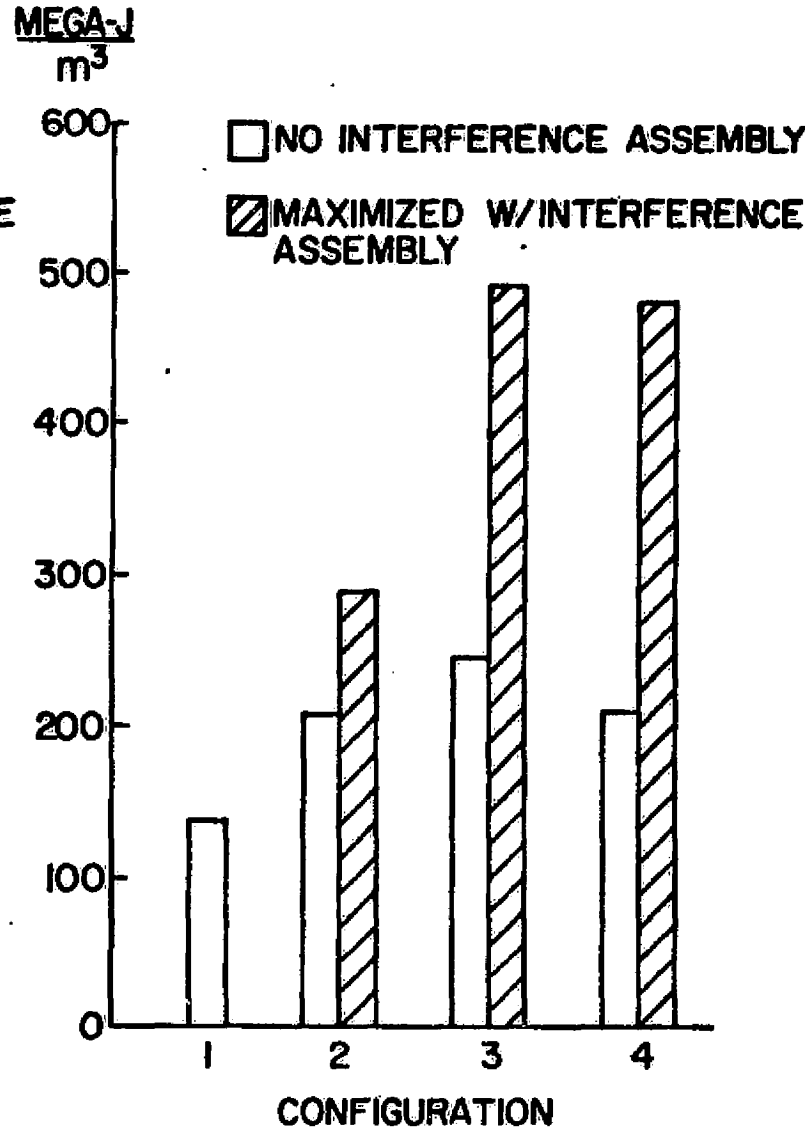

Figure 7. Comparison of volumetric energy density of four example configurations before and after maximization

This is shown by configuration 2 which failed by radial tension both before and after interference assembly. However, a significant increase (36%) in both SED and VED was found with the maximized configuration. In fact, all three multiring configurations failed by radial tension before interference assembly and were significantly improved with maximization. In addition to this means of control, the radial tension in the last two maximized configurations is further reduced by the presence of the iron "dead weight" at the inner surface. This causes a significant compressive radial stress field through these flywheels. With these two controls, the cause of failure returns to tangential stress, as with configuration 1, and the SED comes within 12% of the single ring while the VED surpasses the single ring by 250%.

Conclusions

A stress analysis and energy density maximization procedure has been outlined and demonstrated for a multi-ring disk flywheel. This theoretical analysis assumed a constant thickness, solid or pierced disk flywheel in a state of plane stress. It has been shown that the material working stresses and five non-dimensional parameters for each ring determine the performance of the rotor. It has also been shown that a properly selected interference assembly of the rings will maximize the energy density of the rotor by redistributing tangential stress and by reducing tensile radial stresses.

Results have shown that a six ring configuration with ID/OD = .55 has a specific energy density within 12% of a single ring having ID/OD = .9 while its volumetric energy density surpasses the single ring by 250%. Other results have shown large gains in both SED and VED of maximized multi-ring configurations over the corresponding non-interference assembled rotors.

References

1. Rabenhorst, D. W., "Primary Energy Storage and the Superflywheel," Applied Physics Laboratory ---- Johns Hopkins University, TG-1081, September 1969.

2. Rabenhorst, D. W., "New Concepts in Mechanical Energy Storage," Intersociety Energy Conversion Engineering Conference, Las Vegas, Nevada, 1970, pgs. 2-95 to 2-99.

3. Rabenhorst, D. W., "Potential Applications for the Superflywheel," Intersociety Energy Conversion Engineering Conference, Boston, Massachusetts, 1971, pgs. 1118-1125.

4. Rabenhorst, D. W., "The Application of Wood Technology to Kinetic Energy Storage," APL Technical Digest (Applied Physics Laboratory, The Johns Hopkins University), Volume 2, Number 4, May-June 1972, pgs. 2-12.

5. Rabenhorst, D. W., "Superflywheel Energy Storage System," in Wind Energy Conversion System Workshop (eidtor Savino, J. M.), June 11-13, 1973, Washington, D.C., NASA TM-X-69786, pgs. 137-145.

6. Rabenhorst, D. W. and R. J. Taylor, "Design Considerations for a 100-Megajoule/500 Megawatt Superflywheel," Applied Physics Laboratory/ Johns Hopkins University, TG-1229, December 1973.

7. Rabenhorst, D. W., "The Multirim Superflywheel," Applied Physics Laboratory/Johns Hopkins University, TG-1240, August 1974.

8. Rabenhorst, D. W. and Small, T. R., "Composite Flywheel Development Program Progress Report: March-September 1976," Applied Physics Lab/ Johns Hopkins Univ., #SOD-4616, Oct. 1976.

9. Post, R. F. and S. F. Post, "Flywheels," Scientific American, Vol. 229, Number 6, December 1972, pgs. 17-23.

10. Notti, J. E. et al. "Integrated Power Attitude Control System (IPACS) Study, Volume I - Feasibility Studies," NASA CR-2381.

11. Notti, J. E., et al. "Integrated Power/Attitude Control System (IPACS) Study, Volume II - Conceptual Designs," NASA CR-2382.

12. Notti, J.E., "Design and Test of a Spacecraft Energy Momentum Flywheel," Proceedings 1975 Flywheel Technology Symposium, Lawrence Hall of Science, Berkeley, California, Nov. 10-12, 1975.

13. Kirk, J. A., Studer, P. A., Evans, H. E., "Mechanical Capacitor," NASS TN D-8185, March, 1976.

14. Kirk, J. A., "Flywheel Energy Storage, Part I - Basic Concepts," accepted International Journal of Mechanical Science.

15. Kirk, J. A. and Studer, P. A., "Flywheel Energy Storage - Part II - Magnetically Suspended Superflywheel," accepted International Journal of Mechanical Science.

16. Kirk, J. A., Huntington, R. A., "Stress Analysis and Maximization of Energy Density for a Magnetically Suspended Flywheel," to be published.

17. Wang, C. T., Applied Elasticity, McGraw-Hill Book Co., New York, 1953.

18. Ashton, J. E., Halpin, J. C. and Petit, P. H., Primer on Composite Materials: Analysis, Technomic Publishing Co., Stamford, Conn. 1969.

19. Huntington, R.A., "Stress Analysis, Energy Density Maximization, and Numerical Solution for Arbitrary Shapes Plus Optimization," to be published.

20. Timoshenko, S. and Gere, J. M., Theory of Elastic Stability, McGraw-Hill, New York, 1961.

Appendix A: Computation of Specific and Volumetric Energy Density

define: E_w - Specific Energy Density

E_v - Volumetric Energy Density

$$E_w \equiv \frac{\text{kinetic energy}}{\text{flywheel weight}} \qquad E_v \equiv \frac{\text{kinetic energy}}{\text{flywheel swept vol.}}$$

The kinetic energy (KE) is given, for a rotating mass, as

$$KE = \frac{1}{2} J\omega^2 \tag{A1}$$

where: J is the mass moment of inertia

ω is the angular velocity

The mass moment of inertia for n rings is

$$J = \frac{1}{2} \rho_1 \pi \tau b^4 \left\{\frac{\rho_n}{\rho_1}\left[1-\left(\frac{i_{n-1}}{b}\right)^4\right] + \frac{\rho_{n-1}}{\rho_1}\left[\left(\frac{i_{n-1}}{b}\right)^4-\left(\frac{i_{n-2}}{b}\right)^4\right] + \ldots \left[\left(\frac{i_1}{b}\right)^4-\left(\frac{a}{b}\right)^4\right]\right\} \tag{A2}$$

where: a = inner radius

b = outer radius

i_k = radius of k^{th} ring interface

ρ_k = mass density of k^{th} ring

therefore

$$KE = \frac{1}{4} \rho_1 \omega^2 b^4 \pi \tau \left\{\frac{\rho_n}{\rho_1}\left[1-\left(\frac{i_{n-1}}{b}\right)^4\right] + \ldots \left[\left(\frac{i_1}{b}\right)^4-\left(\frac{a}{b}\right)^4\right]\right\} \tag{A3}$$

Since the weight (W) of the flywheel is given by

$$W = \pi \tau \gamma_1 b^2 \left\{\frac{\rho_n}{\rho_1}\left[1-\left(\frac{i_{n-1}}{b}\right)^2\right] + \ldots\left[\left(\frac{i_1}{b}\right)^2-\left(\frac{a}{b}\right)^2\right]\right\} \tag{A4}$$

where γ_1 is the weight density of ring 1

E_w becomes

$$E_w = \frac{\rho_1 \omega^2 b^2}{4} \gamma_1 \frac{\{\frac{\rho_n}{\rho_1}[1 - (\frac{i_{n-1}}{b})^4] + \ldots [(\frac{i_1}{b})^4 - (\frac{a}{b})^4]\}}{\{\frac{\rho_n}{\rho_1}[1 - (\frac{i_{n-1}}{b})^2 2 + \ldots [(\frac{i_1}{b})^2 - (\frac{a}{b})^2]\}} \quad \text{(A5)}$$

Also, since the swept volume (V_s) is $\pi \tau b^2$

$$E_v = \frac{\rho_1 \omega^2 b^2}{4} \{\frac{\rho_n}{\rho_1}[1 - (\frac{i_{n-1}}{b})^4] + \ldots [(\frac{i_1}{b})^4 - (\frac{a}{b})^4]\} \quad \text{(A6)}$$

It is possible to simplify the expressions for E_w and E_v through the use of the following relationships:

$$\beta_{1j} = \frac{\sigma_{\theta w Tj}}{(\sigma^*_{\theta j} - \nu_{r\theta}\sigma^*_{rj})_{max}} \quad \text{(A7)}$$

$$\beta_{2j} = \frac{\sigma_{rw Tj}}{(\sigma^*_{rj} - \frac{\nu_{r\theta}}{N^2}\sigma^*_{\theta j})_{max}} \quad \text{(A8)}$$

$$\beta_{3j} = \frac{\sigma_{rwcj}}{(\sigma^*_{rj} - \frac{\nu_{r\theta}}{N^2}\sigma^*_{\theta j})_{min}} \quad \text{(A9)}$$

These relationships are the result of applying a strain yield criterion to the nondimensional radial and tangential stresses in each ring (ref. 18). Equations (A7) - (A9) are evaluated for each ring in the flywheel and the smallest value (β) is used in the simplified equations (A10) and (A11).

$$E_w = \frac{1}{4\gamma_1}(\beta) \frac{\{\frac{\rho_n}{\rho_1}[1 - (\frac{i_{n-1}}{b})^4] + \ldots [(\frac{i_1}{b})^4 - (\frac{a}{b})^4]\}}{\{\frac{\rho_n}{\rho_1}[1 - (\frac{i_{n-1}}{b})^2] + \ldots [(\frac{i_1}{b})^2 - (\frac{a}{b})^2]\}} \quad \text{(A10)}$$

$$E_v = \frac{1}{4}(\beta)\{\frac{\rho_n}{\rho_1}[1 - (\frac{i_{n-1}}{b})^4] + \ldots [(\frac{i_1}{b})^4 - (\frac{a}{b})^4]\} \quad \text{(A11)}$$

Appendix B: Interference Fit Stress Analysis

The force equilibrium equation for an axi-symmetric body with no body forces [17] is

$$\frac{\partial \sigma_r}{\partial r} + \frac{\sigma_r - \sigma_\theta}{r} = 0 \tag{B1}$$

The solution to Eq. B1 [14] is

$$\sigma_r = C_1 r^{N-1} + C_2 r^{-N-1}$$

$$\sigma_\theta = C_1 N r^{N-1} - C_2 N r^{-N-1} \tag{B2}$$

where $$N \equiv \sqrt{E_\theta / E_r} \tag{B3}$$

by normalizing Eqs. B2 with the factor $(\rho_1 \omega^2 b^2)$ they become

$$\sigma^*_{r_j} = A_j \left(\frac{r}{b}\right)^{N_j - 1} + B_j \left(\frac{r}{b}\right)^{-N_j - 1}$$

$$\sigma^*_{\theta_j} = A_j N_j \left(\frac{r}{b}\right)^{N-1} - B_j N_j \left(\frac{r}{b}\right)^{-N_j - 1} \tag{B4}$$

$$P^*_k = \frac{P_k}{\rho_1 \omega^2 b^2} \tag{B5}$$

where: j denotes the jth ring

k denotes the kth ring interface

P is the ring interference pressure

The following boundary conditions can be applied to Eqs. B4 and B5

$$\begin{aligned} &@\ r = a && \sigma^*_{r_1} = 0 \\ &@\ r = i_1 && \sigma^*_{r_1} = P^*_1 = \sigma^*_{r_2} \\ &@\ r = i_2 && \sigma^*_{r_2} = P^*_2 = \sigma^*_{r_3} \\ &\quad \vdots \\ &@\ r = b && \sigma^*_{r_n} = 0 \end{aligned} \tag{B6}$$

The solution of Eqs. B6 yield expressions for the constants (A_j & B_j)

$$A_j = \frac{P_k^*\left(\frac{i_k}{b}\right)^{N_j+1}\left(\frac{i_j}{b}\right)^{-2N_j} - P_j^*\left(\frac{i_j}{b}\right)^{-N_j+1}}{\left[\left(\frac{i_k}{i_j}\right)^{2N_j} - 1\right]}$$

$$B_j = \frac{P_j^*\left(\frac{i_k}{b}\right)^{2N_j}\left(\frac{i_j}{b}\right)^{-N_j+1} - P_k^*\left(\frac{i_k}{b}\right)^{N_j+1}}{\left[\left(\frac{i_k}{i_j}\right)^{2N_j} - 1\right]} \qquad \text{(B7)}$$

where $j = 1, 2, 3, \ldots n$ $\qquad k = j-1$

and $\frac{i_o}{b} = \frac{a}{b}$ $\quad \frac{i_n}{b} = \frac{b}{b} = 1$ $\qquad P_o^* = P_n^* = 0$

Eqs. B4 and B7 can now be combined to yield expressions for the stresses in each ring due to the interference pressures at its inner and outer surfaces

$$\sigma_{rsj}^* = \frac{P_k^*\left(\frac{i_k}{b}\right)^{N_j+1}\left\{\left(\frac{i_j}{b}\right)^{-2N_j}\left(\frac{r}{b}\right)^{N_j-1} - \left(\frac{r}{b}\right)^{-N_j-1}\right\} + P_j^*\left(\frac{i_j}{b}\right)^{-N_j+1}\left\{\left(\frac{i_k}{b}\right)^{2N_j}\left(\frac{r}{b}\right)^{-N_j-1} - \left(\frac{r}{b}\right)^{N_j-1}\right\}}{\left[\left(\frac{i_k}{i_j}\right)^{2N_j} - 1\right]}$$

$$\sigma_{\theta sj}^* = \frac{P_k^* N_j\left(\frac{i_k}{b}\right)^{N_j+1}\left\{\left(\frac{i_j}{b}\right)^{-2N_j}\left(\frac{r}{b}\right)^{N_j-1} + \left(\frac{r}{b}\right)^{-N_j-1}\right\} - P_j^* N_j\left(\frac{i_j}{b}\right)^{-N_j+1}\left\{\left(\frac{i_k}{b}\right)^{2N_j}\left(\frac{r}{b}\right)^{-N_j-1} + \left(\frac{r}{b}\right)^{N_j-1}\right\}}{\left[\left(\frac{i_k}{i_j}\right)^{2N_j} - 1\right]} \qquad \text{(B8)}$$

Appendix C: Maximization of Energy Density by Stress Redistribution

Maximum energy storage will occur when each ring of the flywheel reaches its maximum working stress at the same rotational speed. Since this condition is unlikely to occur with normal assembly of the flywheel rings, it must be forced to occur by a pre-selected interference assembly. The following analysis will detail the interference pressure selection procedure.

Since a greater amount of stress will be carried in the circumferential direction, than in the radial it is desirable to maximize the stress attainable in this direction.

Failure will be assumed to be controlled by a maximum failure strain in the tangential (circumferential) direction given by the ratio of working stress and Young's modulus (θ direction).

Therefore, in the j^{th} ring at failure

$$\varepsilon_{\theta j}\Big|_f = \frac{1}{E_{\theta j}} \left(\sigma_{\theta j} - \nu_{r\theta j}\sigma_{rj}\right)\Big|_f = \sigma_{\theta wj}/E_{\theta j} \qquad (C1)$$

where f denote stress or strain states at failure

$$\sigma_{\theta wj} = \left(\sigma_{\theta j} - \nu_{r\theta j}\sigma_{rj}\right)\Big|_f \qquad (C2)$$

In order to maximize the energy storage of the flywheel, ratios of Eq. C2 between each pair of rings must be equal. This is represented as

$$\frac{\sigma_{\theta wj}}{\sigma_{\theta wi}} = \frac{\left(\sigma_{\theta j} - \nu_{r\theta j}\,\sigma_{rj}\right)_{max}}{\sigma_{\theta\kappa} - \nu_{r\theta\kappa}\,\sigma_{r\kappa})_{max}} \qquad (C3)$$

where $j = 1, 2, 3, \ldots n-1$ $\qquad$ $\kappa = j-1$

Eq. C3 can be satisfied if the stresses are considered to be the superposition of rotational and interference stresses. Eq. C3 becomes (for non-dimensional stresses)

$$\frac{\sigma_{\theta wj}}{\sigma_{\theta w\kappa}} = \frac{[\sigma^*_{\theta j} + \sigma^*_{\theta sj} - \nu_{r\theta j}(\sigma^*_{rj} + \sigma^*_{rsj})]_{max}}{[\sigma^*_{\theta\kappa} + \sigma^*_{\theta s\kappa} - \nu_{r\theta\kappa}(\sigma^*_{r\kappa} + \sigma^*_{rs\kappa})]_{max}} \qquad (C4)$$

where the subscript s denotes interference stress.

By combining Eq. C4 with the expressions for interference stress developed in Appendix B, a set of simultaneous equations which yield the interference pressures are found. Since these equations are well behaved and linear, they may be solved by a simple elimination procedure to yield the interference pressures which are necessary to cause each ring to reach its maximum tangential strain at the same rotational speed. This method is also easily adapted to other failure criteria. An example of this set of simultaneous equations in matrix form is given below. Each of the quantities in the equation set must be evaluated at the radius in each ring where tangential failure will first occur.

$$\begin{bmatrix} A_{11} & A_{21} & 0 & 0 & 0 & 0 \\ A_{12} & A_{22} & A_{32} & 0 & 0 & 0 \\ 0 & A_{23} & A_{33} & A_{43} & 0 & 0 \\ 0 & 0 & A_{43} & A_{44} & A_{54} & 0 \\ 0 & 0 & 0 & A_{45} & A_{55} & A_{65} \\ 0 & 0 & 0 & 0 & A_{56} & A_{66} \end{bmatrix} \begin{bmatrix} P^*_1 \\ P^*_2 \\ P^*_3 \\ P^*_4 \\ P^*_5 \\ P^*_6 \end{bmatrix} = \begin{bmatrix} B_1 \\ B_2 \\ B_3 \\ B_4 \\ B_5 \\ B_6 \end{bmatrix} \qquad (C5)$$

where: $k = j - 1$

$$A_{jj} = \left[- \frac{\sigma_{\theta wj}}{\sigma_{\theta wk}} (C_{4k} - \nu_{r\theta k} C_{2k}) + (C_{3j} - \nu_{r\theta j} C_{1j}) \right]$$

$$A_{jk} = (C_{4j} - \nu_{r\theta j} C_{2j}) \qquad A_{kj} = - \frac{\sigma_{\theta wj}}{\sigma_{\theta wk}} (C_{3k} - \nu_{r\theta k} C_{1k})$$

$$B_j = \left[\frac{\sigma_{\theta wj}}{\sigma_{\theta wk}} (\sigma^*_{\theta k} - \nu_{r\theta k} \sigma^*_{rk}) - (\sigma^*_{\theta j} - \nu_{r\theta j} \sigma^*_{rj}) \right]$$

$$C_{1j} = \left(\frac{i_k}{b}\right)^{N_j+1} \left\{ \left(\frac{i_j}{b}\right)^{-2N_j} \left(\frac{r}{b}\right)^{N_j-1} - \left(\frac{r}{b}\right)^{-N_j-1} \right\} / \left[\left(\frac{i_k}{i_j}\right)^{2N_j} - 1 \right]$$

$$C_{2j} = \left(\frac{i_j}{b}\right)^{-N_j+1} \left\{ \left(\frac{i_k}{b}\right)^{2N_j} \left(\frac{r}{b}\right)^{-N_j-1} - \left(\frac{r}{b}\right)^{N_j-1} \right\} / \left[\left(\frac{i_k}{i_j}\right)^{2N_j} - 1 \right]$$

$$C_{3j} = N_j \left(\frac{i_k}{b}\right)^{N_j+1} \left\{ \left(\frac{i_j}{b}\right)^{-2N_j} \left(\frac{r}{b}\right)^{N_j-1} + \left(\frac{r}{b}\right)^{-N_j-1} \right\} / \left[\left(\frac{i_k}{i_j}\right)^{2N_j} - 1 \right]$$

$$C_{4j} = -N_j \left(\frac{i_j}{b}\right)^{-N_j+1} \left\{ \left(\frac{i_k}{b}\right)^{2N_j} \left(\frac{r}{b}\right)^{-N_j-1} + \left(\frac{r}{b}\right)^{N_j-1} \right\} / \left[\left(\frac{i_k}{i_j}\right)^{2N_j} - 1 \right]$$

Appendix D: Buckling Constraint

Consider a thin pierced disk with an inner radius of i_j and an outer radius of i_k, under internal and external pressures P_j and P_k.

From Timoshenko and Gere (ref. 20), the following buckling relation is given for external pressure

$$q_{CR} = \frac{3E_\theta I}{r_o^3} \tag{D1}$$

where q_{CR} = critical pressure per unit length of centerline

E_θ = tangential modulus of elasticity

I = cross sectional moment of inertia

r_o = undeformed mean radius

From the definition of q_{CR}, it follows that

$$P_{CR} = \frac{q_{CR}}{\tau} \tag{D2}$$

where P_{CR} = critical external pressure

τ = axial ring thickness

Also,

$$I = \frac{(i_k - i_j)^3 \tau}{12} \tag{D3}$$

$$r_o \cong \frac{(i_k + i_s)}{2} \tag{D4}$$

by combining Eqs. D-1 through D-4, the following results

$$P_{CR} = -2E_\theta \left[\frac{i_k - i_j}{i_k + i_j}\right]^3 \tag{D5}$$

This equation must now be made nondimensional using the factor $\rho_1 \omega^2 b^2$. A factor of safety is also added.

$$P^*_{CR} = \frac{P_{CR}}{\rho_1 \omega^2 b^2} \frac{1}{FS} = -\frac{2}{FS} \frac{E_\theta}{\rho_1 \omega^2 b^2} \left[\frac{\frac{i_k}{b} - \frac{i_j}{b}}{\frac{i_k}{b} - \frac{i_j}{b}} \right]^3 \qquad (D6)$$

where P^*_{CR} = nondimensional critical pressure

FS = factor of safety

For simplicity of application, it is assumed that the critical pressure can be considered the numeric difference of an external pressure which may buckle the ring and the pressure applied to the interior of ring. Therefore,

$$P^*_{KB} = -\frac{2}{FS} \frac{E_\theta}{\rho_1 \omega^2 b^2} \left[\frac{\frac{i_k}{b} - \frac{i_j}{b}}{\frac{i_k}{b} - \frac{i_j}{b}} \right]^3 - P^*_j \qquad (D7)$$

where: P^*_{KB} = nondimensional external pressure which may buckle the ring

P^*_j = nondimensional internal pressure

Eqn. D-7 is used as the buckling constraint discussed in the text. However, two points must be made. First, the most recent value of B (see Appendix A) (found in the iteration scheme) is used for $\rho_1 \omega^2 b^2$. Secondly, the values of buckling pressure found with this relation are approximate. Thus a sufficient factor of safety is needed. (2.0 is typical.) Also, since the formula was developed for thin rings, $(i_k + i_j) > 10(i_k - i_j)$ for better accuracy. This final restriction is generally not a problem since with the materials considered for this paper, such as Kevlar-49, the value of 10 above yields a buckling pressure of 50 MPa (7500 psi) which would most likely be further restricted by one of the other two constraints.

APPENDIX H

PRICE - A PARAMETRIC COST MODELING METHODOLOGY

PRICE (Programmed Review of Information for Costing and Evaluation) is an RCA-developed parametric cost-modeling technique. It provides reliable estimates of system acquisition costs (development and production), based upon physical parameters such as quantity, size, weight, power consumption, environmental specification, type of packaging, and level of integration; and schedule parameters such as months to first prototype, manufacturing rate, and amount of new design. PRICE has been particularly useful in developing relative costs of competitive systems.

Early cost measurement of concepts is crucial to a new venture, since there is little opportunity to change program costs significantly once a design has been detailed. PRICE was developed to operate with a limited description of a concept so that many alternatives can be cost examined before designs and bills of material are finalized. It is also used extensively for independent assessment of conventionally prepared cost estimates. However, PRICE was never intended to be a substitute for detailed cost estimating; its value lies in the parametric testing of reasonableness of the detailed estimates. If deviations from established trends are indicated by PRICE, the detailed estimates should be investigated.

PRICE does not provide computer software or life-cycle cost predictions. These areas are currently under active study and will be cost-modeled in the near future. PRICE also does not provide costs for brick and mortar, and there are no plans to add such capability to the model.

Numerous parametric cost models exist throughout industry and government agencies, each designed to cover a specific range of products or systems and requiring its set of unique inputs (which include performance features, technologies, and quantities). Numerous models are required because different systems have different cost-significant characteristics that require unique mathematical regressions to quantify the cost effects.

PRICE was formulated as a universal system to generate appropriate regressions or CER's (cost-estimating relationships) for a range of products or systems. In essence, it performs a multi-dimensional extrapolation of past experience to predict cost.

Inputs to PRICE cover an infinite range of systems. Since all products must have weight and size, these are used by PRICE as the principal descriptors. Electronic areas are characterized by their componentry. Mechanical structures can be described in terms of types of material, construction, and densities. Procedures of PRICE have been developed to process situations where weights and sizes are not known. In these cases, the physical characteristics can be generated by the program.

In addition, certain PRICE inputs describe the way an organization operates: its way of doing business. Thus, the model can be customized to reflect appropriate cost element definitions.

PRICE outputs feature costs for the development and production phases. Outputs are categorized by such elements as Drafting, Design, Project Management, Prototype, and Special Tools and Test Equipment. PRICE can also develop an engineering schedule or measure the reasonableness of an input schedule. Variations of parameters such as physical features, componentry, percentage of new design, and reliability (MTBF) can be quickly assessed. Integration and test costs for both engineering and production can be developed by PRICE at any level of the work breakdown structure.

PRICE has provisions to include the costs for GFE and purchased items. It can also evaluate the costs of their testing, modification (if necessary), and integration and test with other equipments.

Fig. 1 shows a PRICE output for a cost study on a hypothetical military airborne radar. The top third of the format lists the program inputs. The

rest of the format includes the derived estimates, schedules, and cost ranges.

PRICE automatically computes the effects of phase interactions between engineering and manufacturing. In addition to considering a normal performance period, PRICE can output cost manifestations due to accelerated or protracted engineering schedules or due to an operation plan that requires stops and restarts of production effort with varying intervals.

PRICE can measure many aspects of a proposed project to determine their significance and their level of influence. It can direct attention to those factors whose modification can be most rewarding. For example, a change of engineering schedule from 8 to 10 months and release of production at the 11th month might result in reduction of the total cost of a particular project even more than reducing the product weight by 10%. Under another set of conditions however, a reduction of assembly weight might far outweigh any conceivable schedule change. On occasion, technology will completely govern the pattern of cost variations.

AIRBORNE RADAR MIL-SPEC OCTOBER 1, 1976

INPUT DATA

QTY	200.	PROTOS	10.0	WT	45.000	VOL	0.780	MODE	1.
QTYSYS	1.	INTEGE	1.000	INTEGS	1.000	AMULTE	125.00%	AMULTM	125.00%

MECH/STRUCT

WS	10.000	MCPLXS	0.000	PRODS	4.200	NEWST	0.900	DESRPS	2.000

ELECTRONICS

USEVOL	1.000	MCPLXE	0.000	PRODE	4.300	NEWEL	0.800	DESRPE	2.000
PWR	0.000	CMPNTS	0.	CMPID	0.000	PWRFAC	1.000	CMPEFF	1.000

ENGINEERING

ENMTHS	6.0	ENMTHP	0.0	ENMTHT	0.0	ECMPLX	1.200	PRNF	0.200

PRODUCTION

PRMTHS	25.0	PRMTHF	0.0	LCURVE	0.000	ECNE	0.000	ECNS	0.000

GLOBAL

YEAR	1976.	ESC	8.30%	PROJCT	1.000	DATA	1.000	TLGTST	1.000
PLATFM	1.800	SYSTEM	1.000	PPROJ	1.000	PDATA	1.000	PTLGTS	1.00

PROGRAM COST	DEVELOPMENT	PRODUCTION	TOTAL COST
ENGINEERING			
DRAFTING	252.	24.	276.
DESIGN	937.	73.	1010.
SYSTEMS	150.	0.	150.
PROJ MGMT	194.	328.	522.
DATA	61.	16.	77.
SUBTOTAL (ENG)	1594.	441.	2036.
MANUFACTURING			
PRODUCTION	0.	6707.	6707.
PROTOTYPE	734.	0.	734.
TOOL-TEST EQ	97.	199.	296.
SUBTOTAL (MFG)	831.	6906.	7738.
TOTAL COST	2426.	7348.	9773.

VOL	0.780	AVCOST	33.54	TOTAL AV PROD COST			36.74	LCURVE	0.897
WT	45.000	ECNE	0.072	ECNS	0.021	DESRPE	0.494	DESRPS	0.210

MECH/STRUCT

WS	10.000	WSCF	12.821	MECID	0.000	PRODS	4.200	MCPLXS	5.602

ELECTRONICS

WE	35.000	WECF	44.872	CMPID	0.000	PRODE	4.300	MCPLXE	7.903
PWR	182.399	CMPNTS	4053.			PWRFAC	1.000	CMPEFF	1.000

SCHEDULES

ENMTHS	6.000	ENMTHP	14.874	ENMTHT	24.679	ECMPLX	1.200	PRNF	0.200
PRMTHS	25.000	PRMTHF	50.229	AVER. PROD RATE PER MONTH					7.928

COST RANGES	DEVELOPMENT	PRODUCTION	TOTAL COST
FROM	2122.	6121.	8243.
CENTER	2426.	7348.	9773.
TO	2874.	9162.	12037.

Fig. 1 — Typical Price Output

There is a mode of PRICE called GEOSYN—an acronym for geometry synthesis, which is truly a design-to-cost procedure. For GEOSYN, the target cost, quantities, product class, and level of technology are entered as inputs. GEOSYN outputs include design limits, i.e., weight, size, component count, and power dissipation. For the design-to-cost project, therefore, if the design is held to the GEOSYN-derived limits, there is a good chance that the cost target will be met.

In 1971, the U.S. Air Force and NASA were the first to contract with RCA for services of the PRICE model. Their usage has increased each year since and several other Government agencies are now using PRICE. Records indicate that the various Government agencies have processed thousands of cost studies.

Many aerospace and electronics companies learned of PRICE through its widespread government use. Because of expressed industry interest, RCA Management chartered the G&CS PRICE Systems Activity to offer PRICE commercially in August 1975.

Since then, agreements for the use of PRICE have been effected with eleven major companies and others are now actively evaluating their potential use of the model.

ROTATING FRAME

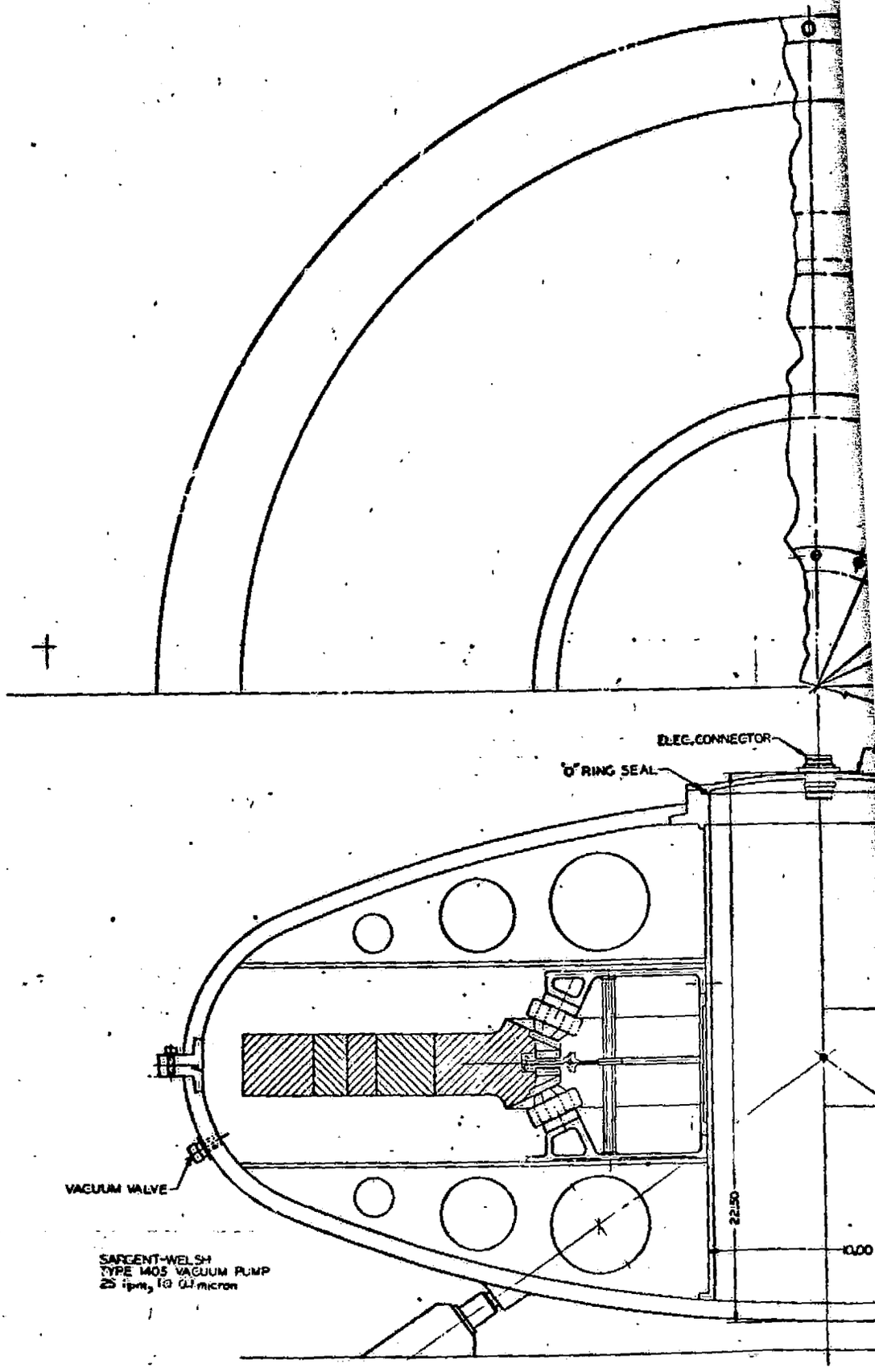

NOTES:
1. MOTOR AIRGAPS & MAGNETIC GAPS TO BE .030 NOM.
2. MFG. TOLERANCES ON WHEEL FOR FLATNESS, PARALLELISM & PERPENDICULARITY TO ROTATIONAL AXIS TO BE ±.002 TIR.

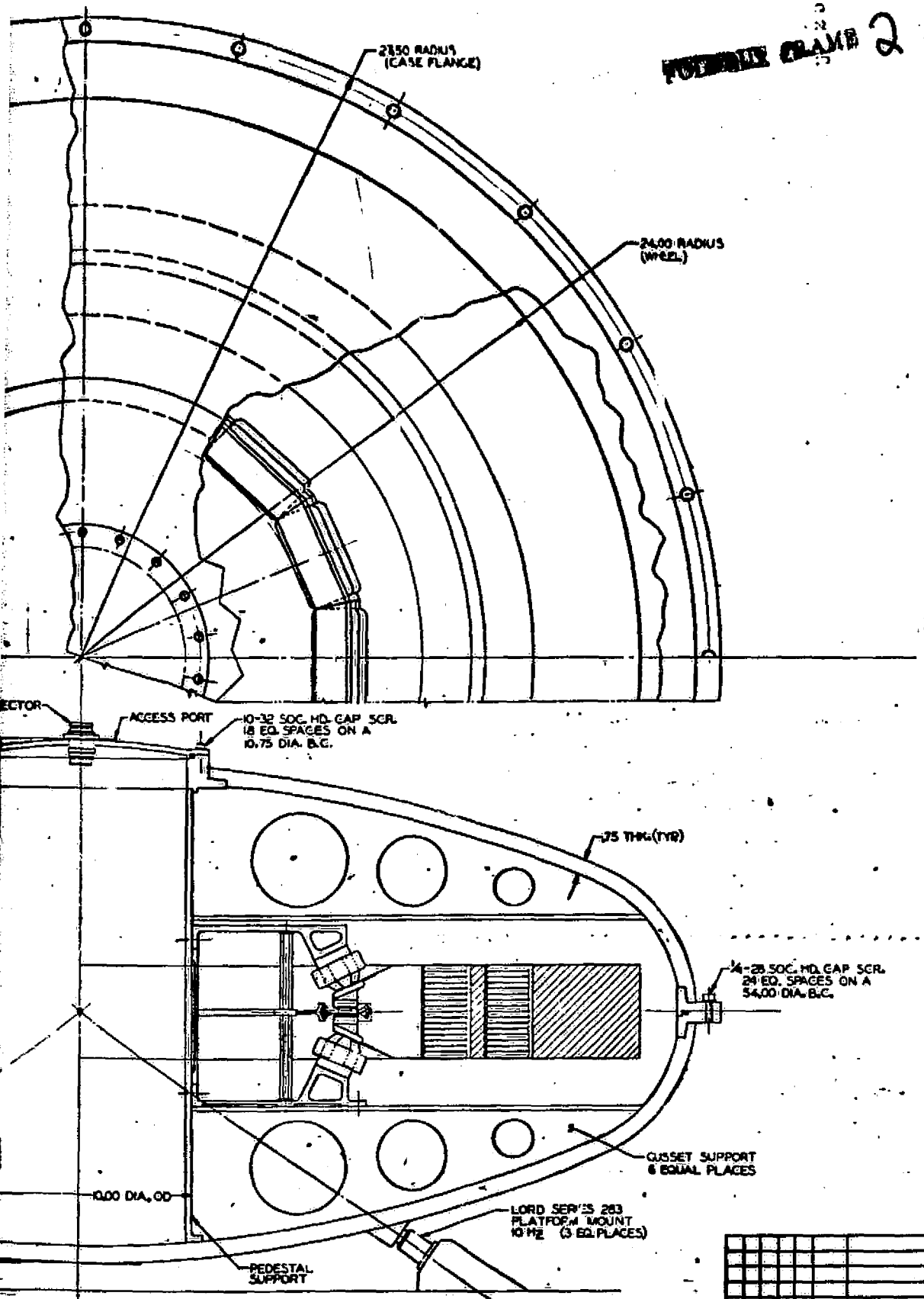

POTENTIAL CLAIM 2

MATERIALS AND SPECIFICATIONS

RCA ELECTRONICS PRINCETON, N.J.

LAYOUT
MECHANICAL CAPACITOR

E | 49671 | SK2294234

C 4

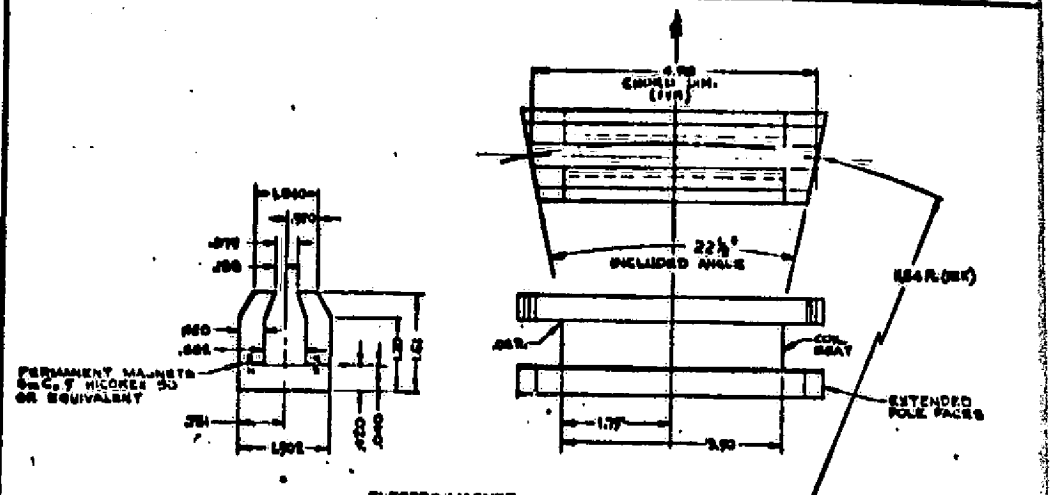

ELECTRO-MAGNET

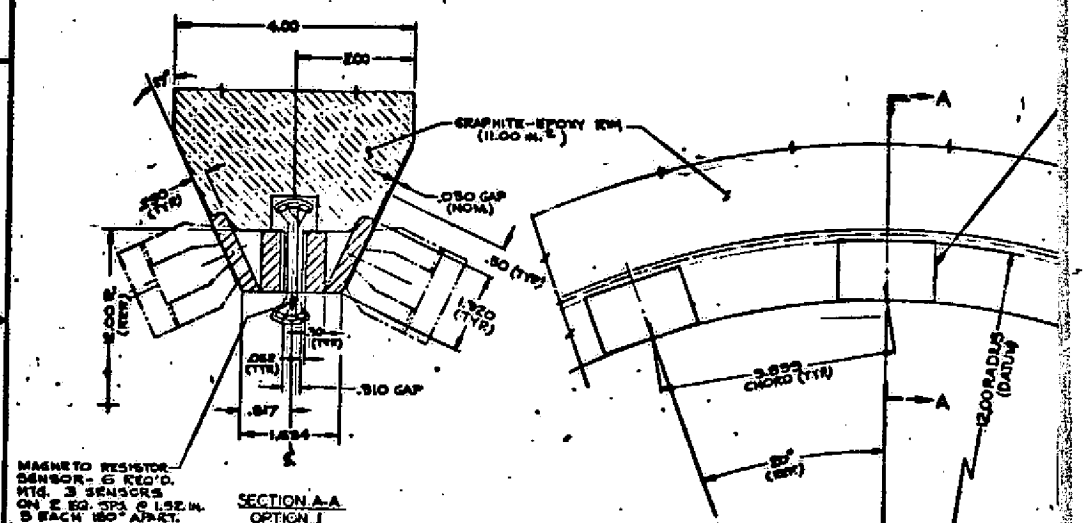

SECTION A-A
OPTION I

SCALE: FULL SIZE

SCALE FULL SIZE

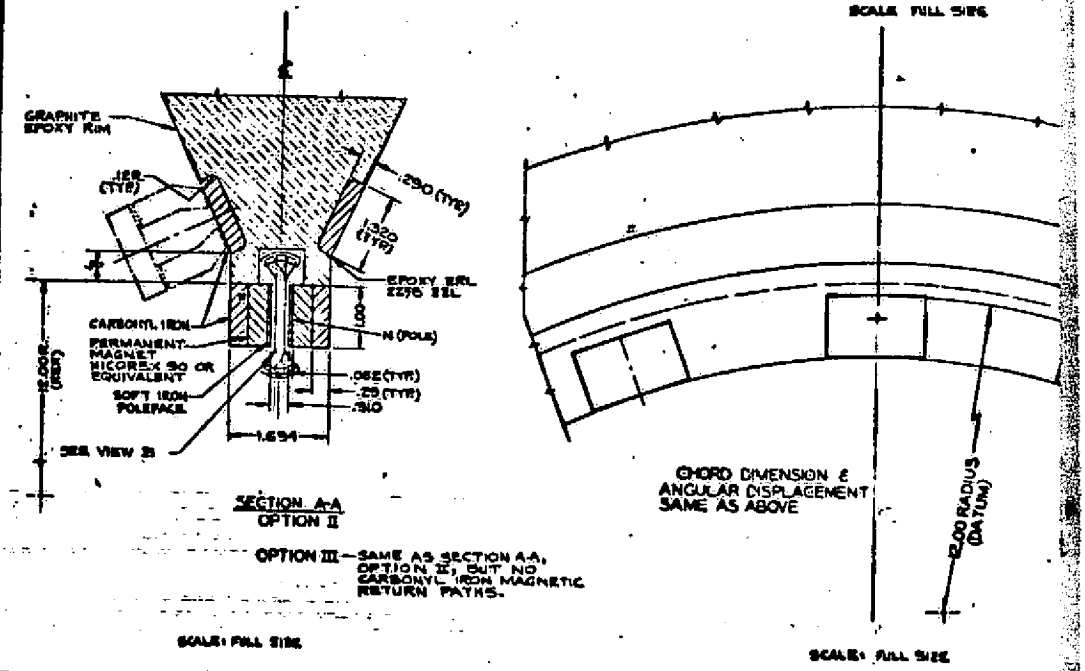

SECTION A-A
OPTION II

OPTION III—SAME AS SECTION A-A, OPTION II, BUT NO CARBONYL IRON MAGNETIC RETURN PATHS.

SCALE: FULL SIZE

SCALE: FULL SIZE

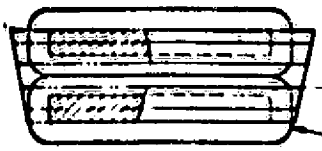

ELECTRO-MAGNETIC BEARING ASSEMBLY (SI REQ'D)

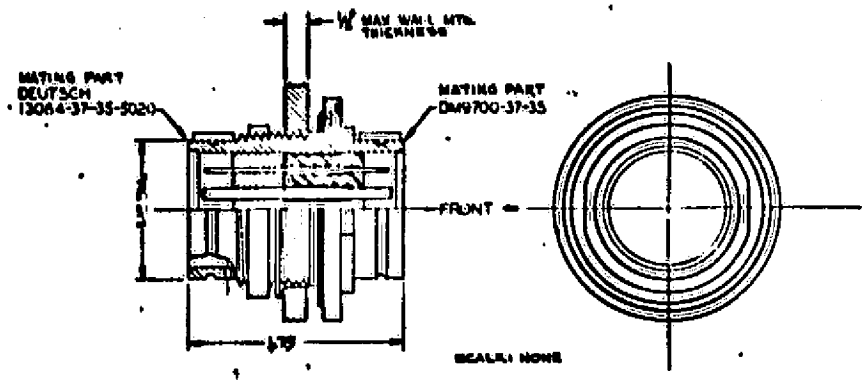

RECEPTACLE, CONNECTOR HERMETICALLY SEALED, MINATURE QUICK DISCONNECT DEUTSCH DM5623-37-3PP

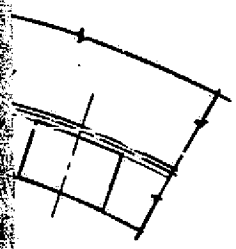

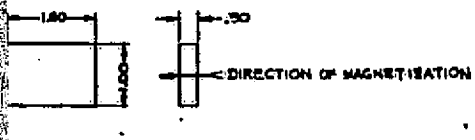

TYPICAL MAGNET FOR M/G NICOREX 50 OR EQUIV.

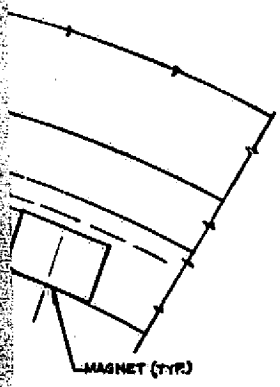

MAGNET (TYP.)

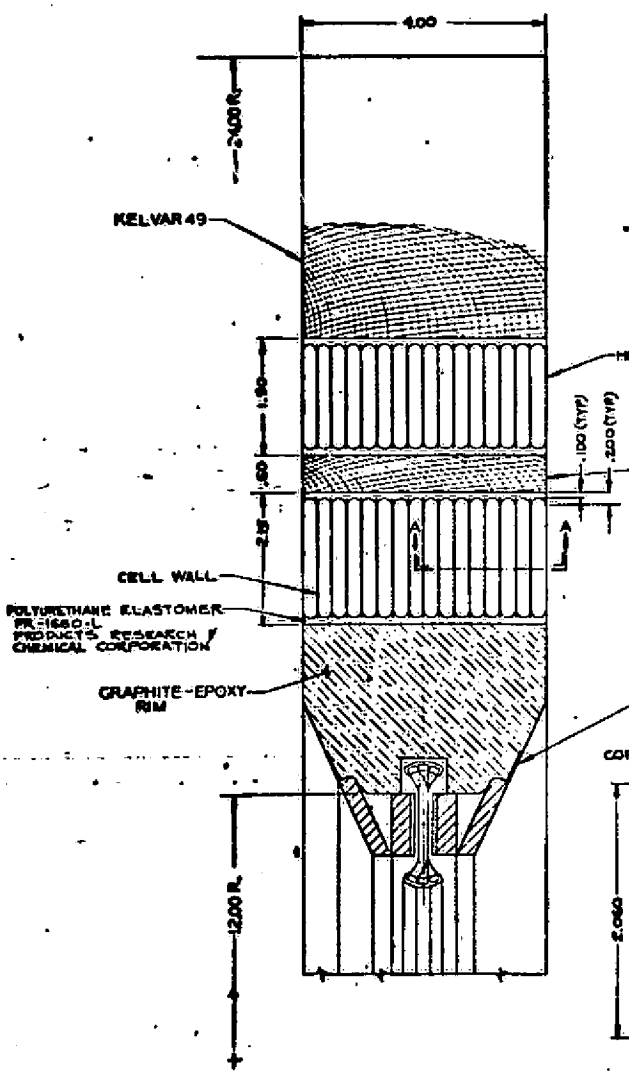

SECTION A-A

HEXCEL AEROSPACE GRADE 5052 ALLOY ALUMINUM HONEYCOMB 1/4-5052-.002, (4.3 LB/CU FT)

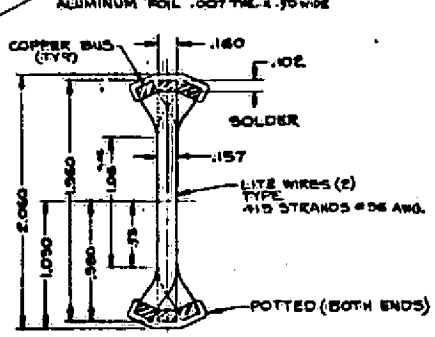

ARMATURE (VIEW B) SECTION THRU SCALE: 2/1

SIZE	CODE IDENT NO.	DRAWING NO.
E	49671	SK2294234

SCALE: NONE SHEET 2